Advance Control Strategies for Maglev Suspension Systems

by

Jonathan E. Paddison

A Doctoral Thesis submitted in partial fulfilment of the requirements

for the award of Doctor of Philosophy of the

Loughborough University of Technology

March, 1995.

Advance Control Strategies for Maglev Suspension Systems

Synopsis

The Birmingham Maglev developed over fifteen years ago has successfully demonstrated the inherent advantages of low speed maglev over comparable wheeled systems. It remains the only commercially operational Maglev in the world today. To develop the next generation of Maglev vehicles which will overcome some of the limitations of the Birmingham system, such as chassis length and cost, the following issues are addressed in this thesis.

1) The possibility of interaction between the chassis resonant frequencies and the suspension control system causing poor ride quality and at worst instability, are formally analysed. In the Birmingham vehicle a stiff chassis (fundamental bending mode 40Hz) is used avoiding significant interaction with the suspension controller. Using advanced control strategies the low frequency chassis resonances can be controlled allowing a vehicle structure to be used with a fundamental bending mode of about 12Hz.

2) A modern control strategy is developed which delivers an improved ride quality compared with the present classical control system despite having to operate with a 'soft' chassis. Kalman filters are digitally implemented and conclusions drawn about their performance. The classical control strategy is also successfully demonstrated on a 3m long 'flexible beam' rig.

3) An associated Maglev suspension problem for the response to ramp inputs such as the transition onto gradients which causes either a large steady state tracking error or a worsening ride quality is addressed by modern control theory using integral feedback techniques and classical theory using third order filters. These controllers are globally optimised by a multi-objective parameter optimisation system which formally considers the conflicts inherent in a suspension system between response to stochastic inputs and deterministic inputs.

Fortschrittliche Reglerauslegung von Magnetschwebebahnfahrzeugen

Übersicht

Seit 1984 hat Großbritannien eine Magnetschwebebahn am Flughafen Birmingham, die sehr gut in einem kommerziellen Umfeld funktioniert. Nach 10 Jahren Erfahrung besteht nun die Möglichkeit, das Birmingham Schwebebahnkonzept zu verbessern.

1. Zur Zeit ist der Wagenkasten der Magnetbahn sehr steif (erste Eigenfrequenz von 40Hz) ausgelegt, um Wechselwirkung zwischen Wagenkasten -strukturdynamik und Regler auf ein Mindestmaß zurückzuführen. Ein steifer Wagenkasten ist teuer und es hat viele Vorteile, einen elastischen Wagenkasten zu bauen. Solche Vorteile sind die geringen Kosten und Gewicht. Nachteile der flexiblen Struktur sind Stabilitäts- und Komfort Probleme. Die vorliegende Arbeit zeigt, daß es mit der modernen Reglungstechnik möglich ist, einen elastischen Wagenkasten zu bauen und dabei auftretende dynamische Probleme zu beherrschen.

2. Die Theorie wurde mit einem Verifikationmodell bestätigt. Ein 3 Meter langes, 200kg 'Half-Car' Modell wurde gebaut. Der Regler wurde auf einem 'Digital-Signal-Processor' implementiert. Die erste Eigenfrequenz dieses Modells ist 12Hz und ist vergleichbar mit normalen Eisenbahnfahrzeugen.

3. Eine voll-aktive Aufhängung hat neben zahlreichen Vorteilen auch Nacheile. Ein Nachteil ist, daß für den Übergang in eine Steigung der Relativweg zwischen Fahrzeug und Fahrweg sehr groß ist. Eine Integral-Rückführung wird zusätzlich zu einer klassischen und modernen Reglerstruktur benutzt und mit einer 'multi-objective parameter optimisation system' verbessert. Ohne mehrzieligen Optimierung gibt es Schwierigkeiten, die verschieden in Konflikt stehenden Ziele zu erreichen.

Table of Contents

Chapter 1: Introduction

A transport system with a non-contacting suspension system has many attractions such as the elimination of friction, with its associated wear and the removal of unwanted forces which would otherwise cause vibration. The reality of the situation is that magnetic suspension offers:

1. Frictionless support.
2. Solid state systems with no moving parts with associated increases in reliability and availability and also low maintenance in terms of time and costs.

All these points have been proven by the experience of the Birmingham Maglev in the period from 1984 to 1994. Yet there are limitations with the Birmingham Maglev Vehicle system design and some of these form the motivation for this Ph.D thesis.

In this thesis a number of problems relating to magnetic levitation (Maglev) vehicle suspensions are considered, principal among them being the use of a relatively flexible chassis. Novel control methods are shown to give a basis for longer and 'softer' chassis. A second subject of the thesis is the consideration of a single degree of freedom Maglev suspension on a gradient or a ramp input. This work shows that the Maglev controller has to be thoughtfully designed to overcome the transition on to slope or ramp which is often neglected in the literature on Maglev suspension design.

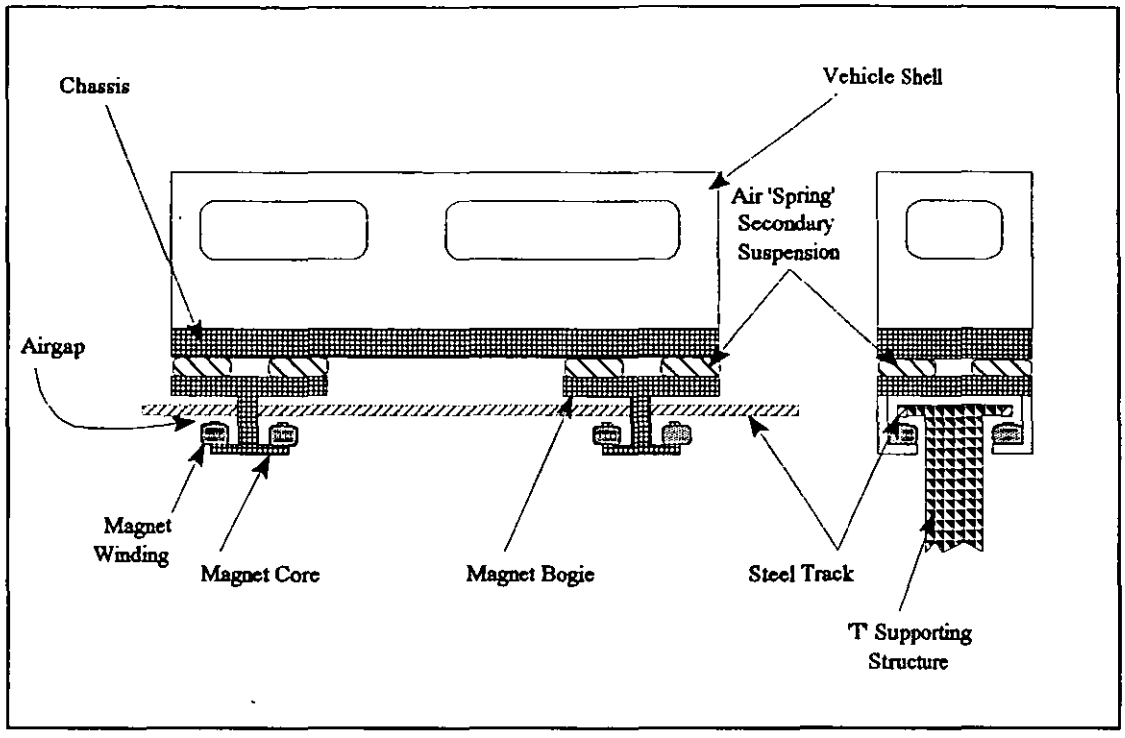

Figure 1.1 A basic Electromagnetic Suspension (EMS) Maglev Vehicle with a secondary suspension identifying the terminology.

1.1 An overview of Maglev development to-date

During the 1960's with the advent of Power Electronics capable of controlling current and voltage the potential of practical magnetic suspension became realisable.

The concept of using a magnetic field to support a vehicle has been around for a considerable time [Earnshaw39] [Braunbek39], but it was the work of a number of teams in Germany, the United Kingdom, the United States of America and Japan during the late 1960's and early 1970's which began to produce significant results.

There are two types of magnetic suspension systems being developed for vehicles. The first, Electro- Magnetic Suspension (EMS), uses the ferromagnetic attraction between an electromagnet and a steel track to suspend the vehicle beneath the track. The attractive forces are inversely proportional to the airgap between vehicle and track and this means EMS is fundamentally unstable. Feedback control is essential to stabilise the system. This

thesis deals only with the EMS system and more precisely the feedback control system requirements which cope not only with the instability but also the ride quality and flexibility of the vehicle chassis. The EMS concept is described in more detail in chapter 4, where the dynamic mathematical models are developed. Figure 1 above shows a generalised EMS Maglev Vehicle. The key elements of the structure are identified to give a basis for further discussion.

The second method called Electro- Dynamic Suspension (EDS) uses the repulsion between conductors (on a vehicle) and currents induced by the vehicle's motion in a reaction plate (on the track) to support a vehicle. As the speed of a vehicle increases the induced eddy currents in the reaction plate are strong enough to produce a vertical force which at high speed is sufficient to carry the weight of the vehicle. The EDS system is dynamically stable because the repulsive forces are inversely proportional to the airgap between vehicle and track. Feedback control is not necessary to stabilise the system but may be used to give the EDS system better suspension characteristics, such as improved damping.

Viewed from the 1990s and through-out the world, Maglev has not fulfilled its early promise. The reasons are complex and it is difficult to identify one single cause. The lack of a coherent transport policy and that in political circles Maglev has been seen, as a way for high-tech military industry to enter the transportation market has dogged Maglev over the last 25 years. Emphasis on high speed transport rather than exploiting the reliability aspects of Maglev for low speed systems has led to rather ambitious and very expensive plans which have required considerable central government funding to be viable.

1.2 Maglev Developments

1.2.1 United Kingdom

The history of Maglev in the UK is one of low level funding in a few universities and at British Rail Research (then a division of British Railways) between the early seventies and the early eighties. The work of the latter group resulted in the development of the Birmingham Maglev, which remains to-date the only commercially operational Maglev in the world.

Most people in the UK associate Maglev with Professor Eric Laithwaite, at Imperial College London, who was at one point the most well known Professional Engineer in the country, due to his Royal Institution Lectures, 'Electrical Machines of the Future' in 1962. His main work was in fact with linear induction motors [Laithwaite65, Laithwaite66] and the systems he proposed were impressive yet ultimately unsuitable for the transport of people, being inefficient and difficult to control.

Perhaps the most significant contributions from the university sector were made by a research group at the University of Sussex [Jayawant81]. The team developed a low speed Maglev prototype during the mid- seventies. This prototype was followed by a series of design studies during the early eighties on various aspects of the technology including consideration of the chassis flexibility [Jayawant83]. Since the mid 1980's the Sussex group has largely concentrated on the applications of Maglev ideas to magnetic bearings [Whorlow93] [CME88].

At Warwick University ambitious plans were developed for an EDS Maglev system during the early 1970's [Rhodes74]. The work begun at Sussex has been further developed at Warwick and Reading Universities using control philosophies for Maglev vehicles based on parallel processing techniques allowing distributed control of the magnets [Sinha87,Sinha91].

Work was carried out during the late 1970's at the University College of North Wales at Bangor and Rutherford Appleton Laboratory into the 'mixed-mu' system of levitation which is based on the principle whereby iron ($\mu>\mu_0$) is levitated in a magnetic field and stabilised by the proximity of diamagnetic materials ($\mu>\mu_0$) [Paul84].

Various propulsion systems for Maglev were investigated by a team at Bath University and interest in Maglev has continued at a lower level [Eastham84].

The team working at the British Rail Research Centre at Derby during the mid 1970's naturally considered Maglev against the backdrop of conventional railway steel wheel on steel rail technology. System studies were carried out to assess the potential for low and high speed Maglev Systems in the UK [Dobbs76], and these yielded two major conclusions. Firstly the fact that the UK is an island meant that high speed Maglev routes would not demonstrate their advantage because the maximum distance would be comparatively small. Also the UK had an extensive mixed rail system. Thus the BR team concentrated on the low speed Maglev (up-to 100km/h). Secondly they identified the inherent reliability as the major 'selling point' of Maglev and endeavoured to concentrate on a simple system utilising a single stage suspension providing the ride quality, stability and guidance properties of a conventional suspension. The fact that the BR team had experience of other transport systems proved to be a significant factor in the success of their work. The work resulted in an experimental 3 tonne vehicle [Goodall77] and this formed the basis for the Birmingham Maglev system. The control ideas were extended to more general railway active systems [Goodall81] and have also provided the basis for application to automobiles [Williams94].

The Birmingham Maglev is described in some detail later in the next section of this chapter and a picture is included at the end of this chapter.

1.2.2 Germany

Germany has had an extensive Maglev programme for the last 20 years. This has been funded in the order of billions of Deutschmarks by the Federal Government, and the work has been mainly undertaken by the large German engineering firms, among them; Thyssen AG, Siemens AG and MBB. In 1981 these firms pooled their resources to form the Transrapid 'Group' under the leadership of Thyssen. Thyssen are now the sole owners of the technology developed.

The goal of Transrapid has always been a high speed Maglev (450km/h) and the programme culminated in a very impressive demonstration Maglev system. This is based in Emsland in North Germany and consists of a 36km long track in a figure of eight shape [Mayer93].

Since the early 1980s there has been very little development of the concept. The emphasis has been on proving the technology. At present the system is used to assess the reliability and demonstrate how it performs with respect to safety and environmental considerations. The Transrapid Europa vehicle has been certified as suitable for public transport in Germany [Schneider91].

The way would now seem to be clear for the development of a real system. The best prospect for the use of the Transrapid is the route between Berlin and Hamburg, which is seen as a symbol of 'high-tech' reunification. A bill to fund the route has passed through both the upper and lower Federal Parliaments [HSTN94a] [SZ94]. The project remains highly political and the political commitment remains uncertain considering the massive investment in high speed (250 km/h), steel wheel on steel rail, intercity infrastructure already made by the Deutsche Bahn (German Railways) in recent years.

The track between Hamburg and Berlin is too short to really demonstrate the ability of high speed Maglev to compete with the airlines (as for instance the TGV route has done

between Paris and Lyon in the south of France). Few people currently fly between the two cities. It is interesting to note that the Transrapid Maglev will be run jointly by Deutsche Bahn and Lufthansa which although both majority state owned are making commercial commitments to the system.

Although there was some early work on low speed (80km/h) Maglev, it seems to be largely forgotten in Germany though recently comments have been made that the Transrapid is simply too complex and a simpler and less ambitious system should have been developed with tax payers' money. A low speed pseudo Maglev called Magnetbahn did exist in West Berlin until 1990 when it was ripped out of the city to make way for the conventional city 'Stadt- Bahn' railway system following the reunification of East and West Germany. No plans exist to develop this Maglev system which used small wheels to provide guidance for the vehicle along an overhead concrete guideway. The suspension force was provided by permanent magnets.

1.2.3 Japan

Japan is widely known throughout the World as being a developer of Maglev. The tendency is to think of the high speed Maglev vehicles using superconducting magnets (an EDS system) but a low speed (100km/h) Maglev being built by the Chubu HSST Development Corporation is very likely to enter service shortly. Public money from the Aichi Prefectural Government has been used to support the building of a test track which it is anticipated will form part of a CHSST Maglev system in Nagoya-City. The vehicle seems to rely on high quality track and a secondary suspension system to attain ride quality which is according to independent sources is 'very satisfactory'. The major problems seem to have been solved and the system seems to be a commercial proposition. It does display the inherent simplicity of low speed Maglev as predicted by the early Maglev advocates. The system is at present undergoing 'assessment of feasibility as a public transportation system' and has passed most of the hurdles [Mizuma93].

The CHSST vehicles are made of two separate cars, each 8.5m long, with an articulated joint. 67 people can be carried per car with a laden weight of 30 tonnes. The operating airgap is about 8mm and the maximum speed is 110km/h.

As well as pursuing developments in Japan, the Chubu HSST Development Corporation have tried to market the technology in North America, most notably in Las Vegas. The lack of legal 'rights-of-way' has prevented and killed many HSST North American projects, and the HSST has dissolved its formal corporate presence in the USA. A feasibility study is under way to supply HSST technology for a $700 million Maglev line linking Rio de Janerio's suburbs with its Airport. The planning regulations are less stringent in Brazil, offering a potential proving ground for the technology. A picture of the HSST-100 vehicle is given at the end of this chapter.

The future of the superconducting vehicles being built by the former Japan National Railways (JNR) now Central Japan Railway (CJR) is under question since their time to market is some way off and high speed Shinkensen trains will shortly be available which can match the target speed of the JNR Maglev vehicles [HSTN94b] [O'Neill93]. This project may well be kept alive because of its high profile use of superconductors but there is confidence that in the long term it will provide the basis for a viable transport system particularly with respect to recent improvements in the performance of high temperature superconductors [Ozeki93]. The CJR and the Railway Technical Research Institute are 'forging ahead' with construction of a 42.8km Maglev test track that could eventually become part of the Tokyo-Osaka Maglev line [MN93].

1.2.4 United States of America

In the US Maglev seems to go in and out of fashion every 15 years. For instance following the signing of the Intermodal Surface Transportation Efficiency Act of 1991, $725 million was allocated to Maglev development over the next six years and was to be managed by the National Magnetic Levitation Prototype Development Program. The

money was for high speed Maglev systems. The funding was achieved on a nationalistic 'ticket' with the threat of having to buy German or Japanese technology in the next ten years as the reason [Stix92]. Some commentators see the money for Maglev as a fillip to hard pressed defence/aerospace firms and research centres which were formerly working on Superconductivity for Defence Applications, such as the 'Star Wars' program.

Unfortunately all of the optimism created by the Act had by the beginning of 1994 evaporated as the funding from central government was completely cut by the Clinton Administration.

At present the National Maglev Initiative remains in tatters. Four consortia developed designs for high speed Maglev systems and a mixture of superconductor and conventional electromagnetic system designs were proposed [Mayer92]. There is still discussion in the US about the viability of these designs both from a commercial and technical perspective. There is a temptation to see the NMI as a paper study.

Nevertheless, the USA Maglev lobby seems to be able to influence minor politicians about the potential of Maglev to their state or city with regard to jobs and supporting defence industries. Hence there is a constant stream of design studies.

1.2.5 Korea

There has been Maglev interest in Korea since 1985, when a team from Hyundai began to investigate the technology. Major influences on their work were the Birmingham Maglev and the Japanese CHSST systems which concentrated on the low speed applications of Maglev.

Hyundai and since 1989, DaeWoo Heavy Industries, with support from the government have made substantial progress and both have developed demonstration vehicles capable of carrying about 40 people. A test track of up to 1km is now under construction to

prove the technology [In-Dae93]. A picture of the DaeWoo vehicle is included at the end of this chapter.

A consortium has been formed to bid for the Seoul-New International Airport Transit system. The future of Maglev in Korea now depends on 'how soon the government fully commits to the Maglev application' [In-Kun93]

1.2.6 Other Countries

Academic interest in Maglev exists in many countries but without funding for practical research. For instance both Italy [Martinelli93] and China [Lian93] have interest in Maglev motivated by their respective infrastructure problems. As yet the work appears to be limited to theoretical studies.

1.3 The Birmingham People Mover Group Maglev

The Birmingham People Mover Group (PMG) Maglev has now been running successfully for 10 years. The Birmingham International Airport PLC management are very satisfied with the system and would like to extend it to new terminals which are currently being planned.

The complete system was built at a total cost of £3.2 million over a three year period beginning in 1981. The supporting guideway structure represented 40% of this cost [North85]. The (PMG) Maglev operates as a low-speed people mover between the airport passenger terminal and Birmingham International Railway Station. As no fee is charged for the service the ridership is not monitored, but officials estimate 1.1 million people used the system in the fiscal year 1991-1992. Total operating costs for the same period were £177,900, which includes labour, material and energy. Cost per passenger trip is estimated at £0.16 (1989 prices). These costs are significantly less than for other airport people movers, such as rubber tyred electric vehicles or moving walkway systems. The

higher cost of these alternative systems are mostly due to their more onerous maintenance requirements [Walker89].

People have accepted the technology and the fact that magnets are used instead of wheels is imperceptible to the passenger except at the station where the 'lift-off' may be felt, this is a significant plus for the Maglev principle, which could be considered by the lay-person to be disconcerting.

The consortium which built the system consisted of the following key players; GEC Transportation Projects Ltd and many other GEC Companies, Metro-Cammell, British Railways Board, British Rail Research, Government, the Railway Inspectorate and West Midlands County Council. The partnership between Private and Public bodies provided the environment to develop the British Rail Research concept in a quasi-development environment. As only three vehicles were built no economies of scale were achieved thus increasing the cost of the system.

British Rail Research provided the fundamental design for the system. This was based on their research prototype Maglev built during the 1970's at the BR Research at Derby [Goodall76]. A key element of the design is that it uses a classically designed modal controller to control four magnets at the corners of each vehicle. The suspension requirements of stability, ride comfort and guidance are provided entirely by the magnets operating with a 15mm airgap between the track and the magnet core. No springs or dampers are used and in fact the only moving parts of the whole vehicle are the automatic sliding doors. In this respect the vehicles are unique in the Maglev world in not using some form of secondary suspension.

Table 1.1 Key details of the Birmingham Maglev System

Vehicle Parameters	
Weight (unladen)	5 tonnes
Weight fully laden with 32 passengers and luggage	8 tonnes
Length	6m
First Body Bending Mode	40Hz
Width	2.2m
Power Consumption	2kWh per vehicle journey
Nominal Source Voltage	600V
Continuous Output Current Rating	335A
Dynamic Parameters	
Nominal Airgap	15mm
Vertical Ride	4.5%g
Lateral Ride	3.3%g
Maximum Forward Speed	15m/s (≈ 34mph)
Forward Acceleration	1.24 m/s^2
System Parameters	
Guideway Length	623m
Maximum Gradient	1.3%
Journey Time	100s

1.4 Motivation for this thesis

That the Birmingham Maglev has been successful is not in doubt. However a number of limitations of the design are outlined below. These form the motivation for the work described in this thesis. The problems and their priority in this thesis are outlined below:

1) High Cost Chassis

The chassis cost was very high compared with a conventional vehicle for the following reasons. The Birmingham Maglev concept relies on a single stage suspension and from the outset the flexibility of the chassis was an issue. During the development of the system a decision was taken that, rather than solve the problem of the flexible structure interacting with the controller, the chassis would be constructed with a first bending mode frequency well outside the controller bandwidth. This decision resulted in the chassis having a first resonant mode of 40Hz [Pollard85].

The suspension controller relies on a degree of certainty about the flexible structure such as identification of resonant bending modes and their variation due to loading and temperature.

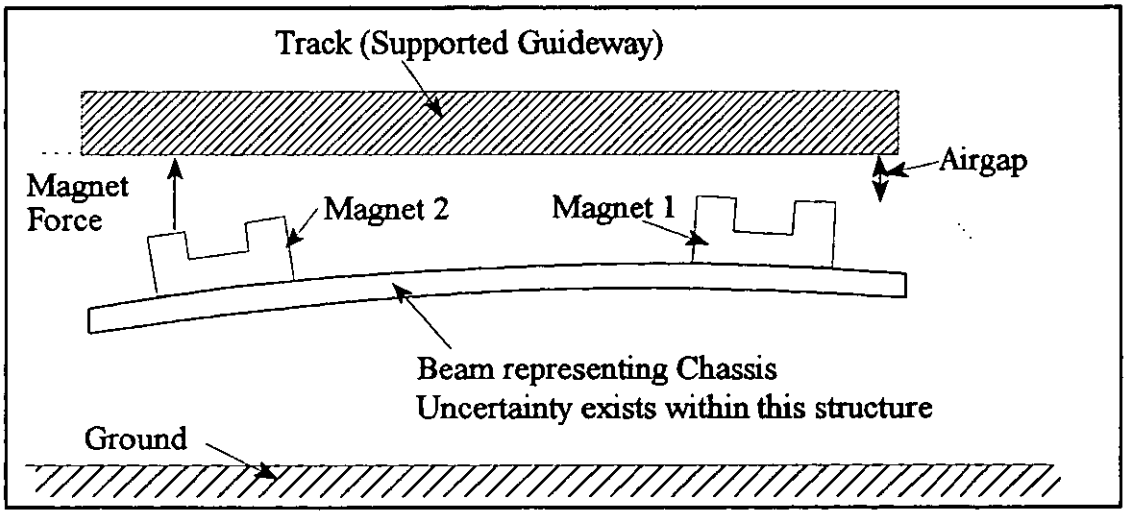

Figure 1.2 Exaggeration of the effects of a flexible Maglev chassis.

The dual requirements of lightness and stiffness resulted in the need for a sophisticated design for the chassis using aerospace type techniques.

2. Out-of-date Components

Advances in electronic component technology such as semiconductor switching devices means that the replacement of components as they fail is increasingly difficult.

3. High Civil Structure Costs

The overhead guideway need not be as rigid and costly as originally specified. A lighter weight structure may well suffice. The problems of vehicle/guideway interaction of high speed transport systems are often quoted but the potential for such effects appear not to have influenced the Birmingham system design.

1.5 Work Addressed in this Thesis

The body of work described in this thesis takes the proven concept of the Birmingham Maglev and enhances it through the use of newer so called 'modern' control techniques. The principal area of investigation is that of control strategies for soft vehicle structures. At present because the vehicles are required to be rigid they are expensive and are limited in length. (The shorter a vehicle is the stiffer its structure can be made.) Longer, cheaper vehicles would be able to compete on favourable terms with conventional transport vehicles. A standard railway carriage is of the order of 20m long, whereas the Birmingham Maglev vehicles are only 6m long. Ideally a Maglev vehicle of 12 to 15m length is envisaged.

Using 'modern' control strategies this inherent limitation on the length of the vehicles can be overcome by using a more sophisticated controller which can actively control the bending modes of a flexible chassis or at least minimise the effects of the flexing.

The use of modern control strategies also allows for the reduction of instrumentation requirements through the use of optimal filters. Maglev vehicles have a large number of sensors and any reduction will simplify the operation of the controller and reduce the overall cost. The effects of limits imposed on the Maglev vehicles as they travel onto gradients or ramps are addressed using a novel control design development system.

The thesis is laid out as follows;

Chapter 2 is a detailed survey of the work involving the control of flexible vehicles, especially those using Maglev suspensions, is presented.

Chapter 3 describes the analysis techniques used in assessment of the control strategies developed. Frequency response and Covariance analysis methods are described and related to basic vehicle ride quality assessment criteria.

Chapter 4 contains the modelling of the basic suspension and then develops the model to incorporate the flexible bending modes and their effects.

Chapter 5 reproduces the 'classical' control strategy on the Birmingham Maglev Controller and investigates its limitations with respect to a flexible chassis. Filter based resonance suppression techniques are analysed.

Chapter 6 develops the so called 'modern' control techniques, firstly using full state feedback and then incorporating Kalman filters.

Chapter 7 considers new control methods with respect to the effects of deterministic and random inputs to a system. A Multi-Objective Optimisation Package is used to trade off different design requirements. This then leads to the reappraisal of the problem in terms of its original model formulation such that the system model dictates the controller performance.

Chapter 8 describes the design and fabrication of rig to demonstrate the control strategies developed in chapters 5 and 6. This section covers the construction of the mechanical structure of the rig, the power supply requirements and construction, the analogue sensor conditioning circuits, the interface with a digital signal processor and the development software used to implement the controller structures.

Chapter 9 describes the testing of a rig and assessment of the results. The rig is assessed in a static situation in the levitation mode.

Chapter 10 contains a conclusion and suggests further work.

1.6 Published Work

Some of the work contained in this thesis has been published in the following papers;

Bals, J. Paddison, J.E., ANDECS-MATLAB Multicriteria design for a Maglev vehicle comparing a 'classical' and a 'modern' control structure. IFAC Conf. on Integrated Systems Engineering, Baden-Baden, Sept.27-29 1994. Invited Session I-2.

Paddison, J.E., MacLeod, C, Goodall, R.M., State Variable Constraints on the Performance of Optimal Maglev Suspension Controllers, 3rd IEEE Conference on Control Applications. Glasgow. August 1994, Pp.599-604.

Paddison, J.E., Goodall, R.M., Bals, J., Grübel, G. Multi-objective design study for a Maglev Suspension Controller using the databased ANDECS-MATLAB environment. IFAC/IEEE Joint CACSD'94/CADCS'94 Conference, Tucson, 7-9 March, 1994 Pp.239-246 .

Paddison, J.E., Goodall, R.M., Controlling Flexible Structures in Maglev Vehicles, 2nd IEEE Conference on Control Applications, 13-16 Sept. 1993 Pp.675-671.

Figure 1.3 Japanese HSST Linear Motor Maglev

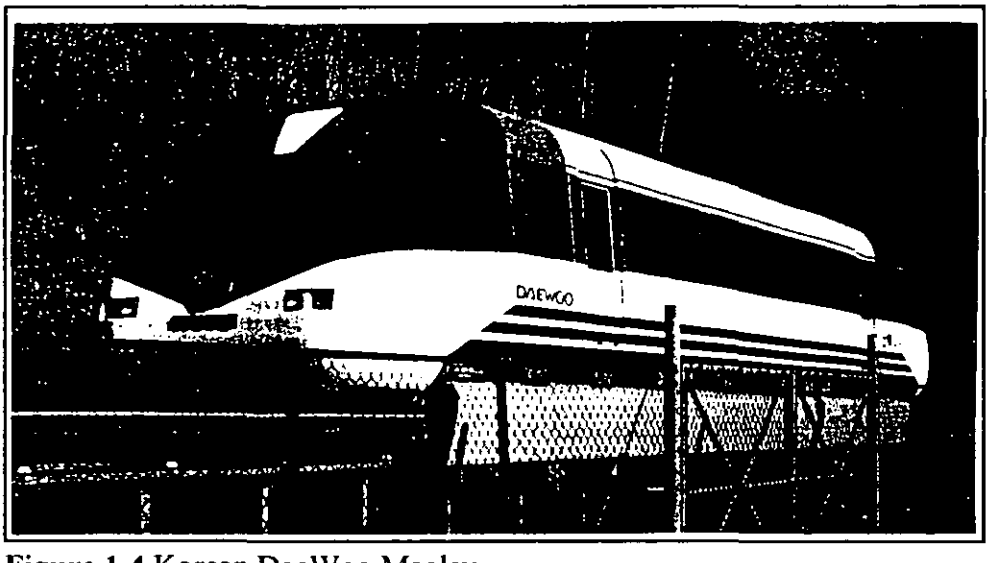

Figure 1.4 Korean DaeWoo Maglev

Figure 1.5 Birmingham Maglev

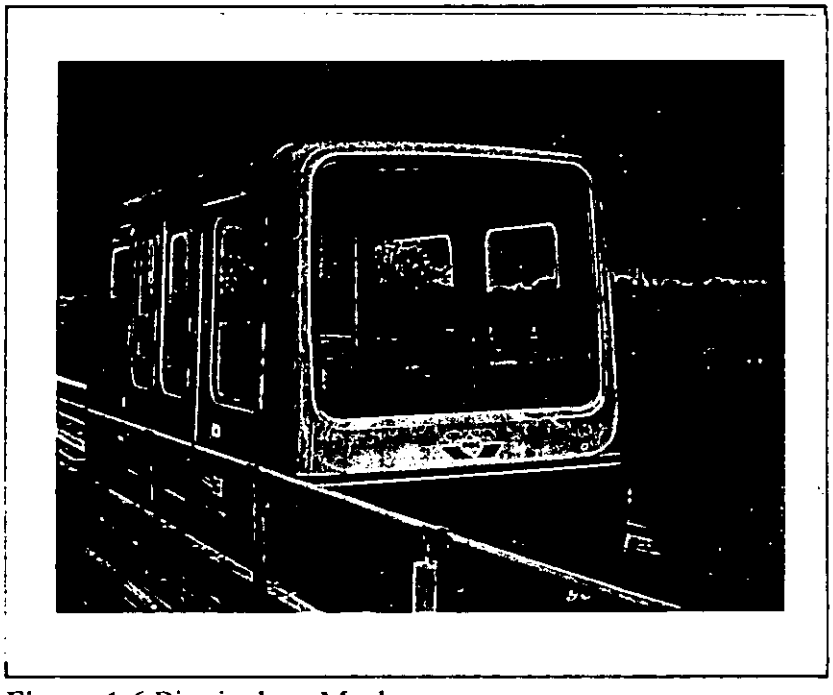

Figure 1.6 Birmingham Maglev

Chapter 2: Literature Survey

Extensive literature surveys have yielded only one reference or work directly applicable to a Maglev vehicle with a 'soft' chassis and using a single stage suspension [Meisinger75]. This is because most Maglev designs incorporate a secondary suspension as well as the magnetic actuators. This lessens the effect of the flexible bending modes on the magnetic suspension control system.

The work presented in this thesis however covers a number of major areas of research each of which has a strong bearing on the project:

1. General active suspensions with respect to both railway vehicles and automobiles.
2. Control techniques, covering the design of the controller and digital implementation aspects.
3. Maglev development
4. Flexible Maglev vehicles
5. Flexible vehicles
6. Methods of modelling and controlling flexible structures

In this chapter the discussion relates to the last three literature areas (i.e. 4, 5 and 6), but the others are referred to in the main text of the thesis. The first section in this chapter covers literature where the flexibility of the Maglev chassis has been considered and clearly shows that the problem has not been practically solved. The second section covers methods of analysing and controlling a flexible conventional wheeled vehicle chassis and this work has mainly been addressed by small academic teams. In these references control techniques are considered but in general the background to the papers is not practically based. Control techniques used on the flexibility problems of space structures are considered in the third section.

2.1 Flexible Magnetic Levitation Vehicles

2.1.1 Sussex University

The work at Sussex University covers many design aspects of a vehicle suspended by four magnets. A great deal is made of the effects of a flexible chassis.

For controlling multi-magnet systems two control strategies are discussed, one using modal control where the rigid body pitch, bounce and heave modes are controlled, and the other using independent control of the magnets at each of the four corners of the vehicle. The authors suggest that independent stabilisation of each magnet has 'the advantage of being able to use well tried methods of compensation'. This it is assumed to mean that the controller developed for a single magnet can be used at each corner magnet [Sinha79].

From experimental and theoretical studies the authors maintain that 'due to the flexibility of the vehicle chassis, the local control scheme provides better dynamic response in terms of position and peak acceleration level'. This is understandable if the 'flexible chassis' provides a degree of decoupling between the magnets. No quantification of the nature of the flexibility such as the natural frequencies of the bending modes or the damping in the structure is provided and this means that the effects of the author's 'chassis flexibility' is difficult to assess. The method of modelling the effect of the fundamental bending mode is difficult to understand since it involves the introduction of a finite stiffness term into the pitching mode. No conventional model of the flexible bending mode is used [Gondhaleker83].

The meaning of the term flexible chassis is not taken to be the same as in the other papers. It is not explicitly stated in this paper but it is seen that the 'flexible chassis' here is more akin to a secondary suspension and its use is similar to the Magnetic Wheel Concept

[Gottzein80].

Developing the idea of decoupling of distributed control being advantageous, further work by the authors introduces the idea of a two-arm chassis which consists of 'a flexible rectangular frame with a rocking arm at each side'. It is stated that the two arm chassis offers the mechanical advantage of a stiff vehicle structure without the disadvantages of increased coupling between the corners. The stiffness and damping present in the model are not quantified and the performance of the suspension is only assessed in response to a time domain step input.

Continuing with the work described in the above paper the local magnet control concept is developed further with a flexible chassis [Gondhaleker83].

2.1.2 Messerschmitt-Bölkow-Blohm GmbH(MBB)

The work undertaken by MBB of Germany during the seventies and early eighties identified many of the design problems for Maglev vehicles. The use of the magnetic wheel concept [Gottzein80] which separates the magnet stability problem from the uncertainty in the chassis by means of a secondary air spring suspension meant that consideration of the flexibility of the chassis was not so important but identifies the problems thereof with the following statement. 'The quantity of unstable eigenvalues of the uncontrolled system is determined by the parameters of the magnets, mechanical suspension elements, and the structure stiffness of the vehicle's body'.

A real worry for the German team appears to have been the vehicle/guideway interaction which for high speed Maglev systems will be very significant. In addition to considering the effects of a flexible guideway the effect of a flexible vehicle was also added [Meisinger75] [Meisinger77].

The guideway and vehicle are modelled as Bernoulli-Euler beams using the assumed modes approach. The first bending modes of the guideway and the vehicle are 4Hz and 6Hz respectively. Most of the thesis considers a Maglev vehicle with a single stage suspension. The Magnetic attractive force is distributed along the length of the free-free vehicle beam in order to simplify the analysis. This seems an over-simplification but it needs to be remembered that the goal of this work was to see how a sinusoidal guideway would excite the flexible modes in the vehicle and the guideway itself. The effects of the guideway roughness are not considered except as noise in the measurements.

Two control strategies are considered, one an LQG controller with fixed gains using a Kalman filter to derive some of the unmeasurable states. The second controller is an adaptive version of the first controller and is described as a periodic observer controller. The adaption is in response to the flexible guideway the effects of which become more pronounced as the Maglev travels faster and the period of the excitation of the vehicle due to the bending of the guideway becomes shorter. The Kalman filter is used to reduce the instrumentation requirements and to provide the key parameters for the gain scheduling of the state feedback in the periodic controller.

A comprehensive set of frequency response theoretical results are presented but are difficult to interpret in terms of practical values. No practical results are shown or even results relating to existing MBB vehicles.

The general conclusion is that, for a high speed Maglev on a flexible guideway, and using a fixed controller a secondary suspension system is the only possible solution from a stability and ride quality point of view. The best results for a single stage EMS suspension are obtained for a correctly tuned periodic observer controller for a given frequency range. No indication is given of the performance of the controlled suspension for variations of speed and its robustness to parameter uncertainty. The work concludes that numerous experiments will be required to extend it further.

2.1.3 National Research Council Canada

The Canadian National Research Council produced an extensive investigation on the structural analysis of a Canadian EDS Maglev Vehicle during the late 1970's [Hayes80]. The authors show that the chassis is limited by what they call vehicle length dependent vibration induced ride quality. They conclude that the characteristics of such a Maglev vehicle prevent the application of vehicle vibration limiting criteria which have been established for aircraft and railway vehicles. The length of the Maglev vehicle must be optimised to obtain acceptable ride quality but a lightweight, long life body shell structure can be produced using conventional technology.

The study does not consider control of the suspension to optimise the ride quality or reduce the effects of bending modes. The problem is considered as one of structural mechanical design.

2.1.4 Railway Technology Research Institute

Work at the Japanese Railway Technology Research Institute has covered many aspect of Maglev design and in particular the high speed EDS Maglev system. The Car Dynamics Laboratory has considered an electrodynamic suspension (EDS) Maglev vehicle with a flexible chassis and various configurations of secondary suspension [Miyamoto80].

The half-car body is modelled in terms of the heave, pitch and first three bending modes of 4.5, 6.3 and 14.1 Hz. The effects of variations in the internal damping due to the position of the connection between the primary and secondary suspensions are considered. The standard damping ratio used is 1% damping.

The main purpose of the paper is to determine which configuration of the primary EDS suspension is most effective in reducing the effect of the flexible body bending modes.

The possibility of improving the damping of the EDS primary suspension is not considered nor is the idea of using an active secondary suspension.

Using frequency response techniques the rms acceleration and power spectral density of the mid-point of each car body are calculated under the influence of a Shinkansen track surface irregularity (i.e. high quality track). The best results are achieved using a secondary configuration most like a conventional rail vehicle, using two bogies attached to the main vehicle at 1/4 and 3/4 the length of the vehicle. Although not stated in the paper such a configuration minimises the excitation of the first flexible bending mode.

2.2 Flexible Vehicles

2.2.1 Nagai and Sawada, (1987) [Nagai87]

This paper considers the use of an active suspension placed between the bogie trucks and the flexible vehicle. The authors hint at the need to pay particular attention to the flexible body modes present in a Maglev vehicle but restrict this paper to a generic non-Maglev vehicle with a two stage suspension. The first stage of the suspension is assumed to be a spring damper pair located between the bogie and the guideway. The second stage consists of a pneumatic actuator in parallel with an air spring.

The advantages given for a flexible vehicle are that it is lighter than a conventional one. This is proposed to be very significant for high speed ground vehicles. The proposed solution uses a full state feedback controller to drive pneumatic actuators to suppress not only the rigid body motions but also the bending vibrations.

The flexible vehicle is modelled as a free-free beam and follows almost exactly the same method described in chapter 4 of this thesis. The authors discuss the effect of changing the actuator and sensor location (which are collocated) with respect to the nodes of the

bending modes and how this alters the controllability of the bending mode in question.

Linear models are used for the suspension stages and the flexible structure. A so called half car model is developed which consists of a vehicle cut away along its length and an actuator at the front and rear of the vehicle.

Two control designs are suggested, one using centralised modal control and the other controlling the actuators at the front and rear of the vehicle independently. Since the bandwidth of the actuators is low (cutoff at 5.19Hz) the authors attempt to control only the first bending mode and the rigid body modes. The first flexible bending mode is 5.1Hz.

State feedback optimal control is used following the Linear Quadratic Gaussian (LQG) approach. The unsymmetrical bending mode gains are not developed optimally but are replaced by the gains corresponding to the symmetrical bending modes. This simplified controller is therefore non-optimal.

The performance index used minimises the rigid body acceleration and the velocity caused by the flexible bending modes. The decentralised control is used only to attempt to minimise the rigid body accelerations.

The disturbance input is a vertical velocity input represented by white noise and a time delay is considered between the front and rear contact points. This delay is not used in the control law formulation.

The conclusions are that the active suspensions improve the ride quality and the stability by suppressing not only the rigid body vibration but also the first order bending vibration, which is excited by the random track surface. The decentralised controller proves less use in suppressing the 1st bending mode than the centralised modal controller.

For the purposes of this thesis the above paper is a very strong contribution.

2.2.2 Hać (1986) [Hać86]

Hać presents a similar model to that previously discussed. The author considers that it is important when applying active suspension techniques to a vehicle with a long wheelbase, to introduce an elastic element into the model. He does not consider Maglev vehicles.

A generic vehicle model is developed using the bond graph method [Margolis79] [Cellier91] leading to an 11m long half-car structure with a first bending frequency of 12.7Hz. Since the controllers are to be developed using the LQG methods, the availability of all the states is essential. A Kalman filter is used to derive the necessary states for feedback and the effects of errors in this estimation are considered in the final analysis. Errors of state estimation depend not only on the measurement noise but also on sensor location.

Hać states that the time delay between the front and rear axles may be accounted for in the analysis but that this 'correlation can be neglected without changing the results considerably'.

The control law development cannot be undertaken on the author's full model since it has uncontrollable elements such as the guideway roughness shaping filter so the model is partitioned.

The controllers are evaluated by considering the variation of the components of the performance indexes with the vehicle stiffness, sensor error and weighting constants.

In conclusion when the stiffness corresponding to a first bending frequency is ten times

that of the rigid body bending frequency then the flexible modes can be neglected from the analysis. Secondly the effect of the active suspension on damping of the rigid body and first bending modes is significant but unquantified in the paper.

This paper does not present a persuasive argument for using active suspensions to suppress vehicle flexible modes. This is undoubtedly because the flexing of the chassis does not represent a serious threat to the vehicle stability.

2.2.3 Allen and Karnopp 1975 [Allen75]

This paper concentrates on the use of semi-active control to reduce the effects of flexible vehicle structural dynamics on the ride and performance quality of a conventional vehicle. The motivation for the work, which is directed at long vehicles such as railway vehicles and truck trailers, is that large structural modal velocities degrade ride quality and contribute to structural fatigue and failure.

The authors discuss the bond graph method of modelling a half car model. A free-free Bernoulli-Euler beam is used to model the elastic body. The purpose, as with the previously discussed papers, is to enhance the secondary stage of the suspension. Also semi-active control concepts are compared with both passive and fully active control strategies.

Linear full state feedback is used to develop the controllers with a 'non-linear field dependent element' used to control the semi-active elements.

The dynamics of the semi-active systems are particularly complex and require performance evaluation in the time domain. The paper provides results demonstrating the positive effects of the semi-active and fully active control schemes on the rigid body mode velocities and the bending mode velocities. Interestingly these results are presented

separately so that the reader can quantify the improvements to the velocity spectra of the bending modes.

The method of choosing the control law for the full active suspension is unclear. It is not an optimal suspension.

This thesis is primarily about single stage Maglev suspensions which are obviously fully active, so that the semi-active suspension strategy is not applicable . The results presented in this paper do show that the semi-active strategy for conventional vehicles should achieve results which are not quite as good as those for a fully active system. Given the fact that no energy is required for the semi-active strategy it offers savings on operating costs.

2.2.4 Capitani and Tibaldi (1988) [Capitani88] [Capitani89]

These papers closely follow the Hać paper [Hać 86]. A very similar model is developed of a half car model. A full model is presented incorporating the rigid body modes (pitch and heave) and the first 10 flexible bending modes. A reduced order model is derived by removing all of the flexible bending modes.

As with the Hać paper a shaping filter is used to provide a coloured noise excitation to the structure. No mention is made of the time delay between the front and rear axles.

Linear Quadratic Regulator (LQR) theory is applied to develop full order and reduced order controllers. The performance of these controllers is considered when they are applied to the full order model.

Again as in the Hać paper the various evaluated elements of the performance index are used to assess the controller performance. This paper goes beyond the Hać method and

evaluates all of the elements of the performance index to give a measure of the suspension characteristics.

How they do this is not completely clear but apparently the solution of the Riccati equation implies the performance index can be reconstructed and then partitioned into the components corresponding to the cost of the individual parameters.

Using this technique all the components of the performance index are evaluated for different levels of control effort. The reduced order and full order controllers are compared and when the reduced order results diverge from those of the full order then a performance limit (of the reduced order controller) has been reached.

The conclusion claims that ' the regulation cost is a suitable tool to establish whether the reduced order LQR gives satisfactory performance'. This statement is difficult to verify since no actual physical results such as acceleration levels are given. The main message of this paper is that reduced order controllers are satisfactory in the case where the controller bandwidth is kept low. This is quite a logical deduction as otherwise high order flexible modes are excited.

The authors state that they have applied Kalman filters to estimate the state variables. A full order Kalman filter does not change the performance much but a reduced order Kalman filter can in some cases increase the performance index, indicating a less than optimal performance. They emphasise however that the effect of errors due to a reduced order controller become more and more relevant with increasing control energy (also meaning an enlarged controller bandwidth).

2.2.5 Lieh(1991) [Lieh91a] [Lieh91b] [Lieh92]

In these papers, Lieh demonstrates the same semi-active suspension applied to a flexible

vehicle. The work is very similar to that of Allen and Karnopp [Allen75] but uses a more complex 8 degree of freedom model derived using the virtual work principle. It incorporates the non-linear elements of the semi-active dampers. Pitch, bounce and one fundamental flexible bending mode are used, the remaining degrees of freedom being accounted for by the semi-active damper models.

Of most interest in this paper is the comparison of the semi-active damper strategy with a fully active suspension derived using standard Linear Optimal Control theory. The two models are compared in the time domain passing over a road obstacle which excites the vehicle structure. The response of the generalised coordinate of the fundamental elastic mode is reduced by the active suspension but exaggerated by the semi-active dampers, as is the high frequency wheel hop. Other performance criteria of the vehicle are improved by both the semiactive damper and fully active suspension strategies.

No performance criteria are presented with respect to a stochastic input and thus it is difficult to quantify the effects of the proposed control strategies on stability and or ride quality. Lieh also investigates the use of dissipative dampers with nonlinearities rather than on-off dampers for the semi-active suspension approach [Lieh91b]. The effect of the semi-active saturation dampers on the flexible bending mode is not an improvement on the on-off dampers. Other aspects of performance such as the low frequency rigid body mode deflections, are improved by using the saturation dampers.

2.2.6 Patten et al (1990) [Patten90]

Similar to the Nagai and Sawada [Nagai87] paper, this work considers the effects of flexibility in a mid-range automobile. The assumed modes method is used to derive the flexible body equations and the first two bending modes are considered which the authors claim is adequate for this study and justify this with subsequent analysis which is not presented. Since an automobile structure is considered the fundamental bending mode has

a resonance at 21Hz, rather higher than in the previous papers which have been discussed.

An LQG controller is developed with the weighting factors for the Riccati equation being selected by trial and error. Ride isolation is deemed the objective for the controller and the square of the inertial displacement and velocity at the seat were selected for the performance index.

Time domain and frequency response results are presented. All show an unquantified improvement particularly at the low frequency region, that is frequencies below 2Hz. It is difficult to assess the specific effect on the flexible body modes of the active controller.

2.2.7 Gevarter (1970) [Gevarter70]

The author in this paper presents a general method of modelling a flexible vehicle. In this case vehicle refers to almost any structure but particularly of the aerospace variety. A 'cybernetic' model of one axis of a flexible vehicle employing a feedback control system with uncoupled control axes is described. The interaction between the rigid and flexible modes is presented clearly in diagrammatic form.

The main body of the paper deals with methods of determining the absolute stability of the flexible structure when employing a simple linear feedback control. The ideas in this section are somewhat outdated which is not surprising given the age of the paper.

2.2.8 Khulief and Sun (1987) [Khulief87]

The significance of this paper is that it demonstrates the use of a finite element model of the elastic vehicle rather than a continuous model using the assumed modes method. A planar vehicle system is presented where the flexible chassis is represented by a finite mesh of 10 beam elements of equal length. The argument for using a finite element model is

that it is more accurate compared with other methods presented in the papers above.

A semi-active suspension using controlled dampers is applied to the vehicle structure along the lines of the Allen and Karnopp paper [Allen75] and then a time domain analysis of the vehicle passing over a bump is analysed.

The most interesting result is that the semi-active control strategy does not have a detrimental effect on the elastic response of the chassis mid-point. This contradicts the previous applications of semi-active dampers to a flexible vehicle where the semi-active control strategy excited the flexible bending modes. No explanation is offered in the paper for this result.

2.2.9 British Railways Research [Goodall81]

This paper describe a programme of work to improve the performance of secondary suspensions for rail vehicles. Historically the project stems from the work on Maglev done by British Rail. The specific point of interest is that, when implementing control strategies for rail vehicles, it was found advantageous to ensure that the main body flexible mode was not excited. This was done by including a notch filter in the main loop compensation stage.

2.3 Control of Flexible Structures

The most prominent area of flexible structure control is that applied to space structures such as solar arrays and antenna. In zero gravity and vacuum conditions there is no inherent damping and residual accelerations caused by thruster corrections or mechanical subsystems can cause the whole structure to vibrate. This may mean that the performance of the space vehicle is reduced or that the experiments are not viable [Jones94]. A very prominent example has been the pointing jitter on the Hubble Space

Telescope(H.S.T) caused by the thermal flutter of the 10m long solar arrays when the satellite passed between sunlight and shadow [Wie92].

There is a great deal of literature on the subject and the problems have encouraged many new control techniques to be developed [Hotz87] [Bernstein85]. The models describing the space structure tend to be of very high order and the problem bending modes are usually of very low frequency (in the case of the H.S.T about 0.12Hz and 0.66Hz).

The most widely used control technique for the large space structure(L.S.S) problem is robust H_∞ control synthesis which has proven adaptable to very large structures [Goh93]. Other authors argue that the application of classical control techniques result in less complex controllers and are equally effective [Wie92]. Classical controllers applied to the L.S.S problem are designed one loop at a time and are generally time consuming to design. H_∞ control synthesis on the other hand allows the designer to make use of more automated control design software to produce a controller for the whole structure but the controller tends to be of an order equivalent to that of the model. For this reason model reduction techniques are under intensive investigation [Grübel83].

Another technique that has been applied to the L.S.S is direct output feedback using a reduced order model [Balas79]. Here the effects of not accounting for all the flexible bending modes, the so called spillover, must be considered in the control law design. The covariance control technique [Liu93] has been developed specifically to tackle the L.S.S problem and takes particular account of the positioning of the dynamic sensors and actuators [Norris89].

2.4 Conclusion on the work reviewed

The problem taken as the central theme of this thesis has not been fully addressed. Meisinger, the one author to have considered the problem of a single stage suspension

Maglev with a flexible chassis analysed the flexible guideway/ flexible vehicle interaction for a vehicle travelling at high speed. His work is a theoretical study with no practical implementation described or indeed results from a practical model.

The Birmingham Maglev suspension controller designed 'out' the problem but for reasons already explained this led to unacceptable cost trade offs. It is interesting to note in table 2.1 below that the Birmingham vehicle chassis is significantly different from all of the other vehicles considered, being short and with a high first bending frequency.

Vehicle Type /Proposer	Vehicle Length [m]	Typical 1st Mode Flexural Bending Frequency		Typical Range of Periodic Input Disturbance. [Hz]	Disturbance Rejection method used.
		Resonance [Hz]	Damping Factor		
Conventional North American passenger carriage (steel-on-steel)	26	16 to 24		0 to 3.4	Secondary Suspension
Transrapid Revenue Maglev (EMS) [Eitlhuber70]	27	5.8 to 6.2		0 to 4.63	Secondary Suspension
Birmingham Maglev (EMS)	6	40			Frequency Rejection Notch Filter
Proposed Canadian Maglev (EDS) [Hayes80]	34.8	4 to 5		0 to 5.4	Secondary Suspension only.
Generic High Speed Vehicle [Nagai87]	20	5.1	0.03		Active State Feedback + Secondary Suspension
Generic Truck Trailer [Hać86]	12	12.7	0.02		Active State Feedback + Secondary Suspension
Pop-Train [Goodall78]	21	15Hz	0.05		Active Secondary + Conventional Secondary

Table 2.1. Comparison of the vehicle parameters where a flexible chassis was considered

Chapter 3: Suspension and Guideway Fundamentals and Analysis

The fundamental role of a suspension is threefold;

1) to support the payload with respect to the track.
2) to follow the intended variations in the position of the track.
3) to provide isolation from the unintentional irregularities in the track position

It is important to note that points 1, 2 and 3 are in conflict, emphasising the compromise nature of a suspension.

This chapter describes what is necessary to ensure that a suspension can meet these requirements and includes a definition of the inputs, methods for analysis, the design goals and the design process itself.

3.1 Inputs to a suspension

There are three types of input to a suspension system: random changes in the track position (the track roughness), deterministic changes such as gradients and curves, and force inputs such as variations in the vehicle load.

3.1.1 Random Inputs

The random inputs represent the inaccuracies of laying track, the lack of straightness of the steel rail and the effects of fixtures and an accurate guideway model to describe the excitation of the suspension is essential to any analysis of performance. Many authors [Robson80] [Dodds73]have written on the subject yet there remain many possible areas of confusion. Appendix 1 deals with some of the definitions used in the following section.

Approximate Stochastic Model of a Guideway

From the results of many studies [Spangler66] [LaBarre70] the track elevation $z_t(x)$ may be considered to be a random process with a spatial spectral density of the form.

$$S_{z_t}(\Omega) = \frac{A_r}{\Omega^2} \quad [m^2/rad\ m^{-1}] \qquad 3.1$$

where A_r is a constant depending on the surface and Ω [rad m^{-1}] is the spatial frequency (an analogue of ω) [Bender67][Hullender72]. It is important to be clear how the above spectral density is derived and in particular which Fourier Transform Pair is used. In this case the definition is that followed by British Rail, which is generally favoured in transportation ride quality analysis. The Fourier Transform of $R_{zt}(\tau)$ and its inverse are defined here by

$$S_{z_t}(\omega) = \frac{1}{2\pi}\int_{-\infty}^{\infty} R_{z_t}(\tau) e^{i\omega\tau} d\tau \qquad 3.2$$

$$R_{z_t}(\tau) = E[\ z_t(t) z_t(t+\tau)\ ] = \int_{-\infty}^{\infty} S_{z_t}(\omega) e^{i\omega\tau} d\omega \qquad 3.3$$

$S_{zt}(\omega)$ is the spectral density of the $z_t(t)$ process and is a function of angular frequency. With a constant forward vehicle velocity of V, $z_t(x)$ may be converted to a function of time using x= Vt and $d\omega$=V $d\Omega$. Thus;

$$S_{z_t(t)}(\omega)\, d\omega = S_{z_t(x)}\left(\Omega = \frac{\omega}{V}\right) d\Omega \qquad 3.4$$

$$S_{z_t}(\omega) = \frac{A_r V}{\omega^2} \qquad 3.5$$

Future calculations are greatly facilitated by the use of an input velocity spectrum (an approximation due to Karnopp), for which the spectrum for dz_r/dt is then just $\omega^2 S_{zr}$ which is

$$S_{z_t}(\omega) = A_r V \qquad \textbf{3.6}$$

It is straightforward to write down the autocorrelation function now in terms of this flat velocity spectrum

$$R_{z_t}(\tau) = 2\pi A_r V \delta(\tau) \qquad \textbf{3.7}$$

When the spectrum is defined in terms of cycles s^{-1} rather than rad s^{-1}

$$R_{z_t}(\tau=0) = E[\, z_t^2 \,] = \int_{-\infty}^{\infty} S_{z_t}(\omega)\, d\omega \qquad \textbf{3.8}$$

$$R_{z_t}(\tau=0) = E[\, z_t^2 \,] = \int_{0}^{\infty} W_{z_t}(f) df \qquad \textbf{3.9}$$

where f is frequency in Hz and $W_{z_t}(f)$ is the equivalent one sided spectral density function. Hence

$$2.S_{z_t}(\omega) d\omega = W_{z_t}\left(f = \frac{\omega}{2\pi}\right)\frac{d\omega}{2\pi} \qquad \textbf{3.10}$$

So the single sided spectrum $W_{z_t}(f)$ is related to the double sided spectrum $S_{z_t}(\omega)$ by

$$W_{z_t}\left(f = \frac{\omega}{2\pi}\right) = 4\pi S_{z_t}(\omega) \qquad \textbf{3.11}$$

or by the equivalent

$$W_{z_t}(f) = 4\pi S_{z_t}(\omega = 2\pi f) \qquad \textbf{3.12}$$

Applying the above theory to the commonly used spectral density [Goodall84] expressed

in terms of cycles rather than radians.

$$W_{z_t}(f_t) = \frac{A_r}{f_t^2} \quad m^2/cycle \quad m^{-1} \qquad \textbf{3.13}$$

where f_t [cycle m^{-1}] is the spatial frequency. Converting to the velocity spectrum gives;

$$W_{\dot{z}_t} = (2\pi)^2 A_r V \qquad \textbf{3.14}$$

Using equation 3.12 above leads to the following result;

$$S_{\dot{z}_t} = (\pi) A_r V \qquad \textbf{3.15}$$

This result is widely used throughout the work presented in this thesis.

Representative Model (following Müller [Müller79] and Hać[Hać85])

This representation accounts for the fact that the guideway does not conform to a white noise and a so called shaping filter is used to give a roll-off at high frequencies.

$$S_\omega(\omega) = \frac{A_r V}{\omega^2 + (A_r V)^2} \frac{\omega^2}{\pi} \qquad \textbf{3.16}$$

$$S_\omega(\omega) = \frac{A_r V}{\omega^2 + (A_r V)^2} \frac{\omega^2}{\pi} = \frac{1}{2\pi}\int_{-\infty}^{\infty} R_w(\tau) e^{-i\omega\tau} d\tau \qquad \textbf{3.17}$$

Considering the magnitude of the process only, the autocorrelation function is:

$$R_w(\tau) = 2A_r V \delta(\tau) \qquad \textbf{3.18}$$

Hence the intensity of the process is

$$Q_w = 2A_r V \qquad 3.19$$

The guideway dynamics (i.e. the shaping filter) must be incorporated into the analysis in the same way as the plant dynamics.

Table 3.1 : Track Roughness Factors

Source	Secondary Quality Track [m]	Best Quality Track [m]	
British Rail	$1x10^{-6}$	$1x10^{-7}$	General
British Rail [BR Vampire Data]	$0.75x10^{-6}$	$0.24x10^{-6}$	Approx. East Coast Main Line

3.1.2 Deterministic Inputs

Deterministic features are most conveniently accounted for by considering the transition when changing from level track onto a gradient, because it is necessary when designing these transitions to limit the superimposed vertical acceleration. For severe gradients such as are often encountered on low speed transport systems it is also necessary to limit the jerk. For this thesis gradients of up to 10% are assumed with superimposed acceleration and jerk levels of $1ms^{-2}$ and $1ms^{-3}$ respectively. These values are broadly representative for low speed systems, but will usually be lower for high speed systems.

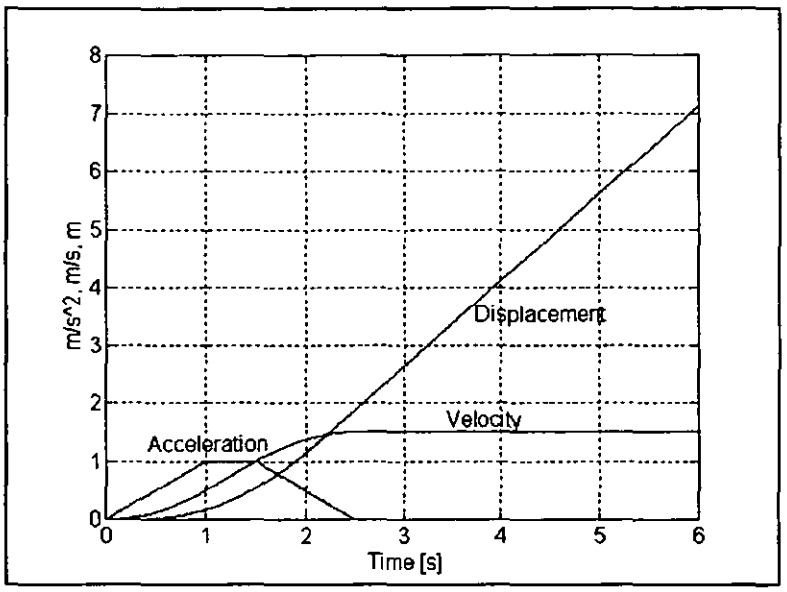

Figure 3.1 Definition of the input experienced by a vehicle travelling at $15ms^{-1}$ onto a 10% gradient.

The figure above shows the deterministic inputs used to assess the effects of a vehicle transition onto a gradient. In the definitions of the gradients a constant forward velocity of $15ms^{-1}$ for the Maglev vehicle has been assumed. For the case of a 10% gradient the above limiting parameters are reached, but in the case of a 5% gradient only the jerk limit applies (since the acceleration limit is not reached).

3.1.3 Force Inputs

Examples of the force inputs to which the suspension must react are the variation in payload and external disturbances such as braking loads and aerodynamic effects. For a small low speed vehicle the payload variation may be as much as 40% from fully laden to unladen. This is particularly significant for vehicles of lightweight construction. Another factor affecting smaller vehicles is that the load may change more rapidly as all the passengers can disembark much faster than for a larger vehicle.

3.2 Response of a Vehicle to Stochastic Inputs

The analysis of the performance of a suspension relies on the calculation of accurate values for the ride quality and track following properties in response to the effects of the guideway roughness.

The ride quality is generally represented by the root mean square (r.m.s) acceleration experienced by the passenger when the vehicle is excited by the roughness of the guideway, and the track following properties are quantified by the corresponding r.m.s relative displacement of the vehicle with respect to the track, i.e. the changes in the airgap.

Two methods of calculating the above values are used extensively in this thesis. One is the well known frequency response analysis approach and the other is the time based technique known as covariance analysis. Having developed reliable analysis techniques the performance of the vehicle suspension under design may be evaluated with respect to the relevant ISO standards (see later). Covariance analysis is a much more convenient analytical tool.

An acceleration frequency response plot of a vehicle travelling across a rough guideway reveals a great deal of information to the suspension designer such as the attenuation of the effects of the excitation process over a specific frequency range.

3.2.1 Frequency Response Techniques

The output power spectrum, $S_y(\omega)$ is equal to the square of the system transfer function multiplied by the input power spectrum, $S_x(\omega)$ [Thomson88];

$$S_y(\omega) = |H(\omega)|^2 S_x(\omega) \qquad \textbf{3.20}$$

For uncorrelated inputs for which the cross-spectral density terms are all zero, the total output power spectrum $S_{y\text{-}total}(\omega)$ may be generalised to;

$$S_{y\text{-}total}(\omega) = \sum_{r=1}^{N} |H(\omega)|^2 S_{x_r}(\omega) \qquad 3.21$$

Having determined the response spectral density the mean square response can be calculated directly from

$$E[y^2] = \int_{-\infty}^{\infty} |H(\omega)|^2 . S_{x_r}(\omega) d\omega \qquad 3.22$$

It is clear that the substitution of the previously defined flat velocity input spectrum for $S_x(\omega)$ yields a method of evaluating the r.m.s. outputs of the system. Again it should be noted which definition of the Fourier Transform is employed in the calculation. The definition by Karnopp and Newland has been followed here. An alternative definition of the Fourier Transform may also be applied at this point;

$$E[y^2] = \frac{1}{2.\pi} \int_{-\infty}^{\infty} |H(\omega)|^2 . S_{x_r}(\omega) d\omega \qquad 3.23$$

and may cause confusion with regard to the frequency integration, but provided the input spectrum autocorrelation function was defined using the same function this is not a problem.

If S_{x_r} is not a flat spectrum then the system response is a product of the plant response and the track spectral density function.

The frequency response of the models of the systems, $H(\omega)$, may be evaluated easily with respect to the above the track spectra to obtain values for r.m.s acceleration and r.m.s change in airgap [Goodall94].

$$\ddot{z}_{rms} = \sqrt{2 \int_0^{\infty} (\pi A_r V)[(j\omega)^2 H_z(j\omega)][(-j\omega)^2 H_z(-j\omega)] d\omega} \qquad 3.24$$

and

$$g_{rms} = \sqrt{2\int_0^{\infty}(\pi A_r V)[H_g(j\omega)][H_g(-j\omega)]d\omega} \qquad 3.25$$

The use of the above equations provides a simple method of obtaining quantifiable results giving a clear indication as to whether the suspension is providing the necessary ride quality and track following.

The main problem with the frequency response method is the need to complete a numerical integration. This can be computationally intensive for even a low-order model. For the best results a variable step integration technique should be used which adds to the complexity of the process.

Frequency Response Analysis with Time Delay

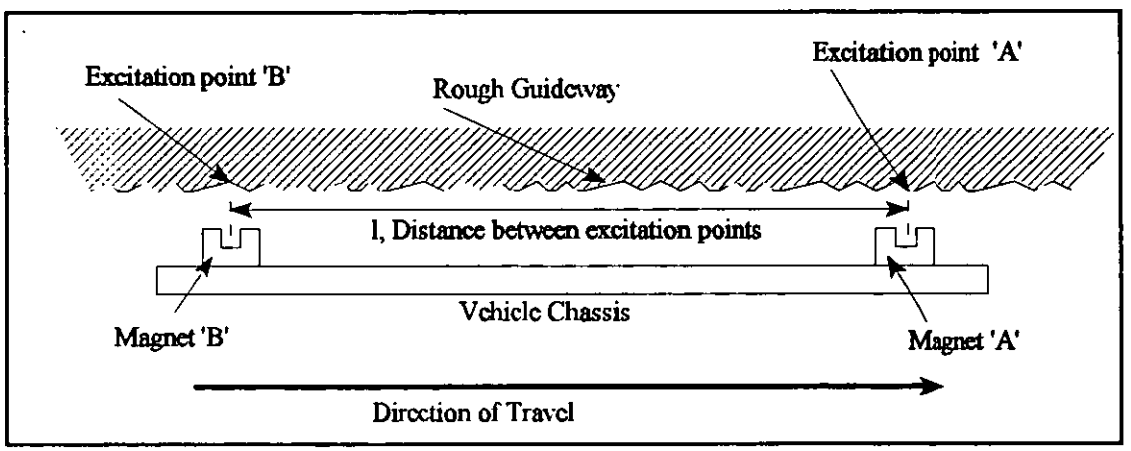

Figure 3.2 Multi-contact point Maglev vehicle

The stochastic excitation process of multi-contact point vehicles is characterised by time delays between front and rear contact points.

$$t_i = \frac{l_i}{V} \qquad i = 1,\ldots,r, \qquad 3.26$$

Where l_i is the distance between the front and rear guideway contact points and V represents the vehicle's speed

The total effect at a particular point in the system due to two (or more) inputs is the sum of the two responses. If the response at the centre position due to excitation point 'A' is $H_{centre\text{-}1}(\omega)$ and due to 'B' , $H_{centre\text{-}2}(\omega)$ then the total response is;

$$H_{centre\text{-}total}(\omega) = |H_{centre\text{-}1}(\omega)|e^{j\Phi_{centre\text{-}1}} + |H_{centre\text{-}2}(\omega)|e^{j(\Phi_{centre\text{-}2}-\frac{L}{V}\omega)} \qquad 3.27$$

in which the exponential terms allow for the relative time delay between the inputs. Adding the two complex response components yields a resultant term which is dealt with in exactly the same way as for the single input system.

3.2.2 Covariance Analysis - Analysis in the time domain

Covariance analysis relies on the Lyapunov matrix stability equation. The covariance analysis is documented in general terms in a number of standard texts [Bryson75] and described more specifically for the time invariant vehicle dynamics case in literature dating from the mid 1970's [Führer83] [Müller79] [Hedrick74] [Karnopp78] [Kortüm94].

Covariance analysis requires two stages: firstly the calculation of the state transition matrix for a stable dynamic system, and secondly the solution of the Lyapunov equation. The State-Transition matrix describes how the state x(t) of the system at some time t evolves into the state $x(\tau)$ at some other time τ. Using the linear system:

$$\dot{x} = Ax + Gw \qquad 3.28$$

where A is the system matrix, G the input matrix and w the disturbance input.

For time invariant systems , the state-transition matrix is the matrix exponential function [Friedland86]:-

$$\Phi(t-\tau) = e^{A(t-\tau)} \qquad 3.29$$

Calculation of the transition matrix is not a trivial problem [Moler78].

$$x(t) = \Phi(t-t_o)x_o + \int_{t_o}^{t}\Phi(t-\tau)Gwd\tau \qquad 3.30$$

Now define the Covariance matrix of the process x as;

$$P_x(t) = E([x(t)-\bar{x}(t)][x(t)-\bar{x}(t)]^T) \qquad 3.31$$

The mean value is given by

$$E[x(t)] = \bar{x}(t) \qquad 3.32$$

For most vehicle dynamics work the mean value is zero so 3.31 simplifies to:

$$P_x(t) = E\{\, x(t)\, x^T(t)\,\} \qquad 3.33$$

and considering the time invariant system;

$$\dot{P}_x = E\{\, \dot{x}\, x^T + x\, \dot{x}^T\,\} \qquad 3.34$$

$$\dot{P}_x = E\{\, Axx^T + xx^TA^T + Gwx^T + xw^TG^T\,\} \qquad 3.35$$

$$\dot{P}_x = AP_x + P_xA^T + G\int_{t_o}^{t}E\{w(t)w(\tau)^T\}G^T\Phi^T(t-\tau)d\tau + [G\int_{t_o}^{t}E\{w(t)\ w(\tau)^T\}G^T\Phi^T(t-\tau)d\tau]^T \qquad 3.36$$

where (as previously) the expected excitation (white noise) process, w, is described;

$$E[w(t)w(t+\tau)] = R_w(\tau) = Q_w\delta(\tau) \qquad 3.37$$

with

$$Q_w = 2\pi S_o \qquad 3.38$$

Reforming the integral components of equation 3.36 gives;

$$\dot{P}_x = AP_x + P_xA^T + G\int_{t_o}^{t} Q_w\delta(t-\tau)G^T\Phi^T(t-\tau)d\tau + [G\int_{t_o}^{t} Q_w\delta(t-\tau)G^T\Phi^T(t-\tau)d\tau]^T \quad 3.39$$

and

$$\dot{P}_x = AP_x + P_xA^T + \frac{1}{2}GQ_wG^T + \frac{1}{2}[GQ_wG^T]^T \quad 3.40$$

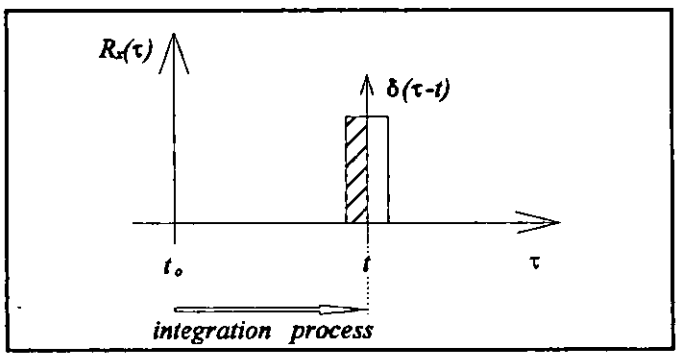

Figure 3.3 Integration of the dirac function.

The half value terms are the result of the fact that the dirac function lies at the end of the integration process as seen in this diagram. Only half of the dirac function lies within the integration range. Since Q_w represents white noise inputs and as there is no correlation between any white noise signals the following equation is obtained;

$$\dot{P}_x = AP_x + P_xA^T + GQ_wG^T \quad 3.41$$

It is normally sufficient to consider the stationary covariance solution which leads to the condition $\dot{P}_x = 0$ and the equation becomes;

$$AP_x + P_xA^T = -GQ_wG^T \quad 3.42$$

This last equation is known as the Lyapunov Equation, solutions for which are well documented [Kreisselmeier72]. The MATLAB® function **lyap(A,G,Q_w)** [Bartels72] used in this thesis has always given reliable results, even for the largest dynamic systems.

The existence of a solution depends upon the dynamic system being asymptotically stable.

Coloured Noise and Covariance Analysis

The above description is sufficient for some approximate solutions but in reality there are no white noise excitation processes of infinite bandwidth hence the need to develop a shaping filter for the so called coloured noise excitation process which modifies the white noise process to model an actual physical process.

Consider the following shaping process;

$$w_{(white\ noise)} \rightarrow H_f(s) \rightarrow \xi_{(coloured\ noise)} \qquad \textbf{3.43}$$

for an excitation model of the form;

$$H_f(s) = \frac{1}{s + A_r V} \qquad \textbf{3.44}$$

Considering the real part;

$$H_f(\omega) = \frac{A_r V}{\omega^2 + (A_r V)^2} \qquad \textbf{3.45}$$

which describes the shaping filter of equation 3.17 with its associated autocorrelation function. For the covariance analysis the filter is expressed in the state space form;

$$\dot{\xi} = -A_r V \xi + w \qquad \zeta = \xi \qquad \textbf{3.46}$$

where ξ is the coloured noise state, and ζ the filter output. Augmenting the plant with the shaping filter thus;

$$\begin{bmatrix} \dot{x} \\ \dot{\xi} \end{bmatrix} = \begin{bmatrix} A & G \\ 0 & A_r V \end{bmatrix} \begin{bmatrix} x \\ \xi \end{bmatrix} + \begin{bmatrix} 0 \\ 1 \end{bmatrix} [w] \qquad \textbf{3.47}$$

and defining the new state vector as x_a which incorporates the guideway and vehicle

dynamics;

$$P_{x_a}(t) = \begin{bmatrix} P_x(t) & P_{x\xi}(t) \\ P_{\xi x}(t) & P_\xi(t) \end{bmatrix} \qquad \textbf{3.48}$$

If the new system matrix is A_a and the shaping filter matrices are indicated with the subscript sf;

$$\dot{P}_{x_a} = A_a P_{x_a} + P_{x_a} A_a^T + \begin{bmatrix} 0 & 0 \\ 0 & Q_w \end{bmatrix} \qquad \textbf{3.49}$$

Shaping filter Lyapunov Equation

$$\dot{P}_\xi = A_{sf} P_\xi + P_\xi A_{sf}^T + G_{sf} Q_w G_{sf}^T \qquad \textbf{3.50}$$

Coupling Lyapunov Equation

$$\dot{P}_{x\xi} = A P_{x\xi} + P_{x\xi} A_f^T + G C_{sf} P_\xi \qquad \textbf{3.51}$$

Principal Lyapunov Equation

$$\dot{P}_x = A P_x + P_x A^T + G C_{sf} P_{x\xi}^T + P_{x\xi} C_{sf}^T G^T \qquad \textbf{3.52}$$

All three equations may be solved separately by the methods previously discussed.

Time Delayed Excitation Process

The stochastic excitation process $\zeta(t)$ of multi-contact-point vehicles is characterised by time delays between the contact points as described earlier.

The multiple excitation term $G\zeta$ may then be written:

$$G\zeta(t) = \sum_{i=1}^{r} g_i \zeta_i(t) \qquad \textbf{3.53}$$

First consider the case for a white noise velocity input which of course simplifies the

situation as no shaping filter is required hence $\zeta_f(t) = w_f(t)$. From equation 3.36:

$$\dot{P}_x = AP_x + P_xA^T + G\int_{t_o}^{t} E[w(t)w(\tau)^T]G^T\Phi^T(t-\tau)d\tau + [G\int_{t_o}^{t} E[w(t)w(\tau)^T]G^T\Phi^T(t-\tau)d\tau]^T \quad 3.54$$

$$E[\,w(t)w^T(\tau)\,] = E\left\{\begin{bmatrix} w(t)w(\tau) & w(t)w(\tau-t_2) \\ w(t)w(\tau-t_2) & w(t-t_2)w(\tau-t_2) \end{bmatrix}\right\} = q\begin{bmatrix} \delta(t-\tau) & \delta(t-\tau+t_2) \\ \delta(t-\tau-t_2) & \delta(t-\tau) \end{bmatrix} \quad 3.55$$

where q is the white noise intensity. Substitution of this expected input result leads to the following integrals

$$\begin{aligned} G\int_{t_o}^{t} E[w(t)w(\tau)^T]G^T\Phi^T(t-\tau)d\tau &= qG\int_0^t \begin{bmatrix} \delta(t-\tau) & 0 \\ 0 & \delta(t-\tau) \end{bmatrix} G^T e^{A^T(t-\tau)}d\tau \\ &+ qG\int_0^t \begin{bmatrix} 0 & 0 \\ \delta(t-\tau-t_2) & 0 \end{bmatrix} G^T e^{A^T(t-\tau)}d\tau \\ &+ qG\int_0^t \begin{bmatrix} 0 & \delta(t-\tau+t_2) \\ 0 & 0 \end{bmatrix} G^T e^{A^T(t-\tau)}d\tau \end{aligned} \quad 3.56$$

The first integral is the same as that for the non-delayed covariance input matrix. The second term only gives a result for time τ' with the condition $t > \tau' = t - t_2 > 0$ [Kortüm94]. The third term is zero for all values of $\tau>0$.

Thus the integral terms result in the following

$$G\int_{t_o}^{t} E[w(t)w(\tau)^T]G^T\Phi^T(t-\tau)d\tau = \frac{1}{2}qGG^T + qG\begin{bmatrix} 0 & 0 \\ 1 & 0 \end{bmatrix} G^T e^{A^T t_2} + 0 \quad 3.57$$

Calculating the transpose of the above integral and integrating and then substituting back into the above Lyapunov Equation.

$$\dot{P}_x = AP_x + P_xA^T + q\left(GG^T + e^{At_2}G\begin{bmatrix}0 & 1\\ 0 & 0\end{bmatrix}G^T + G\begin{bmatrix}0 & 0\\ 1 & 0\end{bmatrix}G^Te^{A^Tt_2}\right) \qquad \textbf{3.58}$$

Considering the stationary process as in the previous cases

$$AP_x + P_xA^T = -q\left(GG^T + e^{At_2}G\begin{bmatrix}0 & 1\\ 0 & 0\end{bmatrix}G^T + G\begin{bmatrix}0 & 0\\ 1 & 0\end{bmatrix}G^Te^{A^Tt_2}\right) \qquad \textbf{3.59}$$

It should be clear that in this case that

$$Q_w = q\left(GG^T + e^{At_2}G\begin{bmatrix}0 & 1\\ 0 & 0\end{bmatrix}G^T + G\begin{bmatrix}0 & 0\\ 1 & 0\end{bmatrix}G^Te^{A^Tt_2}\right) \qquad \textbf{3.60}$$

This may be written in the convenient form [Müller79];

$$AP_x + P_xA^T = -q\left(g_1g_1^T + g_2g_2^T + e^{At_2}g_1g_2^T + g_2g_1^Te^{A^Tt_2}\right) \qquad \textbf{3.61}$$

Where $G = [\, g_1 \; g_2 \,]$ for a two input system.

The above technique is implemented in MATLAB programs developed for this project. Examples are given in appendix 2.

An important point to note is the sometime semi-definite nature of the covariance input description and concerning this Bryson and Ho [Bryson75] (P458-459) in their theorem B7 state:

A linear stationary system dx/dt=Ax has uniform asymptotic global stability if and only if for any positive-definite matrix Q, there exists a positive definite matrix P, which is the unique solution of the linear algebraic equation

$$-Q = A^TP + PA$$

Due to the numerical difficulties in calculating the transition matrix it is often the case that the P matrix has small negative eigenvalues. Strictly speaking it is a negative semi-definite

matrix but it is suggested here that the matrix can be taken as positive semi-definite so long as the negative eigenvalues are small compared with the positive eigenvalues.

The covariance analysis applying the above time shift was checked against the frequency response analysis to ensure that the above numerical inconsistencies are not a problem. The use of the covariance analysis technique in this thesis has shown it to be computationally efficient and at least as accurate as the frequency response analysis. The above proviso from Bryson and Ho has not been found to be significant for the systems analysed which were 28th order models.

Table 3.2 Comparison of the analysis techniques

Time Based Methods Covariance Analysis	Frequency Response Analysis
$E[w(t)w(t+\tau)] = R_w(\tau) = Q_w\delta(\tau)$	$S_y(\omega) = \lvert H(\omega)\rvert^2 S_x(\omega)$
$Q_w = 2\pi S_o$	
$S_o = \pi A_r^2 V$	$S_x(\omega) = S_o = \pi A_r^2 V$
$P_x(t) = E\{ x(t)\, x^T(t) \}$	
$\dot{P}_x = AP_x + P_xA^T + GQ_wG^T$	
$AP_x + P_xA^T = -G\, Q_w\, G^T$	
$E[y^2] = C^T P_x C$	$E[y^2] = \int_{-\infty}^{\infty} \lvert H(\omega)\rvert^2 S_{x_r}(\omega) d\omega$

3.3 Design Goals

ISO Standard 2631 defines ride quality requirements for transport systems and these are quantified in terms of the r.m.s. acceleration experienced by the passengers, usually with a frequency weighting to account for human susceptibility, although this weighting is neglected here. For low speed systems with relatively short journeys the acceptable level of r.m.s. vertical acceleration is usually taken as 4.5% 'g' [Goodall84].

For a Maglev vehicle in which the airgap size is around 15mm (such as the Birmingham Maglev), the r.m.s. variations in airgap should be restricted to 4 or 5mm. Achieving the best trade-off between acceleration and airgap changes due to random inputs, and at the same time ensuring a satisfactory response to the deterministic inputs, is the main problem for the suspension design. The airgap changes which occur at deterministic features must be restricted, and a practical limit is 7.5mm or half the airgap such that there is clearance to accommodate random changes in the airgap even whilst negotiating such features. The specification used to describe the deterministic gradient feature was given in terms of superimposed acceleration and jerk levels of $1ms^{-2}$ and $1ms^{-3}$ Other values are possible but these provide a starting point for the specification [Goodall94].

3.4 Overview of suspension design

Each of the suspension inputs may be considered in turn and their effects minimised and a compromise between conflicting requirements evolved. The following section addresses the optimal suspension and is applicable to both conventional and Maglev suspensions.

3.4.1 Response to random track inputs

Suspensions may be regarded as low pass filters with only low frequency track variations passed onto the vehicle. For the magnetic suspension system the transfer function may

be electronically defined allowing greater control than is possible with passive suspensions where the transfer function is defined by the characteristics of the spring/mass/dampers. A passive suspension has a natural frequency of between 1 and 1.5Hz in order to achieve the necessary ride quality and track following.

The work of a number of authors has shown the optimal suspension to take the form of a 'butterworth filter' transfer function [Bender67] [Hullender72]. These are used to derive expressions for r.m.s acceleration and suspension deflection for the power spectrum inputs described earlier.

The basic transfer function relating the vertical position of the mass of the vehicle z to that of the track is;

$$\frac{z(s)}{z_t(s)} = H_{second}(s) = \frac{1}{1 + \frac{\sqrt{2}}{\omega_o}s + \frac{1}{\omega_o^2}s^2} \qquad \textbf{3.62}$$

In terms of the vertical acceleration of the vehicle in response to a velocity input, we have:

$$\frac{\ddot{z}(s)}{\dot{z}_t(s)} = sH_{second}(s) = \frac{s}{1 + \frac{\sqrt{2}}{\omega_o}s + \frac{1}{\omega_o^2}s^2} \qquad \textbf{3.63}$$

Consideration of a third order filter similarly gives;

$$\frac{z(s)}{z_t(s)} = H_{third}(s) = \frac{1 + \frac{2}{\omega_o}s}{1 + \frac{2}{\omega_o}s + \frac{2}{\omega_o^2}s^2 + \frac{1}{\omega_o^3}s^3} \qquad \textbf{3.64}$$

and for the vertical acceleration;

$$\frac{\ddot{z}(s)}{\dot{z}_t(s)} = sH_{third}(s) = \frac{s + \frac{2}{\omega_o}s^2}{1 + \frac{2}{\omega_o}s + \frac{2}{\omega_o^2}s^2 + \frac{1}{\omega_o^3}s^3} \quad \textbf{3.65}$$

The transfer function for the airgap with respect to z_t is also used in the dynamic analysis. Since airgap is defined as;

$$g = z_t - z \quad \textbf{3.66}$$

$$\frac{g(s)}{z_t(s)} = 1 - H_{second} \quad \textbf{3.67}$$

$$\frac{g(s)}{z_t(s)} = 1 - H_{second}(s) = \frac{\frac{\sqrt{2}}{\omega_o}s + \frac{1}{\omega_o^2}s^2}{1 + \frac{\sqrt{2}}{\omega_o}s + \frac{1}{\omega_o^2}s^2} \quad \textbf{3.68}$$

$$\frac{g(s)}{\dot{z}_t(s)} = \frac{\frac{\sqrt{2}}{\omega_o} + \frac{1}{\omega_o^2}s}{1 + \frac{\sqrt{2}}{\omega_o}s + \frac{1}{\omega_o^2}s^2} \quad \textbf{3.69}$$

Similarly for the third order filter;

$$\frac{g(s)}{\dot{z}_t(s)} = \frac{\frac{2}{\omega_o^2}s + \frac{1}{\omega_o^3}s^2}{1 + \frac{2}{\omega_o}s + \frac{2}{\omega_o^2}s^2 + \frac{1}{\omega_o^3}s^3} \quad \textbf{3.70}$$

Evaluation of the above responses with respect to the flat velocity spectrum is then as follows using the frequency response technique outlined in section 3.2.1:

$$\frac{\ddot{z}(s)}{\dot{z}_r(s)} = sH_{second}(s) = \frac{s}{1 + \frac{\sqrt{2}}{\omega_o}s + \frac{1}{\omega_o^2}s^2} \qquad 3.71$$

$$\left|\frac{\ddot{z}(j\omega)}{\dot{z}_r(j\omega)}\right|^2 = \frac{\omega^2}{1 + \frac{\omega^4}{\omega_o^4}} \qquad 3.72$$

From equation 3.24 the following integral is used;

$$\ddot{z}_{rms}^2 = 2\int_0^{\infty}(\pi A_r V)\,[(H_z(jw)][(H_z(-j\omega)]\,d\omega \qquad 3.73$$

$$\ddot{z}_{rms}^2 = 2\int_0^{\infty}(\pi A_r V)\frac{\omega^2}{1 + \frac{\omega^4}{\omega_o^4}}\,d\omega \qquad 3.74$$

This integral may be evaluated exactly using standard tables.

$$\ddot{z}^2 = \frac{(\pi A_r V)\omega_o^3\pi}{\sqrt{2}} \qquad 3.75$$

Similarly for the airgap

$$g_{rms}^2 = \frac{(\pi A_r V)\,3\,\pi}{\omega_o\sqrt{2}} \qquad 3.76$$

Table 3.3: Typical Values for the Optimal Suspension

Using a forward vehicle velocity V=15ms^{-1} and a secondary quality track with a guideway roughness factor of 1e^{-6}m.

Filter Type	Second Order $\omega_o=2\pi 2$	Third Order $\omega_o=2\pi 1.2$
r.m.s acceleration [ms^{-2}]	0.455	0.4363
r.m.s airgap [mm]	5	6.3

The optimal suspension presented here allows evaluation of the Maglev suspensions developed in this thesis against these optimal benchmarks.

It should be noted that for speeds higher than 50 to 60ms^{-1} which are required for longer journeys the rms acceleration needs to be significantly reduced and the airgap constraint means that this can only be achieved with improved quality track or the introduction of a secondary suspension.

3.4.2 Response to deterministic inputs

The airgap varies to provide isolation from the short wavelength variations of the guideway.

Deterministic features of the track are effectively low frequency inputs and so the steady state suspension deflection must be considered.

From the airgap transfer functions it is possible to calculate the steady state response to gradients, hence from equation 3.69:

$$\frac{g(s)}{\dot{z}_t(s)} = \frac{\frac{\sqrt{2}}{\omega_o} + \frac{1}{\omega_o^2}s}{1 + \frac{\sqrt{2}}{\omega_o}s + \frac{1}{\omega_o^2}s^2} \qquad \textbf{3.77}$$

for the steady state case gives

$$g \approx \frac{\sqrt{2}}{\omega_o}\dot{z}_t \qquad \textbf{3.78}$$

For the third order filter the result is:

$$g_{zz} \approx \frac{2}{\omega_o^2}\ddot{z}_t \qquad 3.79$$

Vertical velocity is not perceived by passengers but is a factor in the determination of the airgap deflection. For a maximum gradient of 10% at a speed of 15ms^{-1} the vertical velocities are 1.5ms^{-1} as shown in section 3.2.2. The maximum vertical acceleration and jerks were introduced in section 3.4.

Table 3.4: Deterministic response of the optimal suspension

Maximum Velocity (ms^{-1})	Maximum Acceleration (ms^{-2})	Maximum Jerk (ms^{-3})	Filter Type/ Frequency	Deflection (mm)
1.5	1.0	1.0	2nd Order 2Hz	175.1
			3rd Order 1.2Hz	37.5

The corresponding deflections are large even for a third order filter suspension characteristic and show the significance of the deterministic response as well as the response to random inputs. This problem is addressed in more detail later in the thesis but it is important to remember that the airgap is only 15±7.5mm showing a deflection of 37.5mm to be unacceptable. The poor performance of the second order filter with respect to the deterministic input is a result of the absolute velocity term, usually referred to as 'skyhook damping'. It is well recognised for its superior performance with random inputs but as shown it creates problems on gradients.

3.4.2 Response to force inputs

With magnetic suspensions it is essential that the static deflection due to load changes does not result in deflections of the same magnitude as in passive suspension systems which for a 1Hz suspension will be of the order of 250mm. Active control allows the suspension to react to forces which are not linked to the suspension (spring/mass)

frequency. Given the small airgap (15mm) it is necessary to limit the maximum deflection due to load changes to ±1mm.

3.4.3 Lateral Suspension Requirements

For lateral suspension it is necessary to avoid transmitting high frequency lateral track movements to the body of the vehicle. Given an optimal vertical suspension producing satisfactory performance the same techniques may be applied equally to achieve the lateral suspension requirements. For this reason the work described in this thesis does not address the lateral suspension requirements. The rig and simulation models described later are considered as half car structures with no lateral components.

3.5 Conclusions

This chapter has introduced many ideas applicable to both Maglev and conventional suspensions. The nature of the guideway is shown to be of paramount importance to the design of a suspension system. A suspension must perform conflicting roles with respect to the stochastic and deterministic effects of the guideway.

The frequency response and covariance analysis methods for the guideway and suspension interaction have been presented. Without accurate analysis the performance of the suspension cannot be assessed.

The design requirements of a suspension are given and then related to the theoretical optimal suspension in which conflicting requirements are shown to exist between the stochastic and deterministic inputs.

Chapter 4: Modelling

4.1 Introduction

In this chapter mathematical models of increasing complexity are developed which encapsulate the dynamics of magnetic suspension systems. A feature of the modelling process is the combination of both electrical and mechanical components in one model.

4.2 Single Degree of Freedom Model (Quarter Car Model)

A controlled electromagnet with a ferromagnetic core is suspended beneath a ferromagnetic rail as shown in figure 4.1 below. Such a configuration represents one degree of freedom of motion and may be thought of as one corner of a vehicle or a quarter car model. The airgap needs to be of the order of 15mm to accommodate the track roughness and by electrical machines standards is therefore large. It is assumed that the reluctance of the airgap will dominate the magnetic circuit. The operating flux density in the airgap will be between 0.7 and 1 T, an upper limit dictated by saturation in the ferro magnetic parts of the magnetic circuit. In the diagram, motion vertically upwards is taken as positive.

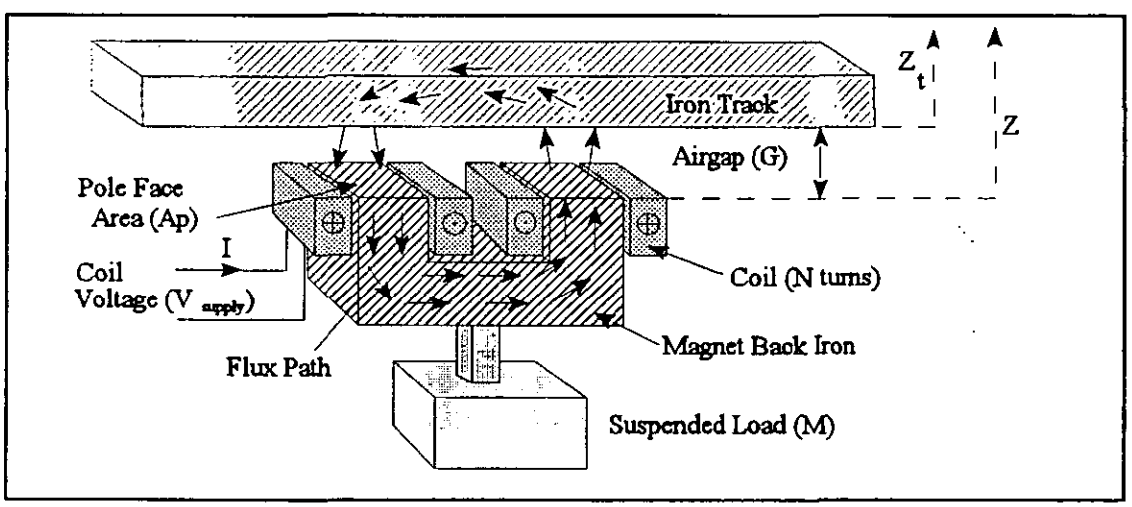

Figure 4.1 Cut-away view of an electromagnet suspended beneath an iron track.

Four important variables in an electromagnet are force F, flux density B, air gap G, the coil current I and the coil voltage V_{coil} and their relationships are considered below.

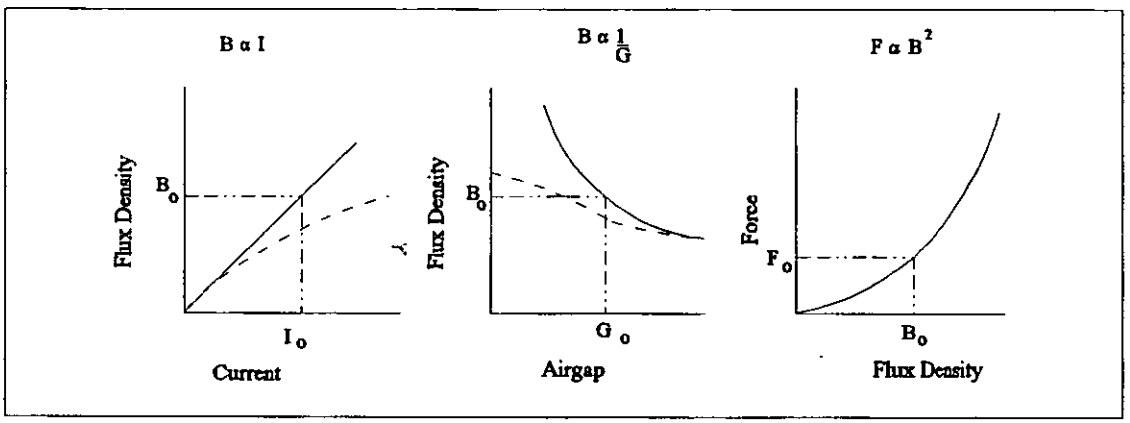

Figure 4.2 Relationship between the key variables describing the magnet. Broken curves represent the actual and the complete lines the theoretical relationships.

These relationships show the system is nonlinear but the nonlinearities are considered 'soft' because:

1. There are no hard nonlinearities present such as discontinuities .
2. The perturbations are not large within the airgap operating space.

The assessment of the 'softness' of the nonlinearities is subjective, but the experience of most magnetic suspension designers is that the system is soft enough to linearise and this allows the successful application of linear analysis and design techniques [Gottzein80] [Jayawant81].

Nonlinear models have been used to develop magnetic vehicle suspension controllers [Cho93,Yao93] but practical systems have as yet not been implemented.

The following definitions are used, in which lower case letters represent a small variation from the nominal operating point, and a subscript 'o' the nominal operating point.

$$B = B_o + b \qquad \textbf{4.1}$$

$$F = F_o + f \tag{4.2}$$

$$I = I_o + i \tag{4.3}$$

$$G = G_o + g \tag{4.4}$$

$$V_{coil} = V_o + v \tag{4.5}$$

The magnetic circuit is described by

$$NI = \int_{L0}^{L2G} H \, dl \tag{4.6}$$

Where the magnetic field strength, H and the airgap flux density, B are related by $B = \mu_o H$. The flux density is then given by $B = \frac{NI\mu_o}{2G}$ if the reluctance of the flux is assumed to be entirely within the two airgaps of each magnet i.e. neglecting the reluctance of the iron. For a constant air gap the flux density is proportional to the magnet current and at constant current it is inversely proportional to the air gap.

Using the exact differentials from the above fundamental relationships yields

$$b = \frac{\partial B}{\partial I} i + \frac{\partial B}{\partial G} g \tag{4.7}$$

which can be shown to give:

$$b = \frac{B_o}{I_o} i - \frac{B_o}{G_o} g \tag{4.8}$$

The attractive force of the magnet towards the track is defined as

$$F = \frac{B^2 A_{pt}}{2\mu_o} \tag{4.9}$$

A_{pt} is the total poleface area, for the electromagnet shown in the figure 4.1 the sum of the two poleface areas, A_p. In terms of the small variations about the nominal point

$$f = \frac{\partial F}{\partial B} b \qquad \textbf{4.10}$$

and because force is proportional to the square of the flux density;

$$f = \frac{2 F_o}{B_o} b \qquad \textbf{4.11}$$

Defining gradients of the relationships in the following manner [Goodall85],

$$K_i = \frac{B_o}{I_o}, \qquad K_g = \frac{B_o}{G_o}, \qquad K_b = 2\frac{Mg_{gravity}}{B_o} = 2\frac{F_o}{B_o} \qquad \textbf{4.12}$$

therefore rewriting the above equations with these constants:

$$b = K_i i - K_g g \qquad \textbf{4.13}$$

$$f = K_b b \qquad \textbf{4.14}$$

Considering Faraday's Law for the induced voltage across the coil

$$v_{coil} = -NA_p \frac{db}{dt} \qquad \textbf{4.15}$$

Here modelling the inductive effect rather than using a pure electrical inductance, means that changes in the airgap affect the magnet voltage. This is significant because for the low levels of acceleration in a suspension system the magnet controller needs to maintain a more or less constant flux density within the airgap. The principles of electromagnetic induction work toward this goal by opposing any change in the flux density. This results in less control effort being required. Now considering the total voltage across the resistive and inductive components which in terms of small variations about the nominal operating

point becomes:

$$v = R\,i + N\,A_p\left(\frac{db}{dt}\right) \qquad \textbf{4.16}$$

Applying Newton's Second Law of Motion the acceleration of the suspended mass is given by

$$F = M\frac{d^2z}{dt^2} - Mg_{gravity} \qquad \textbf{4.17}$$

4.2.1 Block Diagram Description

A block diagram is often used in the control world to help understand the dynamics of the system. Construction of a block diagram using the linearised equations in the Laplace domain is represented by the following equations:

$$v(s) = Ri(s) + s\,b(s)NA_p \qquad \textbf{4.18}$$

and

$$sb(s) = \frac{v(s)-i(s)R}{NA_p} \qquad \textbf{4.19}$$

Then consider the relationships between the flux and current, force and airgap.

$$b(s) = K_i\,i(s) - K_g\,g(s) \qquad \textbf{4.20}$$

$$f(s) = K_b\,b(s) \qquad \textbf{4.21}$$

Defining the airgap as the difference between the absolute coordinate of the track and the absolute coordinate of the magnet.

$$g = z_t - z \qquad \textbf{4.22}$$

The above equations lead directly to the block diagrams shown below.

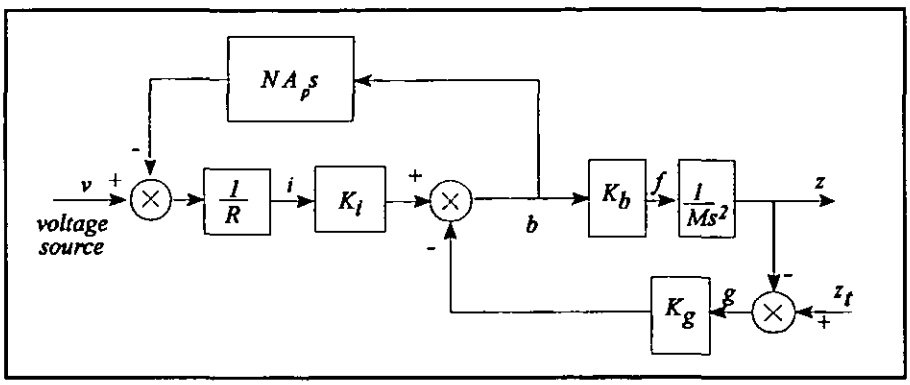

Figure 4.2 Linearised electromagnet model

The instability can be appreciated by considering the dependence of the reluctance upon the airgap which gives a negative stiffness. This means that any variation from the operating point creates a force which further increases the deviation from the equilibrium point.

Considering the simplified transfer function ignoring the flux feedback loop:

$$\frac{z(s)}{z_t(s)} = \frac{-K_g K_b \frac{1}{Ms^2}}{1 - K_g K_b \frac{1}{Ms^2}} \qquad \textbf{4.23}$$

and evaluating the characteristic equation and expressing the above constants in terms of their basic definitions gives:

$$\frac{B_o}{G_o} \frac{2Mg_{gravity}}{B_o} \frac{1}{Ms^2} = 1 \qquad \textbf{4.24}$$

and evaluating this leads to

$$\frac{2g_{gravity}}{G_o s^2} = 1 \qquad \textbf{4.25}$$

hence substituting for the Laplace term with the complex frequency ($j\omega$) gives:

$$\omega_n = \sqrt{\frac{2g_{gravity}}{G_o}} \qquad \textbf{4.26}$$

This indicates the system has a positive real pole (in addition to a negative pole) which means that an impulse to the system would result in a positive exponential term. The above equation shows the unstable pole lies at $(2g_{gravity}/G_o)^{1/2}$ rad s^{-1}. Clearly this is dependent only on the nominal airgap which for a typical Maglev system is 15mm giving a frequency of about 6Hz. This gives an indication of the bandwidth of a control loop required to stabilise the system.

The use of the $NA_p s$ term motivated the development of a rearranged model more suited to analytical modelling. This model has the advantage of being physically precise although the unstable nature of the system is less transparent.

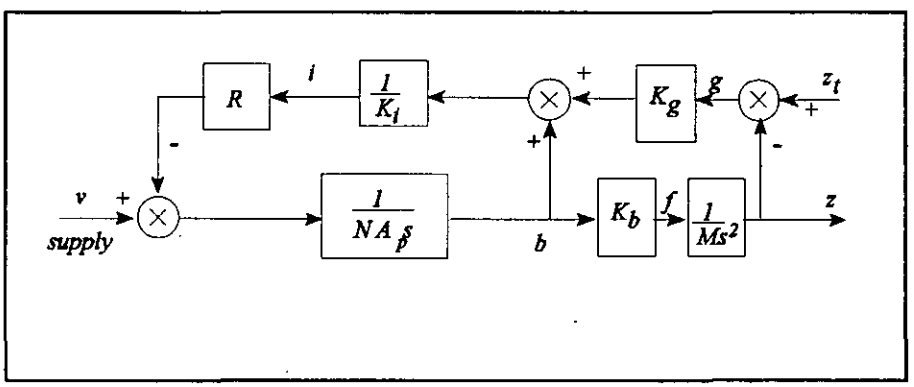

Figure 4.3 Modified linearised electromagnet model

What figure 4.3 does show more clearly is the significance of the correctly modelled inductive effect which inhibits changes in the flux density.

4.2.2 State Space expression of the Linear Model

The model may also be expressed in terms of first order differential equations, the so-

called state space form.

From Newton's 2nd Law

$$M\ddot{z} = f(t) \qquad \textbf{4.27}$$

substituting for the force using equation 4.14

$$M\ddot{z} = K_b\, b \qquad \textbf{4.28}$$

and for the flux density using equation 4.13

$$M\ddot{z} = K_b K_i i - K_g K_b g \qquad \textbf{4.29}$$

Differentiating equation 4.22 to give the equation in terms of velocities

$$\dot{g} = \dot{z}_t - \dot{z} \qquad \textbf{4.30}$$

Differentiating the motion equation

$$M\dddot{z} = K_b K_i \dot{i} - K_g K_b\, \dot{g} \qquad \textbf{4.31}$$

and rearranging in terms of the differential of current

$$\dot{i} = \frac{M\dddot{z}}{K_i K_b} + \frac{K_g}{K_i}\dot{g} \qquad \textbf{4.32}$$

Substituting in equation 4.16 describing the voltage drop across the resistive and inductive components:

$$v = Ri + NA_p(K_i \dot{i} - K_g\, \dot{g}) \qquad \textbf{4.33}$$

$$v = R\left(\frac{M\ddot{z}}{K_i K_b} + \frac{K_g}{K_i} g\right) + NA_p K_i \left(\frac{M\dddot{z}}{K_i K_b}\right) - NA_p K_g \dot{g} \qquad \textbf{4.34}$$

which rearranged in terms of jerk gives

$$\ddot{z} = -\frac{R}{NA_pK_i}\dot{z} - \frac{RK_gK_b}{NA_pMK_i}g + \frac{K_b}{NA_pM}v \qquad 4.35$$

The reason for differentiating to give an equation in terms of jerk becomes apparent when it is seen that equation contains a state for acceleration. The states of acceleration and airgap are explicitly used and the input is a flat velocity spectrum represented by white noise. This combination of states provides a very convenient model which is expressed in the following matrix form.

$$\begin{bmatrix} \dddot{z} \\ \ddot{z} \\ \dot{z} \\ \dot{g} \end{bmatrix} = \begin{bmatrix} -\frac{R}{NA_pK_i} & 0 & -\frac{K_gK_bR}{NA_pMK_i} \\ 1 & 0 & 0 \\ 0 & -1 & 0 \end{bmatrix} \begin{bmatrix} \ddot{z} \\ \dot{z} \\ g \end{bmatrix} + \begin{bmatrix} \frac{K_b}{NA_pM} \\ 0 \\ 0 \end{bmatrix} [v] + \begin{bmatrix} 0 \\ 0 \\ 1 \end{bmatrix} [\dot{z}_t] \qquad 4.36$$

The output equation may obviously be configured to whatever combination of state variables is required or is of interest. Here acceleration, airgap, current and flux density are given.

$$\begin{bmatrix} \ddot{z} \\ g \\ i \\ b \end{bmatrix} = \begin{bmatrix} 1 & 0 & 0 \\ 0 & 0 & 1 \\ \frac{M}{K_iK_b} & 0 & \frac{K_g}{K_i} \\ \frac{M}{K_b} & 0 & 0 \end{bmatrix} \begin{bmatrix} \ddot{z} \\ \dot{z} \\ g \end{bmatrix} \qquad 4.37$$

The choice of state variables has been found to be highly significant to the control strategies which can be developed to stabilise the system with the required performance. This choice allows the emphasis of the control strategy to be modified by the control system designer. The eigenvalues of the system will of course remain the same no matter which states are chosen to describe the system. The table below lists the possible states that can be used to describe the single degree of freedom Maglev model, more details of

which are described elsewhere [Paddison94] (see appendix 3).

Table 4.1: State Variable Choice

Model	1	2	3	4	5	6
State 1	$\ddot{z}$	$\ddot{z}$	$\ddot{z}$	$\ddot{z}$	$\ddot{z}$	$\dot{z}$
State 2	$\dot{z}$	$\dot{z}$	$\dot{g}$	z	g	g
State 3	z	g	g	$\dot{g}$	$\int g dt$	$\int g dt$
Input1	z_t	$\dot{z}_t$	$\ddot{z}_t$	z_t	$\dot{z}_t$	$\dot{z}_t$
Input2	v	v	v	$\dot{z}_t$	v	$\int v dt$
Input3				$\ddot{z}_t$	$\int v dt$	
Input4				v		

The above set of equations form the basis of the standard state space system;

$$\dot{x} = Ax + Bu + G\omega \qquad y = Cx + Du \qquad \textbf{4.38}$$

where A is the system matrix in equation 4.36. B is the control input matrix and G the disturbance input matrix. Only matrix C is present in the output equation 4.37, the feed through matrix D being zero.

4.3 Two Degree of Freedom (Half Car) Model

The following half car model is completely described by two degrees of freedom which are identified as the pitch and bounce modes. Two electromagnets are arranged towards the ends of a rigid I beam as shown in the figure below. The I beam structure allows the effects of beam flexibility to be investigated as its 2nd moment of area can be altered

without significantly changing the mass per unit length, but in this section the beam is perfectly rigid. The so called half-car model is becoming quite common in literature on vehicle dynamics as it allows a much fuller description of the fundamental dynamics than the quarter car model.

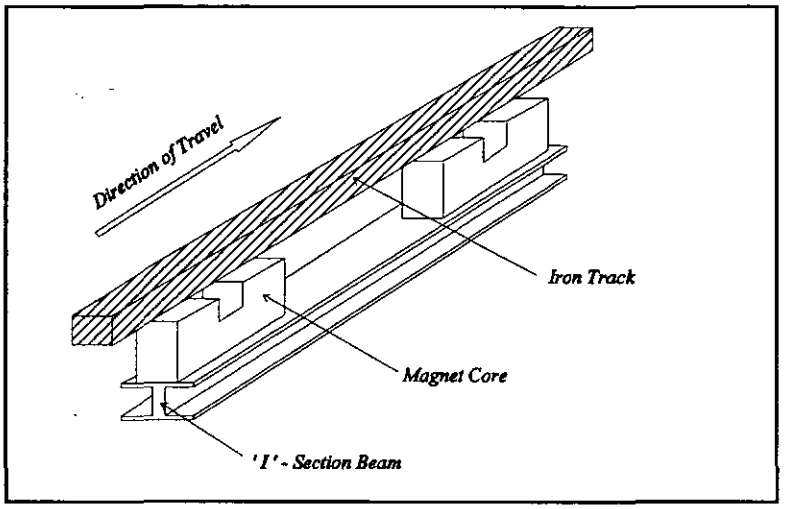

Figure 4.4 Two degree of freedom Maglev model

The diagram below defines the key parameters required to describe the half-car model.

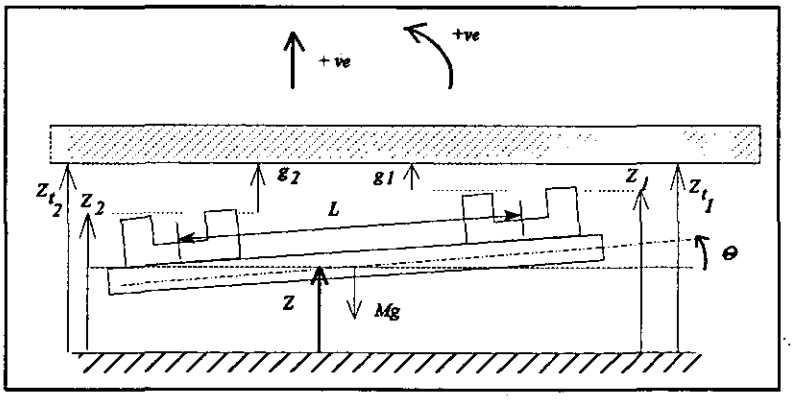

Figure 4.5 Parameters describing the half-car model

Note L is considered to be the distance between the electromagnet centres.

Starting with the fundamental motion equations and applying Newton's Second Law to

the vertical bounce motion

$$M\ddot{z} = f_1 + f_2 \qquad \textbf{4.39}$$

and for the rotational pitch motion

$$I_x \ddot{\theta} = \frac{L}{2}(f_1 - f_2) \qquad \textbf{4.40}$$

substituting for f_1 and f_2 using equations 4.13 and 4.14

$$M\ddot{z} = K_b [K_i i_1 - K_g g_1] + K_b [K_i i_2 - K_g g_2] \qquad \textbf{4.41}$$

Rearranged in terms of i_2

$$i_2 = \frac{M\ddot{z}}{K_b K_i} - i_1 + \frac{K_g}{K_i} g_1 + \frac{K_g}{K_i} g_2 \qquad \textbf{4.42}$$

From the rotational equation:

$$\ddot{\theta} = \frac{L}{2 I_x} [K_b K_i i_1 - K_b K_g g_1 - K_b K_i i_2 + K_b K_g g_2] \qquad \textbf{4.43}$$

Similarly in terms of i_2

$$i_2 = \frac{-2 I_x \ddot{\theta}}{K_b K_i L} + i_1 - \frac{K_g}{K_i} g_1 + \frac{K_g}{K_i} g_2 \qquad \textbf{4.44}$$

Adding equations 4.42 and 4.44

$$i_2 = \frac{M\ddot{z}}{K_b K_i} - \frac{2 I_x \ddot{\theta}}{K_b K_i L} + \frac{K_g}{K_i} g_2 \qquad \textbf{4.45}$$

Subtracting 4.42 from 4.44

$$i_1 = \frac{M\ddot{z}}{K_b K_i} + \frac{2 I_x \ddot{\theta}}{K_b K_i L} + \frac{K_g}{K_i} g_1 \qquad \textbf{4.46}$$

Hence we can obtain di/dt expression for use in the voltage equations.

$$\dot{i}_2 = \frac{M\dddot{z}}{K_b K_i} - \frac{2 I_x \dddot{\theta}}{K_b K_i L} + \frac{K_g}{K_i} \dot{g}_2 \qquad \textbf{4.47}$$

and

$$\dot{i}_1 = \frac{M\dddot{z}}{K_b K_i} + \frac{2 I_x \dddot{\theta}}{K_b K_i L} + \frac{K_g}{K_i} \dot{g}_1 \qquad \textbf{4.48}$$

The voltage equation for magnet 1 is

$$v_1 = R\, i_1 + N A_p K_i \dot{i}_1 - N A_p K_g \dot{g}_1 \qquad \textbf{4.49}$$

Substituting for the current and its derivative.

$$v_1 = R[\frac{M\ddot{z}}{2K_g K_i} + \frac{I_x\ddot{\theta}}{K_b K_i L} + \frac{K_g}{K_i} g_1] + NA_p K_i[\frac{M\dddot{z}}{2K_b K_i} + \frac{I_x\dddot{\theta}}{K_b K_i L} + \frac{K_g}{K_i}\dot{g}_1] - NA_p K_g \dot{g}_1 \qquad \textbf{4.50}$$

Rearranging in terms of the jerk term gives

$$\dddot{z} = \frac{2 K_b v_2}{N A_p M} - \frac{R \ddot{z}}{N A_p K_i} - \frac{2 R I_x \ddot{\theta}}{N A_p M K_i L} - \frac{2 K_b K_g R g_1}{N A_p M K_i} - \frac{2 I_x \dddot{\theta}}{M L} \qquad \textbf{4.51}$$

Similarly for v_2 we derive an equation for the third derivative of z.

$$\dddot{z} = \frac{2 K_b v_1}{N A_p M} - \frac{R \ddot{z}}{N A_p K_i} + \frac{2 R I_x \ddot{\theta}}{N A_p M K_i L} - \frac{2 K_b K_g R g_2}{N A_p M K_i} + \frac{2 I_x \dddot{\theta}}{M L} \qquad \textbf{4.52}$$

Addition of 4.51 and 4.52 gives:

$$\dddot{z} = \frac{K_b v_1}{N A_p M} + \frac{K_b v_2}{N A_p M} - \frac{R \ddot{z}}{N A_p K_i} - \frac{K_b K_g R g_1}{N A_p M K_i} - \frac{K_b K_g R g_2}{N A_p M K_i} \qquad \textbf{4.53}$$

Subtraction of 4.52 from 4.51 gives:

$$\ddot{\theta} = -\frac{K_b v_1 L}{2 I_x N A_p} - \frac{K_b v_2 L}{2 I_x N A_p} - \frac{R \ddot{\theta}}{N A_p K_i} - \frac{L K_b K_g R g_1}{2 I_x N A_p K_i} - \frac{L K_b K_g R g_2}{2 I_x N A_p K_i} \qquad \textbf{4.54}$$

The geometric equations relating g_1 and g_2 to z and θ are also needed:

$$z_1 = z + \frac{L}{2}\theta \;, \quad z_2 = z - \frac{L}{2}\theta \qquad \textbf{4.55}$$

$$g_1 = z_{t_1} - z_1 \;, \quad g_2 = z_{t_2} - z_2 \qquad \textbf{4.56}$$

The state space description of the two degree of freedom system can then be produced:

$$\begin{bmatrix} \dot{z} \\ \ddot{z} \\ \dot{g}_1 \\ \dot{\theta} \\ \ddot{\theta} \\ \dot{g}_2 \end{bmatrix} = \begin{bmatrix} -\frac{R}{N A_p K_i} & 0 & -\frac{K_b K_g R}{N A_p M K_i} & 0 & 0 & -\frac{K_b K_g R}{N A_{p_p} M K_i} \\ 1 & 0 & 0 & 0 & 0 & 0 \\ 0 & -1 & 0 & 0 & -\frac{L}{2} & 0 \\ 0 & 0 & -\frac{L K_b K_g R}{2 I_x N A_p K_i} & -\frac{R}{N A_p K_i} & 0 & \frac{L K_b K_g R}{2 I_x N A_p K_i} \\ 0 & 0 & 0 & 1 & 0 & 0 \\ 0 & -1 & 0 & 0 & \frac{L}{2} & 0 \end{bmatrix} \begin{bmatrix} \dot{z} \\ \ddot{z} \\ g_1 \\ \dot{\theta} \\ \ddot{\theta} \\ g_2 \end{bmatrix}$$

$$+ \begin{bmatrix} \frac{K_b}{N A_p M} & \frac{K_b}{N A_p M} \\ 0 & 0 \\ 0 & 0 \\ \frac{K_b L}{2 I_x N A_p} & -\frac{K_b L}{2 I_x N A_p} \\ 0 & 0 \\ 0 & 0 \end{bmatrix} \begin{bmatrix} v_1 \\ v_2 \end{bmatrix} + \begin{bmatrix} 0 & 0 \\ 0 & 0 \\ 1 & 0 \\ 0 & 0 \\ 0 & 0 \\ 0 & 1 \end{bmatrix} \begin{bmatrix} \dot{z}_{t_1} \\ \dot{z}_{t_2} \end{bmatrix} \qquad \textbf{4.57}$$

The output equation to give the same variables as the single degree of freedom system is:

$$\begin{bmatrix} \ddot{z} \\ g_1 \\ g_2 \\ \ddot{\theta} \\ i_1 \\ i_2 \\ b_1 \\ b_2 \end{bmatrix} = \begin{bmatrix} 1 & 0 & 0 & 0 & 0 & 0 \\ 0 & 0 & 1 & 0 & 0 & 0 \\ 0 & 0 & 0 & 0 & 0 & 1 \\ 0 & 0 & 0 & 1 & 0 & 0 \\ \frac{M}{2 K_i K_b} & 0 & \frac{K_g}{K_i} & \frac{2 I_x}{L K_b Ki} & 0 & 0 \\ \frac{M}{2 K_i K_b} & 0 & 0 & -\frac{2 I_x}{L K_b Ki} & 0 & \frac{K_g}{K_i} \\ \frac{M}{2 K_i K_b} & 0 & 0 & \frac{2 I_x}{L K_b} & 0 & 0 \\ \frac{M}{2 K_i K_b} & 0 & 0 & -\frac{2 I_x}{L K_b} & 0 & 0 \end{bmatrix} \begin{bmatrix} \ddot{z} \\ \dot{z} \\ g_1 \\ \ddot{\theta} \\ \dot{\theta} \\ g_2 \end{bmatrix} \qquad 4.58$$

4.4 Flexible Structure Modelling

In this section the I beam introduced in the last section is allowed to exhibit bending effects. This is done by adding a model of the flexibility to the rigid body modes.

4.4.1 Assumptions about the Flexibility Model

For an analytical model of a flexible structure considerable complexity is needed, whereas an approximate model may be sufficient for modelling the structure for control development and indeed desirable to avoid controller complexity. In this section a simplified model is presented which represents the dynamic characteristics of the flexibility sufficiently for controller design.

Assumptions made include;

1) Only the lowest frequency flexible bending modes are considered, because for bending modes at frequencies above 100Hz the effect of the resonances is negligible. Also, higher frequency flexible bending modes diverge from the model

and are difficult to approximate without a much more complex model (for instance a finite element model).

2) Bending is symmetrical.

3) No divergence from the mode shape.

4) Centre of gravity is at the geometrical centre of the beam or vehicle.

With respect to vehicle dynamics almost all of the authors reviewed in chapter 2 have made the same assumptions [Nagai87] [Hać86].

4.4.2 Bending Theory Model

The analysis method used here is the Bernoulli-Euler theory [Bishop60] [Thompson88] and assumes that the plane cross-sections of a beam remain plane during flexure, i.e. that the radius of curvature of a bent beam is large compared with the beam depth. The flexible model is well described in the above references and an overview is given in appendix 5.

For small deflections, υ of the beam the motion perpendicular to the axis 0-x of the undeflected beam is described by the closed form of the Bernoulli-Euler equation:.

$$\frac{\partial^2 \upsilon}{\partial t^2} + \frac{EI}{A_e \rho} \frac{\partial^4 \upsilon}{\partial x^4} = 0 \qquad \textbf{4.59}$$

For harmonic excitation the solution of this equation is of the form

$$\upsilon = X(x)\, e^{i\omega t} \qquad \textbf{4.60}$$

Substitution leads to the equation:

$$\frac{d^4 X}{dx^4} - \frac{\omega^2 A_e \rho}{EI} X = 0 \qquad \textbf{4.61}$$

The solution of the above equation results in a very unwieldy expression which is

conveniently described in terms of receptance α_{xh}.

$$\upsilon = \alpha_{xh} F e^{i\omega t} \qquad \textbf{4.62}$$

where α_{xh} is the receptance between a point of application of the force at a distance x along the beam, and h the point of measurement:

$$\alpha_{xh} = \sum_{r=1}^{\infty} \frac{\phi_r(x)\phi_r(h)}{M(\omega_r^2 - \omega^2)} \qquad \textbf{4.63}$$

The characteristic function $\phi_r(x)$ represents the effect of a force applied at length x along the beam and $\phi_r(h)$ the measurement of the effect of that force at a point h along the beam, both for the rth frequency.

$$\phi_r(x) = \cosh \lambda_r x + \cos \lambda_r x - \frac{\cosh(\lambda_r l_{beam}) - \cos(\lambda_r l_{beam})}{\sinh(\lambda_r l_{beam}) - \sin(\lambda_r l_{beam})} (\sinh \lambda_r x + \sin \lambda_r x) \qquad \textbf{4.64}$$

The frequency equation of the free-free beam is

$$\cos(\lambda_r l_{beam})(\cosh \lambda_r l_{beam}) - 1 = 0 \qquad \textbf{4.65}$$

and this results in a series which enables the calculation of the corresponding natural frequencies. The end conditions are determined by the end conditions which for the Free-Free beam are:

When x=0, $$\frac{\partial^2 \upsilon}{\partial x^2} = \frac{\partial^3 \upsilon}{\partial x^3} = 0 \qquad \textbf{4.66}$$

When $x = l_{beam}$ $$\frac{\partial^2 \upsilon}{\partial x^2} = \frac{\partial^3 \upsilon}{\partial x^3} = 0 \qquad \textbf{4.67}$$

The deflection and slope at any section of the beam may be found for any position simply by specifying the position of the force application and the measurement output deflection The first four mode shapes are shown below.

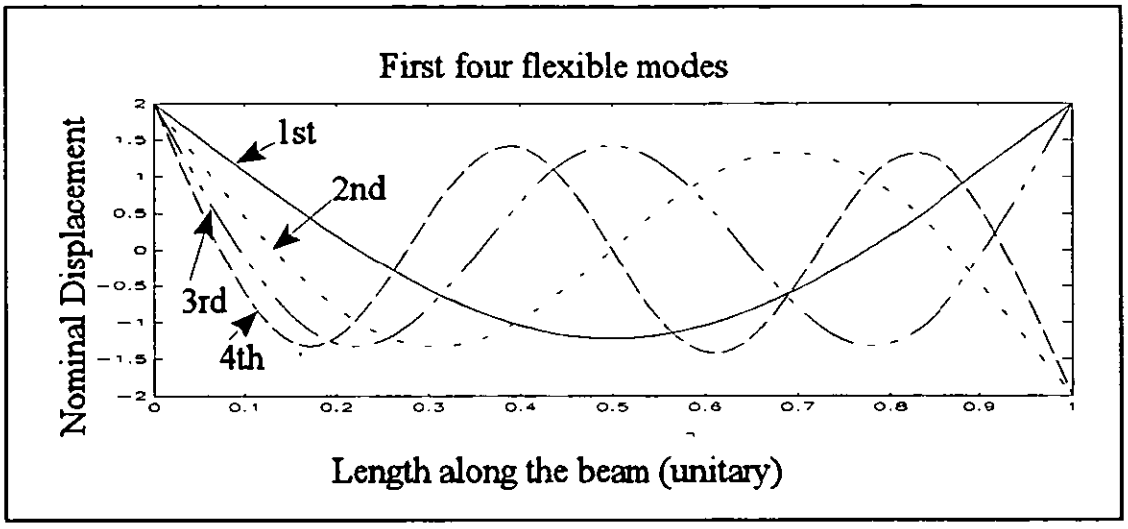

Figure 4.6 Flexible bending mode shapes

4.4.3 Combining of Flexible and Rigid Body Modes

Having described the relative displacement (υ) due to the flexible body modes the integration of the flexible body mode with the rigid body mode is considered. A receptance giving the response to a translational force input is given below:

$$\alpha_{xh} = -\frac{1}{M\omega^2} + \sum_{r=1}^{\infty} \frac{\phi_r(x)\phi_r(h)}{M.(\omega_r^2-\omega^2)} \qquad \textbf{4.68}$$

The mass term represents the vertical translational rigid body mode and the flexible bending modes excited by translational forces are all symmetrical, about the centre of the beam. For rotational motion an inertia term would be present instead of the mass and the flexible bending modes excited by rotational forces would be asymmetric about the beam centre. The above equation represents the harmonic motion with zero damping. By inspection it is fairly clear how to incorporate structural damping into the motion of the flexible modes and the symmetric receptance series is rewritten in the Laplace domain as a transfer function [Wie92]

$$\alpha_{xh} = \frac{1}{Ms^2} + \sum_{r=1}^{\infty} \frac{\phi_r(x)\phi_r(h)}{M(\omega_r^2 + 2\,\zeta\,\omega_r s + s^2)} \qquad \textbf{4.69}$$

Such a representation of the flexible modes may be thought of in terms of the following diagrams.

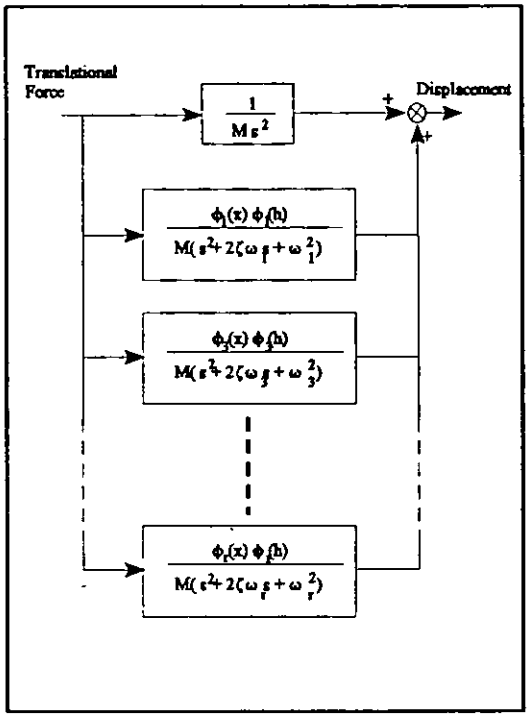

Figure 4.7 Symmetrical bending modes and the translational rigid body mode.

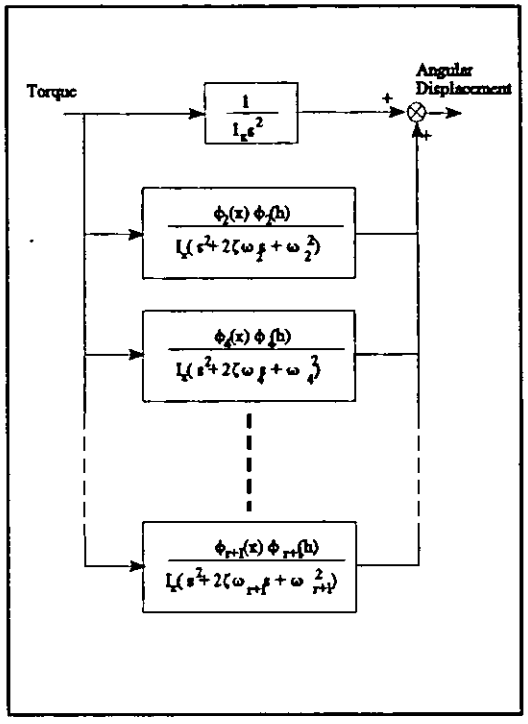

Figure 4.8 Asymmetrical bending modes and the rotational rigid body mode.

The receptance model for each flexible mode considered is easily converted to the state space representation in the following manner.

$$\frac{y(s)}{F(s)} = \frac{\phi_r(x)\phi_r(h)}{M\,[\omega_r^2 + 2\zeta\omega_r s + s^2]} \qquad \textbf{4.70}$$

Where y(s) is a displacement measurement at position h along the beam.

$$\frac{F}{M}\,\phi_r(x)\phi_r(h) = \omega_r^2 y + 2\,\zeta\,\omega_r \dot{y} + \ddot{y} \qquad \textbf{4.71}$$

Defining a generalised coordinate q_r for the rth mode:

$$y(h) = q_r(t)\,\phi_r(h) \qquad \textbf{4.72}$$

Upon substitution and rearrangement gives

$$\ddot{q}_r = \frac{F}{M}\phi_r(x) - q_r\omega_r^2 - 2\zeta\dot{q}_r\omega_r \qquad 4.73$$

which may be written in matrix form for a symmetrical bending mode

$$\begin{bmatrix}\dot{q}_r\\ \ddot{q}_r\end{bmatrix} = \begin{bmatrix}0 & 1\\ -\omega_r^2 & -2\zeta\omega_r\end{bmatrix}\begin{bmatrix}q_r\\ \dot{q}_r\end{bmatrix} + \begin{bmatrix}0\\ \dfrac{\phi_r(x)}{M}\end{bmatrix}F \qquad 4.74$$

It is straightforward to write such an equation in terms of the asymmetrical bending mode due to rotation. Equation 4.74 agrees with the flexible mode descriptions derived by more elegant energy methods [Skelton88].

4.4.4 Coupling between the rigid body model and flexible bending modes

In the preceding sections a rigid body model has been presented which incorporates the magnet electrodynamics and a model of the flexible modes has been derived. Now the coupling between the two models is described and this involves defining the nature of the force which will excite the bending mode.

The force produced by each electromagnet in terms of the vertical and angular accelerations is given by solving equations 4.39 and 4.40 simultaneously this gives:

$$f_1 = M\ddot{z} + \frac{2I_x\ddot{\theta}}{L} \qquad 4.75$$

and

$$f_2 = M\ddot{z} - \frac{2I_x\ddot{\theta}}{L} \qquad 4.76$$

Now incorporating the forces acting on the rigid body modes and the flexible bending modes using the receptance approach described above, consider the vertical motion equation

$$\frac{z(s)}{F(s)} = \frac{1}{Ms^2} + \frac{\phi_1(x)\phi_1(h)}{M\,[\omega_1^2 + 2\zeta\omega_1 s + s^2]} \qquad \textbf{4.77}$$

which in terms of vertical accelerations becomes:

$$\ddot{z}(s) = \frac{f_1 + f_2}{M} + \frac{[f_1\,\phi_1(x_1) + f_2\,\phi_1(x_2)]\,\phi_1(h)\,s^2}{M\,[\omega_1^2 + 2\zeta\omega_1 s + s^2]} \qquad \textbf{4.78}$$

Considering the flexible mode term only and substituting for f_1 and f_2 in terms of the generalised coordinate q_1 for the first bending mode gives:

$$\ddot{q}(s) = \frac{[(M\,\ddot{z} + \frac{2I_x\ddot{\theta}}{L})\,\phi_1(x_1) + (M\,\ddot{z} - \frac{2I_x\ddot{\theta}}{L})\,\phi_1(x_2)]\,s^2}{M\,[\omega_1^2 + 2\zeta\omega_1 s + s^2]} \qquad \textbf{4.79}$$

Clearly for symmetrical bending $\phi_1(x_1)=\phi_1(x_2)$ and rearranging the term gives

$$\ddot{q}_1 + 2\zeta\omega_1\dot{q}_1 + \omega_1^2 q_1 = (\phi_1(x_1) + \phi_1(x_2))\,\ddot{z} \qquad \textbf{4.80}$$

and for asymmetrical bending $\phi_2(x_1)=-\phi_2(x_2)$ so rearranging:

$$\ddot{q}_2 + 2\zeta\omega_2\dot{q}_2 + \omega_2^2 q_2 = (\phi_2(x_1) - \phi_2(x_2))\frac{2I_x}{L}\ddot{\theta} \qquad \textbf{4.81}$$

4.4.5 Coupling between the flexible bending modes and rigid body model

Having seen how the bending mode is excited by the forces which act on the rigid body modes it now remains to describe the coupling of the effects of the bending modes back into the rigid body modes.

Defining the absolute acceleration of the beam as the sum of the rigid body acceleration plus the acceleration due to the bending mode gives:

$$\ddot{z}' = \ddot{z} + \phi_1(h)\ddot{q}_1 \qquad \textbf{4.82}$$

where $\ddot{z}'$ is the absolute vertical acceleration at point h.
From equation 4.80 the bending mode relative acceleration $\ddot{q}_1$ can be substituted into equation 4.82 giving:

$$\ddot{z}' = \ddot{z} + \phi_1(h)[(\phi_1(x_1) + \phi_1(x_2))\ddot{z} - 2\zeta\omega_1\dot{q}_1 - \omega_1^2 q_1] \qquad \textbf{4.83}$$

This equation will enable the effects of the flexibility to be applied to the net velocity and the airgap states, which through the above coupling now represents the real airgap, not the airgap due to the rigid body dynamics alone.

The equation 4.84 combines equation 4.57 with equation 4.83 and shows the coupling of rigid and the fundamental flexible bending mode. The process of constructing a state space model lends itself to defining the various component models and building them into a single large model. This has been done with the MATLAB® models used to simulate the Maglev systems in this thesis (see appendix 4: Model Description).

$$\begin{bmatrix} \dddot{z} \\ \ddot{z}' \\ \ddot{g}_1 \\ \ddot{\theta} \\ \ddot{\delta} \\ \ddot{g}_2 \\ \ddot{q}_1 \\ \ddot{\bar{q}}_1 \end{bmatrix} = \begin{bmatrix} -\frac{R}{N A_p K_t} & 0 & -\frac{K_b K_g R}{N A_p M K_t} & 0 & 0 & -\frac{K_b K_g R}{N A_p M K_t} & 0 & 0 \\ 1 + \phi_1(h)(\phi_1(x_1)+\phi_1(x_2)) & 0 & 0 & 0 & 0 & 0 & -\phi_1(h)[\omega_1^2] & -\phi_1(h)[2\zeta\omega_1] \\ 0 & -1 & 0 & 0 & -\frac{L}{2} & 0 & 0 & 0 \\ 0 & 0 & -\frac{L K_b K_g R}{2 I_x N A_p K_t} & -\frac{R}{N A_p K_t} & 0 & \frac{L K_b K_b R}{2 I_x N A_p K_t} & 0 & 0 \\ 0 & 0 & 0 & 1 & 0 & 0 & 0 & 0 \\ 0 & -1 & 0 & 0 & \frac{L}{2} & 0 & 0 & 0 \\ 0 & 0 & 0 & 0 & 0 & 0 & 0 & 1 \\ \phi_1(x_1)+\phi_1(x_2) & 0 & 0 & 0 & 0 & 0 & -\omega_1^2 & -2\zeta\omega_1 \end{bmatrix} \begin{bmatrix} z \\ \dot{z}' \\ g_1 \\ \dot{\theta} \\ \theta \\ g_2 \\ q_1 \\ \dot{q}_1 \end{bmatrix}$$

$$+ \begin{bmatrix} \frac{K_b}{N A_p M} & \frac{K_b}{N A_p M} \\ 0 & 0 \\ 0 & 0 \\ \frac{K_b L}{2 I_x N A_p} & \frac{K_b L}{2 I_x N A_p} \\ 0 & 0 \\ 0 & 0 \\ 0 & 0 \\ 0 & 0 \end{bmatrix} \begin{bmatrix} v_1 \\ v_2 \end{bmatrix} + \begin{bmatrix} 0 & 0 \\ 0 & 0 \\ 1 & 0 \\ 0 & 0 \\ 0 & 0 \\ 0 & 1 \\ 0 & 0 \\ 0 & 0 \end{bmatrix} \begin{bmatrix} z_{t_1} \\ z_{t_2} \end{bmatrix} \qquad \textbf{4.84}$$

It needs to be emphasised that only the acceleration states are rigid body states in the above equation. The output equation is not shown here because it is similar to equation 4.57 which could be easily modifed to give the absolute acceleration using equation 4.83

$$\begin{bmatrix} \dot{x} \\ \dot{x}_f \end{bmatrix} = \begin{bmatrix} A_r & A_{cfr} \\ A_{crf} & A_f \end{bmatrix} \begin{bmatrix} x \\ x_f \end{bmatrix} + \begin{bmatrix} B \\ B_f \end{bmatrix} u + \begin{bmatrix} G \\ G_f \end{bmatrix} \omega \qquad \textbf{4.85}$$

Equation 4.85 shows the general form of the coupling between the flexible and rigid body modes and shows how equation 4.84 is partitioned into component matrices.

4.5 Comparison of the model with a real vehicle

Within the railway industry the approximation of a vehicle as a simple beam is an accepted part of the conceptual design process. The assumption that the centre of gravity is at the geometrical centre of the vehicle is of course a simplification, but it means that the model remains manageable. The model is not designed to be an accurate representation of the vehicle but a model of sufficient accuracy that a robust controller can be designed around it.

Deviations from the mode shape due to structural irregularities, such as doors, are in amplitude only and may be approximated in the flexibility model by displacement offsets during the analysis stage. The effect of vehicle loading on the resonant frequency of the bending modes has not been considered in the above model development and is a factor which needs to be analysed on the controlled structure. Some studies [Marguet93] indicate that the variation of the natural frequency of the resonant bending modes in response to load changes in a light rail vehicle are up to 10%. The same study also indicates the increase in damping in a vehicle structure introduced by passengers.

Typical values of the structural natural damping ratio ζ for conventional rail vehicles is about 3%.

4.6 Magnet positioning issues

The development of the flexible bending model in this chapter has shown through the use of the receptance transfer function that the displacement at a point on the beam depends on where that point lies with respect to the mode shape and where the magnet force input is with respect to the mode shape.

Placing the magnets at 25 and 75% of the beam means that they are close to the nodes of

the first bending mode (see figure 4.6). The first bending mode will consequently not be excited to any degree by the magnets in these positions, but it is certain that other bending modes will.

The positioning of magnets so as to mininmise the excitation of a number of bending modes is undoubtedly a compromise which depends on the Maglev chassis stiffness and the bandwidth of the magnets. Clearly the position of the magnets will vary during the final design / construction stage as experimental data becomes available for the optimal positioning of the actuators with respect to the control of the bending modes. A phase lead or lag effect will occur depending on which side of the bending mode node the magnet is positioned, but this has more implications for the suspension control law discussed in chapter 5.

Chapter 5: Classical Control Techniques

5.1 Introduction

A number of developers of Maglev vehicles have used a linear classical control strategy to provide the necessary stabilisation and ride control. This chapter describes the classical control approach, with a particular emphasis upon the Birmingham Maglev vehicles, and provides a basis for further investigation of other strategies in chapters 6 and 7. The purpose here is to demonstrate the performance limits of the classical controller, and perhaps more importantly to highlight the significance of the concepts developed for the Birmingham Maglev vehicles.

Chapter 5 is divided into three sections, the first dealing with the control of the single degree of freedom magnet in a levitation and a suspension mode of operation, the second with the development of a modal controller controlling the bounce and pitch motions of the rigid body, and finally the full controller designed to cope with some of the effects of a flexible chassis.

5.2 Control of the Single Degree of Freedom Model

There are many examples of control strategies for single degree of freedom Maglev systems in the general control literature. Due to the nonlinear nature of the problem and the apparently simple description of the problem it is seen as a good demonstrator for new control techniques. Most of the proposed systems are not designed with respect to the role of a suspension as outlined in chapter 3, but are designed and judged purely on control criteria such as tracking performance and robustness to parameter uncertainty.

The approach followed here is to design the controller to achieve the specified suspension performance previously described. Highlighting the key requirements once more:

1) A response equivalent to a passive suspension with a natural frequency of 1 to 2 Hz.
2) A maximum deflection due to load changes of 1mm.
3) Minimisation of the airgap change due to the transition onto a gradient.
4) Operation which is robust to parameter uncertainty.

Considering a quarter car Maglev suspension with a magnet mass of 1000 kg tare and 1200 kg fully laden operating at speeds of $15ms^{-1}$ with an airgap of 15mm the following requirements exist (see appendix 4 for parameter details). A suspension with a natural frequency of 1.5Hz requires an equivalent spring stiffness of $97.7kNm^{-1}$ (for an average mass of 1100 kg) . For a maximum suspension deflection of ±1mm as the load varies by ±100 kg requires a stiffness of 981 kNm^{-1} and this gives a suspension of natural frequency (with average vehicle loading) of 4.72Hz. These are conflicting requirements which must be reconciled in the controller.

Recognising from the outset that these conflicts existed, the designers of the classical suspension sought a method to account for each requirement separately.

In this thesis the emphasis is on the investigation of the effects of a flexible chassis. For this reason some of the other suspension requirements, such as the maximum airgap deflection under loading have been relaxed.

5.2.1 The Basic Suspension Design Problem

Returning to the block diagram model of the magnet developed in chapter 4, it is necessary to compensate for the instability caused by airgap changes. The nature of the instability was shown in control terms to be the result of a positive pole with a frequency of about 6Hz for an airgap of 15mm. It can also be thought of as a spring with a negative stiffness. The most obvious way to compensate for this negative stiffness of the airgap is to create an electronic feedback of the airgap which demands a supply voltage directly

proportional to it. This in effect creates a positive stiffness to compensate for the natural negative stiffness. Such a strategy is shown in the figure below. In most cases it is necessary to control the current in order to overcome the inductive phase lag.

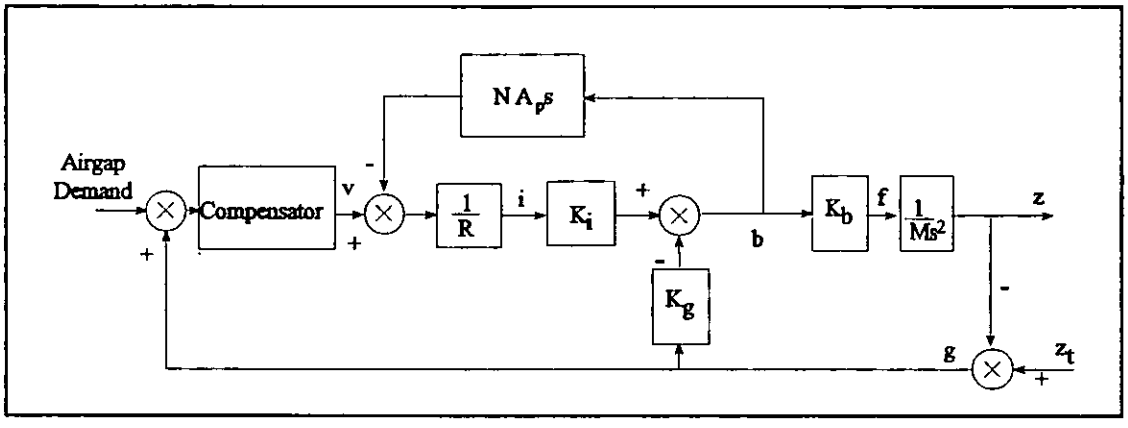

Figure 5.1 Simplest levitation control strategy

The bandwidth of the above compensation will need to be in excess of 6Hz to compensate for the instability but such a suspension would be susceptible to high frequency track irregularities. Lowering the bandwidth to 1.5Hz by reducing the feedback gain makes the control system vulnerable to the nonlinear effects of the magnet and the loop also becomes difficult to compensate. When the airgap varies due to its suspension requirements and the nonlinear effects become more pronounced this will make such a control strategy unworkable in practice.

To overcome this problem additional feedback compensation can be provided. One solution successfully used on the Birmingham Maglev vehicles is to use a fast acting inner flux density feedback loop [Goodall76]. A bandwidth of between 50 and 100Hz, is readily achievable and any changes in the magnet parameters due to the nonlinearities will be compensated for. The flux density feedback loop in effect converts the magnet into an actuator with a predictable force response with only the nonlinearities associated with K_b remaining. An integral term may also be added to the gain of the flux density feedback loop to increase the low frequency response. Such a controller is shown in figure 5.2.

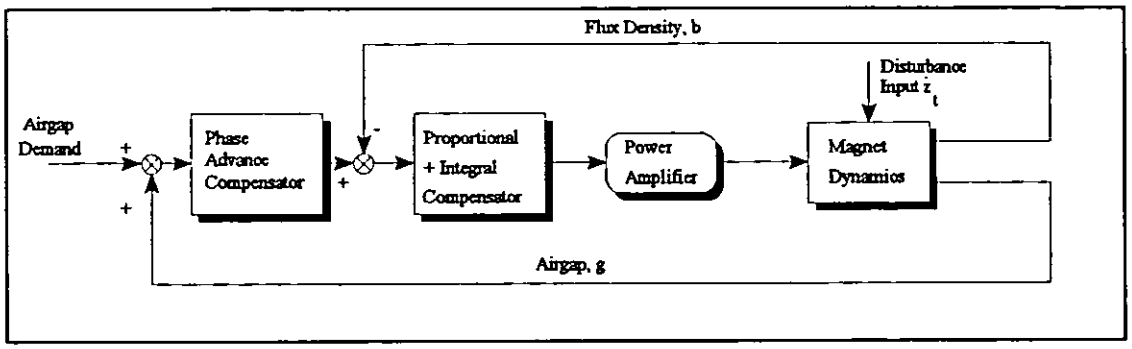

Figure 5.2 Suspension controller

Levitation can be achieved with this control strategy. Using the quarter car Maglev model given in appendix 4 the following main loop phase advance compensator is used

$$H_{pa}(s) = 30\frac{(1 + .06s)}{(1 + .0078s)} \qquad \textbf{5.1}$$

and for the inner flux loop:

$$H_{pi}(s) = 600\,\frac{(1 + .002\,s)}{.002\,s} \qquad \textbf{5.2}$$

The gain in the main loop phase advance compensator will provide a suspension stiffness of $30*2*F_0/B_0$ of 925 kNm^{-1} which will give an airgap deflection of 1mm with a 10% or 100 kg load change.

Design on the Nichols chart has proved the most convenient method and the airgap response is shown below.

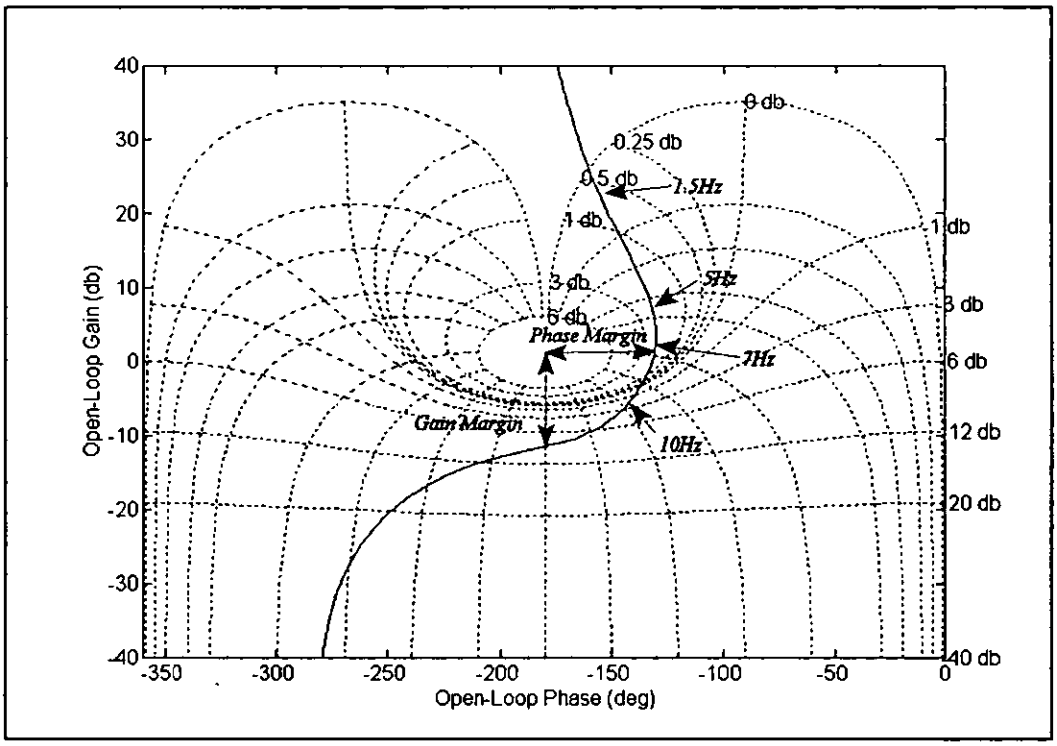

Figure 5.3 Open loop response on a Nichols Chart (flux loop closed)

The gain margin of 10dB and the phase margin of 43° are satisfactory for robust levitation but the ride quality is quite unsatisfactory having a vertical r.m.s vertical acceleration of 13.8ms^{-2} and a r.m.s airgap of 2mm. Reducing the main loop gain to a value much closer to 1 T/m (instead of 20T/m) provides reasonable suspension with an r.m.s vertical acceleration 0.6ms^{-2} and r.m.s airgap of 7mm. The controller is robust to the nonlinear effects, but the maximum load deflection requirement will not be satisfied.

5.2.2 Accommodating Ride Quality and Maximum Load Deflection Requirements

This section explains in detail the control structure adapted for the Birmingham Maglev vehicle, which has been summarised elsewhere [Goodall76]. It is an essential starting point for developing the strategy to include the effects of flexibility, considered a little later in this chapter

To address this specification the suspension requirements need to be examined further.

1) With no forward motion the absolute position (z) of the suspended load and the airgap (g) are identical, and z may therefore be used in place of g.

2) For low frequency track inputs the airgap changes need to be minimised so that the suspension follows the track. For high frequency track inputs the changes in absolute position need to be minimised such that the suspension provides isolation.

A pseudo absolute position coordinate may be derived from a measurement of acceleration by a self-zeroing double integrator which integrates the components above about 0.1Hz. Since the absolute position coordinate is going to be used to minimise high frequency disturbances this frequency limitation is not too significant. The self-zeroing double integrator has the form:

$$H_i(s) = \frac{\frac{1}{\omega_i^3}s}{1 + \frac{2}{\omega_i}s + \frac{2}{\omega_i^2}s^2 + \frac{1}{\omega_i^3}s^3} \qquad \textbf{5.3}$$

where the integrator frequency, ω_i is 0.1Hz or 0.63 rad s^{-1}.

Point (2) above explicitly states what information is necessary for the controller and this can be implemented using a low pass filter on the airgap feedback path and a high pass filter on the absolute position feedback. This is shown in figure 5.4.

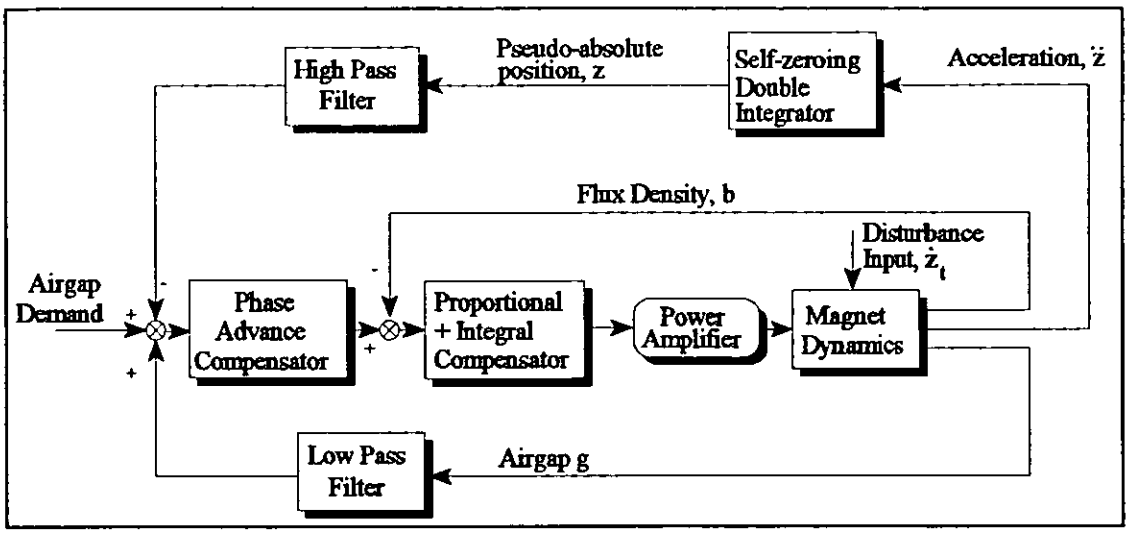

Figure 5.4 Suspension Controller

Complementary high and low pass filters, in which the responses add to unity, allow the two filtered feedbacks to be added to produce a new position coordinate which contains the desired components for satisfactory ride quality. The complementary filter approach has no effect on the control stability but allows the ride quality requirement to be achieved while still having a high gain to reduce the maximum suspension deflection due to loading.

For frequencies within the position control loop bandwidth :

$$g\ H_{lp}(s) - z\ (1 - H_{lp}(s)) \qquad \textbf{5.4}$$

where $H_{lp}(s)$ is the low pass filter. Since the coordinates are related by

$$z = z_t - g \qquad \textbf{5.5}$$

substitution shows that the responses of the suspensions are the same as those of the filters thus:

$$\frac{z}{z_t} = H_{lp}(s) \qquad \textbf{5.6}$$

and

$$\frac{g}{z_t} \cdot (1 - H_{lp}(s)) \cdot H_{hp}(s) \qquad 5.7$$

The low pass filter characteristic can be chosen along the lines identified in chapter 3, and in the Birmingham Maglev Control system they are Butterworth filters, with a frequency of 1 to 1.5Hz and a damping term ζ of 0.707 corresponding to the optimal suspension described in chapter 3.

It has already been shown that the filter characteristic determines the suspension response and this is also true with respect to the steady state deflection produced by the transition of the Maglev vehicle onto a gradient. As was shown in chapter 3 a 3rd order Butterworth filter will reduce the displacement on a gradient but degrades the ride quality in the process. The analysis in chapter 3 is equally applicable when the complementary filters approach is used to dictate the ride quality.

The filter structure may be simplified by considering the above equations and substituting for the high pass filter in terms of the low pass filter.

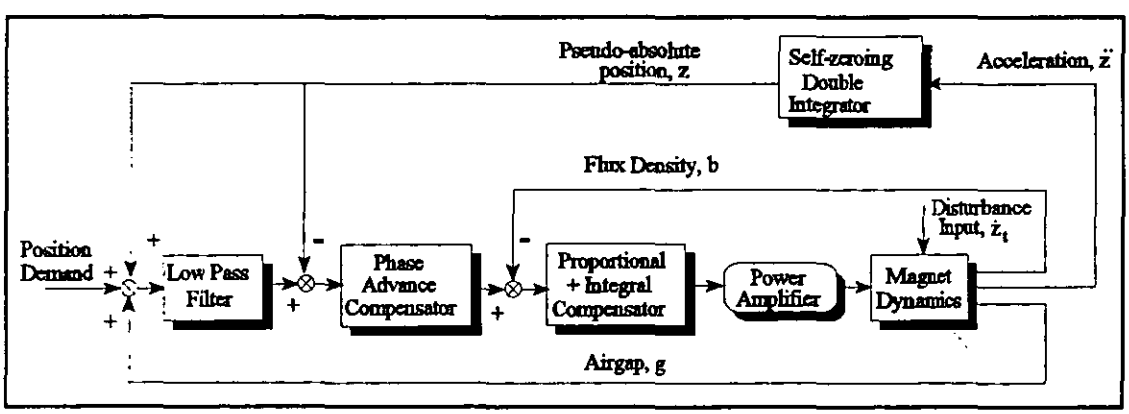

Figure 5.5 Equivalent complementary filter approach with one low pass filter

This control structure now means that the position loop can be designed to meet the maximum load deflection requirements without worrying about ride quality, and the complementary filters can be chosen to provide a suitable ride quality without worrying

about the load deflection. Consequently the flux loop and main position loop compensators remain unchanged from those already presented i.e. equations 5.1 and 5.2.

5.3 Control of the Half-Car Model

A number of methods are possible for the extension of the single degree of freedom controller to the half car model developed in chapter 4. Extending the controller further to a full model is straightforward once the method is established.

1) The magnets at each end of the beam may each have an independent controller identical to the single degree of freedom controller but the controllers will be dynamically coupled via the beam dynamics and so will 'fight' each other. If the beam is sufficiently soft that the loops are effectively decoupled, it may be possible to levitate the system [Jayawant81] but the chassis design will be complex.

2) The most attractive method, because it follows naturally from the modelling process, is to consider control of the rigid body modes, i.e. the bounce and the pitch in the case of the half car model. Leaving each magnet with its own inner flux loop but applying the complementary filters and the position loop in the modal form allows independent control of bounce and pitch. This means that the ride quality, maximum deflection and stability can be each considered individually for each of the rigid modes.

The second method is the one applied to the Birmingham Maglev and is shown for the bounce and pitch modes in the figure below.

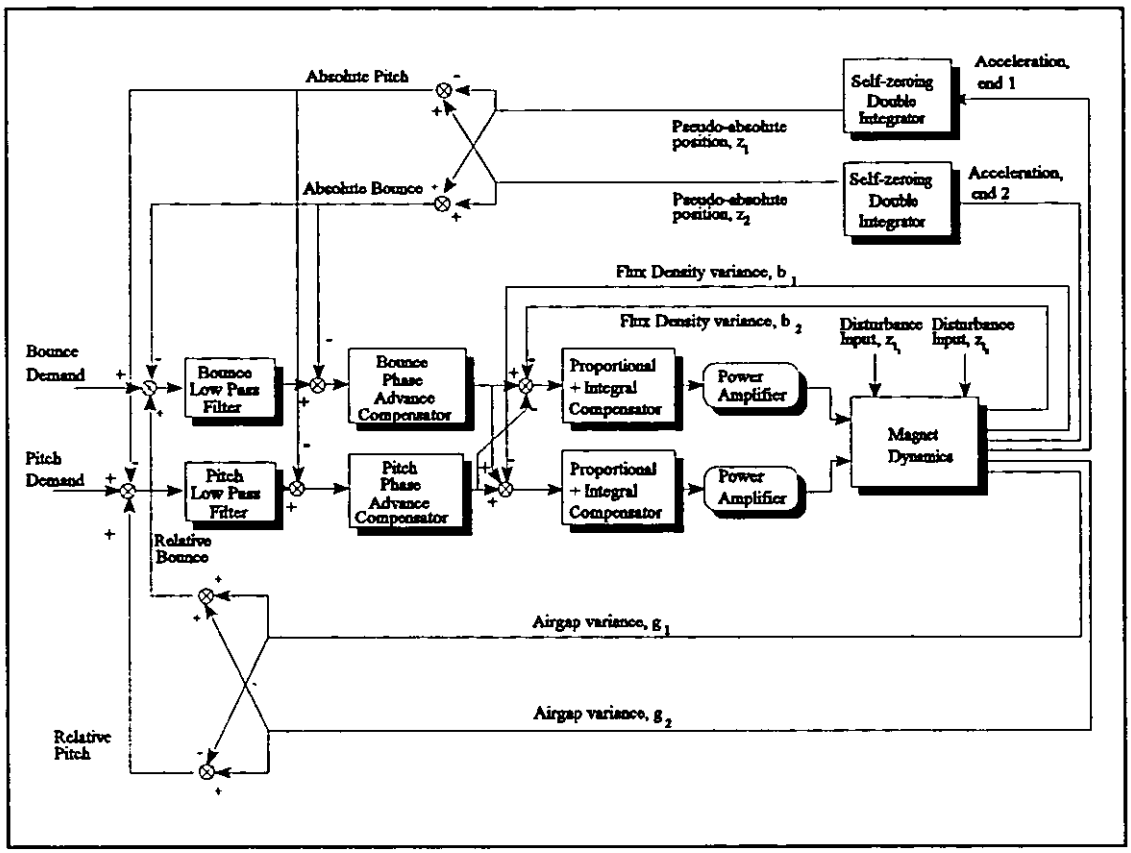

Figure 5.6 Modal Controller for Rigid Body Modes Pitch and Bounce.

The half car model considered has a tare mass of 5000 kg and is 15m in length. The magnets are fixed at 25 and 75% of the beam length and the first bending mode nominally lies at 16.1 Hz. The parameters for the half car model are given in full in appendix 4.

The loop compensators used in the analysis have the following coefficients. The proportional plus integral compensators are the same for both inner flux loops;

$$H_{pi}(s) = 400\,\frac{(1 + .0002\,s)}{.0002\,s} \qquad \textbf{5.8}$$

and for the bounce loop phase advance compensator

$$H_{pa\text{-}bounce}(s) = 17.5\,\frac{(1 + .05s)}{(1 + .01s)} \qquad \textbf{5.9}$$

and for the pitch loop phase advance compensator

$$H_{pa\text{-}pitch}(s) = 27.5\frac{(1 + .08s)}{(1 + .016s)} \qquad 5.10$$

The complementary filters all have filter frequencies of 1Hz and the self zeroing double integrator has a filter frequency of 0.5Hz.

The ride quality achieved with this suspension controller is given in Table 5.2 at the end of this chapter. Stability has proved not to be a problem in the simulations and a 10dB gain margin with a 35° phase margin is attainable.

5.4 Modal Control of the Chassis with flexibility.

In addition to the suspension requirements described earlier (section 5.2) the possibility of the chassis having lower frequency bending modes is now considered.

As has been stated the Birmingham Maglev chassis was constructed to be particularly rigid with a first bending mode of 40Hz. Because the position control loop bandwidth needs to be of the order of 5 to 10Hz the chances of the first bending mode being excited have been minimised from the outset by mechanical construction. Nevertheless the effects of the flexing of the first bending modes were sufficient to warrant a notch or frequency reject filter of the form below to reduce even further the unwanted flexible body dynamics.

$$H_{notch}(s) = \frac{1 + \frac{s^2}{\omega_n^2}}{1 + \frac{2\zeta s}{\omega_n} + \frac{s^2}{\omega_n^2}} \qquad 5.11$$

where ω_n is the notch filter frequency and ζ the damping of the filter where a value of between 5 and 15% is typical [Wie92].

Notch filters for the first symmetrical and first asymmetrical bending modes were placed in the bounce and pitch modal control loops immediately prior to the phase advance compensators.

The approach using notch filters is assessed as the stiffness of the chassis is reduced such that it tends towards the bandwidth of the controller which for the following investigation is 5 Hz.

The results in figures 5.7, 5.8 and 5.9 below show that when considering the first two flexible bending modes there is a clear degradation in the stability of the system, but that this is overshadowed by the effects of the third and fourth bending modes which when included cause instability. The use of notch filters is significant when these bending modes are included as shown when the reduced order controller, which has no notch filters to account for the 3rd and 4th bending modes, is used with a system with 4 bending modes. This so called spillover effect must be accounted for and as the stiffness of the chassis is reduced it is no longer sufficient to consider the two lowest bending modes alone. The reason for the importance of the 3rd and 4th bending modes is that they are strongly excited by the magnets because of their mode shapes. The 1st and 2nd modes have nodes closer to the magnet attachment points and are less excited by the magnet action. For a magnet at 25% of the vehicle length the node for the 1st bending mode is at 24% and for the 2nd bending mode at 13% of the vehicle length. Consequently the 2nd bending mode should be more excited than the 1st bending mode.

Table 5.1 below attempts to summarise the parameters varied in the following results. The Maglev model used in all of the tests is given in full in appendix 4 under the half car column.

Table 5.1 Flexibility investigation

Figure #	Notch Filters Filter Frequency [Hz]				Modes in the Model Bending Mode Frequency [Hz]			
	1st	2nd	3rd	4th	1st	2nd	3rd	4th
5.7	5 to 35	13.8 to 96.6	None	None	5 to 35	13.8 to 96.6	None	None
5.8	5 to 35	13.8 to 96.6	27.1 to 189	44.8 to 313	5 to 35	13.8 to 96.6	27.1 to 189	44.8 to 313
5.9	5 to 35	13.8 to 96.6	None	None	5 to 35	13.8 to 96.6	27.1 to 189	44.8 to 313
5.10	5 to 35	13.8 to 96.6	None	None	5 to 35	13.8 to 96.6	None	None
5.11	5 to 35	13.8 to 96.6	27.1 to 189	44.8 to 313	5 to 35	13.8 to 96.6	27.1 to 189	44.8 to 313
5.12	16.1	44.3	None	None	16.1 ±10%	44.3 ±10%	None	None
5.13	16	44.3	86.9	143.6	16 ±10%	44.3 ±10%	86.9 ±10%	143.6 ±10%
5.14	16	44.3	None	None	16	44.3	None	None
5.15	16	44.3	86.9	143.6	16	44.3	86.9	143.6
5.16	16	44.3	86.9/ None	143.6/ None	16	44.3	86.9	143.6
5.17	16	44.3	86.9/ None	143.6/ None	16	44.3	86.9	143.6

For all of the figures apart from 5.14 and 5.15 the magnets are at the nominal positions of 25 and 75% of the vehicle length except where otherwise indicated.

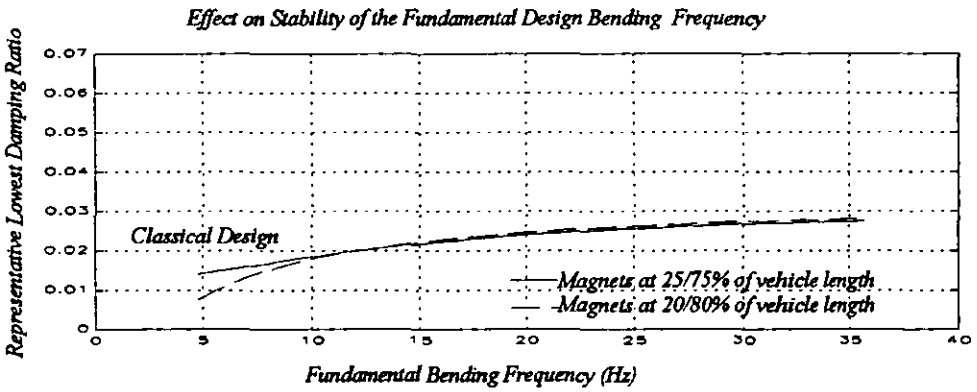

Figure 5.7 2 flexible bending modes

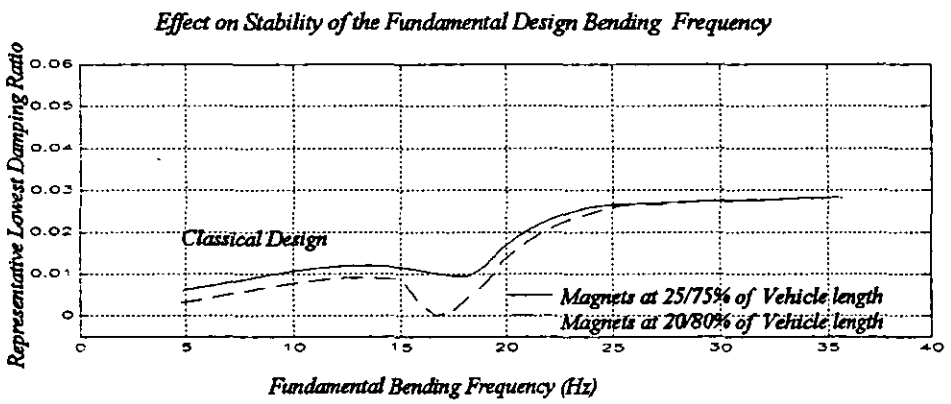

Figure 5.8 4 flexible bending modes

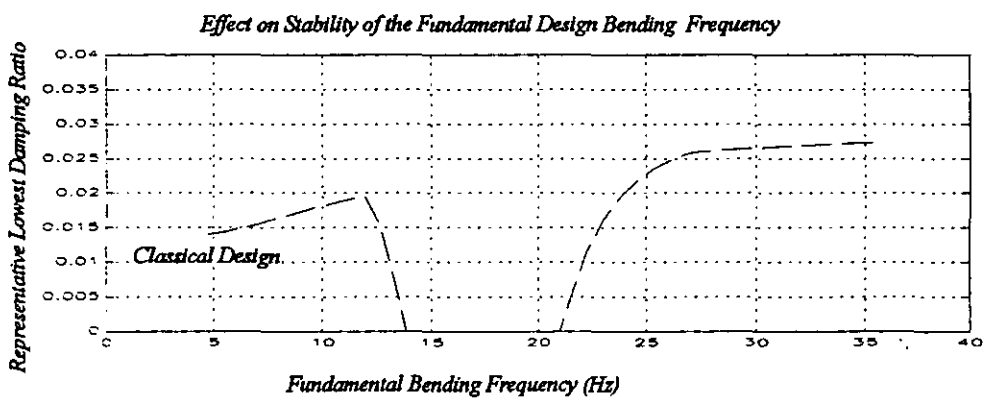

Figure 5.9 Spillover effects (magnets at 25/75% of the length)

Figure 5.9 shows the instability consequences of not using notch filters to minimise the effects of the 3rd and 4th bending modes for a soft chassis when the latter have

corresponding natural frequencies between 80 and 100Hz. Figures 5.10 and 5.11 show how the ride quality is affected by the variation in the design bending frequency. For 2 flexible bending modes this is not significant but the results of 5.11 demonstrates that as the Maglev suspension approaches marginal stability the ride quality deteriorates rapidly. This is due to the highly excited 3rd and 4th bending modes.

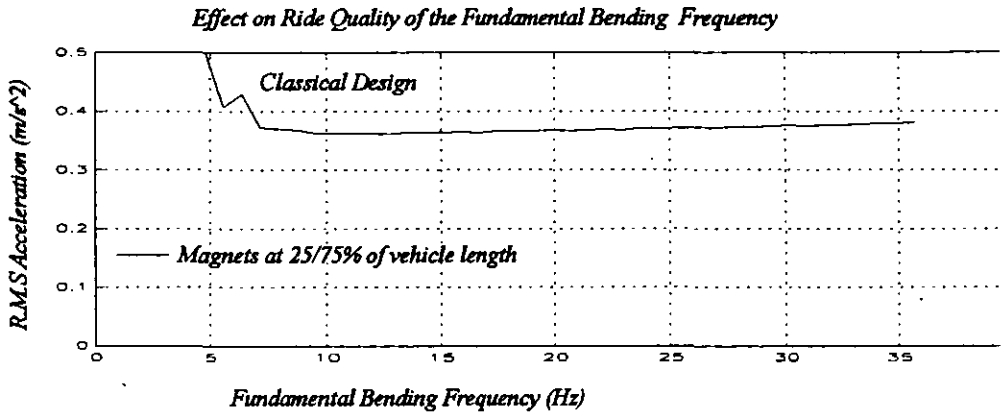

Figure 5.10 2 flexible bending modes

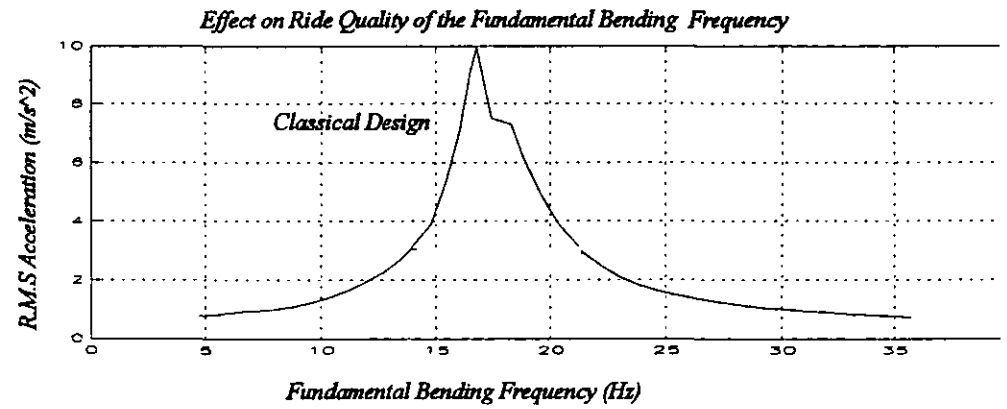

Figure 5.11 4 flexible bending modes

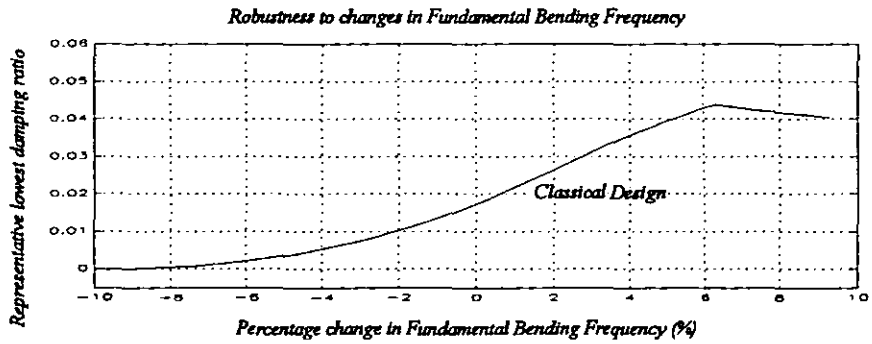

Figure 5.12 Changes in the bending frequency for 2 flexible modes

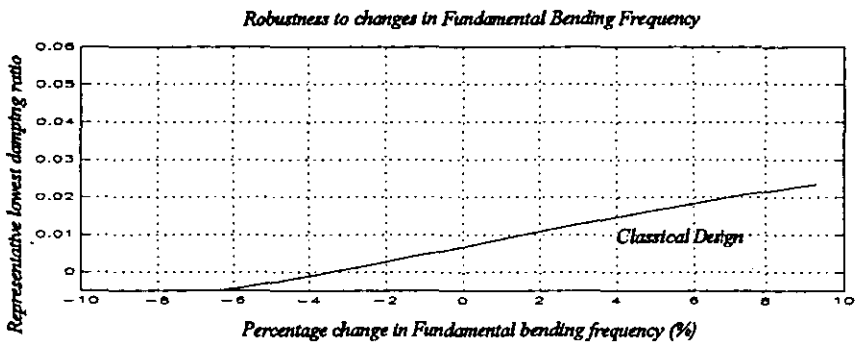

Figure 5.13 Changes in the bending frequency for 4 flexible modes

Variation in the natural frequency from the design is significant in the results above. The system is unstable when the natural frequency diverges by more that about 4% of the design frequency. Divergence of the natural frequency from its design frequency may be caused by temperature or loading changes. Analysis of the effect of passenger load changes suggests that the expected variation in natural frequency should not be more than about 3% [Marquet93].

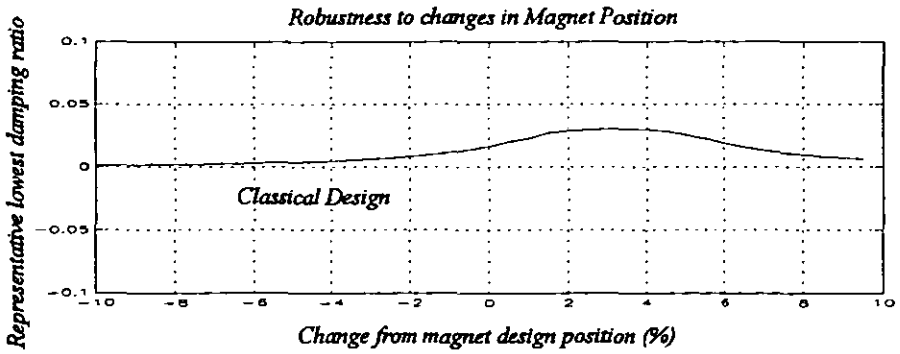

Figure 5.14 2 flexible bending modes (nominal position at 25 and 75% of vehicle length)

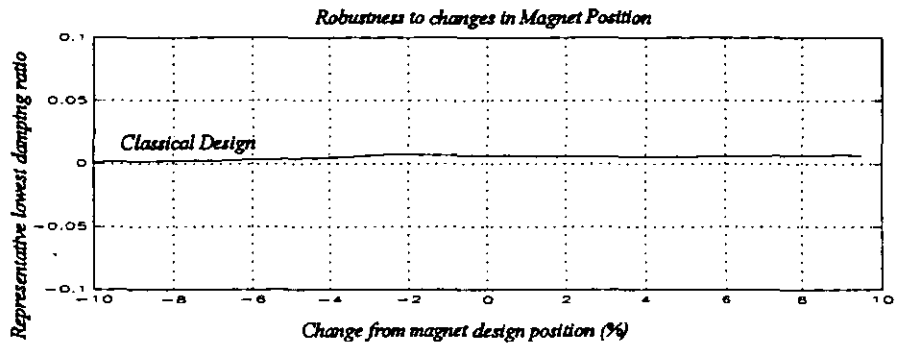

Figure 5.15 4 flexible bending modes (nominal position at 25 and 75% of vehicle length)

Figures 5.14 and 5.15 show the suspension as being only marginally stable at the nominal magnet position. Variation of the magnet's positions along the vehicle decreases the stability such that the Maglev vehicle appears on the verge of instability. The aim of this analysis was to show how stable the Maglev suspension was in response to irregularities in the mode shape.

Figures 5.16 demonstrates the effect of the control strategy on the chassis flexibility when four flexible bending modes are considered. The modal vertical acceleration response is shown with a track velocity input. The 3rd bending mode resonance is very prominent at 87Hz. The figure shows the Maglev suspension with a notch filter at the 3rd bending mode frequency when the system is stable and without when the system is unstable.

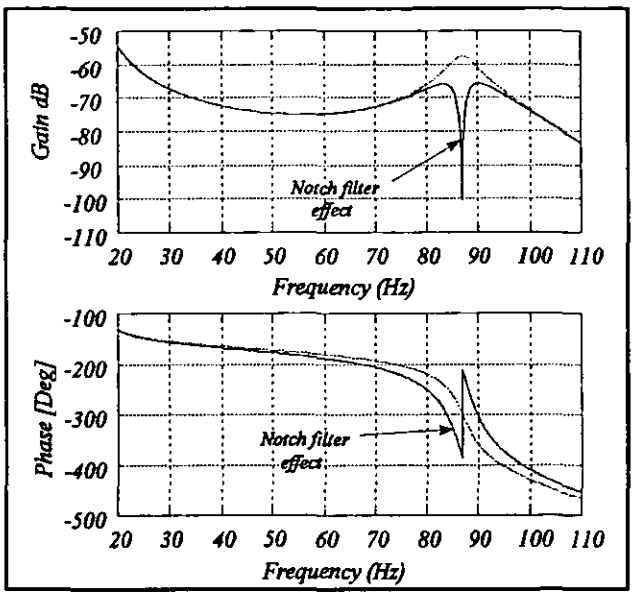

Figure 5.16 Effect on the 3rd bending mode of a notch filter (at 87Hz) which stabilises the suspension.

Extensive investigation of the notch filters found them to be ineffective at minimising the effects of flexibility and as the resonance of the first bending mode approached that of the control bandwidth the notch filter was found to be detrimental to both the ride quality and stability of the suspension. Any reduction in the peak gain due to the resonance was offset by a negative effect on the rigid body mode response. This may be explained by the fact that the phase characteristic of the notch filters will interfere with the stability margins of the main control loops. The Multi-Objective Optimisation System (MOPS) (see chapter 7) was used to tune the notch filters but no improvement could be made in their performance with respect to the lower frequency resonance modes.

Table 5.2 Classical Controller Results
All results completed with secondary quality track (A_r=1x10^{-6}m) with a constant vehicle velocity of 15 ms^{-1}.

Design Model	Quarter Car	Quarter Car	Half Car with rigid chassis	Half Car with 2 flexible bending modes 16.1, 44.3Hz	Half Car with 4 flexible bending modes, 16.1, 44.3, 86.9, 143.6 Hz
Control Method	Flux Density, Airgap	Flux Density, Airgap and Comp. filters	Flux Density, Airgap, Comp. filters	Flux Density, Airgap, Comp. and Notch filters	Flux Density, Airgap, Comp. and Notch filters
Central R.M.S Acceleration (ms^{-2})	0.658	0.45	0.335	0.365	1.11
R.M.S Acceleration at magnets (ms^{-2})	NA	NA	0.434	0.445	1.2
Front R.M.S Airgap (mm)	7.6	5	6.73	6.7	6.73
Rear R.M.S Airgap (mm)	NA	NA	6.72	6.75	6.75

5.5 Conclusions about the Classical Control Strategy

The classical control strategy has been demonstrated to be limited for the use of a 'soft' chassis with a first bending mode much below 20Hz. It may well be possible to use more sophisticated compensation techniques to reduce the effects of the flexible modes but reaching a compromise with such a control method while maintaining the suspension requirements will be difficult. The use of the MOPS system (see chapter 7) to optimise the existing control strategy showed that even when all of the parameters were considered there was no room for improvement and when a performance criteria was bettered it was always at the expense of another parameter.

Chapter 6: 'Modern' Control Techniques

6.1 Introduction

The classical control structure described in chapter 5 has proved highly effective but it has proved difficult to adapt it to account for lower frequency bending modes in a 'soft' chassis. The complexity introduced by the flexibility is such that a classical control technique is not well suited to the problem. The very nature of this type of control means that it will be difficult to achieve a solution without degrading the performance of another aspect of the suspension. Clearly a method is required which will provide similar or better suspension performance as the classical controller while at the same time allowing for the effects of greater chassis flexibility.

Modern Control techniques provide a method by which a number of objectives of the control problem can be addressed at the same time. Rather than considering the controller design one loop at a time the problem is considered as a whole, or in control terminology as a multi-input multi-output (MIMO) system. The theory is well established and has been seen in increasing numbers of practical applications, for instance in the aerospace industry.

A number of modern control techniques are available, but this thesis concentrates on the use of state feedback optimal control to solve the linear quadratic regulator problem (LQR) as it is generally known. Due to the inability to measure all of the states describing a system an optimal Kalman filter is used to derive the unmeasured states. Together these components provide the basis for the solution of the Linear Quadratic Gaussian (LQG) problem. As in chapter 5 the controller is developed first for a single degree of freedom Maglev, the quarter car model, and then for the half-car and finally for a model incorporating flexible bending modes.

6.2 Control of the Single Degree of Freedom (Quarter Car) Model

6.2.1 Full State Feedback

The literature on the optimal control problem is extensive [Friedland87] [Maciejowski89] [Kwakernaak72] [Bryson75] and is covered only briefly in this thesis.

The state space model of the one degree of freedom model developed in chapter 4

$$\dot{x} = Ax + Bu + Gw \qquad \textbf{6.1}$$

$$y = Cx + v \qquad \textbf{6.2}$$

in which vectors ω and v are white noise or zero mean Gaussian stochastic processes which are uncorrelated in time.

The LQG problem is to devise a feedback control law which will minimise a cost function

$$J = \lim_{T\to\infty} E\left\{\int_0^T (x^T Q_k x + u^T R_k u)dt\right\} \qquad \textbf{6.3}$$

where Q_k and R_k are weighting matrices, Q_k for the aforementioned combination of states and R_k for the control vector.

A control feedback matrix is required which will produce the effects of the cost function and the structure of the controller is shown in figure 6.1. The desired control law has the form:

$$u = -K x \qquad \textbf{6.4}$$

and is solved using the matrix Riccati equation:

$$A^T P_c + P_c A + P_c B R^{-1} B^T P_c + Q_k = 0 \qquad \textbf{6.5}$$

giving a positive semi-definite solution for P_c which is substituted into the following equation to give K,

$$K = R_k^{-1} B^T P_c \qquad \textbf{6.6}$$

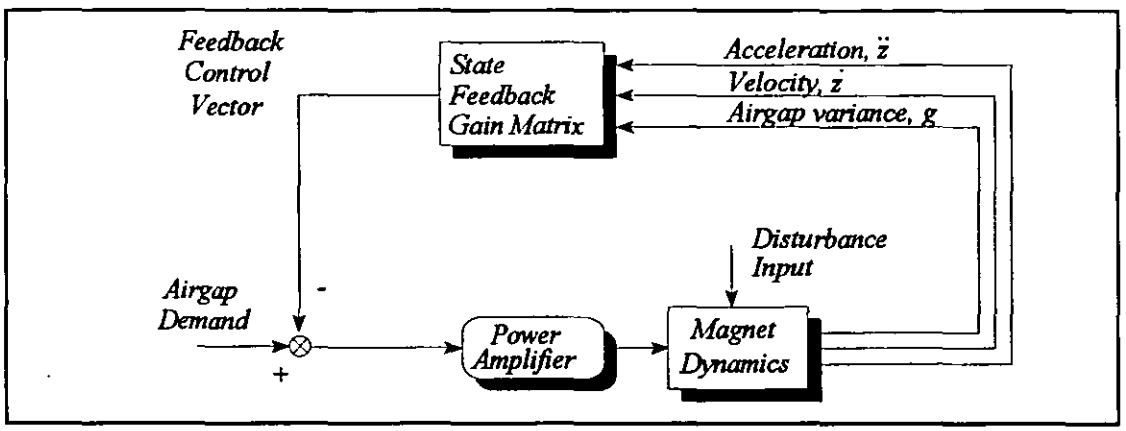

Figure 6.1 Full State Feedback.

The solution of the Riccati equation exists if the state space model is controllable, which means that any modes can be either controlled by an input, or that they are asymptotically stable. The resulting control law is guaranteed to stabilise the plant and yield a global minimum for the cost function given. In addition the stabilised plant now has robustness properties which in terms of classical control are an infinite gain margin (the gain in each channel can be increased indefinitely without losing stability) and a minimum of 60° of phase margin.

The major problem with the above process is the selection of the Q_k and R_k matrices reflecting the relative compromise between elements of the cost function. There is no certain way of making the selection and it may be difficult to relate the weighting parameters to the required performance. However in this problem there is a requirements specification which means that the desired variances of the elements of the cost function are known and a starting point for the design is to place the square of the inverse of the desired values in the leading diagonal of the Q_k matrix. This approach is a modification of what has been proposed elsewhere [Bryson75], and has proved highly effective in the following work although it will be seen that this only enables the random track input aspects to be accommodated. The responses to deterministic inputs and to load changes have to be considered separately. The model described by equations 4.36 and 4.37 uses acceleration, velocity and airgap as states. The suspension requirements given in section

3.5 include an r.m.s vertical acceleration of $0.455ms^{-2}$ and an airgap standard deviation of 0.005m, which gives a first attempt Q_k matrix:

$$x = \begin{bmatrix} \tilde{z} \\ \dot{z} \\ g \end{bmatrix}, \quad Q_k = \begin{bmatrix} \frac{1}{0.455^2} & 0 & 0 \\ 0 & 0 & 0 \\ 0 & 0 & \frac{1}{0.005^2} \end{bmatrix} \qquad 6.7$$

Notice that the element of Q_k on the leading diagonal corresponding to velocity is not weighted. This is done because no specific requirement is placed on the velocity and so no initial value is available. In fact the velocity is inherently constrained by weighting the acceleration, and this has been found to work effectively in practice.

The choice of weighting for the R_k matrix, which represents the cost of control, is rather more difficult. Considering the requirements of the Maglev suspension and the trade off between airgap and acceleration it can be seen that the voltage requirement is a secondary issue. The key design issues are the airgap and acceleration requirements, and the trade off between these also limits the voltage. Ideally the R_k matrix should be as small as possible but the solution of the Riccati equation requires a non-zero value. For this reason a value of $R_k=10^{-9}$ was used. The selection of R_k is discussed during the practical description in chapter 8. It should be noted that making the value of R_k smaller increases the feedback gains making them large and unwieldy and giving a high closed loop bandwidth. Clearly a compromise R_k value needs to be sought which gives a satisfactory response without creating so high a gain that the control demand becomes too large and sensitive to sensor noise.

The final choice of weighting factors is usually made by a trial and error process, but the initial values provide an excellent starting point. A more rigorous method for optimising the choice of weighting factors is described in chapter 7.

MATLAB® is used through-out this thesis for the control law design and analysis. The

MATLAB routine LQR(A,B,Q_k,R_k) provides a stable method for calculating the state feedback gain matrix, K. Using the covariance analysis technique the output can be calculated and the ride quality of the suspension assessed. Results are shown in Table 6.2 at the end of this chapter.

6.2.2 Response to force input

The suspension controller which has been developed is robust due to the inherent properties of the optimal control design process, and satisfies the ride quality requirements. However it is also required that the maximum airgap response with load changes be assessed. The model does not include a force input, and also a load change is not a stochastic process and is not explicitly taken into account in the above design. Remodelling the one degree of freedom model in terms of flux density so that acceleration is no longer a state means that a force input, f_d may be added to simulate load changes. Hence:

$$\begin{bmatrix} \dot{b} \\ \dot{\bar{z}} \\ \dot{g} \end{bmatrix} = \begin{bmatrix} -\frac{R}{NA_pK_i} & 0 & -\frac{K_gR}{NA_pK_i} \\ \frac{K_i}{M} & 0 & 0 \\ 0 & -1 & 0 \end{bmatrix} \begin{bmatrix} b \\ \dot{z} \\ g \end{bmatrix} + \begin{bmatrix} 0 & 0 & \frac{1}{NA_p} \\ 0 & \frac{1}{M} & 0 \\ 1 & 0 & 0 \end{bmatrix} \begin{bmatrix} \dot{z}_t \\ f_d \\ v \end{bmatrix} \qquad 6.8$$

Rather than recalculating the optimal controller using the above matrices, taking the old state feedback gain matrix and multiplying the first gain (corresponding to acceleration) by K_b/M to adjust for the use of flux density as a state, means that only this state is different. The eigenvalues of the model are identical, the control K is identical apart from the factor K_b/M on the acceleration state and a force input has been introduced.

The derivation of the state feedback gain matrix will ignore the force input f_d and the performance of the suspension will be exactly the same as the one using acceleration, velocity and airgap as states. Applying a force input to the above suspension shows that

it is robust to changes of over 40% in the load but the airgap deflection is large. For example a load change of 20% produces a 3mm maximum deflection for a 15mm nominal airgap which is slightly more than for the classical controller.

This deficiency shows clearly that the classical design has advantages in its intuitive nature. The optimal control design is probably robust to changes in the loading but it is not as transparent as the classical controller with respect to this objective. It was mentioned in chapter 4 that the choice of states affects the control law design and it may be possible to enhance the maximum airgap deflection response to load inputs by a new choice of states. A number of issues relating to alternative models have also been investigated [Paddison94] and this paper is included in appendix 3. Additionally in chapter 7 the use of a method to tune the optimal controller to find the best solution given a variable load is discussed.

6.2.3 Response to deterministic input

As with the classical controller the performance on a ramp input or deterministic feature is problematic due to the use of 'skyhook damping' within the control law, which despite giving superior performance for a stochastic input produces large airgaps on gradients. The effect is the result of having a measurement of absolute velocity in the feedback. In chapter 5 the maximum airgap deflection due to the gradient was enhanced through the use of third order complementary filters in place of the second order filters. This degraded the ride quality somewhat but the integral effect of the additional pole reduced the maximum airgap. It is logical that the introduction of an integral term into the above state feedback formulation will have a similar effect Given this motivation a model was developed with the integral of the airgap state as an additional state.

This new augmented model is discussed in chapter 7 where the methods of developing a globally optimised controller are introduced.

6.2.4 Optimal Design using a Kalman Filter

It is very unlikely that all of the states necessary for full state feedback are available. To overcome this drawback an optimal Kalman filter may be used which utilises a model of the system to be controlled to derive an estimate of the full state.

A Kalman filter is shown in block diagram form below. A and B represent the matrices of the model of the Maglev given in equation 4.36 and reproduced in equation 6.9.

$$\begin{bmatrix} \dddot{z} \\ \ddot{z} \\ \dot{z} \\ \dot{g} \end{bmatrix} = \begin{bmatrix} -\frac{R}{NA_pK_i} & 0 & -\frac{K_gK_bR}{NA_pMK_i} \\ 1 & 0 & 0 \\ 0 & -1 & 0 \end{bmatrix} \begin{bmatrix} \ddot{z} \\ \dot{z} \\ g \end{bmatrix} + \begin{bmatrix} \frac{K_b}{NA_pM} \\ 0 \\ 0 \end{bmatrix} [v] \qquad \textbf{6.9}$$

A modified C measurement matrix from equation 4.37 is given in equation 6.10:

$$\begin{bmatrix} g \\ b \end{bmatrix} = \begin{bmatrix} 0 & 0 & 1 \\ \frac{M}{K_b} & 0 & 0 \end{bmatrix} \begin{bmatrix} \ddot{z} \\ \dot{z} \\ g \end{bmatrix} \qquad \textbf{6.10}$$

The inputs to the filter are the control input and the measurement vector from the actual Maglev suspension.

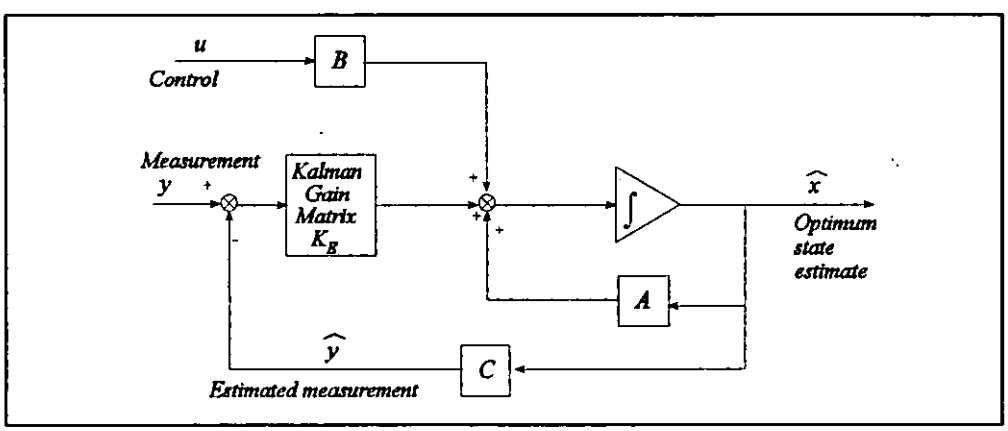

Figure 6.2 Kalman filter as an optimum observer

The Kalman gain matrix is designed to give an optimal response to the effects of the stochastic inputs to the filter such as the disturbance input (the track roughness) and the noisy measurement input. It minimises the mean square estimation error. Calculation of K_E is the dual of the calculation of the state feedback gain matrix, K, utilising the matrix Riccati equation given by

$$P_f A^T + A P_f - P_f C^T R_{ke}^{-1} C P_f + G Q_{ke} G^T = 0 \qquad \textbf{6.11}$$

and the solution of P_f allows the gain matrix to be calculated thus:

$$K_E = P_f C^T R_{ke}^{-1} \qquad \textbf{6.12}$$

Q_{ke} and R_{ke} are covariance matrices representing the expected inputs to the Kalman filter. Q_{ke} corresponds to the process noise which for the Maglev is the track input disturbance covariance and the control variations:

$$Q_{ke} = E\{ w\ w^T \} \qquad \textbf{6.13}$$

R_{ke} represents the measurement noise covariance:

$$R_{ke} = E\{ v\ v^T \} \qquad \textbf{6.14}$$

Usually these matrices are represented by the variances of the expected values of the corresponding vector which are placed along the leading diagonal. Off-diagonal terms may be used if there is information on cross-correlation of the noise elements.

Consider the following Kalman filter which uses measurements of flux density and airgap to estimate the full state of the model.

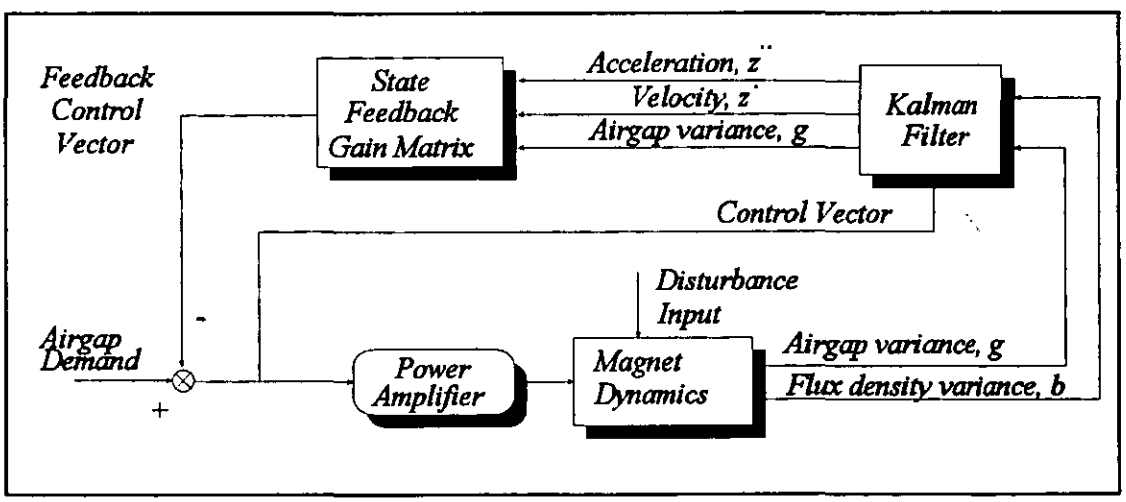

Figure 6.3 State Feedback using a Kalman Filter

The input disturbance is a vertical velocity due to the track input which is represented as a white noise. The description of this is given in chapter 3. But this is not the only input to the system and inclusion of the expected control input variance will help to make the system robust to parameter changes at the control inputs. Here the control standard deviation is assumed to be ±5V, hence:

$$Q_{ke} = \begin{bmatrix} 5^2 & 0 \\ 0 & 2\pi^2 A_r V \end{bmatrix} \qquad \textbf{6.15}$$

The process noise is a consequence of the two inputs which are be correlated. This correlation is not easily defined and is not used here.

The selection of the R_{ke} matrix is based on the noise variance on the measurements for flux density variance which is probably about ±0.02T and an airgap variance of about ±0.005m.

Having approximated the input to the Kalman filter a judgement needs to be made as to the relative weighting between the process and measurement noise covariances. Decreasing the value of R_{ke} relative to Q_{ke} places more reliance on the model than on the measurements. This is of course desirable if the measurements are of poor quality. The decision of the relative weight of Q_{ke} and R_{ke} is difficult to assess and in practice is undertaken during the commissioning stages of the controller when more accurate data about the inputs are available. Ideally the relative weightings of the two covariance matrices Q_{ke} and R_{ke} should be 40dB i.e. R_{ke} is 100 times smaller than Q_{ke} [Goodall89].

$$R_{ke} = \begin{bmatrix} 0.005^2 & 0 \\ 0 & 0.02^2 \end{bmatrix} \qquad \textbf{6.16}$$

The calculation of the Kalman Filter gain K_E has been undertaken using the MATLAB function LQE2(A,G,C_{measm},Q_{ke},R_{ke}/100), where the 100 factor on R_{ke} represents the signal to noise ratio. It should be noted that other structures of the Kalman Filter exist which

offer improvements when implementing the filter digitally [Franklin90].

The Kalman filter may be designed separately from the state feedback gain because of the separation principle which allows the control problem to be divided into two sub-problems the solutions of which are found from the Riccati equation assuming a linear model, a quadratic cost function and Gaussian stochastic processes (w and v). The estimated state is then used in exactly the same way as the full state was used in the LQR controller (as shown in figure 6.3) .

The robustness properties of the LQR technique are no longer guaranteed and LQG designs can exhibit arbitrarily poor stability margins and are consequently sensitive to parameter uncertainty [Doyle79]. Methods exist to overcome this effect of using the Kalman filter in combination with the full state feedback matrix and the properties of the LQG technique may be recovered using Loop Transfer Recovery (LTR) [Maciejowski89]. This is not considered in this thesis since it is considered more appropriate to a final design stage. It is expected that robustness issues will remain to be proved.

6.3 Control of the Half-Car Model

Having developed a satisfactory control strategy for the quarter car model the strategy can be readily extended to the half-car model. The structure of the controller is not altered. Following the successful Modal control approach demonstrated by the classical controller this was also chosen for the full LQG controller.

There is an increase in the number of measurements and the cost function needs to be changed to reflect the modal control approach. Hence the rigid body bounce and pitch accelerations are weighted appropriately. Writing the cost function in the form of equation 6.3 with the new state $x = \{z, \dot{z}, g_1, \theta, \dot{\theta}, g_2\}$.

$$J = \lim_{T\to\infty} E\left\{\int_0^T \left(\frac{1}{0.45^2}\ddot{z}^2 + \frac{1}{0.005^2}g_1^2 + \frac{L^2}{0.45^2}\ddot{\theta}^2 + \frac{1}{0.005^2}g_2^2 + 1e^{-9}(V_1^2+V_2^2)\right)dt\right\} \qquad 6.17$$

Clearly the velocity states do not play a part in this cost function. The distance between the magnets L, on the angular acceleration cost in equation 6.17 allows the translational acceleration criteria to be used for the angular acceleration.

Adding appropriate Kalman weightings to account for the additional measurements the following control structure is straightforward to implement. It should be noted that for a perfect model within the Kalman filter the LQG controller will give the same performance as the equivalent LQR controller.

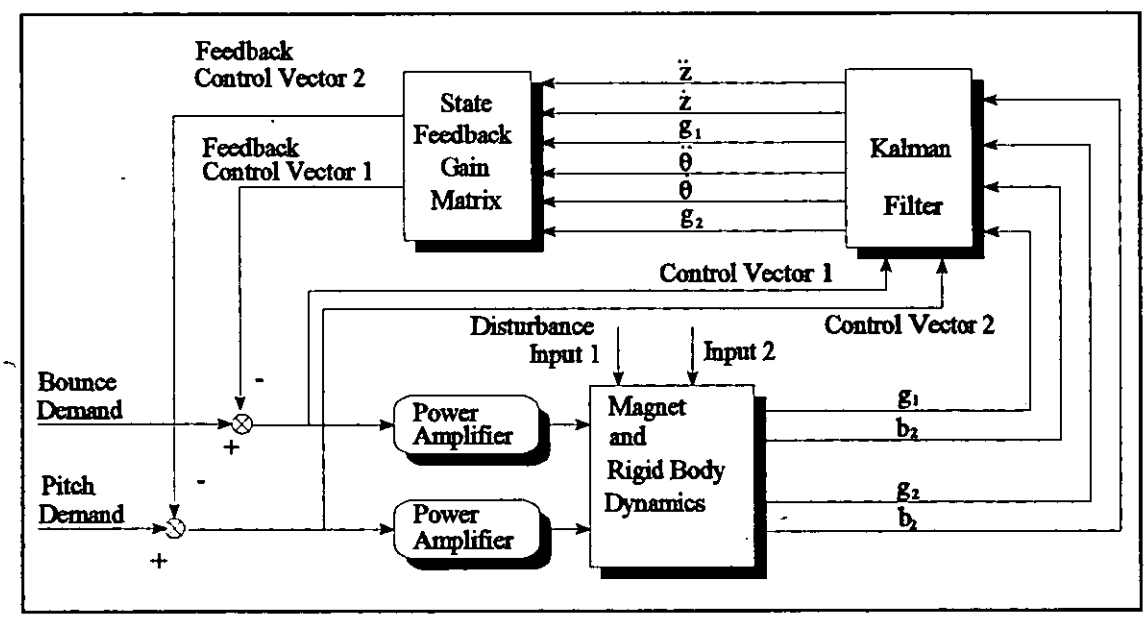

Figure 6.4 LQG Modal Control of the half-car model

The performance of the above controller is presented in table 6.2 in terms of ride quality. The LQG modal suspension performance is equivalent to the quarter car suspension, which is not surprising given the fully controllable nature of the model, the properties of the control approach and the consistency of the cost function.

6.4 Modal Control of the Chassis with Flexibility

The addition of flexibility as described in chapter 4 results in additional coupling into and

out of the rigid body modes. The control structure does not change from that shown in figure 6.4 but a reappraisal of the cost function is required.

Applying the same cost function as given in equation 6.17 will provide a stable suspension but the effects of the flexible bending modes will not be minimised explicitly. The accelerations due to both the rigid and flexible body bending modes need to be minimised because both contribute to what is perceived in terms of ride quality. As was shown in chapter 4 the net acceleration is a linear combination of rigid and flexible body states. Hence it is easy to rewrite the cost function to minimise this net acceleration and this results in a reduction of the effects of flexibility on ride quality and stability

$$J = \lim_{T\to\infty} E\left\{\int_0^T \left(\frac{1}{0.45^2}\ddot{z}_{net}^2 + \frac{L^2}{0.45^2}\ddot{\theta}_{net}^2 + \frac{1}{0.005^2}(g_1^2 + g_2^2) + 1e^{-9}(V_1^2+V_2^2)\right)dt\right\} \qquad \textbf{6.18}$$

where

$$\ddot{z}_{net} = \ddot{z} + \phi_1(h)\ddot{q}_1 + \phi_3(h)\ddot{q}_3 \qquad \textbf{6.19}$$

represents the net vertical acceleration due to the rigid body modes and the first two symmetrical body bending modes at a position h along the beam. The rotational acceleration can be written in a similar form.

The number of flexible bending modes is truncated at 4 because any higher modes are at frequencies well beyond the bandwith of the controller.

The following set of simulation results investigates the effects of varying the resonance frequency on stability and ride quality of the Maglev. Some of the results for the classical controller with notch filters are included to facilitate comparison.

Table 6.1 Flexibility investigation

Figure #	Bending Modes in Cost Function Frequency [Hz]				Modes in the Model Bending Mode Frequency [Hz]			
	1st	2nd	3rd	4th	1st	2nd	3rd	4th
6.5	5 to 35	13.8 to 96.6	None	None	5 to 35	13.8 to 96.6	None	None
6.6	5 to 35	13.8 to 96.6	27.1 to 189	44.8 to 313	5 to 35	13.8 to 96.6	27.1 to 189	44.8 to 313
6.7	5 to 35	13.8 to 96.6	None	None	5 to 35	13.8 to 96.6	27.1 to 189	44.8 to 313
6.8	5 to 35	13.8 to 96.6	None	None	5 to 35	13.8 to 96.6	None	None
6.9	5 to 35	13.8 to 96.6	27.1 to 189	44.8 to 313	5 to 35	13.8 to 96.6	27.1 to 189	44.8 to 313
6.10	16.1	44.3	None	None	16.1 ±10%	44.3 ±10%	None	None
6.11	16	44.3	86.9	143.6	16 ±10%	44.3 ±10%	86.9 ±10%	143.6 ±10%
6.12	16	44.3	None	None	16	44.3	None	None
6.13	16	44.3	86.9	143.6	16	44.3	86.9	143.6
6.14	16	44.3	86.9/ None	143.6/ None	16	44.3	86.9	143.6
6.15	16	44.3	86.9/ None	143.6/ None	16	44.3	86.9	143.6

For all of the figures apart from 6.14 and 6.15 the magnets are at the nominal positions of 25 and 75% of the vehicle length except where otherwise indicated.

Figures 6.5, 6.6 and 6.7 show the limits of the full state feedback and LQG controller designs when the stiffness of the vehicle is decreased. The results point to the significance of the position of the magnets on the modes shapes and the number of flexible bending modes.

The so called spillover effect occurs when the unmodelled dynamics such as flexible modes 'spill over' the region of control and begin to affect the system performance. It is a term usually associated with flexible structures which by their nature have an infinite number of bending modes which cannot be included in the design model used to create the controller. It is something of a contradiction in terms to consider the spillover effect for an LQR full state feedback controller since clearly not all of the states are available but figure 6.7 does demonstrate that a reduced order LQG design in the spillover investigation exhibits no stability variation with stiffness. This is highly significant since it will always be impossible to account for all of the flexible bending modes in a chassis and the reduced order LQG design shows that a truncation of the number of bending modes can be applied without a serious loss of stability. This result agrees with work on reduced order controllers for conventional wheeled vehicles with flexible chassis which was reviewed in chapter 2 [Capitani89].

It should be noted that the lowest representative damping ratio does not always correspond to the same eigenvalue, when a parameter is varied. This means that nonlinear effects appear on the following results where the two lowest representative damping ratios intersect.

With two bending modes and the magnets at 25 and 75% of the vehicle length the stability is very good. This is mainly because these magnet positions are near the nodal points of each of the two flexible bending modes, which are consequently not greatly excited. Moving the magnets (away from the nodes) increases the excitation effect of the magnet action. With four flexible bending modes the magnet positioning is more difficult as every position will be some distance away from at least one node. This is not important for a stiff vehicle but at low stiffnesses the excitation of the third bending mode can be just as destabilising as the first bending mode.

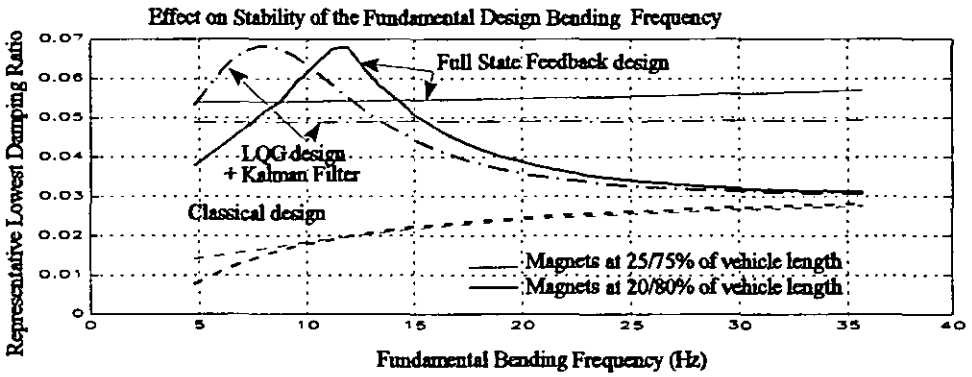

Figure 6.5 Effects of 2 flexible bending modes

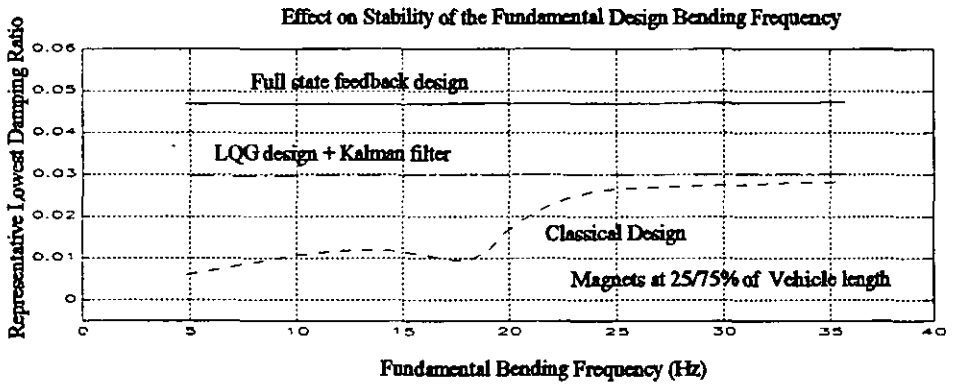

Figure 6.6 Effects 4 flexible bending modes

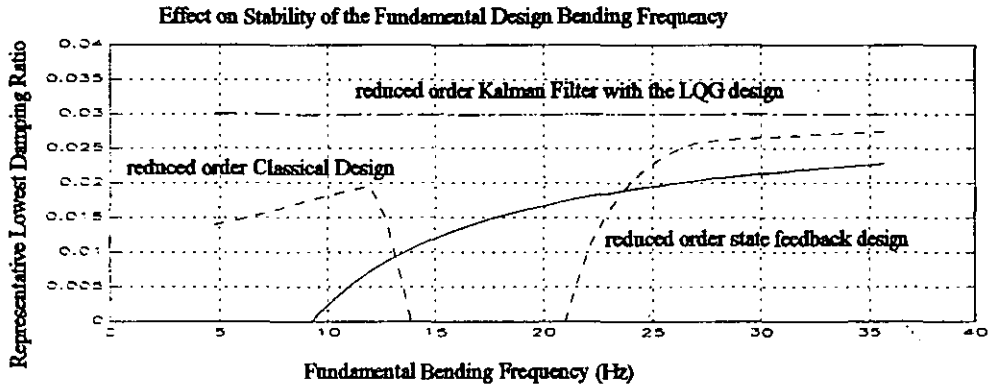

Figure 6.7 Spillover effects (magnets at 25/75% of the vehicle length)

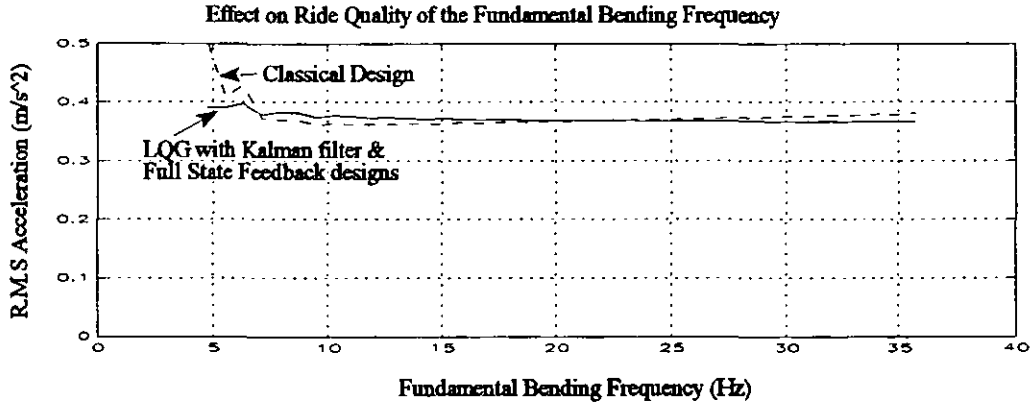

Figure 6.8 Ride Quality variation with stiffness for 2 flexible bending modes

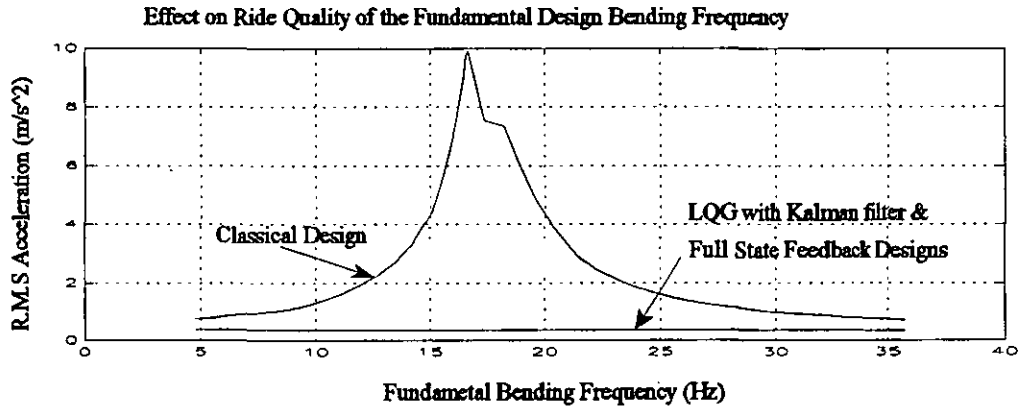

Figure 6.9 Ride Quality variation with stiffness for 4 flexible bending modes.

Clearly the ride quality of the LQG with Kalman filter and full state feedback controllers remains virtually unaffected by variations in the design first bending frequency. This is in marked contrast to the classical design strategy which is limited due to the excitation of the 3rd bending mode when the first four flexible bending modes are considered.

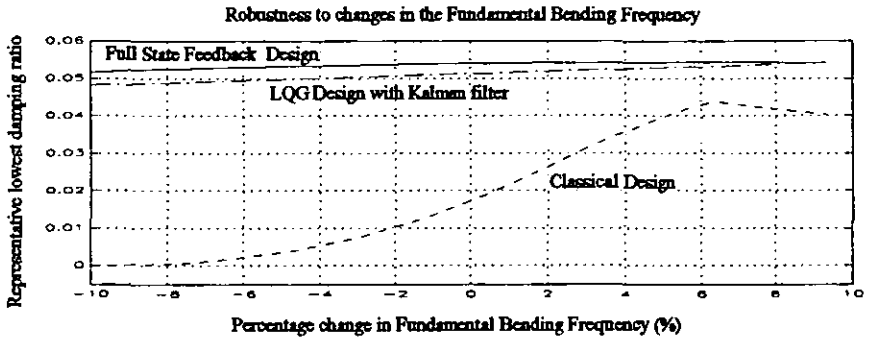

Figure 6.10 Stability variation due to changes in stiffness with 2 flexible bending modes

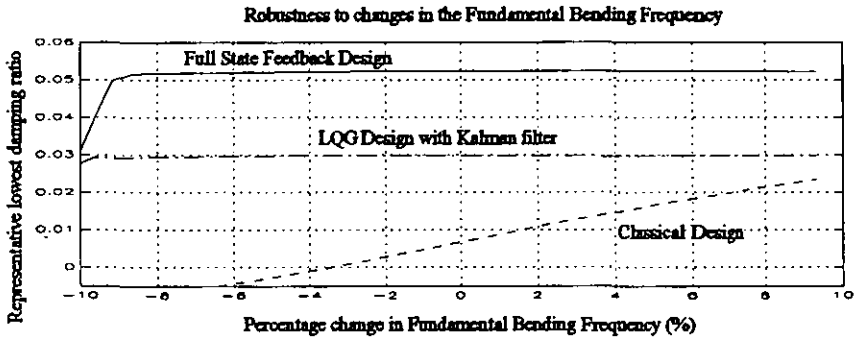

Figure 6.11 Stability variation due to changes in stiffness with 4 flexible bending modes

As the stiffness (represented here by the first bending frequency) is varied from the design frequency both the full state feedback and LQG with Kalman filter designs show stability up to a change of 10%. This shows that the model for the these controllers need not be so accurate. The expected bending frequency deviation due to loading and temperature changes is about 3% and this is well within the capability of the full state feedback and LQG with Kalman filter design approachs which contrasts well with the classical controller which is sensitive to changes in the stiffness.

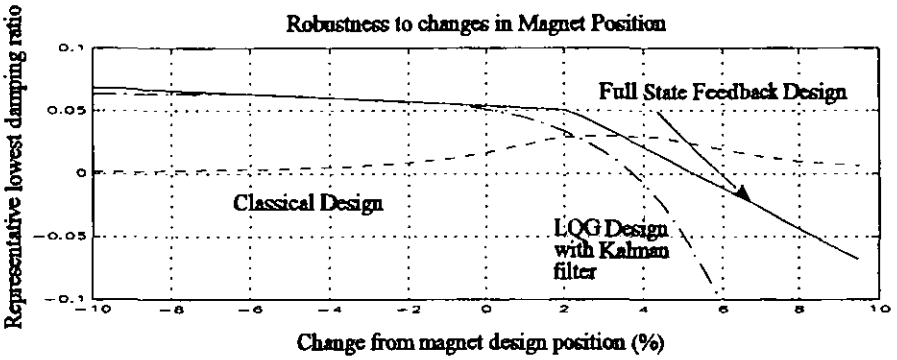

Figure 6.12 Stability variation due to changes in magnet positions with 2 flexible bending modes

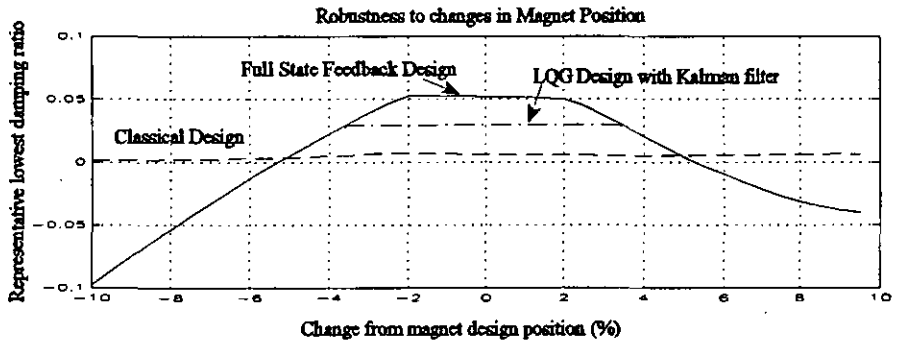

Figure 6.13 Stability variation due to changes in magnet positions with 4 flexible bending modes

Varying the position of the magnet away from the design position represents uncertainty in the bending mode shape, which in reality might be the effect of windows or doors. For two flexible bending modes the stability of the full state feedback and LQG with Kalman filter strategies is limited to a variation of 4 to 5% in the magnet position in one direction only. For the case of four flexible bending modes the magnet cannot be varied by more than 5% in either direction.

Clearly these results reflect the increasing excitation of the modes shapes as the magnets are moved away from the nodes of the bending modes. Earlier results have shown that if exact knowledge of the mode shapes is available there is no difficulty in maintaining stability by the full state feedback and LQG with Kalman filter controllers. It can be concluded from this result that mode shape models for the first four bending modes must

be within 4% of the design amplitude variation. Unlike the classical controller the LQG controller significantly reduces the 3rd resonance mode peak (in the bounce mode). This can be seen in figure 6.16.

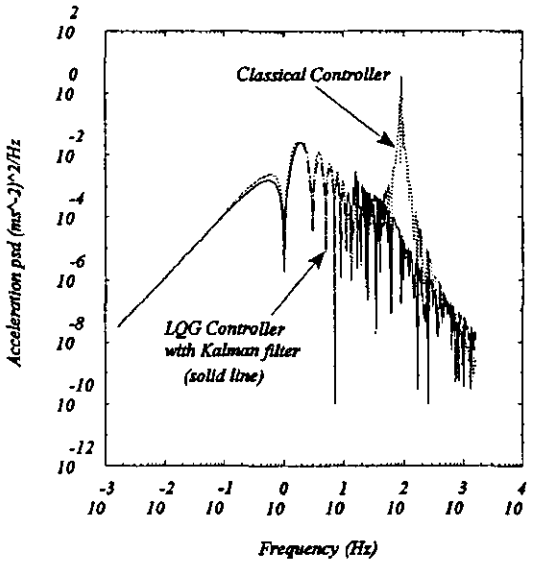

Figure 6.16 Comparison of the LQG Controller with a Kalman filter and Classical Controller acceleration frequency responses.

6.5 Conclusions about the Modern Control Strategy

It has been shown that the 'modern' control approach provides a suspension which can cope with a flexible chassis with a first resonance bending frequency of below 8 Hz. The LQG controller with Kalman filter is stable with respect to variations of up to ±10% in the first bending frequency and up to ±5% in the amplitude variation of the flexible mode shape. The LQG controller with Kalman filter is able to achieve the ride quality to the level specified for all bending frequencies examined.

The suspension deflection due to loading has been considered for the LQG control design with a Kalman filter but not specifically designed for. The maximum deflection due to a 20% loading was about 3mm instead of ideally being below 1mm. The problem is considered further in chapter 7.

Table 6.2 : Suspension Performance with secondary track (A_r=1x10^{-6})

Design Model	Quarter Car Suspension		Half Car Model			
			rigid chassis	flexible chassis		
				2 flex modes; 16.1,44.3Hz	4 flexible modes; 16.1,44.3,87,140 Hz	
Control Method	Optimal Full State Feedback	LQG & Kalman Filter	LQG & Kalman Filter	LQG & Kalman Filter	Optimal Full State Feedback	LQG & Kalman Filter
R.M.S central Acceleration (ms^{-2})	0.46	0.46	0.365	0.371	0.352	0.353
R.M.S Acceleration at leading airgap (ms^{-2})	NA	NA	0.513	0.511	0.47	0.47
R.M.S Airgap leading (mm)	4.99	5.0	4.81	4.82	5.00	5.00
R.M.S Airgap trailing (mm)	NA	NA	4.81	4.83	5.00	5.00
Maximum Airgap for a 10% gradient (mm).	168	165	NA	NA	NA	NA
Maximum Airgap change for a 20% load change (mm)	3.0	3.0	3.0	3.0	3.0	3.0

Chapter 7: Optimisation Studies

7.1 Introduction

One of the themes of this thesis has been the inherent conflicts present in the design of a suspension. This chapter presents a concurrent control technique which helps a designer to resolve the conflicting demands of a suspension specification and to produce a globally optimised controller.

The design study presented here uses the ANDECS®-MATLAB® design environment to satisfy simultaneously the suspension requirements corresponding to both random and deterministic inputs. The classical and 'modern' control strategies for the quarter car suspension models presented in chapters 5 and 6 are optimised and contrasted, and their respective performance limits are investigated.

7.2 ANDECS-MATLAB Environment

7.2.1 Design Philosophy

The Analysis and Design of Controlled Systems (ANDECS) design environment has been developed with the philosophy that the design objective and the corresponding specifications need to be iteratively adapted in order to find the best compromise between potentially conflicting design goals [Grübel93].

ANDECS has been evolved over many years as an open engineering software environment and allows many different software tools from different software companies to operate within it. ANDECS has various in-built design tools, among them the Multi-Objective Programming System (MOPS) which is a databased design environment specifically for multi-objective design optimisation. Design history is recorded on an automatically evolving database which allows a comparison of different designs and access to self

documenting facilities [Joos91]. This is particularly important for control design with modern computer aided control system design (CACSD) software which allows the designer a (sometimes) bewildering multitude of design choices.

Figure 7.1 shows the ANDECS-MOPS design logic and also shows where the MATLAB component of the design process is incorporated for the study described here. It should be stressed that this need not be MATLAB, and interfaces to other design software are possible.

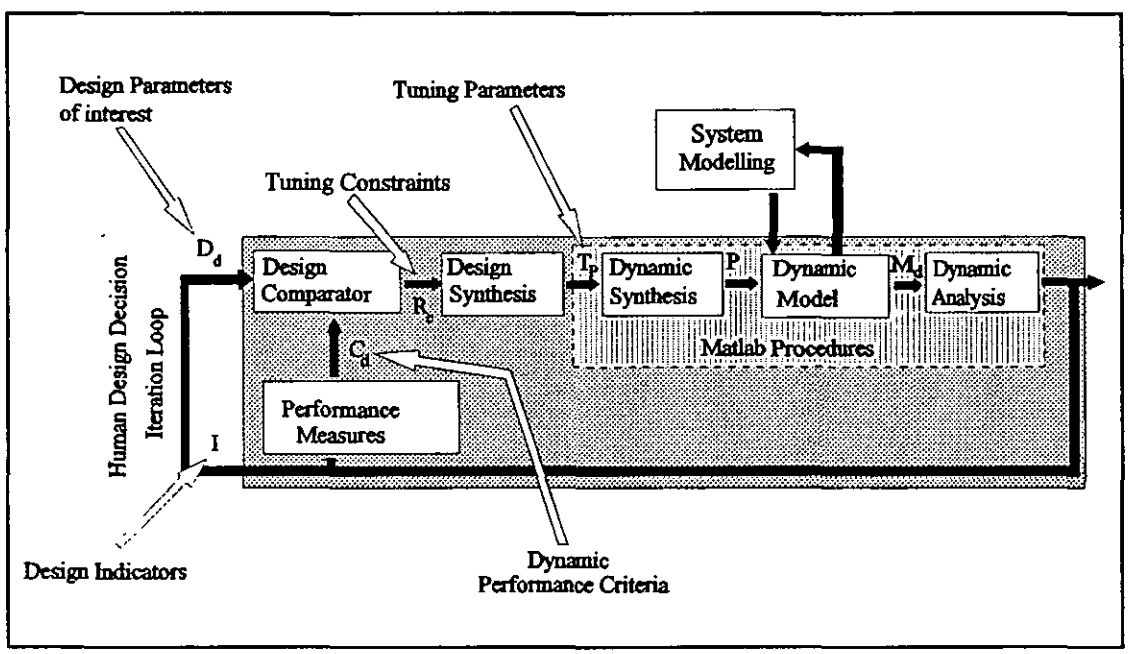

Figure 7.1 ANDECS-MOPS Design Logic for Maglev suspension design

The objective of the design synthesis is to calculate a control law $P(T_p)$ from a set of tuning parameters T_p. T_p may consist of any parameters which affect the controller design: for the Maglev suspension they will be either the weighting coefficients of a Riccati equation for the optimal controller or the coefficients of compensation filters etc for the classical controller.

The dynamic model M_d contains both the system dynamics and the controller, which are analysed as a complete system in the dynamic analysis module. In this case the dynamic

analysis consists of time and frequency responses which are transformed into a set of dynamic performance criteria C_d. With reference to the results of the analysis which are shown to the designer as a set of performance indicators, I_p the designer can then shape the so-called design director vector D_d. The iterative loop then compares the criteria C_d with the design director vector D_d in the design comparator and searches for a combination of tuning parameters T_p, which, while remaining within performance or tuning constraints R_c, leads to the best compromise controller.

A min- max vector optimisation is used across the design comparator and design synthesis blocks. Different numerical methods for vector optimisation are available in the control subroutine library of ANDECS called Reliable Numerical Algorithms for Control System Analysis and Design (RASP) [Grübel91]. To find the 'best' solution it was found to be advantageous to experiment with different numerical solvers for the optimisation process, as a change in initial conditions or solver could lead to an improved solution.

The design comparator is the key to the process, and the maximum function is used:

$$\alpha = \max\left\{\frac{c_i(T_p)}{d_i}\right\} \qquad 7.1$$

where c_i and d_i are components of the criteria vector C_d and the design director vector D_d and for $\alpha<1$

$$C_d \leq \alpha D_d < D_d \qquad 7.2$$

The smaller the criteria vector C_d is compared to the design director vector D_d the better is the design. The max function α should be minimised as a function of the tuning parameters T_p of the dynamics synthesis procedure.

Design synthesis uses the minimum function:

$$\min\ \alpha(T_p) \rightarrow T_p \qquad 7.3$$

subject to the performance and tuning constraints R_c which may be expressed by for the performance criteria as

$$c_j(T_p) \leq c_{j\text{-max}} \qquad 7.4$$

and for the tuning constraints as

$$T_{p\ k\text{-min}} \leq T_{p\ k} \leq T_{p\ k\text{-max}} \qquad 7.5$$

The procedure may on first sight seem fairly automatic, yet the role of the designer in the loop is very significant in steering the design via the design director vector.

ANDECS provides a visual environment Visual and Interactive Steering for Task Activation (VISTA) which allows an online appreciation of conflicts arising in a multiple criteria optimisation. This helps to avoid unfeasible criteria and supports the designer in making locally consistent design decisions and is one of the main advantages of using the ANDECS environment. The diagram below shows the criteria conflict editor for a generic active suspension problem. This is actually the optimisation of the control structure given later and demonstrates how some of the criteria have been improved (arrows down) while others have deteriorated (arrows up). The thick black line represents the best control achieved with this search process. The playoff between MAXG (the maximum airgap deflection on a gradient) and the ACC1 (r.m.s acceleration) is clearly seen.

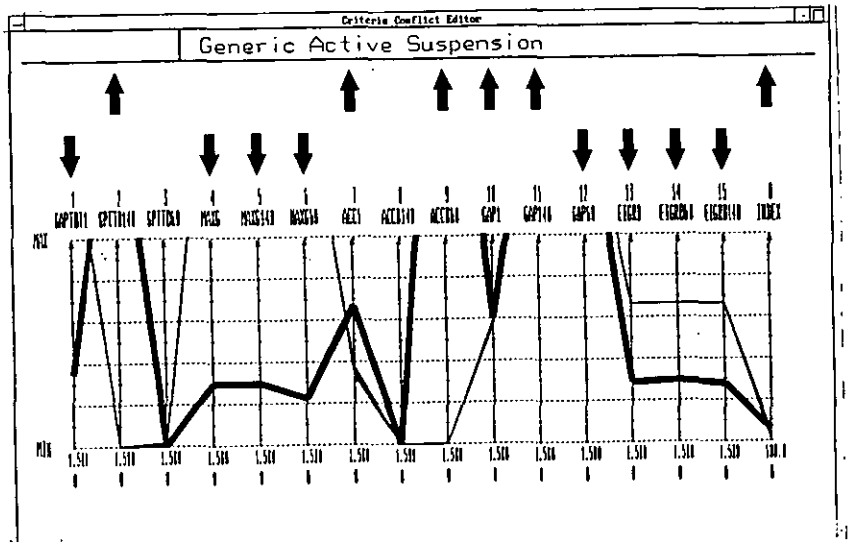

Figure 7.2 MOPS Criteria Conflict Editor

Figure 7.3 shows examples of the time domain and frequency domain responses indicating how the optimisation is progressing. The effect of a step response on the acceleration is shown, as well as a Bode plot of the acceleration response.

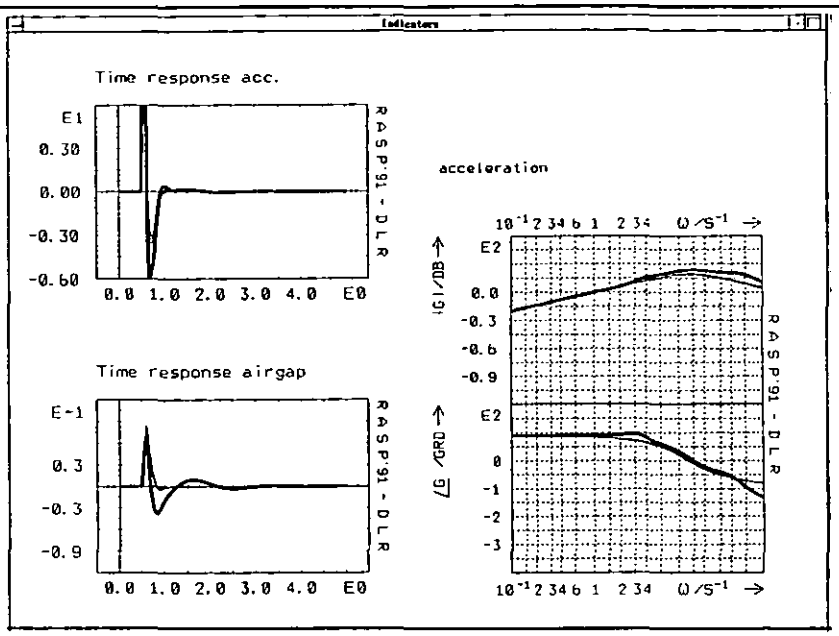

Figure 7.3 MOPS Indicators which are in this case time and frequency domain responses.

7.2.2 Integration of ANDECS and MATLAB

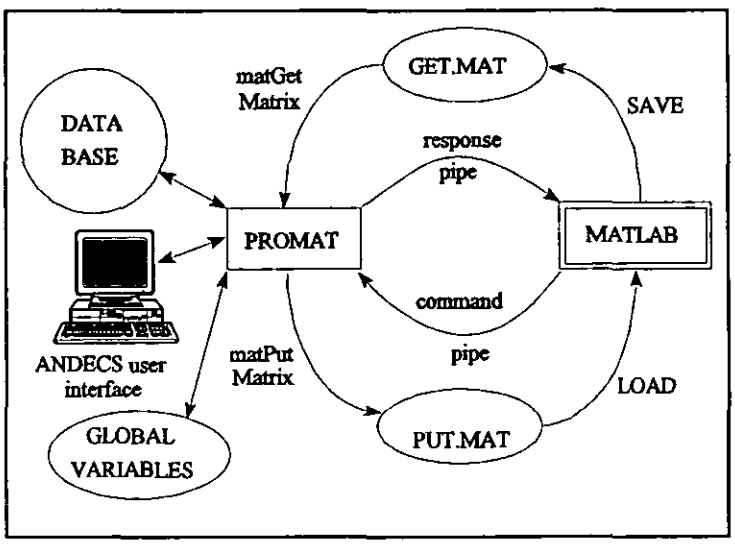

Figure 7.4 ANDECS-MATLAB communication

The ANDECS-MATLAB coupling is based on the MATLAB external interface library and allows access to the complete functionality of MATLAB [Bals94].

The ANDECS module PROMAT is connected with MATLAB via two pipes for passing commands from the master process ANDECS to the slave process MATLAB and for returning the results. For transferring data between the ANDECS database and the MATLAB workspace two binary files put.mat and get.mat are used.

The benefits of using the ANDECS-MATLAB interface are:

1. Access to an automatically evolving database of design steps allowing back tracking of the design history.
2. Online visualisation of the optimisation indicating conflicts and compromises which may have to be made.
3. A proven Multi-Objective Optimisation System with a choice of optimisation routines and individual criteria and constraint formulations.

The advantages of providing MATLAB functionality within ANDECS are:

1. Transportability of models developed in MATLAB which is rapidly becoming a standard tool in virtually every laboratory.
2. Access to the expanding range of MATLAB toolboxes.
3. Familiarity with MATLAB enables ANDECS to be understood faster.

7.3 Controller Designs

Chapters 5 and 6 have described two control strategies for the quarter car Maglev suspension. Both strategies provided satisfactory ride quality and guidance for the Maglev on flat track in response to the random track roughness. This was not the case however when the performance of the suspension on a deterministic feature such as the transition onto a gradient was considered. For such a deterministic input the airgap changes were found in most cases to be orders of magnitude too large. Hence when designing a controller the airgap changes due to the deterministic features must be restricted to about half the airgap (about 7.5mm) such that there is still clearance to

accommodate random changes in the airgap due to the guideway roughness. Also it was shown in chapters 5 and 6 that the maximum airgap deflection due to a load change could be independently designed in the classical control formulation, but the LQG formulation gave no method of implicitly accommodating this design requirement. Using the MOPS module it is possible to incorporate all of the suspension requirements for both control strategies, and to search for a compromise control law.

7.3.1 Application to the Classical Control Strategy

The classical control strategy consists of four tunable functions; the flux loop with a proportional plus integral (P+I) stage, the main position loop with a phase advance compensator and the ride control filter and finally the double integrator.

The coefficients of all four functions could be tuned by MOPS but the flux loop compensator has been excluded because the 50Hz bandwidth is easy to achieve, and changes to the compensator then only have a minimal effect on the system performance.

The three remaining components of the suspension were tuned using the MOPS module. The gain of the main loop determines the response to load changes, and the double integrator and ride quality filter frequencies determine the response to track inputs.

Using MOPS it would be possible to vary all of the coefficients of each filter during the optimisation process, but in practice prior knowledge is available which not only reduces the number of variables, but also avoids unstable filter responses which might occur if MOPS was allowed complete freedom of coefficient choice. Butterworth filter responses have been found effective in the Birmingham Maglev controllers and so are used to dictate sets of coefficients for a given filter frequency.

The use of third order filters with a zero on the numerator for the ride filters $H_r(s)$ is suggested since this form has already shown better performance with respect to

deterministic inputs than the second order filter [Goodall78]. Here ω_r is the tunable parameter.

$$H_r(s) = \frac{1 + \frac{2}{\omega_r}s}{1 + \frac{2}{\omega_r}s + \frac{2}{\omega_r^2}s^2 + \frac{1}{\omega_r^3}s^3} \qquad 7.6$$

The double integrator needs to be self zeroing in the presence of a d.c. offset so a third order response of the form $H_i(s)$ is necessary. Clearly the filter frequency ω_i is the tuning parameter.

$$H_i(s) = \frac{\frac{1}{\omega_i^3}s}{1 + \frac{2}{\omega_i}s + \frac{2}{\omega_i^2}s^2 + \frac{1}{\omega_i^3}s^3} \qquad 7.7$$

The tuning of the phase advance compensator involves tuning the time constant, τ_{pa} and the gain K_{pa}. The filter has the form:

$$H_{pa}(s) = K_{pa}\frac{1 + s\tau_{pa}}{1 + s\alpha_{pa}\tau_{pa}} \qquad 7.8$$

and α_{pa} is a constant ($\alpha_{pa} < 1$).

The tuning parameters to be used by MOPS for the classical design are then:

$$T_p = \{ K_{pa}, \tau_{pa}, \omega_i, \omega_r \} \qquad 7.9$$

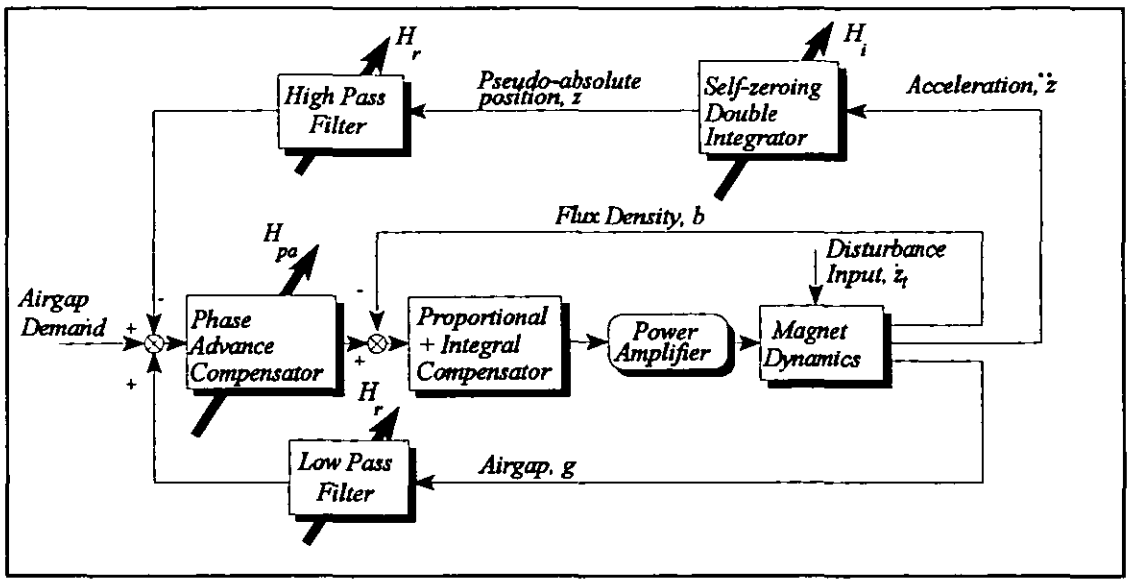

Figure 7.5 Classical controller showing the functions to be tuned.

7.3.2 Application to the Modern Control Strategy

Chapter 6 presented the LQG controller and stated that the separation principle allowed the calculation of the state feedback gain matrix independently of the Kalman filter gain.

The Kalman filter is used to estimate all of the states while still using the same measurements as the classical controller, which is done to ensure that the two controllers are comparable. The Kalman filter weighting matrices, Q_e and R_e are specified by the nature of the process and measurement noises which are known and therefore not available for tuning. The relative weighting of the two matrices could be tuned using the MOPS system but this would result in an unrealistic Kalman filter gain which would bear little relation to the physical system. For this reason the 40dB signal to noise ratio discussed in chapter 6 was used to indicate the relative gain of Q_e with respect to R_e [Goodall89]. Hence the Kalman filter does not figure in the MOPS optimisation of the system.

The selection of the state feedback matrix was seen to depend on the relative weightings of Q_k and R_k used in the Riccati equation. All elements of these matrices could be chosen

by MOPS but this would result in R_k being made as small as possible, making the control gains unrealistically large. For this reason R_k was left as the value given in chapter 6 of 10^{-9}. The values along the leading diagonal of Q_k have given satisfactory results and so, to simplify the optimisation, only these terms will be used as tuning parameters.

Adjustment of the weighting factors will alter the response to the deterministic input though there is no direct relationship showing how this can be done to improve the suspension. To overcome the skyhook damping effect on deterministic features a more direct approach is to augment the model by including the first and second integral of the airgap in the feedback. This will have the effect of reducing low frequency variations in the airgap and the degree to which this is done is influenced by the size of the gains placed in the integral feedback path. The process of choosing these gains is ideally suited to the use of MOPS. The use of integral feedback to improve the response to deterministic inputs is an extension to an approach discussed for a conventional vehicle [Davis88].

The structure of the controller to be tuned is shown in figure 7.6.

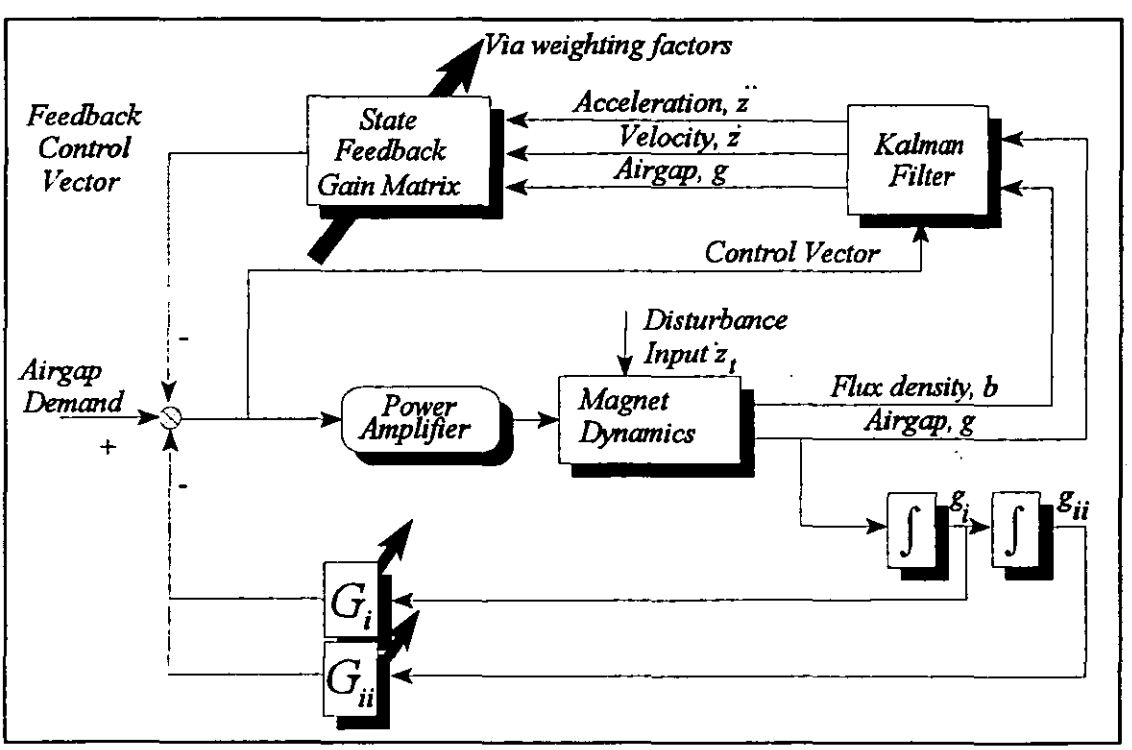

Figure 7.6 LQG Control strategy with elements to be tuned by MOPS

The tuning parameters then become for the LQG design:

$$T = \{ Q_{kz}, Q_{kv}, Q_{kg}, G_{ii}, G_{ii} \} \qquad 7.10$$

where the first three terms refer to the weighting factors for the states: acceleration, velocity and airgap.

7.4 Analysis and Simulation

The most difficult part of the MOPS process is to formulate the performance criteria such that a reducing criteria corresponds to satisfying a goal better. In addition to minimising the performance index, constraints may be applied to certain performance measures which they cannot exceed. For the Maglev suspension the acceleration is to be minimised within the constraint of the limited airgap. The performance criteria are as follows:

1. r.m.s acceleration level with random track - minimise relative to 0.45ms^{-2} target.
2. r.m.s airgap change with random track - constrained to no more than 5mm.
3. maximum airgap change in response to a transition onto a gradient - constrain to no more than ±7.5mm
4. constrain eigenvalues to the left hand side of the complex plane to ensure stability (an in built MOPS function).

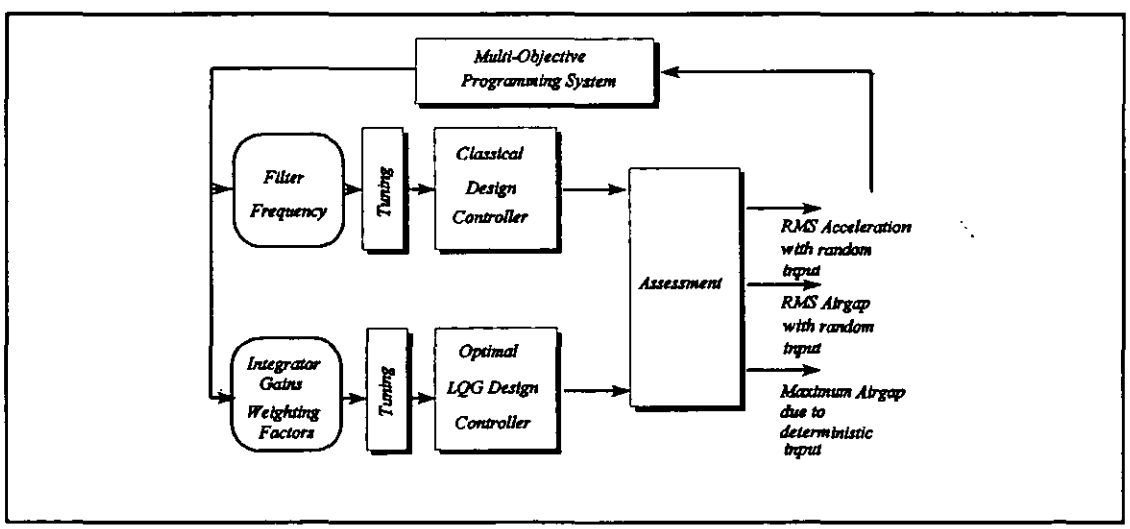

Figure 7.7 Assessment strategy

The assessment strategy is shown in figure 7.7 and consists of a covariance analysis to determine the r.m.s acceleration and airgap in response to secondary quality track and a time response which determines the maximum deflection of the airgap during the transition on to either a 10% or 5% gradient. Note that separate optimisations of the LQG and Classical controllers are performed using the appropriate tuning parameters, but in each case the assessment is on the basis of identical performance criteria

7.5 Results

Table 7.1 : Performance comparison

Design Method	Classical Controller		LQG Controller		LQG Controller (No deterministic input requirement)	
Gradient	10%	5%	10%	5%	10%	5%
R.M.S Acceleration (ms^{-2})	0.7	0.57	0.62	0.52	0.46	0.46
R.M.S airgap (mm) (random input)	5.0	5.0	5.0	5.0	5	5.0
Maximum Airgap (mm) (deterministic input)	7.5	7.5	7.5	7.56	165	82

The above set of results show that the required r.m.s acceleration cannot be achieved by either of the controllers even with the a reduced gradient of 5%. The LQG controller achieves a slightly better performance, although with the Kalman filter it will be more complex than the classical controller. The r.m.s and maximum airgap changes are included to demonstrate that MOPS has satisfied the specified constraints on their values.

The last two columns show the effect when the maximum airgap is not constrained. In this case the r.m.s acceleration is satisfactory but the deflections due the transition onto a gradient are very large. The comparison between the last column and the results for the full optimisation applied to both the classical and LQG controllers shows that MOPS with integral feedback has reduced the deterministic airgap changes by a factor of 20 with only a 50% degradation in ride quality which may be expressed diagrammatically by figure 7.8.

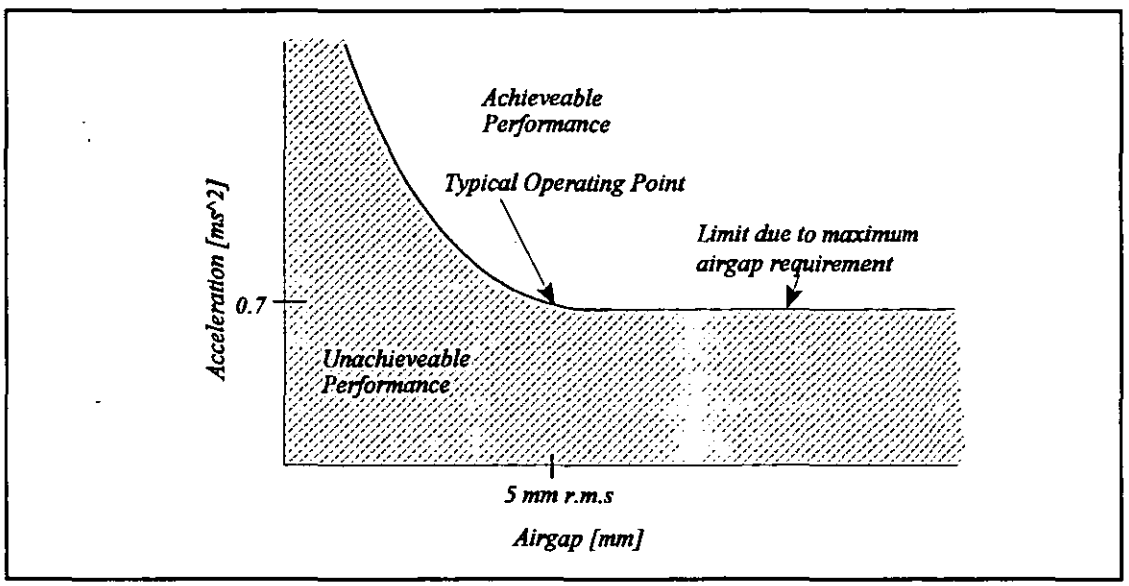

Figure 7.8 Acceleration and Airgap conflicting requirements

The above results represent the Maglev with a nominal operating load. As described in chapter 6 the original model which was used when the MOPS optimisation was undertaken did not account for force inputs and so the controller optimisation excluded minimisation of the maximum airgap deflection due to loading. Using the model discussed in chapter 6 this requirement could easily be incorporated.

The time response of the airgap changes during the transition of both Maglev suspensions onto a gradient is of interest. It shows that despite the different control law formulation, the 7.5mm limit is adhered to even though the transient responses are quite different.

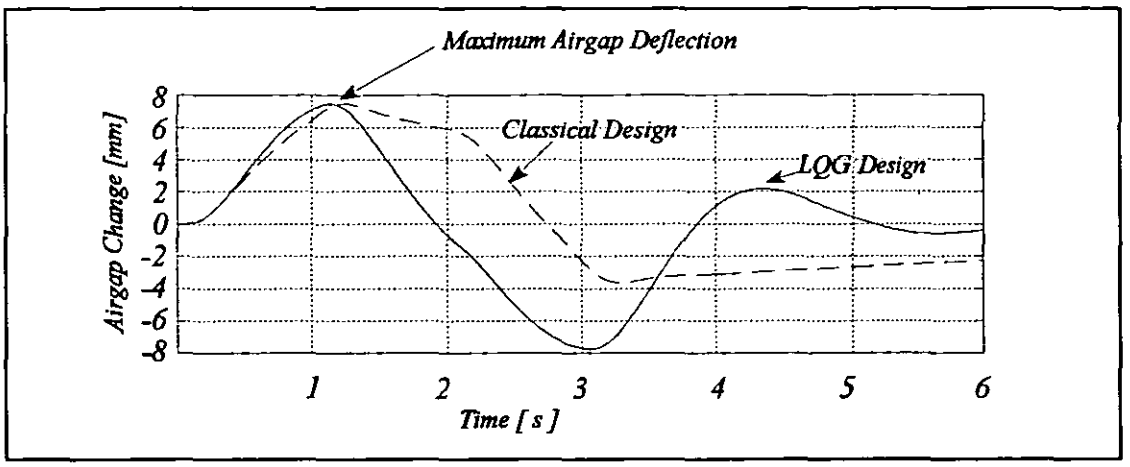

Figure 7.9 Airgap response for a transition onto a 5% gradient

7.6 Conclusions

The performance of the two controllers are similar both in terms of ride quality and maximum airgap deflection during a transition onto a gradient. The difficulty in reconciling the conflicting requirements of the suspension is clearly demonstrated.

Although showing slightly worse ride quality performance than the LQG controller , the classical controller is far more practical and may be implemented on the Birmingham Maglev directly. The LQG controller requires high gains of the order of $4x10^5$ in the integral airgap feedback path which may not be practical in a real system and this motivated further studies using the integral of airgap in the model formulation [Paddison94] (See Appendix 3). This new model has not as yet been optimised using MOPS. The classical controller is also an inherently simpler structure but requires a greater degree of knowledge to create the basic design. The insight gained through the classical controller undoubtedly helps in the LQG formulation.

The work presented in this chapter has provided a deeper insight into the conflicts inherent in a Maglev suspension. While performing the optimisation using the ANDECS-MOPS-MATLAB software the designer is 'forced' to appreciate the problem in a more intuitive way.

Chapter 8: Experimental Rig Design and Construction

8.1 Introduction

The objective of the rig is to demonstrate the limitations of the classical controller in coping with a 'soft' Maglev chassis which has a first bending frequency of about 12Hz. It should also show whether the modern control strategy can be successfully implemented given all the conflicting requirements of the suspension. From the outset of the project a fairly substantial rig was envisaged which would allow the results to be translated to a real vehicle without significant scaling difficulties.

Constructing a scaled Maglev suspension is difficult because the magnet characteristics do not scale well. For example the magnet lift to weight ratio is less favourable for a small magnet than a large one. In addition in this investigation the relationship between the resonances of the chassis structure and the controller response are of key importance. A shorter scaled vehicle inevitably has a higher first bending frequency which has less effect on the controller. Altering the controller by increasing the bandwidth to suit the scaled chassis is not feasible since this would result in a system which would be susceptible to instability. For these reasons the longest practical rig of 3m was constructed and the airgap and flux densities were kept as close to realistic values as possible, that is 10mm and 0.7T respectively.

Electromagnet design can be a complex process, but the intention has been to produce a simple magnet using basic materials without endeavouring to optimise the design.

It is also clear from the design process that the components (magnets, chassis etc.) that go to make up a Maglev vehicle are highly interdependent and cannot be specified in isolation.

8.2 Mechanical Construction

8.2.1 Flexible Beam Design and Construction

With reference to the theoretical study so far presented in this thesis, the beam representing the chassis is designed to have the following attributes:

1. First bending frequency of approximately 12Hz.
2. A natural damping factor of below 3%. In mechanical structures damping will be increased by fretting at frictional joints and these need to be avoided.
3. The original idea was to have a single beam with some adjustment to vary the natural frequency, and see how well the controller could cope with the variation. However this proved impossible to achieve without joints which could have introduced fretting and therefore too high a damping factor. For this reason two beams (A and B) with the same mass were used, designed to have fundamental bending frequencies at 12Hz ±5%. i.e. 12.6Hz and 11.4Hz [Marquet93].
4. To have sufficient mass per unit length that the lumped masses of the two magnets have a negligible effect on the system's dynamics. Loading the free-free beam towards the ends has a tendency to raise the natural frequency as well as altering the mode shape. Dynamic simulations suggest the total lumped magnet masses should be a maximum of 25% of the total mass.
5. Attachment points to allow the magnets to be moved by ±5% along the beam length with respect to their nominal positions at 25 and 75% of the beam length.

Figure 8.1 below shows the beam with the magnet cores bolted on. The sandwich construction adopted for the beam is clearly shown. The side plates, which are the 'contents' of the sandwich, may be altered in height and width while keeping their cross sectional area and mass constant, and this provides a method of altering the 2nd moment of area of the beam which in turn alters the stiffness of the beam.

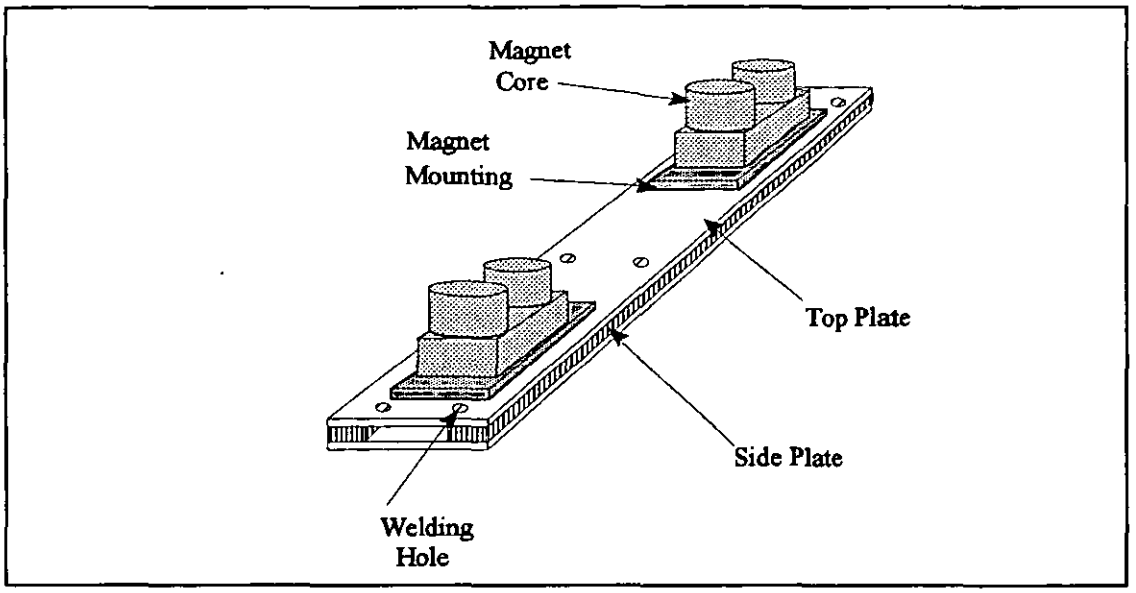

Figure 8.1 Beam with magnet cores

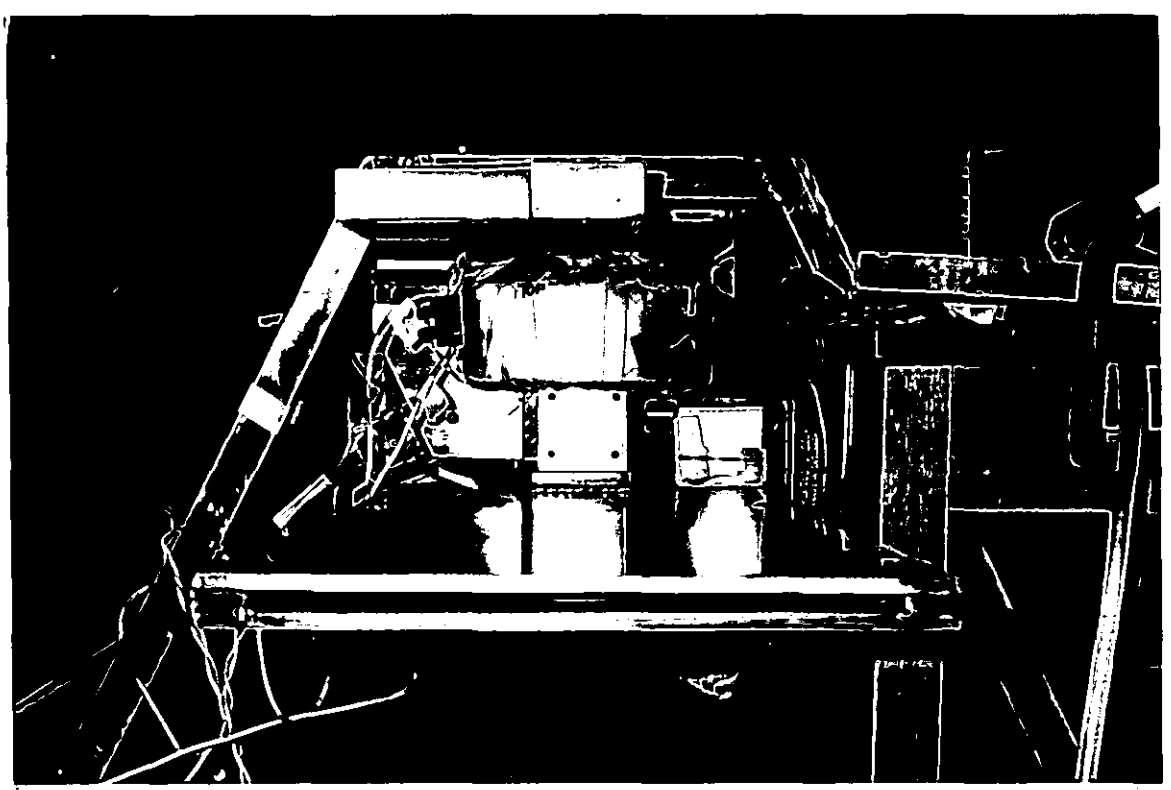

Figure 8.2 View into the rig showing the beam cross-section

The second moment of area for this construction is

$$I_2 = \frac{B_b D_b^3 - b_b d_b^3}{12} \qquad 8.1$$

where B_b and D_b are the beam overall breadth and depth respectively and b_b and d_b are the internal space breadth and depth. Bending theory (appendix 5) then allows the natural frequency to be calculated given the constraining conditions and the bending mode of interest..

Potential problems for the beam construction were 'warping' of the structure due to the welding process and the effect of welding the magnet supporting plate to the top plate. The uncertainties due to welding mean that the resonant bending frequencies cannot be expected to lie exactly where specified.

Bead welds are applied along the top plate to ensure no motion relative to the side plate which would introduce friction and thus damping into the structure.

Due to the very nature of a Maglev vehicle it is advantageous to minimise the chassis weight. Aluminium is the obvious choice due to its low density and high tensile strength. The problems in building an experimental rig from aluminium are similar to those encountered on the Birmingham vehicles, namely the specialist knowledge needed to do so and the associated high cost of fabrication. Aluminium is difficult to work with, and this is particularly so with longer lengths where ' warping' would be highly likely. Making the beam from plate mild steel means that the mass of the magnets can be kept in proportion to the mass of the total structure.

For the above reasons aluminium was dismissed as a suitable material early in the rig design process.

8.2.2 Resonance and Damping Analysis

Having designed and constructed two beams it is essential to check that their frequency response characteristics relate to the problem under consideration. Attaching the magnets and applying an impulse to the beam, the resonant frequencies can be measured with accelerometers attached to the beam. This test was performed on the beams when they were resting on the supporting structure and this means that they are not strictly free-free beams.

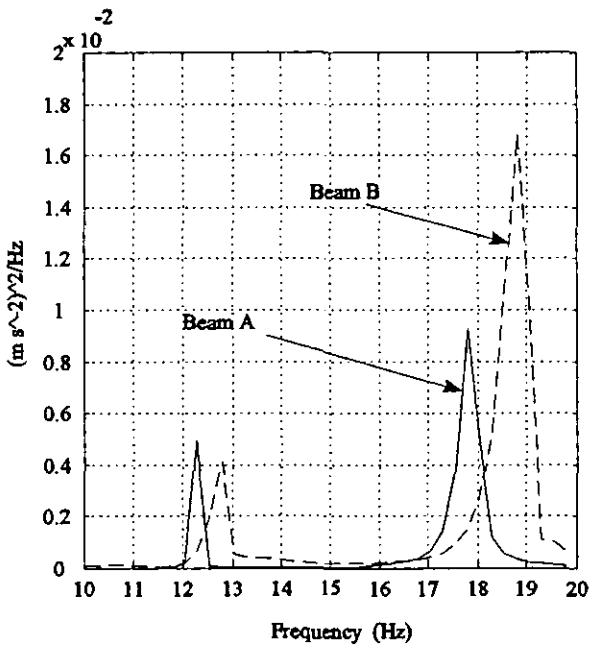

Figure 8.3 Acceleration p.s.d derived from the impulse response of the two beams.

The above power spectral density (p.s.d) shows that the first two resonances lie at 12.2 and 17.8Hz for the beam A (solid line) and at 12.75 and 18.8Hz for the beam B. These resonance frequencies are very close to the design values.

The third and fourth resonances are at 32.2 and 48Hz for beam A and 36 and 52Hz for the beam B and have magnitudes significantly less than the first two bending modes. Hitting the beam to obtain the resonances does not cause enough excitation to identify any

more than the first two bending modes with real confidence.

The damping factor may be calculated through the use of the logarithmic decrement [Thompson88]. This procedure requires analysis of the time response of the decaying vibrations and can be calculated from the following response.

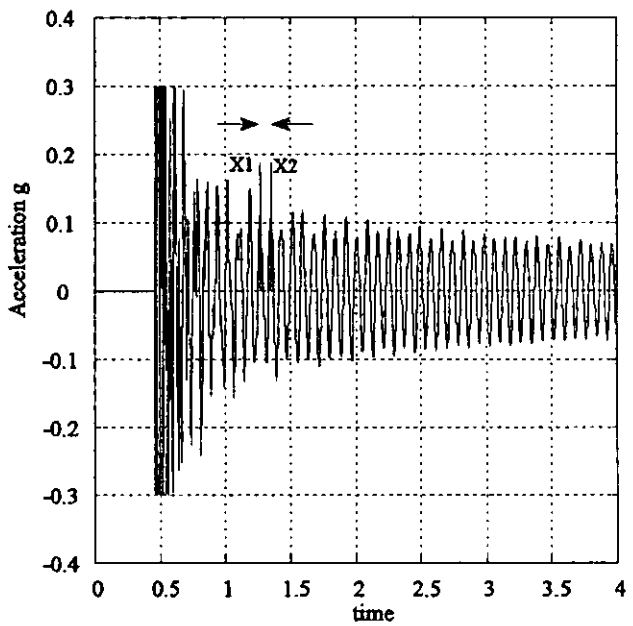

Figure 8.4 Calculation of the logarithmic decrement from two successive amplitudes X1 and X2.

X_1 and X_2 are two successive amplitudes.

$$\delta_{ln} = \ln\left[\frac{X_1}{X_2}\right] = \frac{2\pi\zeta}{\sqrt{1-\zeta^2}} \qquad 8.2$$

The average decrement over about 10 successive periods is taken here. Substitution of the values from the above graph gives a value for the natural damping ratio ζ of 0.213%. A typical vehicle structure would have a damping factor of 3% and shows that damping within this structure is very low, which presents a more rigorous test for the controller than would be encountered with a real vehicle.

8.2.3 Supporting Frame

The frame supports two short track sections and the anti-roll system which prevent the beam from rolling along its axis.

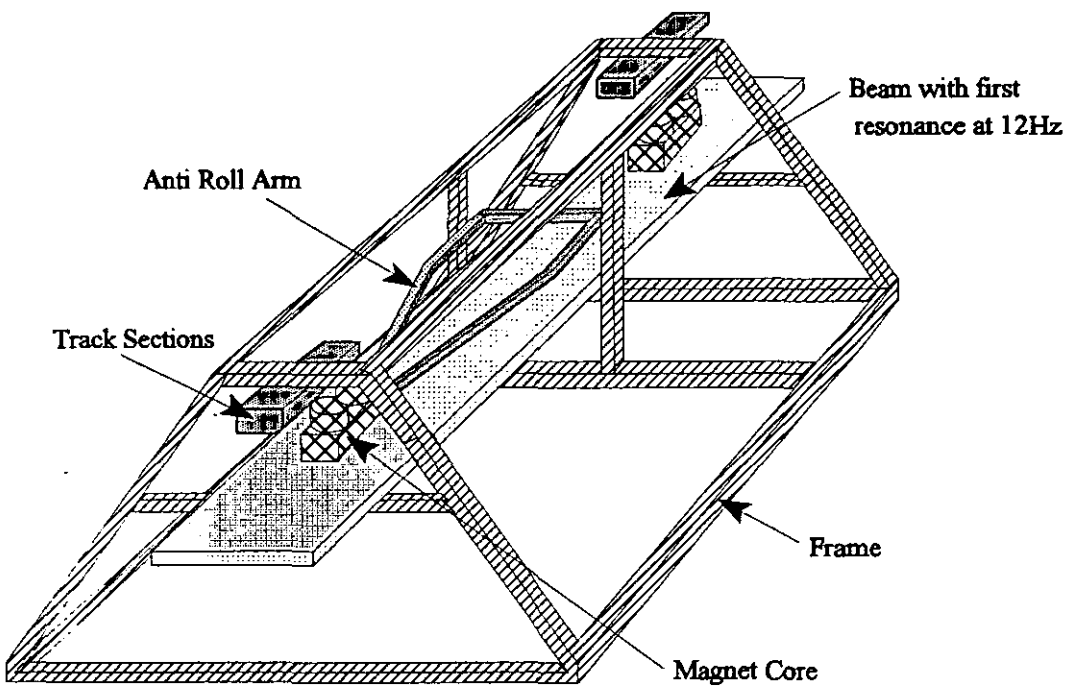

Figure 8.5 Maglev rig and frame

Impulse response tests show for the above frame that the first significant resonance is at about 90Hz. It was found during testing of the Maglev that the lateral modes along the length of the frame are the most susceptible to excitation but that this was not significant if the Maglev was in stable levitation. It is also worth noting that the rig had to be situated on a level surface to reduce the possibility of the frame being excited torsionally. The frame does not have any resonances which could interfere or be confused with the resonances of the suspended beam.

The anti-roll bar provides stability for the assembly in the roll mode. Its mass is comparatively small compared with the beam and magnets. It also has the benefit of preventing longitudinal motion of the beam when levitated.

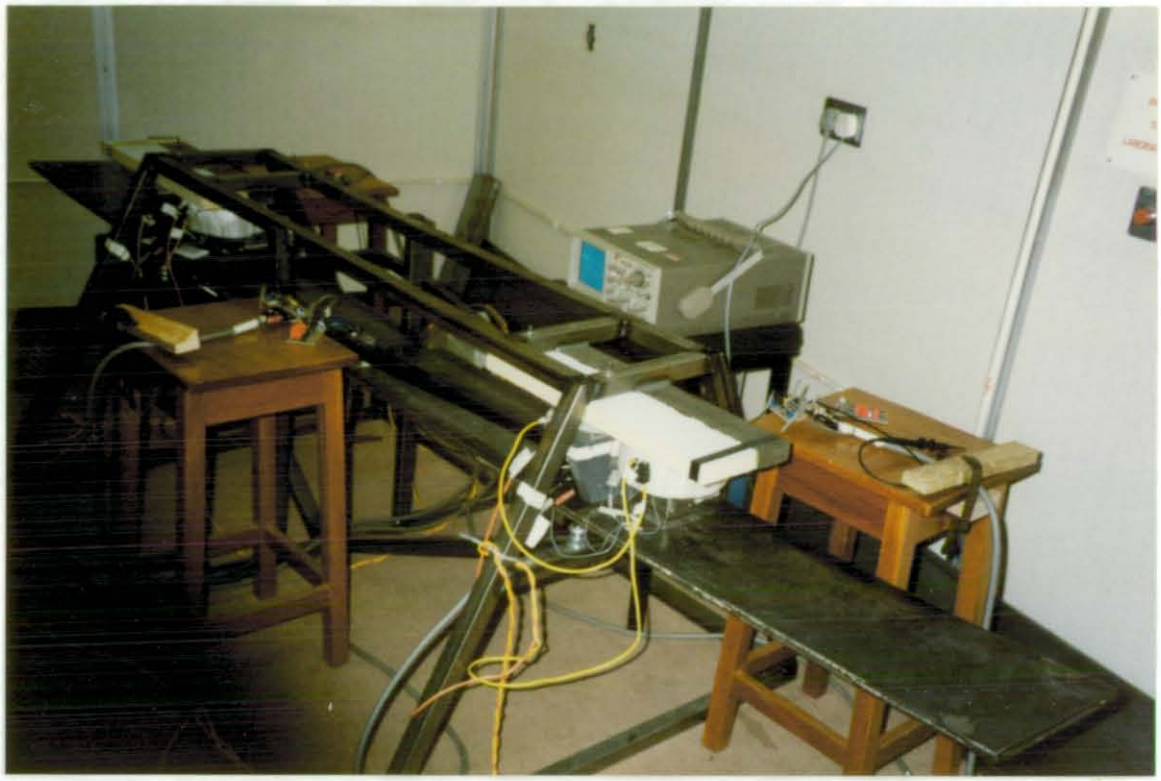

Figure 8.6 View of the assembled rig and frame

8.3 Electromagnets and Power Supply Design

8.3.1 Magnet Design

Two magnets are required for the system and have the following requirements;

1. To suspend the structure at a nominal air gap of 10mm. The total load to be supported is a maximum of 200kg when laden.
2. To have a minimal mass compared with that of the beam (see above). This should be less than 25% of the beam to avoid alteration of the dynamic characteristics of the beam.

8.3.2 Fundamental Equations for Magnet Design

Starting the design with the flux density equation:

$$B_o = \frac{N I_o \mu_o}{2 G_o} \qquad 8.3$$

The nominal values are selected largely through experience. A conservative nominal flux density, B_o, of 0.7T is easily reachable with electrical steel and a nominal current, I_o, of 12A can be supplied by a reasonably sized power amplifier. Given the nominal airgap size of 10mm the required excitation ($N I_o$) is 11160 ampere-turns, i.e. N as 930 turns.

The second fundamental equation relates the flux density to the force obtained and this will allow the pole face area to be determined.

$$F_o = \frac{B_o^2 A_{ptotal}}{2\mu_o} \qquad 8.4$$

One magnet will be required to lift approximately 1000 N which dictates a total pole face area of $A_{ptotal}=5.03\times10^{-3}$ m^2, from which each pole face has an area, of 2.5×10^{-3} m^2. A square pole would have sides of 0.05m, or a circular poleface would have a radius 0.0283m. A circular pole face is easier to build and simplifies the coil construction, but does not give such a defined magnetic field with respect to the square track. This has been found to be a disadvantage during the magnet lift-off where guidance is particularly important. During the lift-off condition the airgap is about 24mm and the nonlinear aspects most pronounced. Also the magnet may be attracted to other objects such as the frame rather than the track. These effects make the attainment of stable levitation more difficult.

The third empirical equation relates the ampere-turns to the cross-sectional area of the conductor, A_{wc}, given the limits of how much current can be conducted by the material

chosen.

$$N I_o = A_{wc} J \qquad 8.5$$

Aluminum or copper conductor may be used. The choice of whether to use copper or aluminium windings is very significant to the weight implications for the magnets. Despite the increased current density possible with the copper foil conductor, the copper turns have a mass twice that of the aluminium, for the same airgap flux density. For this reason aluminium foil was chosen as the conductor.

Working on a coil current density of 2 A mm^{-2}, and assuming a slot twice as wide as it is deep to avoid too much leakage [Goodall85] a window of dimensions 103 by 62mm was used.

Details of the magnet design are included in the appendix 6 but a summary of the key parameters is given in table 8.1.

Table 8.1: Theoretical Magnet Parameters

Parameter	Theoretical
Magnet Mass [kg]	12.34
Lift [N]	981
Lift/Weight ratio	8.1
Power [W]	255.68
Resistance [Ω]	1.8
Power/Lift [W/kg]	2.56

Detailed testing of the magnets has not been carried out, but they were found to deliver 0.7T at 12A and proved well able to levitate the beam.

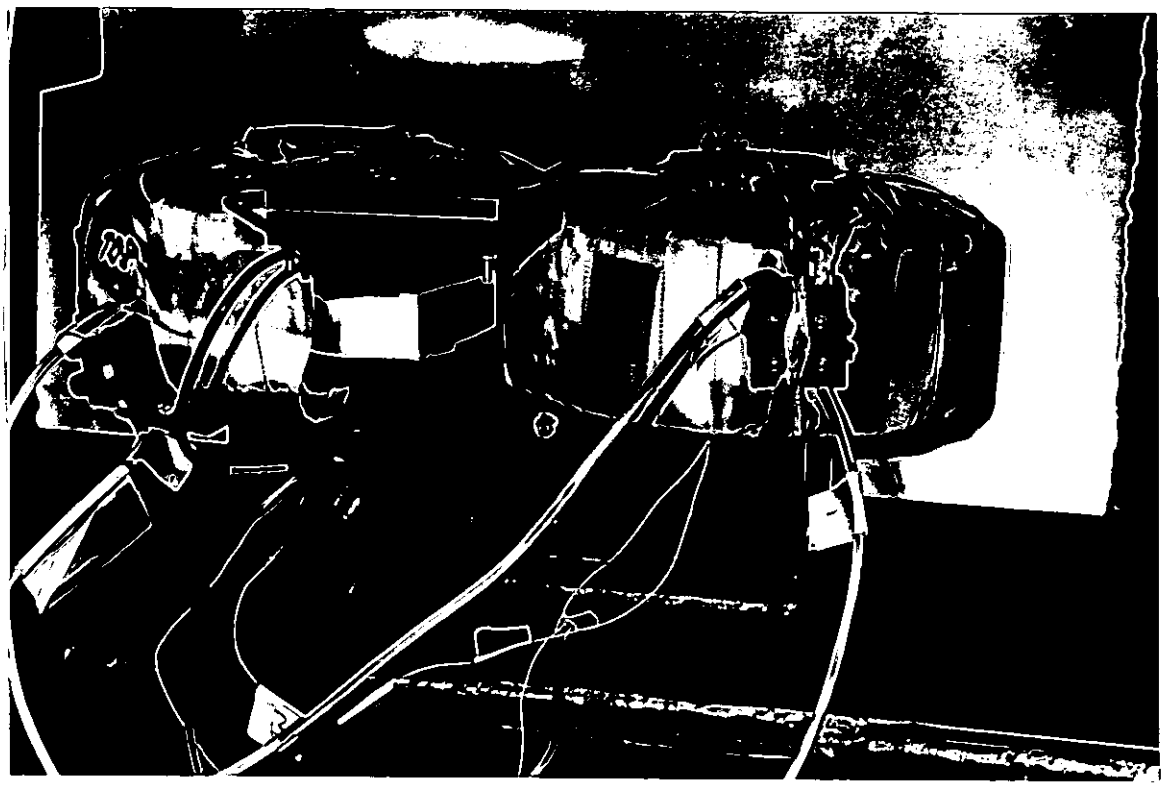

Figure 8.7 Assembled magnet bolted to the beam

8.3.3 Magnet Power Amplifier

The power amplifier is one of the most critical requirements of the Maglev rig. A fast response is required to achieve the high bandwidth flux control. Most suspensions use a pulse-width modulated transistor power amplifier where the switching devices are switched on and off at high frequency. The inductance of the magnets provides smoothing of the current.

Although many Maglev applications use current feedback in the power amplifier, as mentioned in chapter 4, this neutralises the stabilising induced voltage effect. Accordingly the amplifiers are voltage controlled, with the drive signal determining the mark/period ratio.

Two quadrant power amplifiers were used, delivering uni-directional current with bi-directional voltage; negative forcing voltages are important to maintain controllability under certain conditions.

The power amplifier was used with a maximum current of 18A and a continuous current rating of 12A with a maximum voltage of 56V.

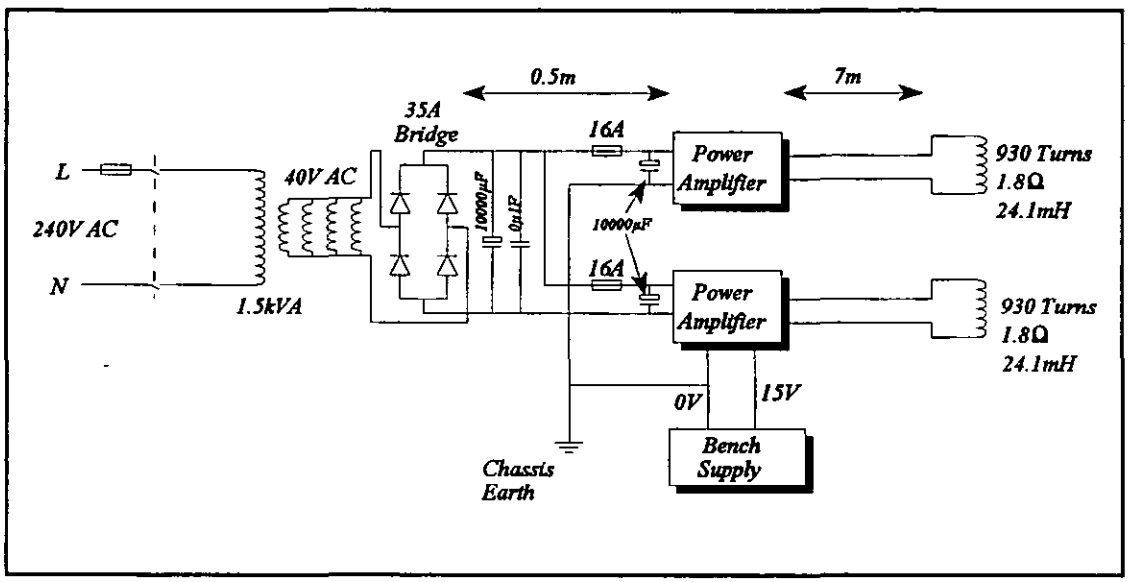

Figure 8.8 Power Amplifier arrangement for the Maglev rig

The power amplifiers used in this rig have a switching frequency of about 15kHz. Considerable care was taken to twist and screen the leads to the magnets in order to minimise electro-magnetic compatibility problems with regard to the transducers.

8.4 Transducers and Signal Conditioning

8.4.1 Accelerometers

The project requires accelerometers which have a good linear response down to low frequencies, ideally DC, and are compact and robust. The acceleration experienced by the accelerometers is a maximum of about 2.5g; for this reason 5g accelerometers were

selected. (Ideally the rig should be producing accelerations of a maximum of 5%g (approximately $0.5ms^{-2}$) but during the commissioning stages and the investigation of the flexibility effects the accelerations are much higher.)

Piezoresistive machined silicon accelerometers from Euro Sensor Ltd were used . The accelerometers have a linear response from 0 to 350Hz and have a sensitivity of 10mV per g which is rather low and results in noise problems in the accelerometer conditioning circuitry. This noise has been found to be particularly pronounced when the magnets are carrying operating currents i.e. 12A.

The accelerometer and its conditioning circuit are inside an aluminium box with the accelerometer bolted to the base of the box to provide good mechanical contact with the suspended mass.

The output of the conditioning circuit is fed into a self-zeroing double integrator which integrates the acceleration to give a pseudo- absolute position. The double integrator is implemented both in analogue and digital form. The double integrator is effective down to about 0.2Hz. As has been explained the classical controller requires an absolute position coordinate for frequencies above about 1.5Hz, so the low frequency component of the result is not particularly important.

The double integrator is represented by the following transfer function;

$$H_I(s) = \frac{\frac{1}{\omega_i^3}s}{1 + \frac{2}{\omega_i}s + \frac{2}{\omega_i^2}s^2 + \frac{1}{\omega_i^3}s^3} \qquad \textbf{8.6}$$

and is implemented practically by:

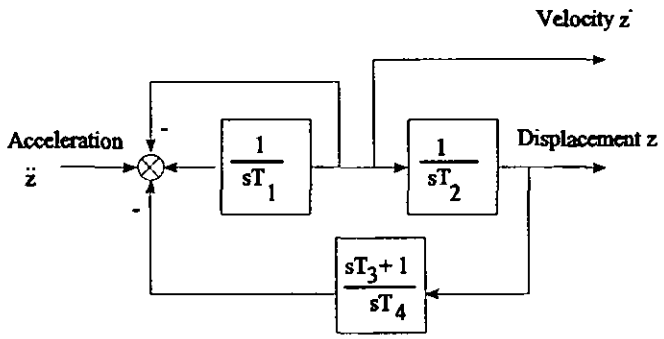

Figure 8.9 Block diagram of the self zeroing double integrator, where T_1=0.47, T_2=0.946, T_3=T_4=2.2.

The frequency response of the above filter structure is shown below;

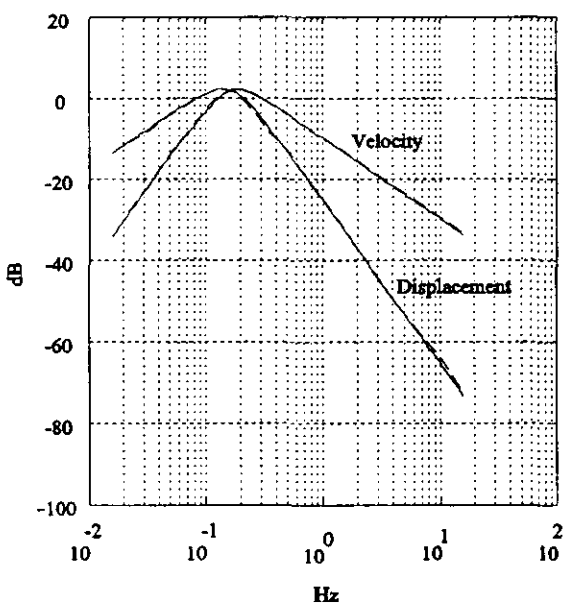

Figure 8.10 Double Integrator response actual and theoretical

The digital (software) implementation of the double integrator proved more effective than the analogue realisation for a combination of reasons, particularly because scaling of the results of the integration processes is so much easier.

8.4.2 Airgap Position Sensors - Linear Proximity Sensors

Non-contacting Sensagap displacement transducers from RDP Electronics were used on the rig. These are capacitive devices which operate over a range of 33mm when the target is earthed. They have a linear response which is flat up to about 150Hz and very robust and totally unaffected by the magnetic field. They are also comparatively inexpensive compared with the alternative sensors which use the inductive effect.

These sensors are intended to measure the distance between the magnet pole face and the track, but were fitted to the side of the pole faces due to the limited space. Initially a steel 'target' was used but this was found to divert the magnetic field, particularly on lift-off and was prone to cause instability due the lack of magnet guidance provided by the distorted field. Replacing these with Aluminium targets proved to solve the problem, shown diagrammatically below where the magnetic field in 'B' is not entirely directed through the track.

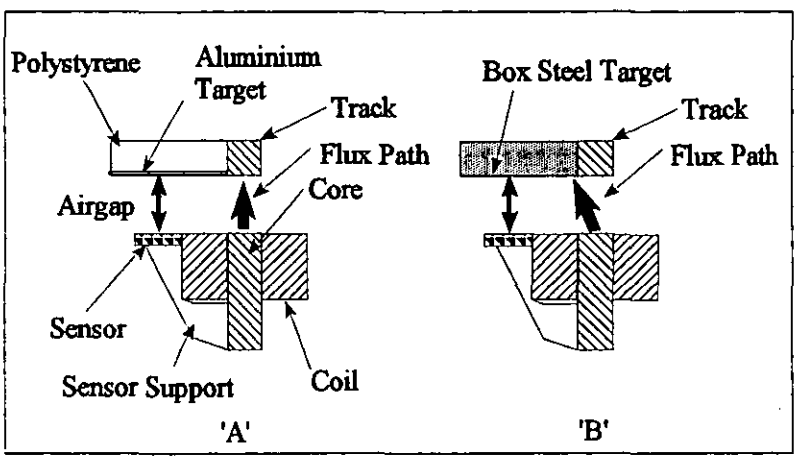

Figure 8.11 End view of magnets showing 'A' the suspension with a non-magnetic target and 'B' the flux following a path through the airgap sensor's steel target.

8.4.3 Flux sensors

The flux sensor consists of a search coil and an analogue self-zeroing integrator. The search coil made of 20 turns of plastic coated copper wire wound into a circular groove of 2mm depth on each pole face. A finite element analysis of the flux distribution is required to determine the optimal shape and dimensions of the search coil.

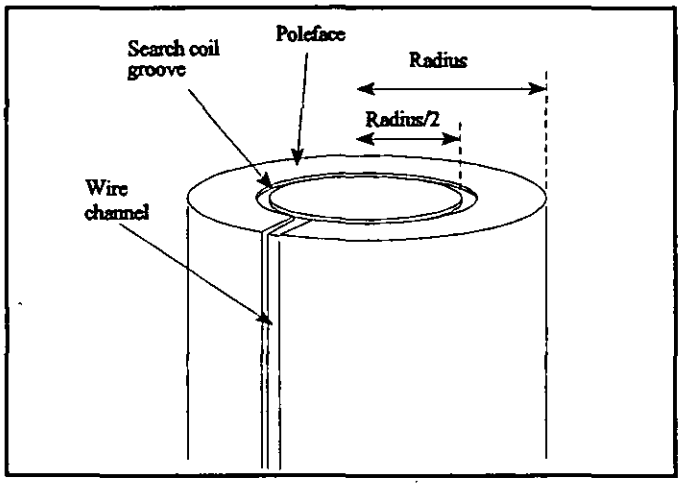

Figure 8.11 Search coil embedded in the pole face

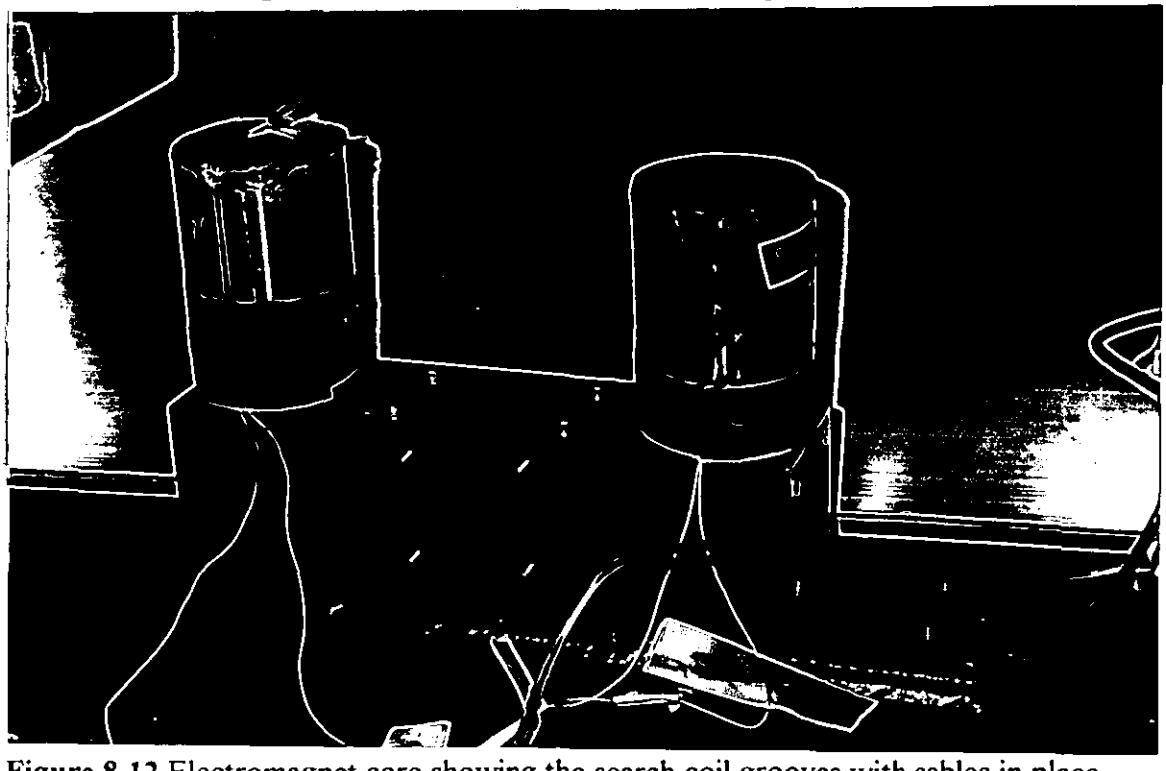

Figure 8.12 Electromagnet core showing the search coil grooves with cables in place

The search coil is embedded in the groove and fixed with an epoxy resin in order to make it robust with the magnet pole face impacting on the track. As the flux density changes a voltage is induced in the search coil. The area of the search coil is known, so simply by integrating and scaling the resulting voltage the change in flux density can be determined. The circuit is self zeroing so as to prevent the integrator drifting, and has the following transfer function:

$$H_{tf} = \frac{\frac{1}{\omega_{fi}}s}{1 + \frac{1}{\omega_{fi}}s + \frac{1}{\omega_{fi}^2}s^2} \qquad 8.7$$

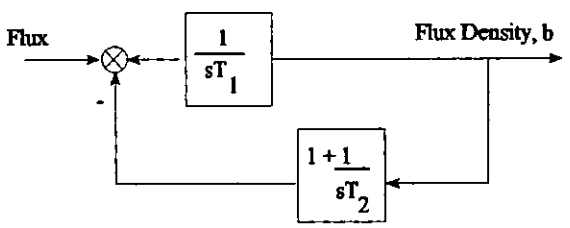

Figure 8.13 Block diagram of the self zeroing integrator, where T_1=0.0018, T_2=1.5.

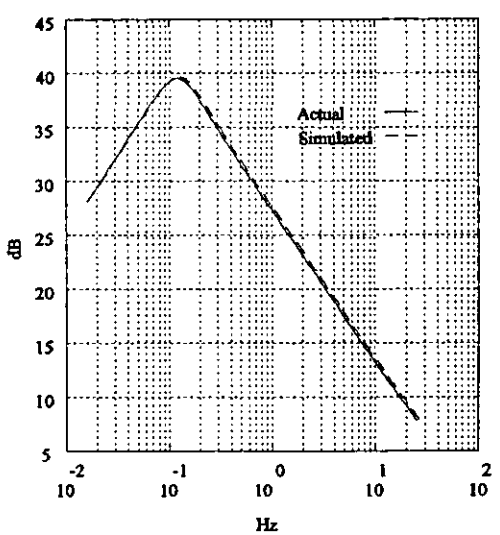

Figure 8.14 Flux integrator response

One of the problems with this configuration of sensor is the lack of a low frequency response. This can lead to some interesting effects which are discussed with the experimental results in chapter 9.

8.4.4 Current Sensors

The current sensor used is very simple consisting of a 0.1Ω resistor in series with the magnet coil. The conditioning circuit must reject the common-mode voltage from the power amplifiers - a maximum of 56V.

8.5 Digital Signal Processor

Fifteen years ago the Birmingham Maglev controller was successfully implemented using analogue electronics which has the advantage of being cheap and rugged but it is also difficult to alter. Nowadays digital processors are relatively cheap and offer a great deal of flexibility to the control designer during the implementation phase. This is particularly significant for the implementation of sophisticated control structures which can be altered easily in software rather than hardware, which would of course require changing a physical connection. This is the main reason why a digital approach was chosen for this project. Secondary reasons are the fact that any future Maglev vehicles are likely to use digital controllers since the 'single chip' solution can be cheaper and more reliable.

8.5.1 Hardware

An AT&T DSP32C digital signal processor on a Surrey Medical Imaging Systems Ltd (SMIS) card with 256k of on board memory has been used to provide the processing requirements for both the classical and modern controllers developed in this thesis. The DSP32C is capable of 25×10^6 floating point operations per second with a 24 bit mantissa and an 8 bit exponent. The DSP32C comes with a floating point C language compiler,

assembler and linker with a variety of library functions which are modified by bundled software from SMIS in order to function on the above processor card [SMIS91].

A 32 channel 12bit analogue to digital (ADC) input card [LSI92] and a 16 channel 12 bit digital to analogue (DAC) zero order hold output card [LSI88], both from Loughborough Sound Images Ltd (LSI), are used to provide interfacing with the rig. The LSI cards come with some software from ONYX Software Ltd which is designed specifically for the DSP32C and the LSIADC and LSIDAC cards.

This hardware is configured in the form shown below. The DSPLINK provides a high speed, bi-directional bus that allows input/output directly to/from the DSP32C avoiding having to use the IBM PC bus.

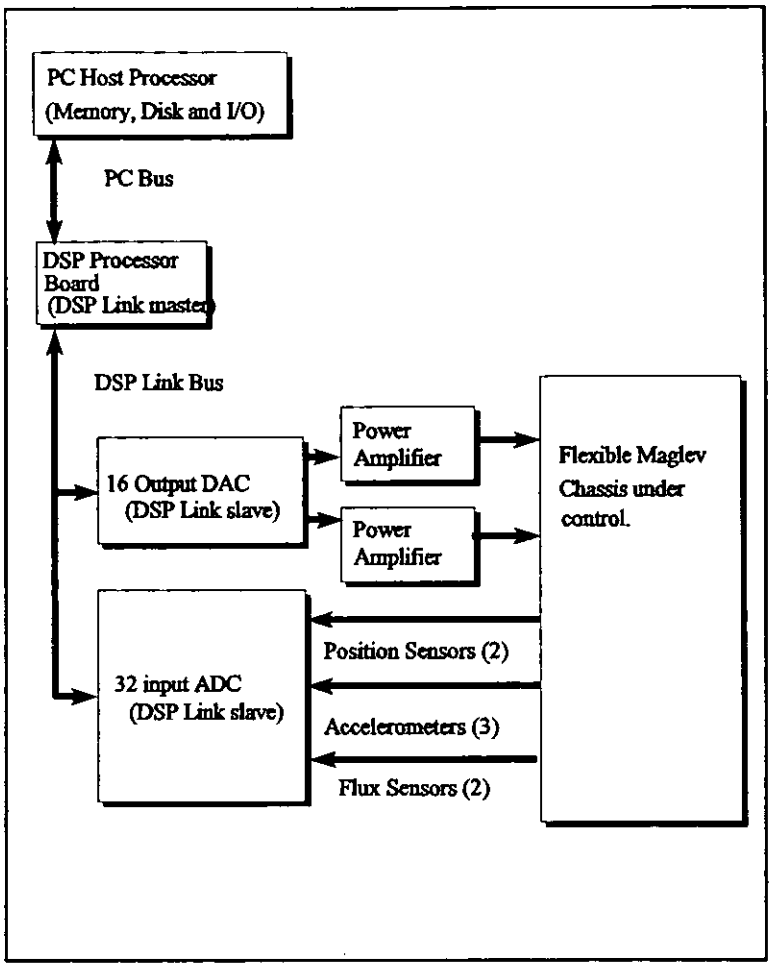

Figure 8.15 Digital Processor/Rig interface

8.6 Controller Implementation

8.6.1 Software Issues

The first priority is to determine the sample rate required to give an accurate enough set of data for the continuous system to be controlled. It is generally considered that a sample rate 10 times the bandwidth of the controller is required. So in the case of the classical controller described in chapter 5 which has an inner loop bandwidth of up to 100Hz a 1000Hz sample rate is suggested. This requirement is comfortably within the specification of the DSP32C.

The software structure used in all of the controllers implemented in this thesis is shown below.

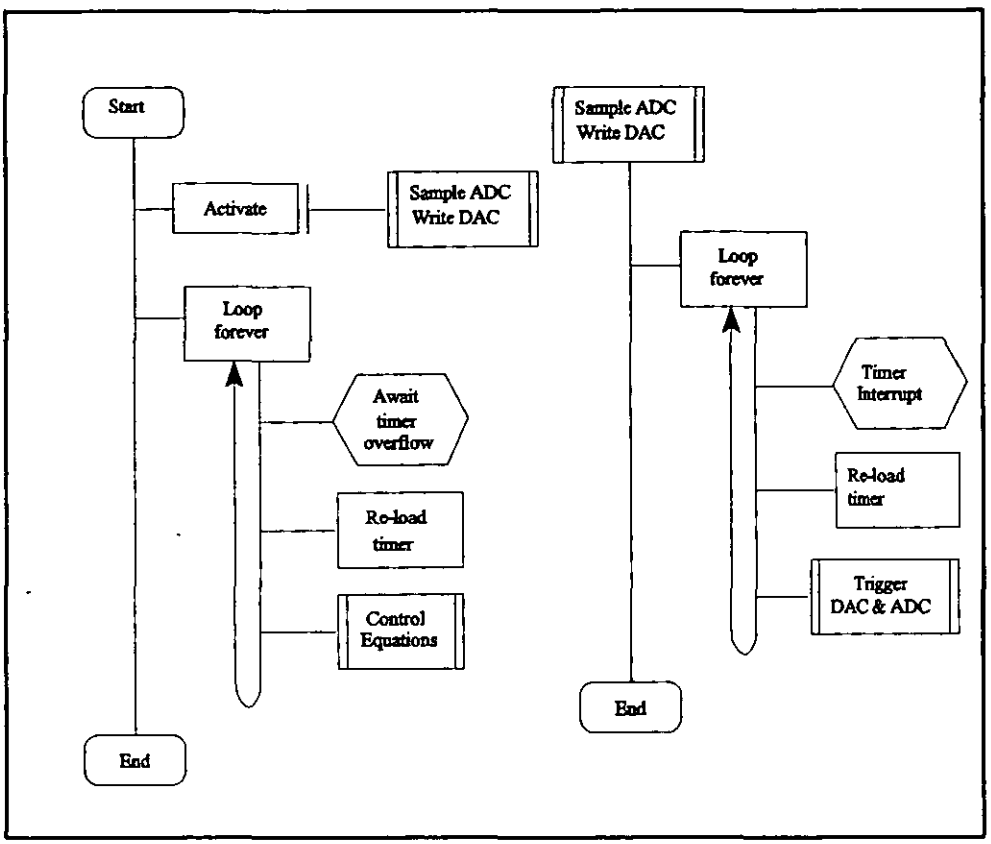

Figure 8.16 Digital control structure.

The interrupt routine is the basis of the above structure, providing data at regular 0.001second intervals. The ability to synchronise the interrupt with the controller is essential and to do this access is required to the input/output card registers. This is provided by a fast assembly coded program.

The AT&T 'C' compiler version 1.6.1 has proved limited in its facilities for implementing quite simple code. This version of 'C' has proved fairly non-ANSI standard and the code developed has proved rather difficult to transport.

8.6.2 Controller Emulation

To implement the controllers developed in chapters 5 and 6, whether they be designed with classical or modern control theory they need to be discretised. Controllers developed in the continuous domain are converted to the discrete domain using emulation techniques in a straightforward manner. Other techniques are available and the controller may indeed be designed in the discrete domain from the outset, but in this work emulation is the technique used.

Classical Controller Implementation

For the classically designed controllers a decision was taken to use the δ-operator rather than the z-operator for the purpose of digital implementation [Forsythe91] [Middleton90]. The δ-operator has superior properties with respect to coefficient sensitivity and internal variable overflow. With a 32 bit floating point processor the advantages of the δ-operator are less significant than for a 16 or 8 bit processor.

The bilinear transform or δ-operator emulation tables are used to convert all the filters to the discrete form.

$$s = \frac{2\,\delta}{T(2 + \delta)} \qquad 8.8$$

In most cases the modified canonic form of the discrete filter was used because it gives unity feedback in the structure which naturally is less computationally intensive.

The emulation process is such that it is easy to calculate the discrete filter coefficients for each filter within the overall C program as shown in appendix 7 for the phase advance compensator and this done in the first function. The second function performs the filter operation. The iterative nature of the filters means that the state of the filter must be

stored until it is called again. The storage of internal and external variables in a structure has been the method used to do this. Clearly the accuracy of the coefficients then depends on the numerical format used and the C float variable (32 bit) was found to be sufficient in all cases.

'Modern' Controller Implementation

The LQG controllers were re-evaluated in the discrete domain using the z-operator. The change to using the z-operator was prompted by the software tools available within MATLAB for this conversion which is more involved than for the classical approach.

All of the LQG controllers had to be further tuned but approximately the same weighting factors were used as in the original continuous design. The design process was as follows:

1. Convert the continuous system to discrete form using the MATLAB command c2dm using the bilinear (Tustin) approximation option.
2. Recalculate the discrete K_E and K matrices for the Kalman filter and state feedback gain matrices.
3. Store the system in an ASCII format to be read by the DSP32C.

This process had to be followed for every controller variation in order to ensure the matrix coefficients were sufficiently accurate. They could not be calculated on the DSP as easily as in the case of the classical controller implementation.

An example of the code used to implement the discrete Kalman filter and state feedback gain matrix is given in appendix 7. The discrete matrix equations implemented in this code are:

$$\hat{x}_{k+1} = A\hat{x}_k + Bu_k + K_E(y_k + C\hat{x}_k) \qquad \textbf{8.9}$$

Equation 8.9 is the Kalman filter and 8.10 the state feedback control. Some examples of

$$u = -K\hat{x}_k \qquad 8.10$$

discrete LQG controllers are given in the literature [Lewis94] [Ahmed91] [Franklin90] but as the code in appendix 7 shows the process is quite involved compared with the discrete classical equivalent.

Chapter 9 discusses the problems encountered in the implementation and commissioning of the Kalman filter.

8.7 Rig Commissioning

The rig as a whole was assembled as initially envisaged without problems. The mechanical assembly proved to be particularly successful with the desired beam stiffness being achieved with quite simple construction techniques.

Problems were encountered in two areas. Firstly proprietary amplifiers were bought, but after a period of testing proved unsatisfactory in particular with respect to their conversion to voltage drive format. Secondly the software supplied to drive the ADC proved to be unreliable and incapable of supplying interrupt driven data at 1kHz. The C compiler also proved unsatisfactory and non-ANSI standard.

Chapter 9: Experimental Results

9.1 Introduction

This chapter presents the practical investigation of the theory developed in chapters 5 and 6 using the rig described in chapter 8.

The classical controller is discussed together with interesting aspects of the design which came to the fore during the commissioning process. The LQG controller is then considered with the implementation problems encountered. Reliability problems were encountered with the compiler and the input/output card driver software and this certainly delayed and restricted the use of the DSP development system.

9.2 Single Degree of Freedom Magnet using the Classical Controller

The implementation of a Maglev suspension is a particularly complex process because of the need to overcome the essential instability as well as getting the instrumentation and control processing correct. Clearly it is best to set up the controller in stages, but open loop testing is prohibited by the unstable nature of the suspension. For the single degree of freedom magnet operation the rig was used in the configuration shown in figure 9.1.

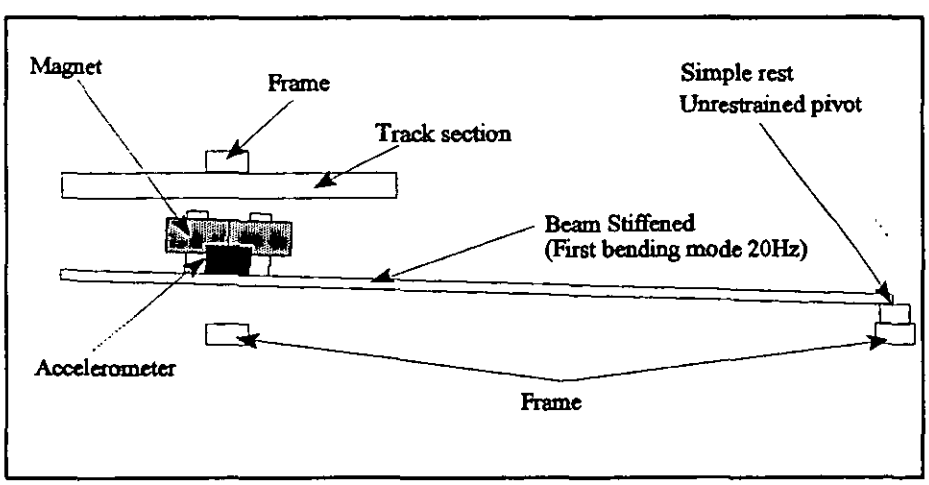

Figure 9.1 Single Degree of freedom magnet test arrangement

The theoretical models developed earlier in this thesis provided a starting point for the controller design.

The r.m.s vertical accelerations are generated by structural feedback of the flexible modes and no additional excitation was injected since this was deemed sufficient to demonstrate the principles being investigated. Analysis of the raw acceleration data using a Fast Fourier Transform (f.f.t) allows the calculation of the power spectral density and the r.m.s vertical acceleration.

Experimentation was required to achieve stable levitation and this was achieved with the following controller configuration.

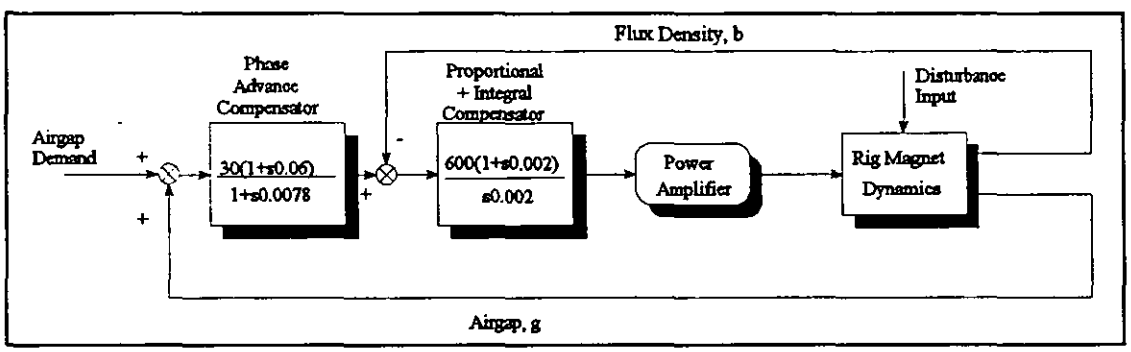

Figure 9.2 Simple controller providing robust single degree-of-freedom levitation

This suspension produced a vertical r.m.s acceleration of 0.776ms^{-2}. The control bandwidth was about 5Hz but the suspension deflection was not quantified.

Introducing second order high and low pass complementary filters with corner frequencies of 1.5Hz and the self-zeroing double integrator with a 0.1Hz corner frequency, improved the vertical r.m.s acceleration by a factor of 10 to 0.076ms^{-2}. Figure 9.3 below shows the airgap time response during the lift-off period and provides a time domain comparison between the controller with and without the ride filters, and shows the generally slower response with the ride filters in place. The period up to 10 seconds represents the effect of the ramp command used to slowly increase the current to give the self zeroing flux integrator time to respond.

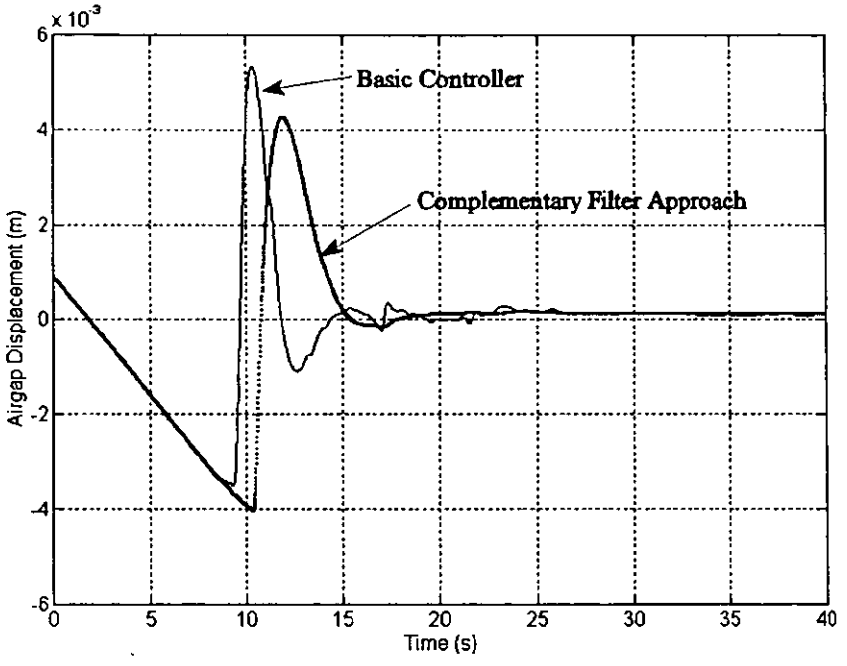

Figure 9.3 Comparison of the basic controller and controller using the complementary filter approach during lift-off.

9.2.1 Effects of search coil imperfections

Investigation of the frequency response of the main position loop shown in figure 9.4 demonstrated features which were not expected. The main open loop response is of Type 2 and should not therefore have a constant low frequency gain, neither should there be the resonance effect at about 2.5Hz. This was surmised to be due to imperfections in the flux density measurement, as explained below.

The flux feedback is intended to be representative of force, for which ideally a value for the r.m.s flux density over the whole pole face is required. Since the search coil measures the average flux over the area contained by its turns, this is clearly an approximation for the r.m.s flux density over the whole pole face and therefore does not properly represent forces, and this is particularly true as the airgap changes and the flux is distributed differently.

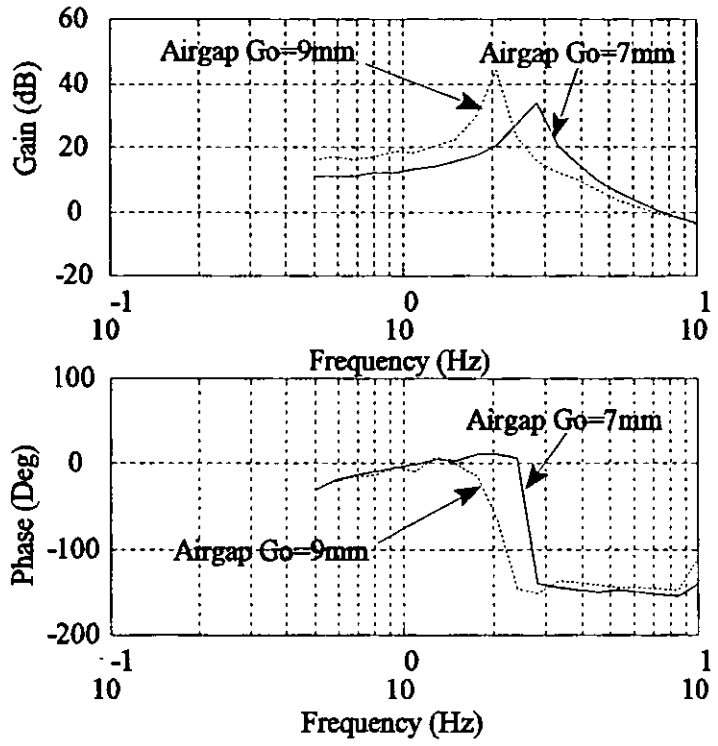

Figure 9.4 Effect of varying the nominal airgap on the position open loop response.

The same size of airgap change requires a force variation which becomes smaller as the frequency decreases, and a frequency will be reached at which the effect on the flux measurement caused by the redistribution of the flux over the pole face (due to the low frequency changes in airgap) is larger than the changing force.

The flux distribution is difficult to predict and probably needs a finite element analysis to appreciate, however the coupling of the airgap into the flux density measurement could be taken into account with the following simplified representation.

$$b' = b + C_g g \qquad \textbf{9.1}$$

where b' is the compensated flux density and C_g a coupling factor.

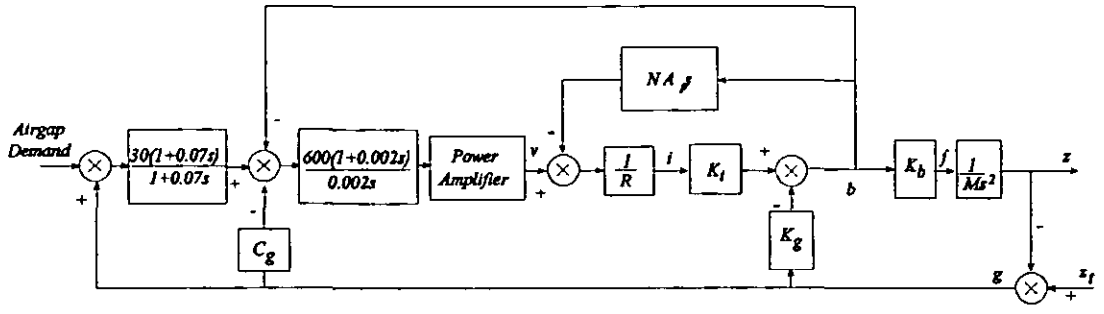

Figure 9.5 Application of the airgap coupling term.

Rearranging equation 9.1

$$\frac{b}{b'} = 1 - C_g \frac{g}{b'} \qquad \textbf{9.2}$$

If there is no input from the track (z_t=0) then

$$\frac{g}{b} = -\frac{K_b}{Ms^2} \qquad \textbf{9.3}$$

Multiplying equations 9.3 and 9.2 gives after some rearrangement

$$\frac{g}{b'} = -\frac{K_b}{Ms^2}\left[\frac{Ms^2}{Ms^2 - K_b C_g}\right] \qquad \textbf{9.4}$$

and on substitution of the nominal values and the resonant frequency of 2.5Hz yields a value for C_g of -8.64 T/m. This explanation was obtained by measuring the open loop response at a different nominal airgap, for which the flux distribution would be different and hence giving a different resonant frequency.

Further confirmation was obtained by including the coupling factor in the simulation model of the rig (values in appendix 4 and controller parameters in figure 9.5) and this produced a very similar result to those from the experimental results.

Having identified the nature of the imperfection it may be compensated for in the controller by including a positive value of C_g in the same position as in figure 9.5, and the modified open loop response is shown in figure 9.6. The compensated response has a lower roll-off over the control bandwidth.

The compensation minimises the effects of the resonance, and the main position loop proved to be much easier to tune with this compensation factor.

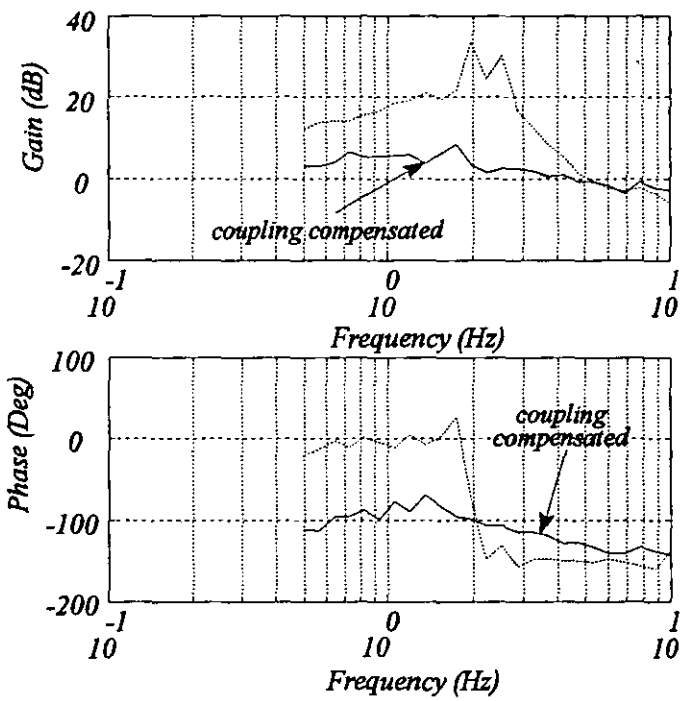

Figure 9.6 Effect of the coupling factor to compensate for the deficiency in the flux sensor.

The effect of the resonance due to the airgap coupling into the flux density feedback, while not destabilising, is to create uncertainty between the magnet model and the rig model. This possibly accounts for some of the experimentation required to achieve a stable suspension.

The use of the coupling term should improve future theoretical models and help with the interpretation of results.

9.3 Classical Controller for the half-car rigid beam

In this section the effect of the classical modal controller on a semi-rigid beam with a first resonance at 20Hz is examined.

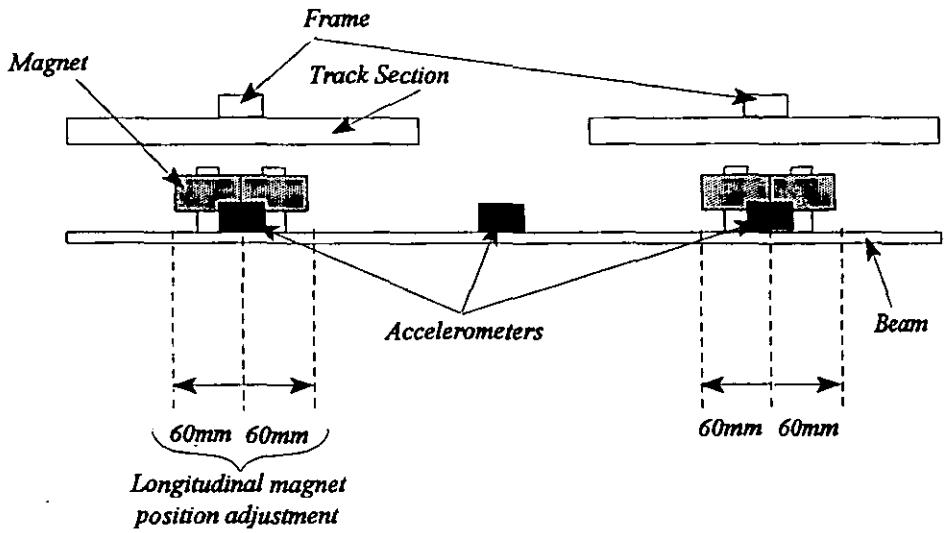

Figure 9.7 Rig configuration for investigation of the half car suspension

During the commissioning process it was logical to use a stiffened beam initially in order to get straightforward levitation without significant effects of beam flexibility. To stiffen the beam a 3m long section of square tubing was secured along the length of the beam using clamps. Being in suspension it should behave as an ideal free-free beam and a first bending frequency of 20Hz was measured. It was therefore significantly stiffened, but the fundamental resonant frequency is not particularly high. Due to the magnet positions the fundamental resonant frequency (i.e. the first symmetrical bending mode) is never significantly excited and for this reason does not figure in the experimental results. It should be noted that readings from all three accelerometers shown in figure 9.7 are presented in all of the results which means that low frequency bending modes can be identified without ambiguity.

Suspension with the stiffened beam was readily achieved using the following structure and compensator coefficients.

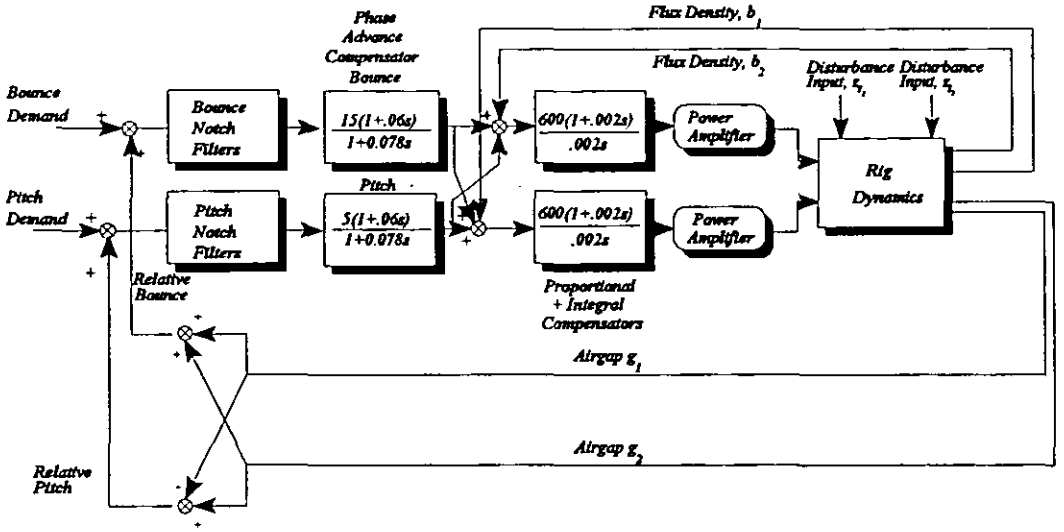

Figure 9.8 The classical controller used for tests on the flexible beam.

Two points that should be noted from figure 9.8 are that the controller does not use the complementary filter approach to allow the ride quality to be achieved and secondly the gains on the phase advance bounce and pitch filters are low giving a comparatively low bandwidth controller. The controller settings were the result of compromises due to one of the power amplifiers causing interference to the accelerometer and airgap sensor conditioning circuitry. This electromagnetic incompatibility problem was never fully explained. Nevertheless tests could be made with this controller to demonstrate the effects of low frequency bending modes.

A large number of conditions were assessed with this controller. These are summarised in table 9.1 and the results are presented and discussed on the following pages. Notch filters can be added in series with the bounce and pitch modes. The r.m.s vertical accelerations at the three accelerometer positions for each condition are expressed in response to the excitation of the beam by suspension alone and no other input is present. The acceleration power spectral densities presented are the result of 4 seconds of accelerometer output measured, scaled and then processed using an f.f.t technique.

Table 9.1: RMS Accelerations

			Notch Filter Frequencies [Hz]			R.M.S Acceleration [ms^{-2}] Measurement Position			Stable
Fig.	Beam	Magnet Position	Pitch (1st)	Bounce (3rd)	Pitch (2nd)	One	Two	Centre	
None	None	1DOF	None	None	None	0.776	NA	NA	Yes
None[1]		1DOF	None	None	None	0.076	NA	NA	Yes
9.9	Stiff-ened	Nom	None	None	None	0.56	0.775	0.601	Yes
None		Nom	None	19.6	None	0.57	0.65	0.703	Yes
None		Nom	40.2	None	None	0.486	0.624	1.0	Yes
9.10		Nom	40.2	67.65	None	0.357	0.414	0.59	Yes
9.11/ 9.12	A	Nom	None	None	None	NA	NA	NA	No
9.13	A	Nom	28.8	None	None	2.735	2.729	2.796	Yes
None	A	Nom	28.8	51.9	None	2.258	2.25	2.704	Yes
9.14	A	Nom	28.8	51.9	51.9	2.162	2.17	2.668	Yes
None	A	+60	None	None	None	NA	NA	NA	No
9.15	A	+60	28.8	51.9	51.9	1.378	1.586	0.499	Yes
9.16	A	-60	None	None	None	2.828	2.811	1.252	Yes
9.17	A	-60	28.8	51.9	51.9	0.22	0.23	0.346	Yes
9.18/ 9.19	B	Nom	None	None	None	NA	NA	NA	No
None	B	Nom	28.8	51.9	51.9	2.613	2.627	2.78	Yes
None	B	Nom	30.1	55.4	55.4	1.908	2.037	1.388	Yes

[1] Complementary ride filters used.

Table 9.2: Measured Beam Frequencies (Hz)

Beam	1st symmetrical	2nd asymmetrical	3rd symmetrical	4th asymmetrical
Stiffened (levitated)	20	40	67.65	unknown
A (levitated)	7.2	28.8	51.9	unknown
A (impulse)	12.2	17.8	32.2	48
B (levitated)	12.5	30.1	55.4	unknown
B (impulse)	12.75	18.8	36	52

9.3.1 Half-car rig with a stiffened beam

Using the stiffened beam and the controller in figure 9.8 the following p.s.d results were obtained. Note the 20Hz fundamental bending mode is too small to be seen on these results as it is only mariginally excited.

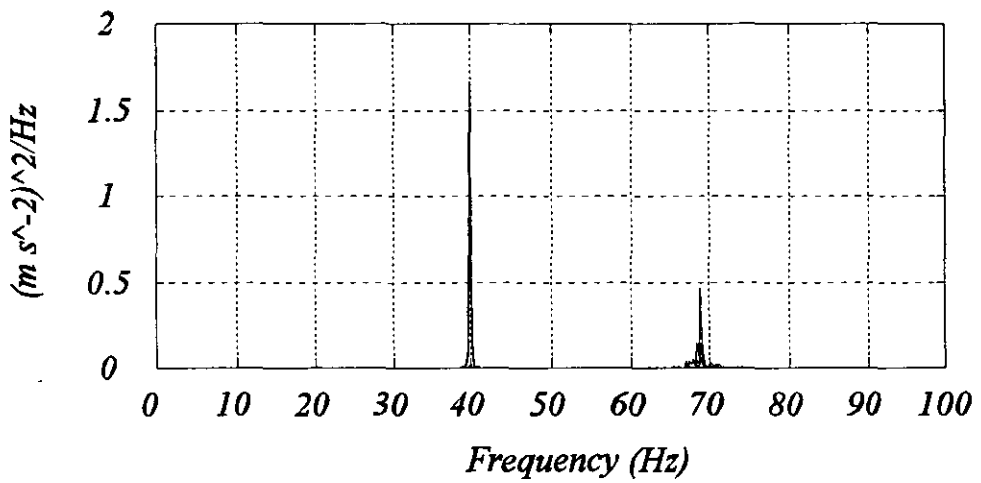

Figure 9.9 Resonances of the stiffened beam.

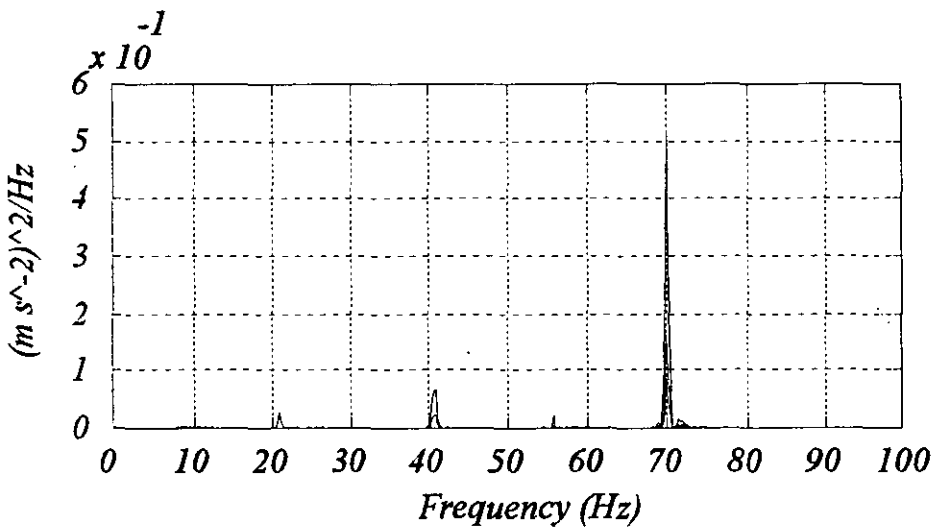

Figure 9.10 Effect of notch filters at frequencies of 40.2 and 67.65Hz in the pitch and bounce modes respectively for the stiffened beam

The magnitude ratio of the resonance at 40Hz is reduced by 83% by the introduction of the notch filters at 40.2Hz in the pitch mode and 67.65Hz in the bounce mode. Note the difference in scale between the two p.s.ds. The notch filter at 67.65Hz appears not to have sufficient attenuation however reduction in the magnnitude of the mode at 40.2Hz implies a transfer of energy to the 67.65 mode.

In this case the flexible bending modes are not a threat to the stability of the suspension. The notch filters improve the ride (in terms of acceleration) by 36% at the magnets but the ride at the centre of the vehicle shows no improvement.

9.3.2 Half-car rig and the normal beam

Analysis of the beam in levitation without any stiffening produces the following result, which demonstrates that the fundamental bending mode (nominally at about 12Hz) is not significantly excited. Indeed without this enlarged scale it would be hardly visible compared with the magnitude of the second mode.

Another significant result is that the central accelerometer, which should strongly detect the symmetrical bending mode, detects the 2nd bending mode which is in the asymmetric (pitch) mode showing a degree of cross-coupling due to the accelerometers not being positioned on the nodes of the flexible bending modes.

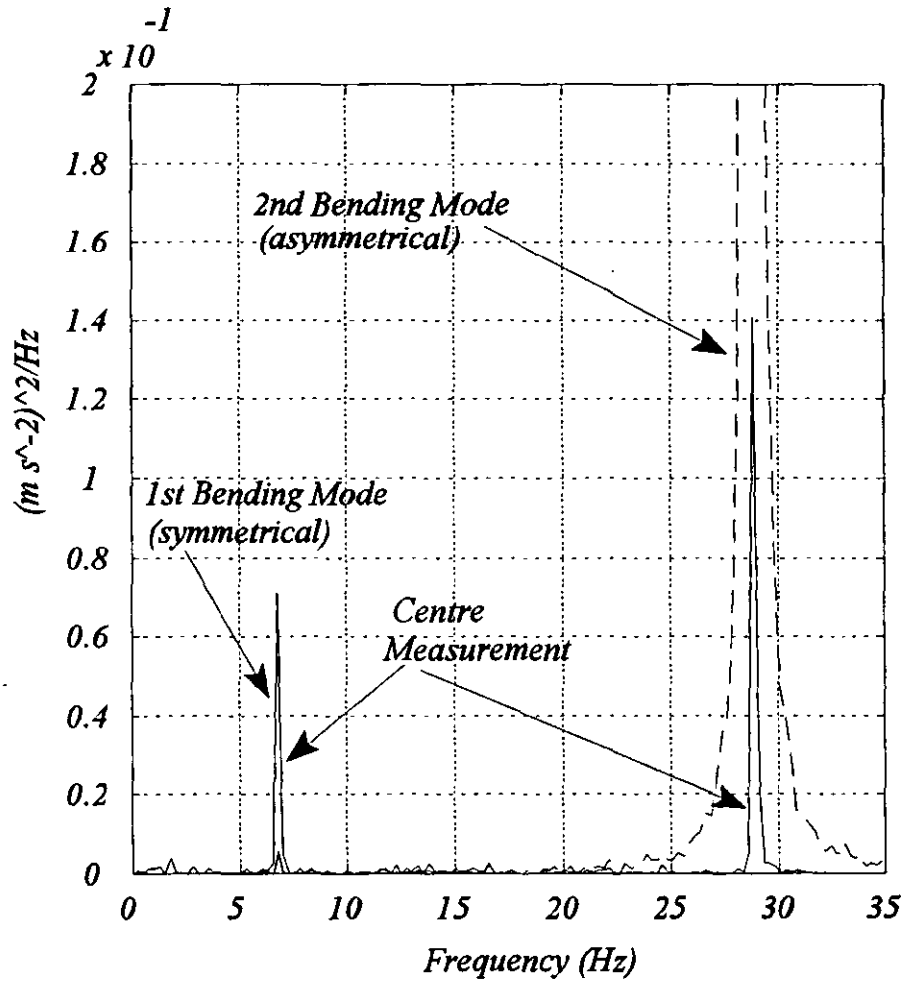

Figure 9.11 Acceleration power spectrum showing the limited excitation of the first bending mode, which has been shifted to 7Hz by the controller.

Why the fundamental bending mode appears to have been shifted to 7.2Hz from 12.2Hz is difficult to explain but is possibly due to interactions between the bending mode and the main position loop.

Figures 9.12 shows the resonances of the Maglev beam without any notch filters present. What the results do not show is that the Maglev eventually becomes unstable due to the increasing energy in the bending modes. The energy build-up due to the resonances is slow enough to be able to obtain the results shown before the system becomes unstable.

Figure 9.13 demonstrates the effective introduction of one notch filter at the first asymmetric bending mode. This stabilises the system by virtually eliminating the excitation of the 28.8Hz mode. It has the effect of increasing the excitation of the 2nd symmetrical bending mode at 51.9Hz in the bounce mode but this is not destabilising. After some experimentation it was found most effective to add two more notch filters of 51.9Hz in both the pitch and bounce modes. Strictly it should not be necessary to add both filters, but there clearly is coupling between the pitch and bounce modes due to the practical beam diverging from the theoretical ideal and the fact that the magnets produce a distributed force.

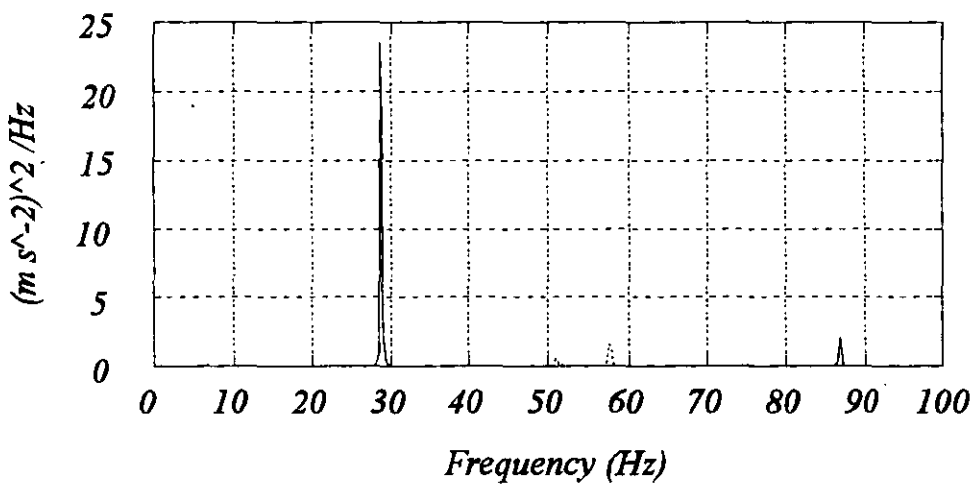

Figure 9.12 No notch filters present, and system becomes unstable due to the bending modes.

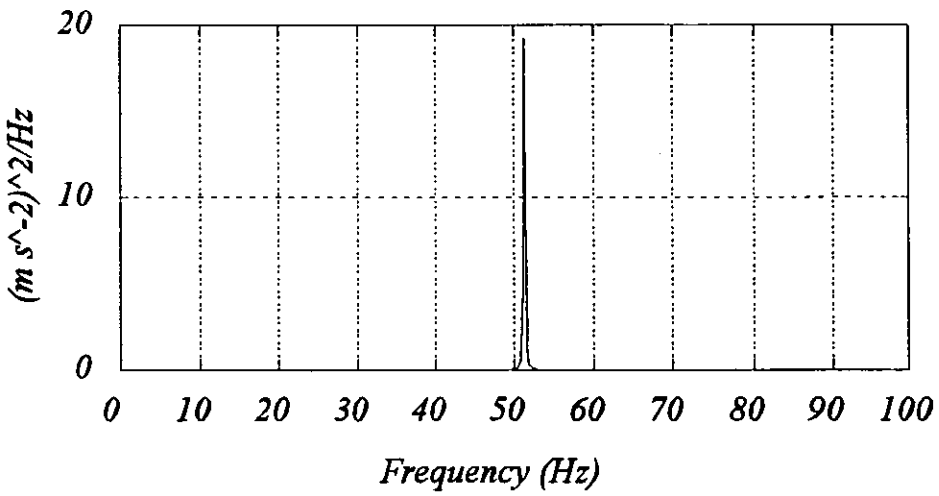

Figure 9.13 One notch filter at 28.8Hz in the pitch mode stabilises the suspension

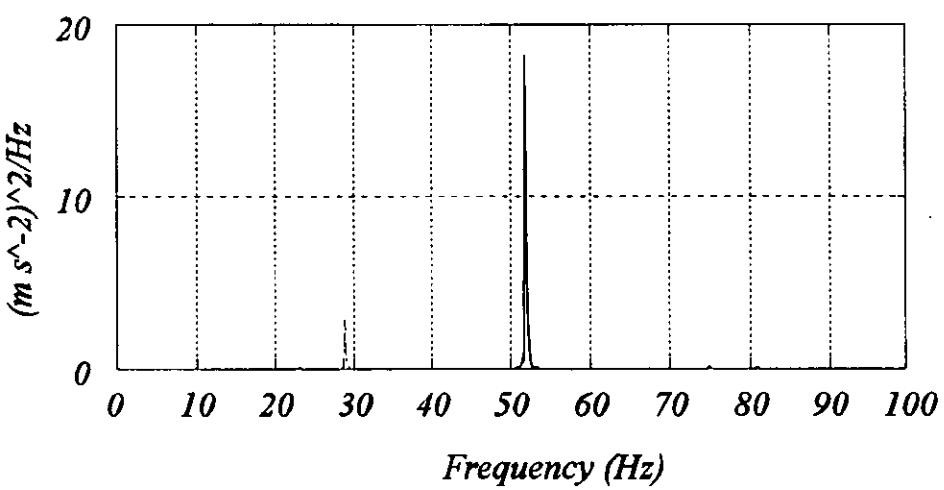

Figure 9.14 Notch filters of 51.9Hz present in both the bounce and pitch modes in addition to notch at 28.8Hz in the pitch mode.

Moving the magnets from their nominal positions (while keeping the accelerometers in the same positions) towards the ends of the beam by 60mm accentuates the excitation of some of the bending modes. On the basis of the theoretical mode shapes the 2nd bending mode should be less excited, while the 1st, 3rd and 4th bending modes should be more excited.

The system is in fact very unstable without notch filters and only with notches at 28.8Hz and 51.9Hz in the pitch mode and 51.9Hz in the bounce mode is it stable. Because of the shallow slope of the 1st bending mode it is only slightly more excited by the new magnet position, but is still hardly visible on the acceleration p.s.d.

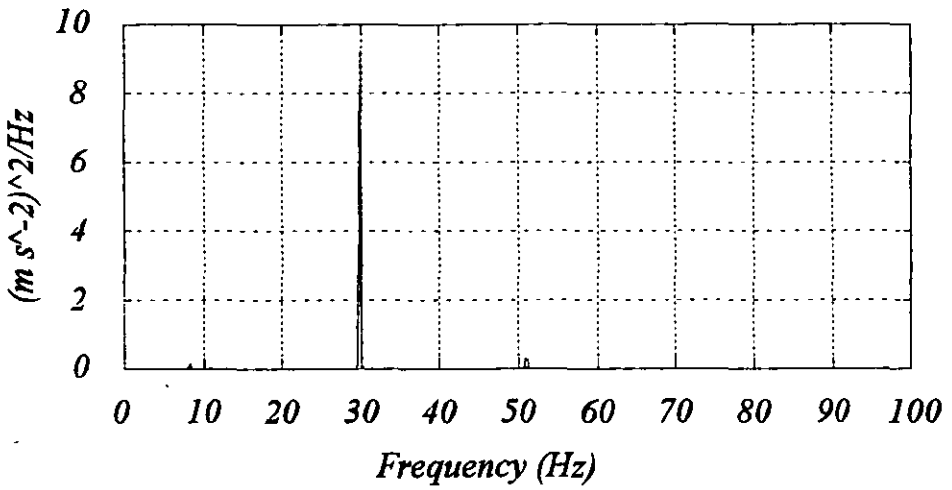

Figure 9.15 Magnets moved 60mm outwards from the beam centre, the system is only stable with notch filters at 51.9Hz in the bounce and 28.8 and 51.9Hz in the pitch modes.

Moving the magnets towards the centre of the beam in contrast has a stabilising effect, and the system is stable even without the use of notch filters. When notch filters are introduced the vertical acceleration level is the best of any of these tests. Clearly the movement of the magnets towards the beam centre reduces the excitation of the 3rd and 4th bending modes significantly, and only slightly increases the excitation of the 1st and 2nd bending modes. This 60mm or 2% change in the magnet position therefore has a surprisingly large effect on the stability. The acceleration p.s.ds are given for the Maglev suspension without and with notch filters in figures 9.16 and 9.17.

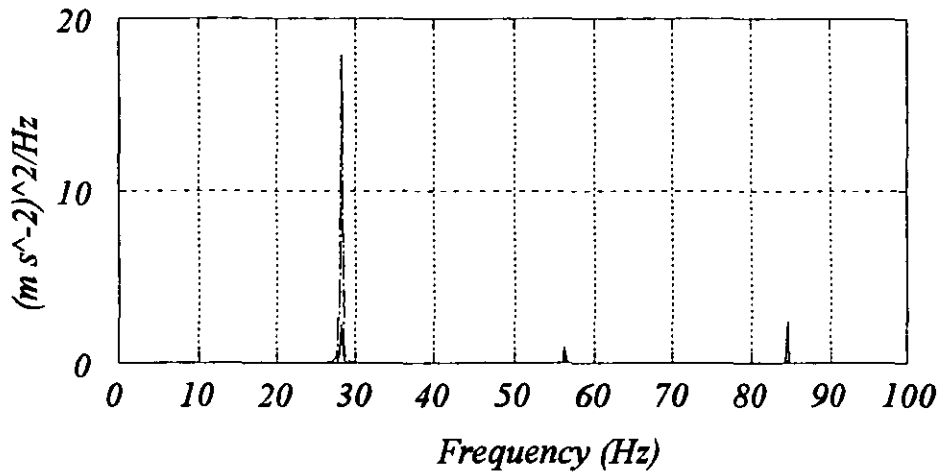

Figure 9.16 Magnets moved by 60mm towards the beam centre. No Notch filters used.

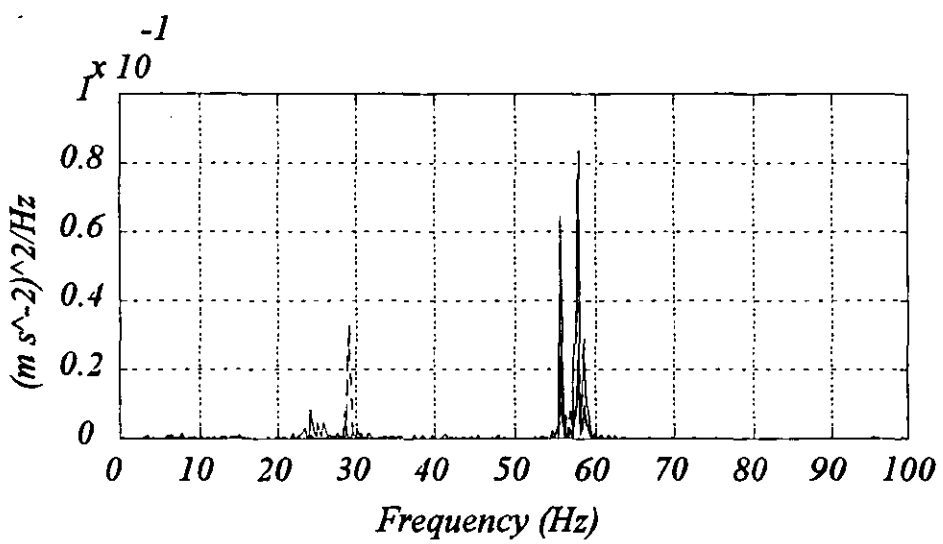

Figure 9.17 Magnets moved 60mm towards the centre and notch filters present on key modes.

The final experiment was to keep the controller the same but to change to the other beam in order to investigate the robustness of the controller. Changing from beam A to the slightly stiffer beam B did not produce any surprises. The slightly higher frequencies meant that the stiffer system was perceptibly more stable, but still required the use of

notch filters with the magnets in their nominal positions.

Figures 9.18 and 9.19 show the differences between the two beams. Figure 9.19 is a repeat of the result with an enlarged scale to show some of the less excited bending modes.

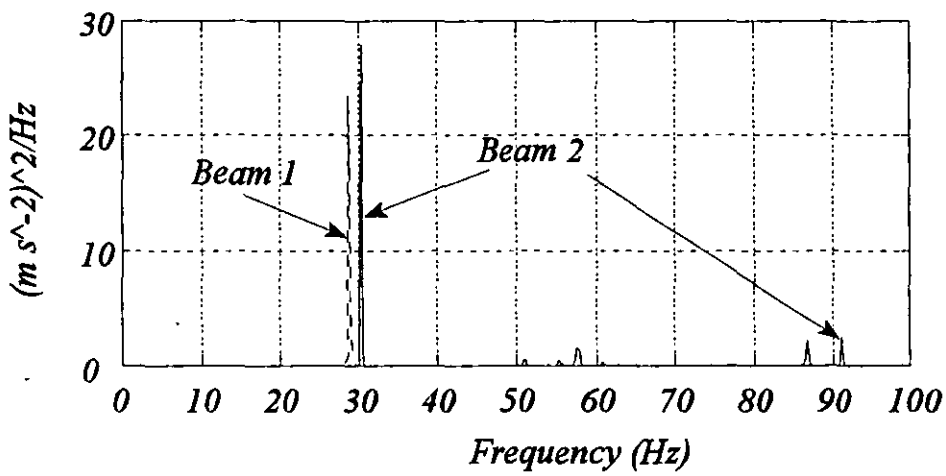

Figure 9.18 Comparison of the two beams (in levitation)

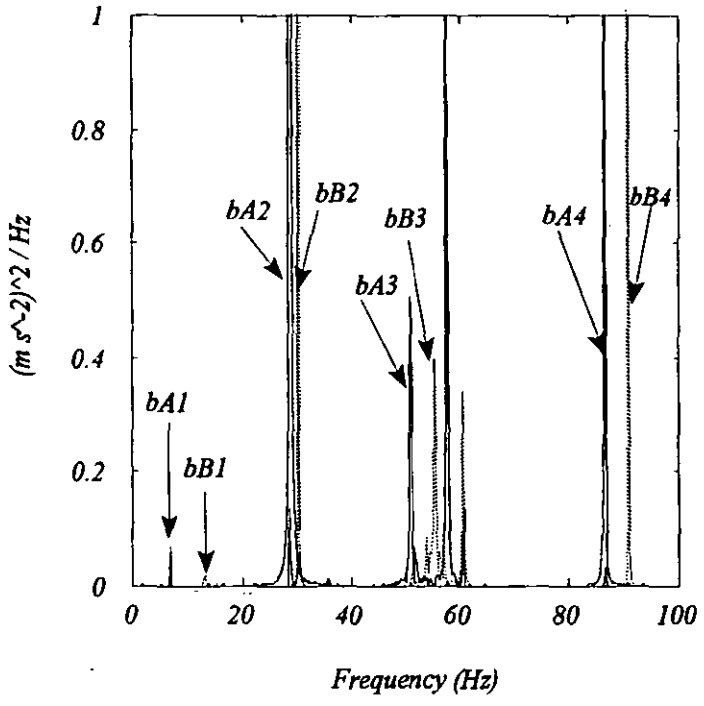

Figure 9.19 Comparison of the two beams where bA1 is the first beam and fundamental bending mode and bB1 is the second beam fundamental bending mode.

The frequencies around 60Hz are difficult to explain and need to be analysed using a finite element package. The two fundamental bending frequencies were originally shown to be at 12.2 and 12.75 Hz. The fundamental bending frequency of the second beam (bB1) remains close to this position at 12.5Hz but the beam A fundamental bending frequency (bA1) has shifted to about 7Hz. The reason for this difference in behaviour is unclear given the identical fabrication techniques used on each beam but the beam A's fundamental frequency may be that much closer to the main loop bandwidth that it is more strongly effected by the control action. These fundamental bending frequencies are not very significant to the control problem because they are barely excited which is a consequence of the magnet positions. The results in table 9.1 show that, while having the exact frequency of the bending mode in the notch filter is significant, it is not crucial. If the notch filter frequency is out by about 5% , as in this case, then the stability is not jeopardised though the ride quality performance does deteriorate by 50% in the worst case.

9.4 LQG Controller Implementation

Suspension was not achieved with the LQG controller within the time available for the project, this section presents an analysis of the difficulties which were encountered. The primary problem was that it was not possible to achieve satisfactory operation of the Kalman filter state estimator, and without this the state feedback control cannot work. Some attempt was made to reduce the controller gains in order to try and achieve stability, but these proved unsuccessful and so attention was turned to the Kalman filter on its own. From the outset is was found to be difficult to reconcile the differences between all of the estimates and their corresponding actual measurements. Any two of the estimated states could be adjusted through the weighting factors to give values close to the actual values, but the third estimated state then diverged from its corresponding actual state.

Another problem found when tuning the Kalman filter was the assessment of the bandwidth of the estimated state. For instance the acceleration measurements have a large high frequency component and to what degree these high frequency components need to be modelled is difficult to verify - other than by a trial and error process.

The Kalman filter was converted into discrete form using MATLAB® and tested with data from the classical controller system. Measurements from the rig were recorded onto disk and then fed into the Kalman Filter model in the MATLAB environment. This enabled off-line experimentation to be carried out with the filter design parameters.

The investigation was restricted to the single degree of freedom (quarter car) model used in chapter 6 given by equations 6.9 and 6.10, using the appropriate values for the rig (given in appendix 4 under the column 'rig' in table A4.1). The measurement data was obtained using the single degree of freedom Maglev suspension with the classical controller presented in section 9.2 and the rig configuration shown in figure 9.1. All of the results presented are produced with the Kalman filter operating in real-time in parallel with the classical controller.

The Kalman Filter gain was calculated using the following weighting factors;

$$\begin{bmatrix} v \\ \dot{i}_f \end{bmatrix}, \qquad Q_{kf} = \begin{bmatrix} 3.2^2 & 0 \\ 0 & 0.1^2 \end{bmatrix} \tag{9.5}$$

and

$$y = \begin{bmatrix} g \\ b \end{bmatrix}, \qquad R_{kf} = \begin{bmatrix} \frac{0.00005^2}{100} & 0 \\ 0 & \frac{0.0025^2}{100} \end{bmatrix} \tag{9.6}$$

The measurements used were airgap and flux density because these had proved themselves to be reliable for the classical controller implementation, and a typical example is describe below, in which the rig was driven with a 2Hz sinusoidal command signal. It was thought that the use of flux density and airgap would be sufficient and that the use of acceleration would cause additional complication. The assessment of the relative weightings for three input measurements is clearly a more complex problem.

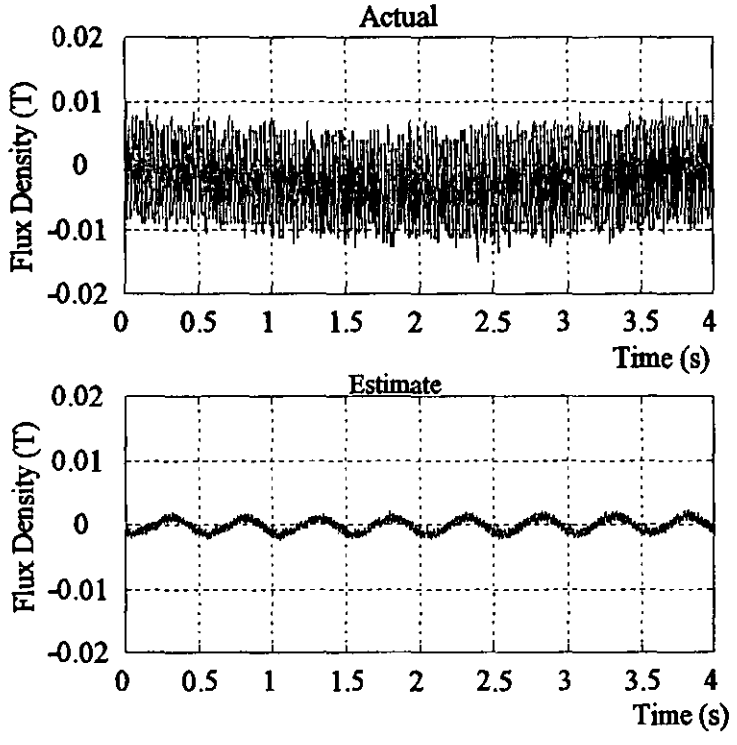

Figure 9.20 Flux Density actual and estimated time response when the Maglev is driven with a 2Hz command signal.

Clearly the flux density estimate (which is not used in the optimal control law) shows significant differences compared with the actual measurement. This difference is possibly due to the unmodelled dynamics which are removed from the estimate as noise should be. An f.f.t analysis of the actual flux measurements might reveal more information about the various components present.

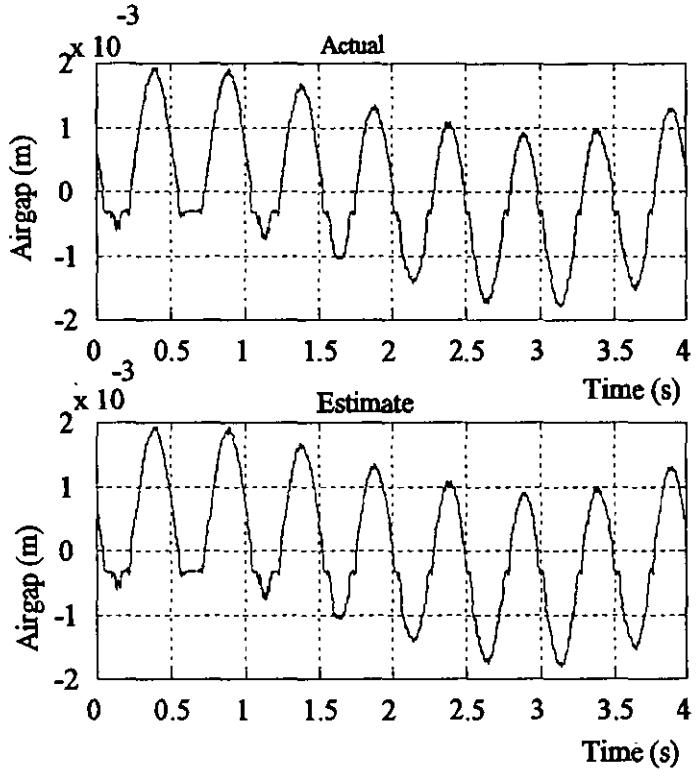

Figure 9.21 Actual and estimated airgap for a 2Hz command signal.

The actual and estimate airgap are shown in figure 9.21 and the estimate is very good. The distortion on the sinusoidal waveform results is due to a high frequency signal but its source is unknown.

The airgap and flux density estimates presented suggest that the Kalman filter is operating as it should be with respect to noise and higher order unmodelled dynamics. The estimated state consisting of airgap, velocity and acceleration produced a control vector, when fed into the state feedback gain matrix, of very high voltage demand and this seemed to be due to the velocity estimate component being unrealistic. This suggests mismatch

between the Kalman filter model and the rig.

9.5 Summary

The classical controller has been tested successfully and the experimental findings on the whole agree with the theoretical results presented in chapter 5. The work was also limited by problems with electromagnetic incompatibility between the transducers and one power amplifier, and although this was not explained it shows the importance of getting the signal conditioning right. A particular problem with the flux measurement was identified, and a compensation method investigated.

The LQG control strategy while theoretically promising so much has been very difficult to implement. The experimental results have provided some evidence of deficiencies in the Kalman filter, but time has not permitted further investigation. The problems with the flux measurement outlined earlier in this chapter almost certainly contribute to these deficiencies.

Chapter 10: Conclusions

A number of problems relating to the design of Maglev suspensions have been addressed. The use of a 'soft' chassis with a single stage Maglev suspension suitable for a low speed Maglev vehicle is a problem recognised from designing the Birmingham Maglev vehicles. The conflicting requirements of a suspension and in particular a single stage suspension mean that the introduction of additional suspension criteria is difficult. In addition the Maglev suspension requirements of a transition onto a gradient are given theoretical consideration.

10.1 Coping with a Soft Chassis

The existing classical control strategy has been fully investigated both theoretically and practically on a half-car rig. The introduction of lower frequency bending modes (of the order of 12Hz) into the chassis structure has been shown to cause difficulties with the Maglev suspension's stability and performance.

The conventional way to cope with the excitation of mechanical resonances in a controlled system is through the introduction of narrow band-reject or notch filters. The theoretical studies in this thesis demonstrate that the notch filters, while having the significant effect of avoiding the excitation of higher frequency bending modes, have a limited effect on low frequency bending modes. Simulation shows that the interaction between magnet position, bending mode shapes and stiffness of the chassis is a complex problem. For a soft chassis with magnets at 25 and 75% of the vehicle length the fundamental bending mode is not greatly excited. However the second and third bending modes are significantly excited. The third bending mode (which is symmetrical) has a destabilising effect on the system even when its resonance frequency (20Hz) is well above the main loop bandwidth (5Hz). Movement of the magnets towards the vehicle centre to reduce the excitation of the third bending mode has a positive effect with regard to this mode but increases the excitation of some other modes. The use of notch filters avoids the

destabilising effects of the higher bending modes (3rd and 4th) but ride quality is reduced for a particularly low chassis stiffness.

A classical modal controller using four notch filters for the first four bending modes is robust to changes in the mode shape though the degree of stability is reduced. Variation in the stiffness or uncertainty about the natural frequencies of the first four bending modes does limit the classical strategy of using notch filters. For instance a reduction in the fundamental bending frequency by 3% (at low frequencies) produces instability because the notch filters no longer match the resonant frequencies.

Practical investigations of the classical controller using a purpose built rig give very good agreement with the theoretical studies. The approximate nature of the Bernoulli-Euler model of the free-free beam means that other than for the fundamental bending mode the frequencies of the model do not agree with those of the rig. The trends shown in the theoretical studies are all confirmed by the practical investigations. The classical strategy lends itself to tuning during the commissioning stages of implementation, for instance by adjusting notch filters to the relevant bending frequencies. Practical tests very quickly allow the identification of the flexible bending modes causing stability problems. It was not found necessary to get the notch filter frequencies exactly tuned to the corresponding natural bending frequencies in order to provide stability, but exact agreement certainly improved ride quality. The movement of the magnets towards the centre of the beam relative to their nominal position had a very beneficial effect on stability and performance, suggesting that a greater understanding of the flexible mode shapes would allow further optimisation of the design. The degree to which the fundamental bending mode is not excited in the practical rig is surprising, so much so that it does not figure in the control problem.

The LQG controller promises a great deal. Theoretically, stability and performance are superior to the classical control strategy and it provides stability and ride quality for a very soft chassis (fundamental bending frequencies of 8Hz and less). Its robustness to changes

in the stiffness and consequently the bending mode frequencies was very good being able to cope with changes of up to 10% . Notably the robustness to changes in the bending mode shape was not quite as good as the classical controller. If the mode shape changed by ±5% the LQG controlled suspension became unstable, though for changes within this range the suspension was considerably more robust than the classical controller.

Implementation and commissioning of the LQG controller has proved very difficult. The Kalman filter was the component of the LQG strategy causing the problems. The practical results suggest that the model of the electromagnet rig used within the Kalman filter to derive its optimal gains was deficient in a number of respects. Firstly it did not adequately take account of the coupling identified between the low frequency airgap changes and the flux measurement. Secondly the flux input to the Kalman filter was not actually true flux density but was in fact the product of a self zeroing integrator, the dynamics of which were not included in the Kalman filter model.

The problems of the Kalman filter meant that the LQG controller for even the single degree of freedom magnet could not be implemented. The process of Kalman filter implementation were more complex than for the classical controller because the gain matrix and the discrete Maglev model could not easily be calculated within the development system, and had to be read from a file. This made the commissioning unwieldy compared with the implementation of the discrete compensation filters of the classical controller. This experience with LQG controllers is reflected in a recent article which states 'having designed a powerful controller and tested it in a simulation environment, the control engineer usually does not have the inclination, let alone the skill, to then code the control law in C and link it to some real time environment' [Williams95].

The problems encountered with the practical implementation of the LQG controller may well be overcome with a better model incorporating the flux measurement/airgap coupling and the flux density self-zeroing double integrator, but these issues remain to be tackled.

10.2 Theoretical Studies of the Response to Deterministic Inputs

The problem of large airgap deflections for Maglev suspensions using the skyhook damping effect following transitions onto gradients has been addressed for both the LQG and the classical control strategies. The classical controller uses a particular form of third order ride filter which inhibits the airgap deflection to a certain extent through integral action. An LQG controller has been developed with additional integral feedback of the airgap to reduce the deflection. Incorporating deterministic performance criteria into the suspension is difficult because of the conflicting requirements of a suspension, however using the ANDECS module MOPS in connection with MATLAB a technique of tuning both LQG and classical controllers was developed which allowed the response to both deterministic and stochastic inputs to be addressed together. The results were significant in that the classical and augmented LQG controllers both achieved approximately the same performance. The classical controller should be readily implementable because it has the same structure as the proven control strategy used on the Birmingham Maglev vehicles.

This study using the ANDECS environment provides a very powerful example of the use of multi-objective optimisation software to resolve conflicting requirements in a suspension.

The use of integral feedback has prompted further work on remodelling the Maglev suspension to implicitly incorporate integral airgap as a state in full state feedback controllers. Problems still remain in the tuning of such a controller, and how well the integral term can be estimated using a Kalman filter is an open question, especially in view of the practical experience on this project.

10.3 Implementation Issues

The mechanical rig and magnet construction have been successful. The flexible bending modes were very close to the desired resonances, and the magnets have achieved all of the

necessary requirements. Both of these crucial elements for a Maglev system were designed in a straightforward manner using conventional materials and standard workshop equipment.

The use of a digital signal processor was chosen to provide flexibility to the controller implementation and design. In fact, the use of quite a sophisticated floating point device has created problems due to the complexity of the software interface and the input/output requirements. The bundled software available with the DSP and the ADC/DAC cards was not suited to real time control. Its lack of transparency meant that it was impossible to alter, so new software (such as interrupt routines) had to be written. Because of the complexity of the DSP and associated elements this was not as straightforward as it could have been, particularly because the C compiler and linker used with this DSP proved to be unreliable. In retrospect it would have been better to have used a simpler DSP (fixed point, 16bit) and to program using a lower level language because the operation of the program would have been clearer, but such an approach however means that the code is less transportable or understandable to future workers. The problems encountered were specific to the choices made for this project and the conclusion should not be generalised.

In addition to the DSP problems, the interference problems caused by one of the power amplifiers remain unexplained. This emphasises the need to ensure the construction quality of the signal conditioning and in particular that for the accelerometers. The accelerometers used had a comparatively low sensitivity and the voltage output was 10mV/g making them susceptible to interference.

10.4 Suggestions for Further Work

The discrepancy between the Bernoulli-Euler beam model and the rig beam needs to be investigated, firstly to predict the bending mode resonances more accurately and secondly to show the effect of a distributed supporting force (i.e. the magnetic field) on the beam. This would best be done with a finite element package. Also a finite element model needs

to be used to optimise the magnet positions relative to the first four flexible bending modes. For a full vehicle rather than a half car model the additional roll and torsional modes must also be accounted for. In the experimental tests only the magnet positions were varied and the effect of varying the position of the accelerometers with respect to the mode shapes may identify positive phase effects to the complementary filter approach (which requires the use of an absolute position coordinate).

The magnetic field distribution and its interaction with the search coil in the pole face is an area of future work. Again analysis using finite element software is probably required. This is necessary to enhance the model of the flux density / force changes. This has been seen to be crucial to the LQG controller which seems to be sensitive to this model uncertainty.

The effect of the self-zeroing flux integrator and the airgap coupling need to be incorporated into the model dynamics of the Kalman filter. Uncertainty still remains in the design process of a Kalman filter and in particular the choice of weighting factors and their relationship to the expected input measurement and process noise.

If the noise problem caused by the power amplifiers was rectified it would allow the classical controller to be used with a higher position loop bandwidth to cope with 40% load changes and the introduction of the ride filters. If the controller operating at this higher bandwidth and supplying good quality ride exhibits the same properties as have been demonstrate by the rig, then it is possible that an extension of the use of notch filters may allow the use of a flexible chassis. The digital classical controller could be further developed with either more sophisticated frequency reject filters or even some form of adaptive notch filter. The DSP has inbuilt functions for calculating on line the fast Fourier transform, and it should not be too difficult for the exact resonance frequencies to be calculated and the notch filters tuned to these frequencies.

To assess the controllers with respect to a track input it will be necessary to shake the

track sections. It should be possible to approximate the track velocity spectra with these vibrations and assess the level of ride quality of the suspension.

10.5 Concluding Summary

The following key conclusions can be drawn from this thesis:

1. The LQG controller is theoretically superior in terms of robustness and performance compared with the Classical controller in terms of coping with flexibility and stochastic excitation.
2. The LQG controller is however more difficult to implement and the classical controller has proved itself during commissioning. The classical controllers advantages are that it can be implemented a loop at a time and that it does not require an accurate model of the system dynamics.
3. The results taken as a whole indicate that it is possible for a Maglev controller to cope with soft chassis. The results suggest that the classical controller may be a reasonable solution for the controller of a longer Maglev vehicle, but if the optimal strategy can be achieved in practice then it offers greater performance and robustness potential.
4. The use of a form of integral feedback seems to be the best method of coping with the transition onto a gradient given a controller using the sky hook damper. Limits to the performance of a Maglev system on gradients have been identified, and entail either using high quality track on the gradients or lowering the speed during the transition period.

References

[MN93] Japanese Test New MLU-002 Prototype on Miyazaki Track, Maglev News, Vol.11,No.6,Pp.1, 31st May 1993.

[HSTN94a] Bundesrat Ratifies Law Boosting German Maglev, High Speed Transport News, Vol.2, No.24, Pp.1-3, 3rd October 1994.

[HSTN94b] Central Japan Railways (CJR) working on next generation Shinkansen, High Speed Transport News, Vol.2, No.27, Pp.12, 14th November 1994.

[SZ94] Bundesrat genehmigt endgueltig die Transrapid-Strecke, Sud-Deutsche Zeitung, 2nd October 1994.

[Ahmed91] Ahmed, I., Digital Control Applications with the TMS320 Family, Texas Instruments 1991.

[Allen75] Allen,R.R., Karnopp,D.C., Semi-Active Control of Ground Vehicle Structure Dynamics, AIAA 16th Structures, Dynamics and Materials Conference, AIAA Paper 75-821, 27-29th May 1975.

[Balas79] Balas, M.J., Direct Output Feedback Control of Large space Structures, Journal of Astronautical Sciences, Vol. 27, No.2, Pp. 157-180, April 1979.

[Bals94] Bals,J., Joos,H.-D., Gruebel,G., The ANDECS-Matlab Environment for Databased Computational Control Experimenting, IEEE Joint Symp.on Computer Aided Control System Design, Tuscon, Pp.233-238, March 7th-9th 1994.

[Bartels72] Bartels,R.H., Stewart,G.W., Algorithm 432: Solution of the Matrix Equation AX+XB=C, Comm.ACM, Pp.159, September 1972.

[Bender67] Bender, E.R., Optimisation of the Random Vibration Characteristics of Vehicle Suspensions, MIT Thesis 1967.

[Benham85] Benham,P.P., Crawford,R.J., Mechanics of Engineering Materials, Longman 1987.

[Bernstein] Bernstein,D.S., Hyland,D.C., Optimal Projection / Maximum Entropy: Stochastic Modelling and Reduced Order Design Synthesis, IFAC Model Error Concepts and Compensation Workshop, Pp. 47-54, June 1985.

[Bishop60] Bishop,R.E.D, Johnson,D.C., The Mechanics of Vibration, University Press Cambridge, 1960.

[Braunbek39] Braunbek,Werner, Freischwebendende Körper im elektrischen und magnetischen Feld, Zeitschrift für Physik, Vol.112, No.11, Pp.753-763, April 1939.

[Bryson75] Bryson,Arthur, Yu-Chi, Ho, Applied Optimal Control, Hemisphere 1975.

[Capitani88] Capitani,G., Tibaldi,M., Reduced-order controllers for Active Suspension of Vehicles with Flexible Body, IASTED International Symposium MIC'88 Grindelwald, Pp. 305-307., February 1988.

[Capitani89] Capitani,G.,Tibaldi,M., Reduced-order controllers for Active

Suspension of Vehicles with Flexible Body, IMACS Conference, Cetaro,Italy, Pp.201-206, February 1989.

[Cellier91] Cellier,F.E., Continuous System Modeling, Springer-Verlag 1991.

[Cho93] Cho,Dan, Kato,Yoshifumi, Spilman,Darin, Sliding Mode and Classical Controllers in Magnetic Levitation Systems, IEEE Control Systems, Pp. 42-48, February 1993.

[CME88] Politics holds up maglev development, Chartered Mechanical Engineer No.3, Pp.16-17, March 1988.

[Davis88] Davis,B.R., Thomspson,A.G., Optimal Linear Active Suspensions with Integral Constraint, Vehicle System Dynamics, Vol.17, 357-366, 1988.

[Dobbs76] Dobbs, Magnetically levitated and wheeled Mini tram comparison study, British Rail Research & Dynamics Division report 5. 1976.

[Dodds73] Dodds, C.J., Robson, J.D., The description of Road Roughness, Journal of Sound and Vibration, Vol.31, No.2, Pp.175-183, 1973.

[Doyle79] Doyle, J.C., Stein, G., Multivariable feedback design: Concepts for a classical/modern sunthesis, IEEE Transactions on Automatic Control, Vol.AC-24, Pp.607-611.

[Earshaw39] Earnshaw,S, On the Nature of the Molecular Forces which regulate the Constitution of the Luminiferous Ether, Transactions of the Cambridge Philosphical Society, Vol.7, No.1, Pp.97-112, March 1839.

[Eastham84] Eastham,J.F., Balchin,M.J., Rodger,D., A comparison of some propulsion methods for magnetically-levitated vehicles, IMechE, Conference Maglev Now and for the Future, Pp.111-118, October 1984.

[Eitlhuber79] Eitlhuber, E., Purpose and Design of the Transrapid Experimental Facility Emsland, Proceedings of the International Symposium on Traffic and Transportation Technologies, Vol B11, 18-20th June, 1979.

[Forsythe91] Forsythe,W., Goodall,R.M., Digital Control, Macmillan New Electronics 1991.

[Franklin90] Franklin,Gene.F., Powell,J.David., Workman,Michael,L., Digital Control of Dynamic Systems, Addison Wesley 1990.

[Friedland86] Friedland,Bernard, Control System Design, An introduction to State Space Methods, McGraw-Hill 1986.

[Führer83] Führer,Claus, Dolan,John, Kovarianzanalyse bei zeitlichversetzten Erregerprozessen mit Anwendung auf mehrachsige Schienenfahrzeuge, DLR Institut für Fahrzeugtechnik Report 515-81-8, November 1983.

[Gevarter70] Gevarter,William, B., Basic Relations for Control of Flexible Vehicles, AIAA Journal, Vol.8, Pp. 666-672, April 1970.

[Goh93] Goh, Cher-Hiang, Anwendung der Positivitaets- und H_inf -Theorie zum Entwurf robuster Regelungen fuer flexible Strukturen. VDI Verlag Reihe8: Mess-, Steuerungs- und

Regelungstechnik, No. 334, 1993.

[Gondhalekar83] Gondhalekar, V.M., Jayawant, B.V., Chassis dynamics related to a low-cost magnetically suspended vehicle, IEE Proceedings, Vol.130, Pt.D, No.2, Pp.83-92, March 1983.

[Goodall76] Goodall,R.M., Suspension and Guidance Control for a d.c attraction Maglev vehicle IEE Conference Publication No.142, Pp.100-103, 1976.

[Goodall77] Goodall,R.M., British Rail Magnetically Suspended Vehicle -a description of its design, commissioning and testing, British Rail Research and Development Division Technical Report TR EDYN, 8th March, 1977.

[Goodall78a] Goodall,R.M, Control System Studies of an active lateral suspension to be fitted to POP-train, Internal British Rail Research Report IMDOS57, November 1978.

[Goodall78b] Goodall,R.M., Williams,R.A., Barwick,R.W., Ride Quality specification controller design for a magnetically suspended vehicle, Institute of Measurement and Control Symposium Dynamic Analysis of Vehicle Ride and Manoeuvring Characteristics, Pp.79-89, November 1978.

[Goodall81] Goodall,R.M, Williams,R.A., Lawton,A., Harborough,P.R., Railway vehicle active suspension in theory and practice. Proceedings 7th IAVSD Symposium, Cambridge, Pp.301-317, September, 1981.

[Goodall84] Goodall, R.M., Williams, R.A., Dynamic criteria in the design of Maglev suspension systems, IMechE Maglev Transport - now and for the future C393/84, Pp.77-86, October 1984.

[Goodall85] Goodall,R.M., The Theory of Electromagnetic Levitation, Journal of Institute of Physics, Vol.16, No.5, Pp.207-213, 1985.

[Goodall89] Goodall,R.M., Electromagnetic Suspension control without airgap measurement, Transactions Institution of Measurement and Control, Vol.11, No.2, Pp.92-98, April 1989.

[Goodall94] Goodall, R.M, Dynamic characteristics in the design of Maglev suspension, Proceedings IMechE Part F: Journal of Rail and Rapid Transit, Vol. 208, Pp.33-41, April 1994.

[Gottzein80] Gottzein,E., Meisinger,R., Miller,L., The 'magnetic wheel' in the suspension of high speed ground transportation vehicles, IEEE Transactionson Vehicular Technology, Vol.VT29, No.1, Pp.17-23., February 1980.

[Grübel83] Grübel,G., Kreisselmeier,G., Systematic Computer Aided Control Design, AGRARD Lecture Series, 1/09/83, No.28.

[Grübel91] Grübel,G, Joos,H-D, RASP and RSYST- Two Complementary Program Libraries for Concurrent Control Engineering, IFAC/IMACS 5th Symp. CADCS'91 Swansea., Pp.101-106, 15th July 1991.

[Grübel93] Grübel,G., The ANDECS Design Environment for Control Engineering, Proceedings 12th IFAC Congress,Sydney, July 1993.

[Hać85] Hać, A., Suspension Optimization of a 2-DOF vehicle model using a stochastic optimal control technique, Journal of Sound and Vibration, Vol.100, No.3, Pp.343-357, July 1985.

[Hać86] Hać, A., Stochastic Optimal Control of Vehicle With Elastic Body and Active Suspension, ASME Journal of Dynamic Systems, Measurements and Control, Vol.108, Pp.106-110, June 1986.

[Hayes80] Hayes,W.F., Tucker,H.G., Flannery,S.J., Rule,W.K., Structural Analysis of Proposed Maglev Vehicle Body Shell, NRC Canada 1980.

[Hedrick74] Hedrick,J.K., Billington,G.F., Dreesbach,D.A., Analysis, Design, and Optimization of High Speed Vehicle Suspensions Using State Variable Techniques ASME Journal of Dynamics Systems,Measurements, and Control, Vol.100, No.4, Pp.193-203, June 1975.

[Hotz87] Hotz,A, Skelton,R,E., Covariance Control Theory, International Journal of Control, Vol. 46, No.1, Pp.13-32, January 1987.

[Hullender72] Hullender,D.A., Wormley, D.N., Richardson, H.H., Active Control of Vehicle Air Cushion Suspensions, ASME Journal of Dynamic Systems, Measurement and Control, Vol.94, No.1, Pp. 41-49, March 1972.

[In-Dae93] In-Dae, Chung, Dal_Ho,Im, Chan-il,Park, Status of Development and Future Prospects of DaeWoo Maglev System in Korea, International Conference on Speedup Technology for Railway and Maglev Vehicles'93, , Pp.150-155. 22-26th November, 1993.

[In_Kun93] In_Kun,Kim, Chanil,Park, Kook_Hun,Kim, Maglev Programs in Korea, Argonne 13th International Conference Magnetic Levitation and Li, Pp.41-45, 19th May, 1993.

[ISO74] International Standard ISO2631: Guide for the Evaluation of Human Exposure to Whole-Body Vibrations, International Standards, ISO 1974.

[Jayawant81] Jayawant,B.V., Electromagnetic Levitation and suspension technique, Edward Arnold, 1981.

[Jayawant83] Jayawant,B.V., Gondhalekar,V.M., Chassis dynamics related to a low cost magnetically suspended vehicle. IEE Proceedings, Vol.130, No.2,Pp.83-92., March 1983.

[Jones94] Jones, D.I., Vibration control in Space, IEE Computing and Control Engineering Journal, Vol.5, No.2, Pp.89-95, April, 1994.

[Joos91] Joos,H.-D, Automatic Evolution of a Decision Supporting Design -Project Data base in Concurrent Control Engineering, IFAC/IMACS Symposium on Computer Aided Design in Control Systems, Pp.113-117, 7th July, 1991.

[Karnopp78] Karnopp,D.C., Vehicle Response to Stochastic Roadways, Vehicle System Dynamics, Vol.7, Pp.97-109, January 1978.

[Karnopp86] Karnopp,D.C., Theoretical Limitations in Active Vehicle Suspensions, Vehicle System Dynamics, Vol.15, Pp.41-54, June 1986.

[Khulief87] Khulief,Y.A., Sun,S.P., Finite Element Modeling and Semi-Active Control of Vibrations in Road Vehicles, ASME Winter Annual Meeting 87-WA-DSC-39, Boston, December 1987.

[Kortüm94] Kortüm,W., Lugner,P., Systemdynamik und Regelung von Fahrzeugen, Einführung und Beispiele, Springer 1994.

[Kreisselmeier72] Kreisselmeier,G., A solution of the Bilinear Matrix Equation AY+YB=-Q, SIAM Journal of Applied Mathematics, Vol.233, Pp.334-338, November 1972.

[Kwakernaak72] Kwakernaak,H., Sivan,R., Linear optimal Control Systems, Wiley-Interscience 1972.

[LaBarre70] La Barre,R.P., Forbes,R.T., Andrew,S., The Measurement and Analysis of Road Surface Roughnes, MIRA Report 1970/5, 1969.

[Laithwaite65] Laithwaite,E.R., Electromagnetic Levitation, Proceedings IEE, Vol.112, No.12, Pp.2361-2375, January 1965.

[Laithwaite66] Laithwaite,E.R., Propulsion without Wheels, The English Universities Press Ltd 1966.

[Lewis94] Lewis,F., L., Applied Optimal Control & Estimation, Digital Design and Implementation, PrenticeHall/TexasInstruments 1994.

[Lian93] Lian,J.S., Zhou,J.W., Zhang,K.L., Jiang,H., A General Survey of Chinese Maglev Train. Argonne 13th Conference on Magnetically Leviated Systems, Pp.146-150, May 1993.

[Lieh91a] Lieh, J., Control of Vibrations in Elastic Vehicles using Saturation Nonlinear Semiactive Dampers, ASME Winter Annual Meeting 91-WA-DSC, Pp.1-6, Winter 1991.

[Lieh91b] Lieh, J., Modeling and Simulation of an elastic vehicle with semiactive suspensions, ASME Advanced Automotive Technologies, DE-Vol.40, Pp.315-326.

[Lieh92] Lieh,J., Damping Control of Ride Quality for Flexible Vehicle, ASME DSC-Transportation Systems, Vol.44, Pp.113-127, January 1992.

[Liu93] Liu, K., Integrated Modelling and Controller Design with Application to Flexible Struture Control, IFAC Automatica, Vol.29, No.5, 1291-1314, October 1993.

[LSI92] 32 Channel Analog Data Acquisition User Manual, LSI 1992.

[LSI88] 16 Channel Analog Output Card User Manual, LSI 1988.

[Maciejowski89] Maciejowski, J.M., Multivariable Feedback Design, Addison-Wesley 1989.

[Margolis79] Margolis,D.L .Karnopp,D.C., Bond Graphs for Flexible Multibody Systems, ASME Journal of Dynamic Systems, Measurements, and Control, Vol.10, No.1, Pp.50-56, March 1979.

[Marguet93] Marguet,B., Theoretical and Experimental Study of the influence of Furniture Elements on the Modal Properties of an Underground Vehicle, GEC-Alsthom Report, unpublished 1993.

[Martinelli93] Martinelli,G., Morini,A., Present Status of Research for Maglev in Italy, Argonne 13th Conference on Magnetically Levitated Systems, Pp.51-53, 5th June 1993.

[Mayer93] Mayer,W.J., Rogg,D., Wiescholek,U.,The TRANSRAPID High-Speed Maglev System in Germany -Development Program and Future Prospects, International Conference on Speedup Technology for Railway and Maglev Vehicles, Vol.1, Pp.369-374, 22-26th November 1993.

[Mayer92] Mayer,W.J., Neue Magnetbahnkonzepte in den USA, ETR Forschungsinformation Bahntechnik 1/12/92, Vol.41, No.12, Pp.859-860.

[Meisinger75] Meisinger,R., Beitraege zur Regelung einer Magnetschwebebahn auf elastischem Fahrweg, VDI 1975.

[Meisinger77] Meisinger,R., Control Systems for flexible MAGLEV vehicles riding over flexible guideways, Proceedings IUTAM-IAVSD Symposium, Delft Summary, Pp. 200-202., 1975.

[Middleton90] Middleton,R.H., Goodwin,G.C., Digital Control and Estimation, A Unified Approach, Prentice-Hall, 1990.

[Miyamoto80] Miyamoto, M, A Dynamic Response of Magnetically Levitated Flexible Vehicle to Random Track Irregularities, RTRI Quarterly Reports, Vol.21, No.1, Pp.44-48, 1980.

[Mizuma93] Mizuma,T., Matsumoto,A., Masada,E., Technology and Safety Evalusation of EMS Maglev Transport H100, International

Conference on Speedup Technology for Railway and Maglev Vehicles'93, International Conference on Speedup Technology for Railway and Maglev Vehicles Conference, Vol.1, Pp.393-398, 22-26th November 1993.

[Moler78] Moler,C., VanLoan,C., Nineteen Dubious Ways to Compute the Exponential of a Matrix, SIAM Review, Vol.204,Pp.801-837, 1978.

[Müller79] Müller,P.C., Popp,K., Schiehlen,W.O., Covariance Analysis of Nonlinear Stochastic Guideway Vehicle Systems, 6th IAVSD Symposium, Pp.337-351, 3rd September 1979.

[Nagai87] Nagai,M., Sawada,Y., Active Suspension for Flexible Structure Control of High Speed Ground Vehicles, IFAC 10th congress of Automatic control, Vol.3, Pp.197-202, 27th July 1987.

[Newland93] Newland,D.E., An introduction to Random Vibrations, spectral and wavelet analysis, Longman Scientific 1993.

[Norris89] Norris,G.A, Skelton,R.E., Selection of Dynamic Sensors and Actuators in the Control of Linear Systems, ASME Journal of Dynamic Systems, Measurements & Control, Vol.111, Pp.389-397, 1989.

[North85] North,B., Maglev- Magnetically Levitated Transit System, Birmingham Airport, England, Railtech Conference 1985.

[O'Neill93] O'Neill,W., Beating the bullet, New Scientist, Pp.36, 2nd October 1993.

[Ozeki93] Ozeki,M., Current Status of Research and Development of Superconducting Maglev Systems in Japan, International Conference on Speedup Technology for Railway and Maglev Vehicles Conference, Vol.1, Pp.7-11, 22-26th November 1993.

[Paddison94] Paddison, J.E., MacLeod, C., Goodall, R.M., State Variable Constraints on the Performance of Optimal Maglev Suspension Controllers, 3rd IEEE Conference on Control Applications, Glasgow, August, Pp. 599-604, 1994.

[Patten90] Patten,W., Chalasani,R.M., Allsup,D., Blanks,J., Analysis of Control Issues for a Flexible One-Half Car Suspension Model,Ameican Control Conference,(SanDiego), Pp.1363-1368, 1st June 1990.

[Paul84] Paul,R.J.A, Asher,G.M., Williams,J.T., Brown,J., A new form of magnetic suspension for high speed maglev transport, ImechE Maglev Now and for the Future, Pp.67-76, October 1984.

[Pollard85] Pollard,M..G., Riches,E.E., Birmingham Maglev: Development for the Future, International Conference on MAGLEV Transport85, Pp.11-14, 17th September 1985.

[Rhodes74] Rhodes, R.G., Mulhall, B.E., Abel, E., Maglev Vehicle Oscillations and Damping Mechanisms, IEE Conference on new forms of Guide Transport, 1974, No.117.

[Robson80] Robson,J.D., Cross spectral densities in random vibration analysis, International Journal of Vehicle Design, Vol.12, Pp.121-129, February 1980.

[SIMS91] XCC & XCX Standard Library, S.M.I.S 1991.

[Schneider91] Schneider,M., Towards the magnetic unification of Germany?, German Research Service, Applied Science, Vol.3, Pp.4, August 1991.

[Sinha79] Sinha,P.K., Jayawant,B.V., Analytical and design aspects of Magnetically Suspended Vehicles, IFAC Automatica & Proceedings Symposium on MultivariableTechniques, Vol. 15, Pp.539-552, 1979.

[Sinha87] Sinha,P.K., Electromagnetic Suspension, Dynamics and Control, Peter Peregrinus Ltd 1987.

[Sinha91] Sinha, P.K, Pech, G., Abbassi, H.A., Digital Control of an Electromagnetic Suspension System using the TMS-3200 Signal Processor, Automatica, Vol.27, No.6, Pp.1051-1054, 1991.

[Skelton88] Skelton,R.E., Dynamic Systems and Control -Linear Systems Analysis and Synthesis, JohnWiley and Sons1988.

[Spangler66] Spangler,E.B, Marta,H.A, Dynamic Measurement of Rail Profile and Related Locomotive Truck Motions, ASME-IEEE Railroad Conference, SanFransisco, Paper 66-RR-1, 1966.

[Stix92] Stix,G., Riding on Air, Scientific American, Pp.82-83, 1st February 1992.

[Thomson88] Thomson,W.T., Theory of Vibration with applications, Unwin-Hyman 1988.

[Walker89] Walker,J.N., Birmingham's experience with the Maglev System, Airport Forum, Vol.5, Pp.15-18, April 1989.

[Whorlow93] Whorlow,R.J.,.Jayawant,B.V., Apparatus for the electromagnetic control of the suspension of an object, European Patent Application, European Patents 1993.

[Wie92] Wie,B., Experimental Demonstration of a Classical Approach to Flexible Structure Control, AIAA Journal of Guidance and Control, Vol.15, No.6, Pp.1327-1333, 1st November 1992.

[Williams81] Williams,R.A., Railway Suspensions enter the electroinc age, IEE Conference Publication 203, November 1981.

[Williams94] Williams,R.A., Electronically controlled automotive suspensions, IEE Computing and Control Engineering Journal, Vol. 5, No. 3, Pp.143-148, June 94.

[Williams95] Williams,S., Making Advanced Control Work, IEE Computing and Control Engineering Journal, Vol.6, No.1, Pp.5-10, February 1995.

[Yao93] Yao,W.H., Hedrick,J.K., Adaptive Sliding Mode Control of a Magnetic Suspension System using Output Feedback, Elsevier Studies in Automation and Control 1993. (Ed. K.D.Young).

Glossary of Symbols

A	system matrix	
A_a	augmented system matrix	
A_{cfr}	coupling between flexible and rigid body mode	
A_{crf}	coupling between rigid and flexible body mode	
A_c	cross sectional area of element	$[m^2]$
A_p	pole face area	$[m^2]$
A_{pt}	total pole face area	$[m^2]$
A_r	track roughness / rigid body dynamics matrix	[m]
A_{sf}	shaping filter system matrix	
A_t	magnet surface area	$[m^2]$
B	control input matrx / flux density	
B_f	control input to flexible body modes	
B_o	nominal flux density	[T]
b	small variation in flux density	[T]
$c_j(T_p)$	individual criteria function (chapter 7)	
C	output matrix	
C_d	dynamic performance criteria (chapter 7)	
C_{sf}	shaping filter output matrix	
d_i	individual design director vector (chapter 7)	
D	feed-through matrix	
D_d	design director vector (chapter 7)	
E	Young's modulus of elasticity	$[N\ m^{-2}]$
f	frequency / small variation in force	$[cycle\ s^{-1}]$ / [N]
f_t	spacial frequency	$[cycle\ m^{-1}]$
f_i	force from the ith magnet	[N]
F	force	[N]
F_o	nominal force	[N]
g	airgap variation	[m]

g_1,g_2	airgap variation for magnet 1 / 2	[m]
g_{ss}	steady state airgap deflection	[m]
g_i	ith disturbance input matrix	
g_i, g_{ii}	first and second integrals of airgap g (chapter 7).	
$g_{gravity}$	acceleration due to gravity	[m s^{-2}]
G	disturbance input matrix / airgap	
G_i, G_{ii}	integral airgap gains (chapter 7)	
G_f	disturbance input matrix for flexible body modes	
G_a	augmented disturbance matrix	
G_o	Nominal airgap	
h	measurement coordinate for a bending mode shape	[m]
h_t	film coefficient	[W m^{-1} K^{-1}]
H	magnetic field strength	
$H(\omega)$	general filter function	
$H_{pa}(s)$	phase advance compensator	
$H_{pi}(s)$	proportional + integral compensator	
$H_{lp}(s)$	low pass filter	
$H_{hp}(s)$	high pass filter	
$H_{notch}(s)$	notch filter	
$H_r(s)$	ride filter	
$H_i(s)$	double integrator filter	
$H_{second}(\omega)$	second order suspension transfer function	
$H_{third}(\omega)$	third order suspension transfer function	
$H_{centre-i}$	vehicle transfer function between ith axle and centre	
$H_{centre-total}$	vehicle transfer function between all axles and centre	
i	small variation in current	[A]
I	current	[A]
I_p	performance indicators (chapter 7)	
I_2	second moment of area	[m^4]
I_o	nominal magnet current	[A]

I_x	moment of inertia for pitch mode	[Kg m^{-2}]
K_i	flux density, current gradient	[T/A]
K_g	flux density, airgap gradient	[T/m]
K_b	force, flux density gradient	[N/T]
K_{pa}	phase advance gain	[T/m]
M	total mass of magnet and load	[Kg]
Mo_i	ith bending moment	
l_{beam}	total beam length	[m]
L	distance between magnets	[m]
N	number of coil turns	
P	control law (chapter 7)	
P_x	covariance matrix for the x state	
$P_{x\xi}$	covariance matrix for the noise cross-coupling state	
P_ξ	covariance matrix for the coloured noise state	
Q_w	noise intensity	
Q_e	process noise weighting matrix for Riccati equation (Kalman filter)	
Q_k	weighting matrix for Riccati equation (LQR design)	
q_{kz}	acceleration weighting for Riccati equation (LQR design) (chapter 7)	
q_{kz}	velocity weighting for Riccati equation (LQR design) (chapter 7)	
q_{kg}	airgap weighting for Riccati equation (LQR design) (chapter 7)	
q_t	energy change per unit volume	[J m^{-3}]
q	white noise intensity	
q_r	generalised coordinate for the rth bending mode	
R	magnet resistance	[Ω]
R_e	measurement noise weighting matrix for Riccati equation (Kalman filter)	
R_k	cost of control weighting matrix for Riccati equation (LQR design)	
R_x	autocorrelation function [x^2]	
R_{zt}	track displacement autocorrelation function	[m^2]
R_w	noise autocorrelation function	
S_i	ith shear force	[N]

S_o	flat vertical track velocity spectrum	
S_x	input spectral density [x^2 time]	
S_{xr}	rth input spectral density [x^2 time]	
S_y	output spectral density	
S_{zt}	spatial spectral density	[m^2/rad m^{-1}]
$S_{\dot{z}_t}$	one side vertical spatial track velocity	[$(ms^{-1})^2/(rads^{-1})$]
t	time	[s]
t_i	time delay between i axles	[s]
T	time period	[s]
T_p	set of tuning parameters	
T_{max}	Maximum temperature rise of the device	[°C]
u	control input vector	[V]
V	velocity	[m s^{-1}]
V_{supply}	voltage supplied to suspension	[V]
V_{coil}	coil voltage	[V]
V_o	nominal coil voltage	[V]
v	small variation in coil voltage	[V]
$W_{\dot{z}_t}$	one side vertical spatial track velocity	[$(ms^{-1})^2$/Hz]
x	general state vector/horizontal distance travelled	[m]
x_a	augmented state vector	
x_f	state vector for flexible body modes	
X	general solution of the closed form Bernoulli-Euler equation	
y	mean response	
z	absolute position coordinate	[m]
z'	rigid body absolute position coordinate	[m]
z_1,z_2	absolute position coordinate of magnet 1 / 2	[m]
z_t	vertical track displacement	[m]
z_{t1},z_{t2}	vertical track displacement at magnet 1 / 2	[m]
α	max- min function (chapter 7)	

α_{xh}	receptance between force application point x and measurement point h	
α_{pa}	phase advance term	
δ	dirac function [1/time]	
ζ	damping factor/output coloured noise	
λ_r	solution of the rth frequency equation	
ξ	coloured noise state	
ρ	correlation coefficient / density	
θ	angular rotation	[rad]
$\phi_{centre\text{-}i}$	phase response centre of vehicle and ith axle	
Φ	transition matrix	
ϕ_r	characteristic function for mode shape r	
Ω	spatial frequency	[rad m^{-1}]
τ	time period / time constant	[s]
τ_{pa}	phase advance time constant	[s]
ν	measurement noise	
υ	displacement of flexible mode	[m]
ω	angular frequency / process noise	[rad s^{-1}]
ω_o	filter frequency	[rad s^{-1}]
ω_n	filter frequency/notch filter frequency	[rad s^{-1}]
ω_r	ride filter frequency	[rad s^{-1}]
ω_i	double integrator frequency	[rad s^{-1}]

Acknowledgements

The author wishes to thank the following individuals and organisations for their support during the course of this learning experience.

Professor Roger Goodall for introducing me to Maglev and giving me the opportunity to work on such an interesting problem.

Dr Colin MacLeod for taking an interest in my work and helping me to formalise the theory.

Professor Willi Kortüm and his department for providing me with the opportunity to work at the DLR and making my year in Germany so rewarding and enjoyable.

Professor Georg Grübel and his department for making the ANDECS software available to me.

To my fellow colleagues who gave their time freely to help me during the practical stages.

And lastly my parents who have provided unstinting support and encouragement, particularly over the last year of the Ph.D.

Thanks are also due to GEC-Alsthom Metro-Cammel Limited for providing both financial support and industrial experience to the project and the Engineering and Physical Sciences Research Council for the CASE Studentship.

Additional funding was financial support was provided by the Deutsche Akademischer Austauschdienst, the Royal Academy and the IMechE.

Appendix 1: Spectral Density Basic Theory

The autocorrelation function for a random process x(t) is defined as the average value of the product x(t)x(t+τ). Where the process is sampled at time t and then at time t+τ. The mean value of the product E[x(t)x(t+τ)] and the standard deviation, σ are independent of absolute time provided the process is stationary and is dependent only on the time separation τ. Hence the definition:

$$E[x(t)x(t+\tau)] = R_x(\tau) \qquad \text{A1.1}$$

The autocorrelation function $R_x(\tau)$ indirectly gives information about the frequencies present in a random process. The frequency content of a graph of $R_x(\tau)$ against τ reflects the frequency content of samples of the random process x(t). At very large time intervals, $\tau \to \infty$, a random process will be uncorrelated since there will not be a coherent relationship between x(t) and x(t+τ). In this case the correlation coefficient, ρ will tend to zero so defining the mean value of x as m=E[x];

$$\rho = \frac{E[(x(t)-m)(x(t+\tau)-m)]}{\sigma^2} \qquad \text{A1.2}$$

$$\rho = \frac{R_x(\tau)-m^2}{\sigma^2} \qquad \text{A1.3}$$

hence $R_x(\tau \to \infty) = m^2$. Also it should be noted for a stationary process $R_x(\tau)$ depends only on the separation time τ and not absolute time t.

When the random process x(t) is normalised about a zero value such that the mean value of the process m=E[x] is zero, then provided x(t) has no periodic components, $R_x(\tau \to \infty) = 0$ and the Dirichlet condition $\int_{-\infty}^{\infty} |R_x(\tau)| d\tau < \infty$ is satisfied and thus the Fourier Transform of $R_x(\tau)$

may then be calculated (Classical Fourier Analysis theory applies only to functions which decay to zero when $|t| \to \infty$).

The Fourier Transform of $R_x(\tau)$ and its inverse are defined here by

$$S_x(\omega) = \frac{1}{2\pi}\int_{-\infty}^{\infty} R_x(\tau) e^{i\omega\tau} d\tau \qquad \textbf{A1.4}$$

$$R_x(\tau) = E[\, x(t).x(t+\tau)\,] = \int_{-\infty}^{\infty} S_x(\omega) e^{i\omega\tau} d\omega \qquad \textbf{A1.5}$$

$S_x(\omega)$ is the spectral density of the x process and is a function of angular frequency.

It is important to note that many authors differ over the position of the factor $1/2\pi$ which appears in these equations. The above definition is the one more popular in random vibration theory [Newland93] [Karnopp78].

Consider the case when $\tau=0$:

$$R_x(\tau=0) = E[\, x^2\,] = \int_{-\infty}^{\infty} S_x(\omega) d\omega \qquad \textbf{A1.6}$$

The mean square of the stationary process x is therefore given by the area under a graph of spectral density $S_x(\omega)$ against ω.

The units of $S_x(\omega)$ are those (mean square of process)/(unit of frequency).

$S_x(\omega)$ is better named the mean square spectral sensity. The mean square spectral density of a stationary random process x(t) is a real, even and non-negative value of ω.

Obviously the mean square value of a white noise process is infinite so white noise is a theoretical concept only, but practically the term is used to describe a broad band noise whose bandwidth extends well past all frequencies of interest.

From the the inverse Fourier transform of $R_x(\tau)$

$$R_x(\tau)=\int_{-\infty}^{\infty} S_x(\omega)\cos\omega\tau\, d\omega \qquad \textbf{A1.7}$$

$$R_x(\tau)=2\int_{\omega_1}^{\omega_2} S_o\cos\omega\tau\, d\omega \qquad \textbf{A1.8}$$

$$R_x(\tau)=\frac{2S_o}{\tau}\cos\left(\frac{\omega_1+\omega_2}{2}\right)\tau\sin\left(\frac{\omega_2-\omega_1}{2}\right)\tau \qquad \textbf{A1.9}$$

When $\omega_1=0$,

$$R_x(\tau)=\frac{2S_o\sin(\omega_2)\tau}{\tau} \qquad \textbf{A1.10}$$

As $\omega\to\infty$ the cycles of the random process pack together such that they form a single vertical spike of infinite height, zero width and finite area. This behaviour is represented mathematically by using Dirac's delta function $\delta(\tau)$ which is so defined that it is zero every where except at $\tau=0$ which is infinite in such a way that:

$$\int_{-\infty}^{\infty}\delta(\tau)d\tau = 1 \qquad \textbf{A1.11}$$

More generally $\delta(\tau - T)$ is zero everywhere except $\tau = T$ and has the sifting property:

$$\int_{-\infty}^{\infty}\delta(\tau - T)\, f(\tau)\, d\tau = f(\tau = T) \qquad \textbf{A1.12}$$

where $f(\tau)$ is any arbitary continuous function of τ. Using this 'delta function' notation the autocorrelation function for a stationary random white noise process with spectral density S_o is written.

$$R_x(\tau) = 2\pi S_o \delta(\tau) \qquad \textbf{A1.13}$$

This term is zero every where except $\tau = 0$ where it is infinite. This area under $R_x(\tau)$ at $\tau=0$ is $2\pi S_o$ and this can be verified by calculation of the Fourier transform of $R_x(\tau)$ to regain $S_x(\omega)$ thus:

$$S_x(\omega) = \frac{1}{2\pi}\int_{-\infty}^{\infty} 2\pi S_o \delta(\tau) e^{-j\omega\tau} d\tau \quad \rightarrow \quad S_x(\omega) = S_o \qquad \textbf{A1.14}$$

Dimensions of S_o are those of (x^2)x(time), for the $\delta(\tau)$ are 1/(time) and so the dimensions of the autocorrelation function $R_x(\tau)$ are those of (x^2).

Appendix 2: Covariance Analysis

Covariance Analysis for i inputs (following [Kortüm94])

Generalising for an i axle vehicle and incorporating the shaping filter input description gives the following equations:

$$\dot{x}_a = A_a x_a + \sum_{i=1}^{r} G_i \zeta(t-t_i) \qquad \text{A2.1}$$

$$\dot{\xi} = A_f \xi + G_f w \qquad \text{A2.2}$$

$$\zeta(t-t_i) = C_f \xi(t-t_i) \qquad \text{A2.3}$$

Where :

$$A_a = \begin{bmatrix} A & g_1 c_f & g_2 C_f & \cdots & g_r C_f \\ 0 & A_f & 0 & 0 & 0 \\ \cdots & \cdots & \cdots & \cdots & \cdots \\ 0 & 0 & 0 & 0 & A_f \end{bmatrix} \quad G_a = \begin{bmatrix} 0 & \cdots & 0 \\ 1 & \cdots & \cdots \\ \cdots & \cdots & \cdots \\ 0 & \cdots & 1 \end{bmatrix}, \quad x_a(t) = \begin{bmatrix} x(t) \\ \xi(t-t_1) \\ \cdots \\ \cdots \\ \xi(t-t_r) \end{bmatrix} \quad x_a(t) = \begin{bmatrix} w(t-t_1) \\ \cdots \\ \cdots \\ w(t-t_r) \end{bmatrix}$$

Defining also a Covariance Matrix P_x

$$P_x = \begin{bmatrix} P_x & P_{x1} & P_{x2} & \cdots & P_{xr} \\ P_{x1}^T & P_{x1} & 0 & 0 & 0 \\ \cdots & \cdots & \cdots & \cdots & \cdots \\ P_{xr}^T & P_{1r}^T & 0 & 0 & P_{rr} \end{bmatrix}$$

As before solving the following three equations (for the time invariant system).

Form filter 'Lyapunov Equation'

$$A_f \bar{P}_{x_{a\,ij}} + \bar{P}_{a\,ij} A_f^T + e^{A_f(t_f - t_i)} G_f Q_w G_f^T = 0 \quad , i = 1 \ldots\ldots j \ , \qquad j = 1,\ldots\ldots r, \qquad t > t_o + t_i \qquad \textbf{A2.4}$$

Where for the covariance matrix of the process ξ gives:

$$\bar{P}_{ij} = \bar{P}_{ij}^T \ , \qquad i = 1,\ldots\ldots j \qquad j = 1,\ldots\ldots r. \qquad \textbf{A2.5}$$

Coupling 'Lyapunov Equation'

$$A P_{x\,j} + P_x A_f^T + \sum_{i=1}^{r} g_i P_{ij} + S_j G_f Q_w G_f^T = 0 \qquad j = 1 \ldots\ldots r \ , \qquad \textbf{A2.6}$$

$$S_j = \sum_{i=1}^{j} \int_0^{t_j - t_i} e^{A(t_j - t_i - \tau)} g_i e^{A_f \tau} d\tau \qquad \textbf{A2.7}$$

$$A S_j + S_j A_f = \sum_{i=1}^{j} \left[e^{A(t_j - t_i)} g_i - g_i e^{A_f(t_f - t_i)} \right] \qquad \textbf{A2.8}$$

Principal 'Lyapunov Equation'

$$A P_x + P_x A_f^T + \sum_{i=1}^{r} (G_i P_{x\,i}^T + P_x g_i^T) = 0 \qquad \textbf{A2.9}$$

Implementation of the Covariance Analysis using MATLAB

Firstly for a single input system:

```
% Analysis of the butterworth filter response with covariance and frequency
% response techniques.
% Using the definition of the Fourier Transform pair according to Karnopp and
% Newland.
```

```
Ar=1e-6;                          % Track Roughness [m]
V=15;                             % Vehicle Speed [m/s]
wo=2*2*pi;                        % Butterworth Filter Rolloff Frequency [rad/s]
zeta=1/sqrt(2);                   % Damping Factor
w=logspace(-1,5,1000);            % Develops a uniform step size

num=[1 0];                        % Transfer Function represents acceleration
den=[1/wo^2 2*zeta/wo 1];         % over track  elevation velocity

[mag,phase]=bode(num,den,w);      % Calculate the frequency response of the filter
[A,B,C,D]=tf2ss(num,den);         % Convert the filter to state space form

% Covariance Analysis

r=(pi*Ar*V)*(2*pi);               % Define covariance input  R_{z_r}(τ=0)

Qstate=lyap(A,B*r*B');            % Apply Lyapunov equation
Qout=C*Qstate*C';
rmsac2i=sqrt(Qout);               % R.M.S responses

% Frequency Response Analysis
ma=((mag).^2);

m=0;                              % Variables used for the integration
h1=0;
w1=0;
Area=0;

for i=1:999.;                     % Integration loop
        Area=Area+(w(i)-w1)*(m+ma(i))/2;
        m=ma(i);
        w1=w(i);
end
% Integral is double sided (in rad/s) so we must multiply by 2
```

```
% The flat input spectrum in radians is pi.A.v

rmsac2ii=sqrt((pi*Ar*V)*(2*Area));
rmsac2iii=sqrt((pi*Ar*V)*wo^3*pi/(sqrt(2)));        % Optimal suspension formula as
                                                    % described by Hullender et al

fprintf('RMS a time derivation %g m/s^2\n\n',rmsac2i);      % 0.455 ms⁻²
fprintf('RMS a frequency derivation %g m \n\n',rmsac2ii);   % 0.455 ms⁻²
fprintf('RMS a formula derivation %g m \n\n',rmsac2iii);    % 0.455 ms⁻²
```

For a two input system system matrix ac and inputs b1 and b2 with an autocorrelation function rdint:

```
b1=b(:,1);
b2=b(:,2);
exd=expm(ac*L/v);                                   % Calculate the transition matrices
exdt=expm(ac'*L/v);
Qdist=b1*b1'+b2*b2'+exd*b1*b2'+b2*b1'*exdt;         % Calculate the covariance input matrix
X=lyap(ac,Qdist*rdint);                             % Solve the Lyapanov equation
p=c*X*c';                                           % Extract the output variables
rms=sqrt(abs(diag(p,0)));                           % Determine the rms values
```

Appendix 3: Choice of State Variables

Copy of paper:

State Variable Constraints on the Performance of Optimal Maglev Suspension Controllers.

J.E.Paddison, C. MacLeod, R.M.Goodall

Published in the Proceeding of the IEEE Conference on Control and its Applications. Glasgow, UK, August 1994, pp.599-604.

The impetus for the following paper came from the work presented in chapter 7. My contribution was the basic model, the analysis techniques and the problem description together with the formal analysis.

Appendix 4: System Models

Table A4.1: Model Comparison

Model Parameter	Birmingham Maglev	Quarter Car	Half Car	Rig	Goodall Rig [Goodall89]
Tare Mass, M [Kg]	5000	1000	5052	105	0.075
Fully laden Mass [Kg]	8000	1200	8000	160	NA
Airgap, Go [mm]	0.015	0.015	0.015	0.01	0.004
Flux Density B_o [T]	1	0.7	0.7	0.7	0.07
Current, I_o [A]	100	100	100	12	0.5
Nominal Force Fo / magnet [N]	16000	9810	24784	981	0.7
Pole Face Area A_p [m^2]	0.04	0.025	0.0318	0.0025	0.0004
Turns, N	≈240	167	167	930	830
Resistance [Ω]	≈1	0.5	4	1.8	10
Length [m]	6	NA	15	3	NA
Resonances					
f_1 (symm)[Hz]	40	NA	16.1	7.2	NA
f_2 (asym) [Hz]	≈96.6	NA	44.3	28.8	NA
f_3 (sym) [Hz]	≈189	NA	86.9	51.9	NA
f_4(asym) [Hz]	≈313	NA	143.6	75	NA
Damping Factor	≈0.03	NA	0.03	0.002	NA

Matlab Programs

Program 1: Rig parameter definitions "para1.m"

```
%%%%%%%%%%%%%%%%%%%%%%%%%%%%%%%%%%%%%%%%%%%%%%%%%%%%%%%
%        General Parameters for Flexible Maglev                    %
%                                                                  %
%        Flexible Modes Defined                                    %
%                                                                  %
%        FIGURES BASED ON THE BIRMINGHAM PEOPLE MOVER              %
%                                                                  %
%                                                                  %
%%%%%%%%%%%%%%%%%%%%%%%%%%%%%%%%%%%%%%%%%%%%%%%%%%%%%%%

Dept1=0.7;                          % method of varying w1, w2
Bred1=0.5;
f1=0.75;                            % variation of actuator position 0.7-1
senpos=1;                           % variation in sensor position 0.8-1.2 step 0.05
moderr=1;                           % modal displacement error 0.8-1.2 step 0.05
massch=1;                           % load variation

% ***** Vehicle and Roadway Parameters ********************************

rough=pi*1e-6;                      % Track surface roughness (m)
v=15;                               % Vehicle Speed (m/s)
rdint=2*pi*v*rough;                 % White Noise Intensity

% ***** Beam dimensions ************************************************

bred1=0.72*Bred1;
dept1=0.9*Dept1;

beam(1)=Bred1;                      % Beam breadth
beam(2)=Dept1;                      % Beam depth
beam(3)=bred1;                      % Beam inner breadth
beam(4)=dept1;                      % Beam inner depth
L=15;                               % Beam length

% ***** Magnet parameters **********************************************
mu=1.257e-6;                        % Permeability of free space
gravity=9.81;                       % Acceleration due to Gravity [m/s^2]
Bo=0.7;                             % Flux density [T]
Go=0.015;                           % Nominal Air gap
Io=100;                             % Nominal Current
N=(Bo*(2*Go))/(mu*Io);              % Turns, using nominal current
bmass=(beam(1)*beam(2)-beam(3)*beam(4))*L*2626;   % Beam mass Aluminium (Kg)
magmass=100;                        % Magnet Mass (Kg)
M=bmass+2*magmass;                  % Total suspended mass
R=4;                                % Resistance (Ohms)
Ix=magmass*(L/4)^2+bmass*(L^2)/12;  % System moment of inertia
Iz=(beam(1)*(beam(2))^3-beam(3)*(beam(4))^3)/12;  % 2nd Moment of Area
Fo=(M/2)*gravity;                   % Nominal force  for 1 magnet
Ap=Fo*2*Go^2/(mu*(N*Io)^2);         % Pole Face Area (Note reduction to effect operating force reduction)
Lo=0.005;                           % Leakage reactance
E=12E9;                             %  Young's Modulus

% ***** Linearised Parameters ******************************************

Ki=Bo/Io;                           % Magnet Parameters
Kg=Bo/Go;
Kb=2*Fo/Bo;
```

```
% ************ Mode Shapes ***********************************************************************************

lambdal=[4.73004 7.85320 10.9956 14.1372 17.2788];

% ************ First Mode Shape ******************************************************************************
zeta1=0.03;                                          % damping factor
w1=(lambdal(1)^2)*sqrt(E*Iz/((bmass/L)*L^4));        % 1st Nat Freq.
lamda1=(((w1^2)*(bmass/L))/(E*Iz))^0.25;             % Eigenfunc result
m1e1=frefre(lambdal(1),(fl*L)/L,L/L);                % Mode shape free end
m1e2=frefre(lambdal(1),((1-fl)*L)/L,L/L);            % Mode shape free end
m1c=frefre(lambdal(1),(L/2)/L,L/L);                  % Mode shape centre

m1e1s=frefre(lambdal(1),((senpos*fl)*L)/L,L/L);      % Mode shape free end (to vary position of sensor)
m1e2s=frefre(lambdal(1),((1-(senpos*fl))*L)/L,L/L);  % Mode shape free end (to vary position of sensor)

% ************ Second Mode Shape *****************************************************************************

zeta2=0.03;                                          % damping factor
w2=(lambdal(2)^2)*sqrt(E*Iz/((bmass/L)*L^4));        % 2nd Nat Freq.
lamda2=(((w2^2)*(bmass/L))/(E*Iz))^0.25;             % Eigenfunc result

%.....Amplitudes.....

m2e1o=frefre(lambdal(2),(L*fl)/L,L/L);               % Mode shape free end output
m2e2o=frefre(lambdal(2),(L*(1-fl))/L,L/L);           % Mode shape free end output
m2co=frefre(lambdal(2),(L/2)/L,L/L);                 % Mode shape centre output

m2e1os=frefre(lambdal(2),(L*(fl*senpos))/L,L/L);     % Mode shape free end output (to vary sensor position)
m2e2os=frefre(lambdal(2),(L*(1-(senpos*fl)))/L,L/L); % Mode shape free end output (to vary sensor position)

%.....Gradients.....

m2e1=ffasym(lambdal(2),(L*fl)/L,L/L);                % Mode shape free end
m2e2=ffasym(lambdal(2),(L*(1-fl))/L,L/L);            % Mode shape free end
m2c=ffasym(lambdal(2),(L/2)/L,L/L);                  % Mode shape centre (very nearly zero)

m2e1s=ffasym(lambdal(2),(L*(senpos*fl))/L,L/L);      % Mode shape free end (to vary sensor position)
m2e2s=ffasym(lambdal(2),(L*(1-(fl*senpos)))/L,L/L);  % Mode shape free end (to vary sensor position)


% ************ Third Mode Shape ******************************************************************************

zeta1=0.03;                                          % damping factor
w3=(lambdal(3)^2)*sqrt(E*Iz/((bmass/L)*L^4));        % 3rd Nat Freq.
lamda3=(((w3^2)*(bmass/L))/(E*Iz))^0.25;             % Eigenfunc re
m3e1=frefre(lambdal(3),(fl*L)/L,L/L);                % Mode shape free end
m3e2=frefre(lambdal(3),((1-fl)*L)/L,L/L);            % Mode shape free end
m3c=frefre(lambdal(3),(L/2)/L,L/L);                  % Mode shape centre

m3e1s=frefre(lambdal(3),((senpos*fl)*L)/L,L/L);      % Mode shape free end (to vary position of sensor)
m3e2s=frefre(lambdal(3),((1-(senpos*fl))*L)/L,L/L);  % Mode shape free end (to vary position of sensor)

% ************ Fourth Mode Shape *****************************************************************************
zeta2=0.03;                                          % damping factor
w4=(lambdal(4)^2)*sqrt(E*Iz/((bmass/L)*L^4));        % 2nd Nat Freq.
lamda4=(((w4^2)*(bmass/L))/(E*Iz))^0.25;             % Eigenfunc result

%.....Amplitudes.....

m4e1o=frefre(lambdal(4),(L*fl)/L,L/L);               % Mode shape free end output
m4e2o=frefre(lambdal(4),(L*(1-fl))/L,L/L);           % Mode shape free end output
m4co=frefre(lambdal(4),(L/2)/L,L/L);                 % Mode shape centre output
```

```
m4e1os=frefre(lambdal(4),(L*(f1*senpos))/L,L/L);          % Mode shape free end output (to vary sensor position)
m4e2os=frefre(lambdal(4),(L*(1-(senpos*f1)))/L,L/L);      % Mode shape free end output (to vary sensor position)

%......Gradients..........................................................

m4e1=ffasym(lambdal(4),(L*f1)/L,L/L);                     % Mode shape free end
m4e2=ffasym(lambdal(4),(L*(1-f1))/L,L/L);                 % Mode shape free end
m4c=ffasym(lambdal(4),(L/2)/L,L/L);                       % Mode shape centre

m4e1s=ffasym(lambdal(4),(L*(senpos*f1))/L,L/L);           % Mode shape free end (to vary sensor position)
m4e2s=ffasym(lambdal(4),(L*(1-(f1*senpos)))/L,L/L);       % Mode shape free end (to vary sensor position)

m4e1=m4e1*lamda4;                                         % Torque Input (as per B&J p.358)
m4e2=m4e2*lamda4;                                         % Torque Input
m4c=m4c*lamda4;
%.........................................................................................................
```

Flexible Structure Model: flxsys6.m

```
%%%%%%%%%%%%%%%%%%%%%%%%%%%%%%%%%%%%%%%%%%%%%%%%%%%%%%%%%%%%%%%%%%%%
%                                                                  %
%           Maglev  Plant Description                              %
%                                                                  %
%                                                                  %
%%%%%%%%%%%%%%%%%%%%%%%%%%%%%%%%%%%%%%%%%%%%%%%%%%%%%%%%%%%%%%%%%%%%


% ***** DESIGN FOR 4 FLEXIBLE MODES ************************************************************


% ***** Fundamental system matrix *************************************************************

ar=[-R/(N*Ap*Ki)          0  -(Kb*Kg*R)/(N*Ap*M*Ki)       0             0  -(Kb*Kg*R)/(N*Ap*M*Ki);
1+m1c*(m1e1+m1e2)+m3c*(m3e1+m3e2) 0       0          0                0        0;
   0                     -1        0          0                -L/2       0;
   0                      0  -(L*Kb*Kg*R)/(2*Ix*N*Ap*Ki)   -R/(N*Ap*Ki)    0  (L*Kb*Kg*R)/(2*Ix*N*Ap*Ki);
   0                      0        0      1+(m2c*(m2e1o-m2e2o)+m4c*(m4e1o-m4e2o))*2/L  0      0;
   0                     -1        0          0                +L/2       0];


% ***** Cross coupling matrix - is the moderr the correct method to vary parameters
acc1=[0      0 0   0        0 0;
   m1e1-m1e2 0 0   0          0 0;
   0      0 0   0        0 0;
   0      0 0 (m2e1o-m2e2o)*2/L  0 0;
   0      0 0   0        0 0;
   m3e1-m3e2 0 0   0          0 0;
   0      0 0   0        0 0;
   0      0 0 (m4e1o-m4e2o)*2/L  0 0];

% ***** Flexible Mode Description ****************************

af=[ 0       1       0       0   0   0     0   0;
   -w1^2  -2*zeta1*w1    0       0   0   0     0   0;
    0       0       0       1   0   0     0   0;
    0       0     -w2^2   -2*zeta1*w2 0   0     0   0;
    0       0       0       0   0   1     0   0;
    0       0       0       0  -w3^2 -2*zeta1*w3 0   0;
    0       0       0       0   0   0     0   1;
    0       0       0       0   0   0    -w4^2 -2*zeta1*w4];

% ***** Coupling into the rigid body mode ********************
```

```
%    q1      dq1/dt    q2  dq2/dt
acc2=[ 0          0          0  0          0      0          0   0;
  m1c*(-w1^2) m1c*(-2*zeta1*w1) 0   0        m3c*(-w3^2) m3c*(-2*zeta1*w3)  0    0;
    0         0          0   0          0      0          0   0;
    0         0          0   0          0      0          0   0;
    0         0    m2c*(-w2^2) m2c*(-2*zeta1*w2)  0        0      m4c*(-w4^2) m4c*(-2*zeta1*w4);
    0         0          0   0          0      0          0   0];


% ****** Disturbance Input Matrix *******************************

brd=[0 0;0 0;1 0;0 0;0 0;0 1];

% ****** Disturbance Input Matrix to Flexible Modes ************

bfd=[0 0;0 0;0 0;0 0;0 0;0 0;0 0;0 0;0 0];

% ****** Control Input ******************************************************

brc=[Kb/(N*Ap*M) Kb/(N*Ap*M);0 0;0 0;Kb*L/(2*N*Ap*Ix) -Kb*L/(2*N*Ap*Ix);0 0;0 0];

% ****** Control Input to Flexible Modes ************************************

bfc=[0 0;0 0;0 0;0 0;0 0;0 0;0 0;0 0;0 0];

% ****** Output Description *************************************************

% ****** Output from Rigid Body Mode ****************************************

ar=[0      0 0     1          0 0;     % rigid body angular acceleration
   0      0 1     0          0 0;     % g1
   0      0 0     0          0 1;     % g2
   1      0 0     0          0 0;     % acceleration for z  {d2z/dt2}
(m1e1+m1e2) 0 0     0          0 0;          % acceleration due to 1st body mode
   0      0 0 (m2e1o-m2e2o)*2/L  0 0;        % angular acceleration due to 2nd body mode
(m3e1+m3e2) 0 0     0          0 0;          % acceleration due to 3rd body mode
   0      0 0 (m4e1o-m4e2o)*2/L  0 0;        % angular acceleration due to 4th body mode
M/(2*Kb)   0 0  2*Ix/(L*Kb)      0 0;        % b1;
M/(2*Kb)   0 0 -2*Ix/(L*Kb)      0 0;        % b2;
M/(2*Ki*Kb) 0 Kg/Ki 2*Ix/(L*Kb*Ki)  0 0;  % i1; f1 = [  M     0 0    2*Ix/L      0 0];
M/(2*Ki*Kb) 0 0   -2*Ix/(L*Kb*Ki)  0 Kg/Ki];          % i2;

% ****** Output from Flexible Body Mode *************************************

cf=[zeros(4,8);
   -w1^2 -2*zeta1*w1  0     0     0     0     0     0;   % acceleration due to 1st body mode
      0     0     -w2^2 -2*zeta1*w2  0     0     0     0;   % acceleration due to 2nd body mode
      0     0     0     0     -w3^2 -2*zeta1*w3  0     0;   % acceleration due to 2nd body mode
      0     0     0     0     0     0     -w4^2 -2*zeta1*w4;% acceleration due to 2nd body mode
      0     0     0     0     0     0     0     0;
      0     0     0     0     0     0     0     0;
      0     0     0     0     0     0     0     0;
      0     0     0     0     0     0     0     0];


% ****** Assemble Required System Matrix ************************************

a=[ar    acc2;
   acc1   af];

% ****** Complete Disturbance Input *****************************************

bd=[brd;bfd];
```

```
% ****** Complete Control Input ************************************************

bc=[brc; bfc];

% ****** Assemble Complete Input Matrix ***********************************

b=[brd    brc;
  bfd    bfc];

% ****** Output from Complete Modes ***************************************

ctemp=[cr cf];

c=[ctemp;
  ctemp(4,:)+m1c*ctemp(5,:)+m3c*ctemp(7,:);                          % net vertical acceleration
  ctemp(1,:)+m2c*ctemp(6,:)+m4c*ctemp(8,:);                          % angular acceleration due to rigid + 2nd flex body mode;
  ctemp(4,:)+m1e1*ctemp(5,:)+ctemp(1,:)*L/2+m2e1o*ctemp(6,:)+m3e1*ctemp(7,:)+m4e1o*ctemp(8,:);
                                                                     % acceleration at airgap 1
  ctemp(4,:)+m1e2*ctemp(5,:)-ctemp(1,:)*L/2+m2e2o*ctemp(6,:)+m3e2*ctemp(7,:)+m4e2o*ctemp(8,:)];
                                                                     % acceleration at airgap 2
d=zeros(length(c(:,1)),length(b(1,:)));
```

Appendix 5: Flexible Structure Description

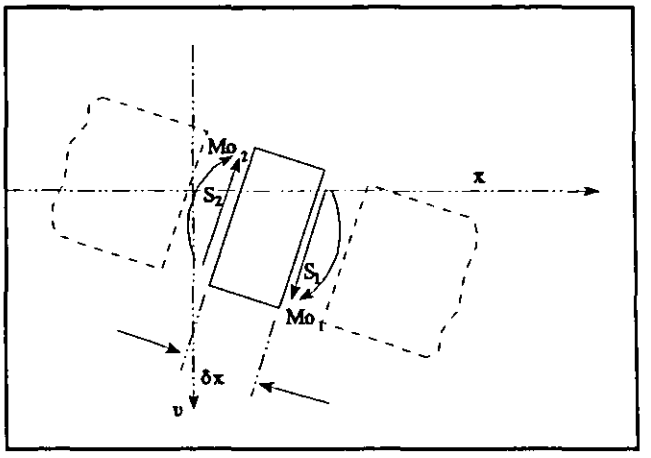

Figure A5.1 Short element of a beam of length δx.

In the figure above the shear forces S_1 and S_2 and the bending moments Mo_1 and Mo_2 act on the bounded plane faces of the beam element.

For small deflections, υ of the beam the motion perpendicular to the axis 0-x of the undeflected beam is given by

$$S_1 - S_2 = (\rho A_e \delta x)\frac{\partial^2 \upsilon}{\partial t^2} \qquad \textbf{A5.1}$$

and as the element length tends to zero

$$\frac{\partial S}{\partial x} = (\rho A_e)\frac{\partial^2 \upsilon}{\partial t^2} \qquad \textbf{A5.2}$$

Assuming that the rate of change of the moment of momentum of the element about its centre of gravity can be neglected, then for the rotational motion

$$S\partial x + Mo_1 - Mo_2 = 0 \qquad \textbf{A5.3}$$

which as the element length becomes small becomes

$$S = -\frac{\partial Mo}{\partial x} \qquad \textbf{A5.4}$$

Simple bending theory [Benham87] provides the relation

$$M = -EI_2 \frac{\partial^2 \upsilon}{\partial x^2} \qquad \textbf{A5.5}$$

This can be combined with equation to give A5.4

$$S = -EI_2 \frac{\partial^3 \upsilon}{\partial x^3} \qquad \textbf{A5.6}$$

Substituting for the shear force in equation A5.2 provides a method of describing the motion of the beam due to flexure.

$$\frac{\partial^2 \upsilon}{\partial t^2} + \frac{EI}{A_e \rho} \frac{\partial^4 \upsilon}{\partial x^4} = 0 \qquad \textbf{A5.7}$$

For harmonic excitation with frequency ω the solution of this equation is of the form

$$\upsilon = X(x)\, e^{i\omega t} \qquad \textbf{A5.8}$$

Substitution leads to the equation:

$$\frac{d^4 X}{dx^4} - \frac{\omega^2 A_e \rho}{EI} X = 0 \qquad \textbf{A5.9}$$

Defining the term

$$\lambda^4 = \frac{\omega^2 A_e \rho}{EI_2} \qquad \textbf{A5.10}$$

The general form of the function X(x) becomes

$$X(x) = A_c \cos(\lambda x) + B_c \sin(\lambda x) + C_c \cosh(\lambda x) + D_c \sinh(\lambda x) \qquad \textbf{A5.11}$$

The constants A_c, B_c, C_c, and D_c may be determined if the end conditions are known, which when substituted back into equation A5.8 using A5.11 gives a relationship between the excitation and the displacement for specified force input and measurement points (x and h respectively). The solution of the above equation results in a very unwieldy transfer function which is conveniently described in terms of receptance α_{xh}.

$$v = \alpha_{xh} F e^{i\omega t} \qquad \textbf{A5.12}$$

Where α_{xh} is the receptance between a point of application of the force at a distance x along the beam, and h the point of measurement:

$$\alpha_{xh} = \sum_{r=1}^{\infty} \frac{\phi_r(x)\phi_r(h)}{M(\omega_r^2 - \omega^2)} \qquad \textbf{A5.13}$$

The characteristic function $\phi_r(x)$ represents the effect of a force applied at length x along the beam and $\phi_r(h)$ the measurement of the effect of that force at a point h along the beam both for the rth frequency.

$$\phi_r(x) = \cosh \lambda_r x + \cos \lambda_r x - \frac{\cosh(\lambda_r l) - \cos(\lambda_r l)}{\sinh(\lambda_r l) - \sin(\lambda_r l)} (\sinh \lambda_r x + \sin \lambda_r x) \qquad \textbf{A5.14}$$

The frequency equation of the free-free beam is

$$\cos(\lambda_r l)(\cosh \lambda_r l) - 1 = 0 \qquad \textbf{A5.15}$$

and this results in a series which enables the calculation of the corresponding natural frequencies using equation A5.10 where λ and ω become specific to the r th frequency, that is λ_r and ω_r. Consider the following diagram for a free-free beam.

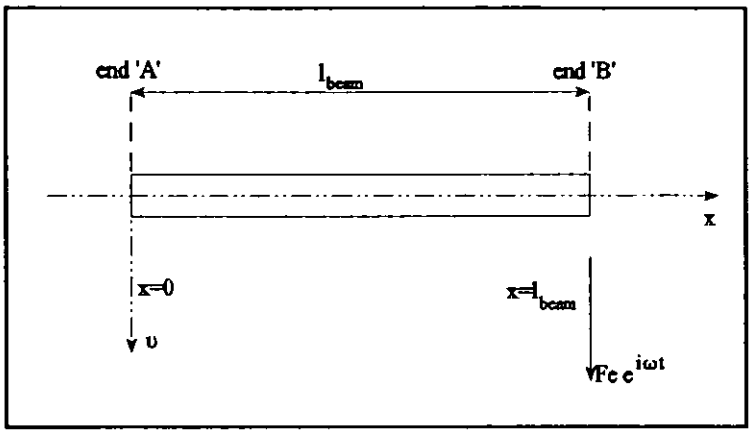

Figure A5.2 End 'B' of a free-free beam being acted upon by a vertical harmonic component forces.

The end conditions are determined by the end conditions which for the Free-Free beam are:

When $x = 0$, $$\frac{\partial^2 \upsilon}{\partial x^2} = \frac{\partial^3 \upsilon}{\partial x^3} = 0 \qquad \textbf{A5.16}$$

When $x = l_{beam}$ $$\frac{\partial^2 \upsilon}{\partial x^2} = 0, \quad \frac{\partial^3 \upsilon}{\partial x^3} = \frac{F_e}{EI_2} e^{i\omega t} \qquad \textbf{A5.17}$$

The deflection and slope at any section of the beam may be found for any position simply by specifying the position of the force application and the measurement output deflection.

The diagram below shows the free-free beam with the condition given in equation 4.74 occuring at both ends.

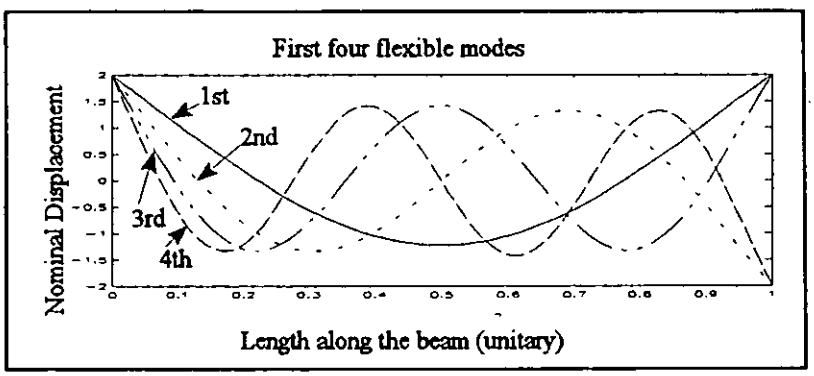

Figure A5.3 Flexible bending modes

Appendix 6: Rig Design

MAGNET ROUND CORE WITH GROOVE FOR FLUX SENSORS

Material: Mild Steel
(4 off)

RIG DESIGN

FLEXIBLE MAGLEV PROJECT

Jonathan Paddison. ext 4178, email JPADDISO

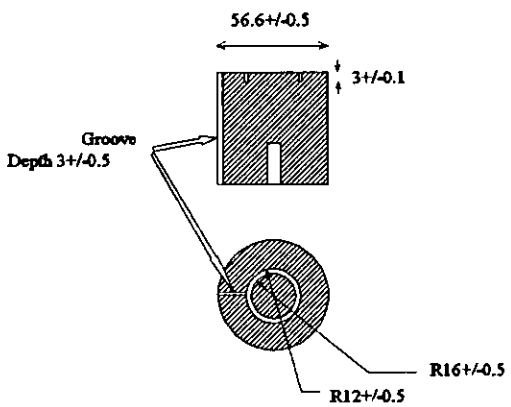

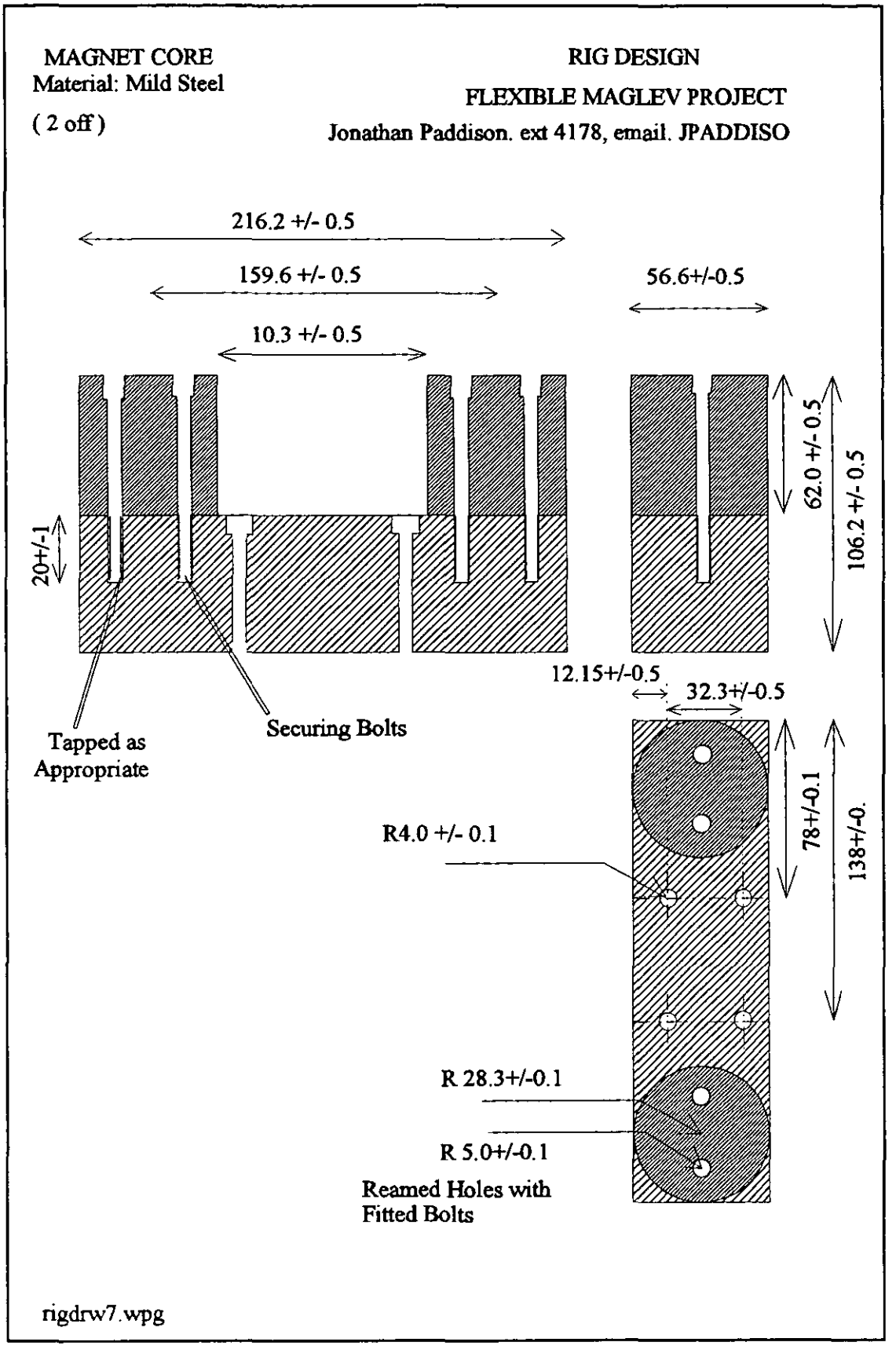
MAGNET CORE
Material: Mild Steel
(2 off)
RIG DESIGN
FLEXIBLE MAGLEV PROJECT
Jonathan Paddison. ext 4178, email. JPADDISO
216.2 +/- 0.5
159.6 +/- 0.5
56.6+/-0.5
10.3 +/- 0.5
62.0 +/- 0.5
106.2 +/- 0.5
20+/-1
12.15+/-0.5
32.3+/-0.5
Tapped as
Appropriate
Securing Bolts
R4.0 +/- 0.1
78+/-0.1
138+/-0.
R 28.3+/-0.1
R 5.0+/-0.1
Reamed Holes with
Fitted Bolts
rigdrw7.wpg

FRAME CONSTRUCTION
(1 off)

RIG DESIGN
FLEXIBLE MAGLEV PROJECT
Jonathan Paddison, ext 4178, email JPADDISO

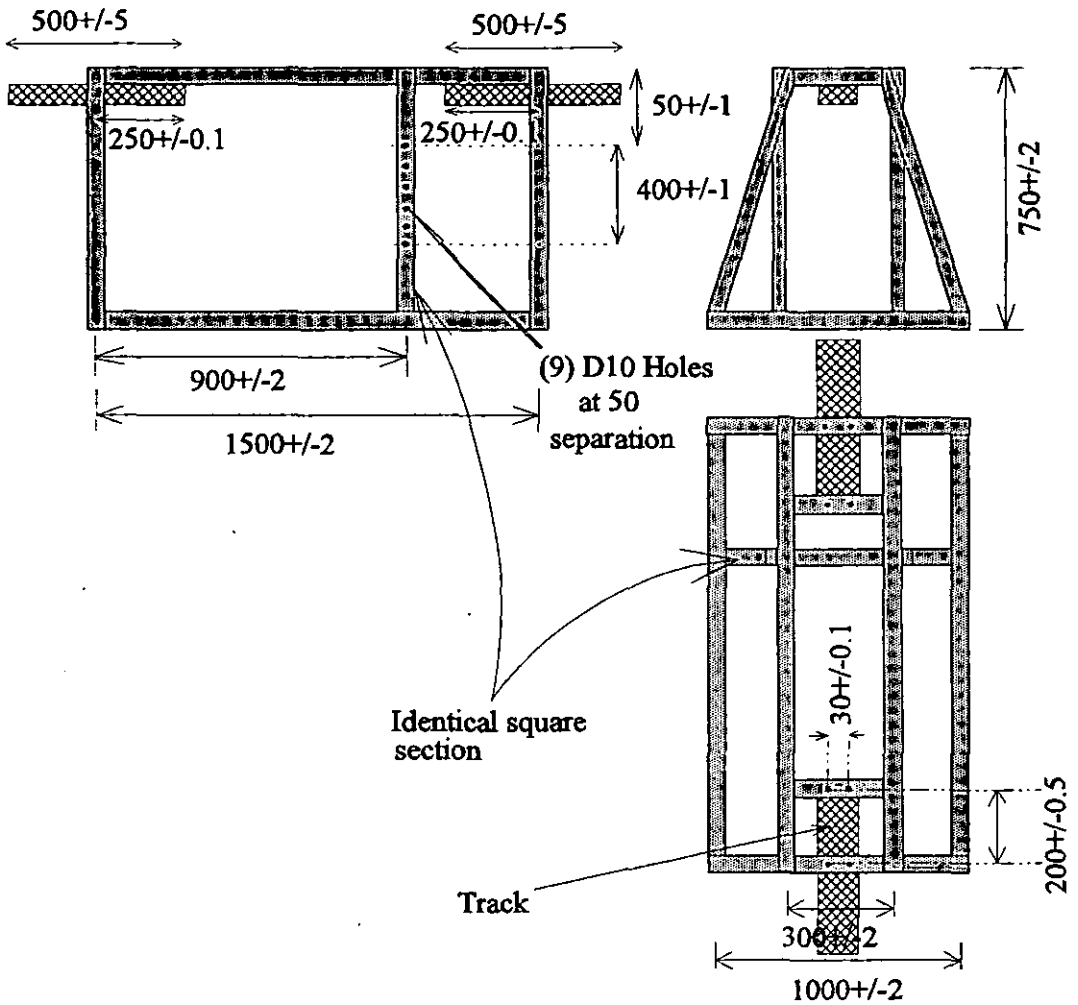

Standard square section steel should be suitable (1 1/4 inch)

Total amount estimated to be: 12.0 m

rigdrw9.wpg

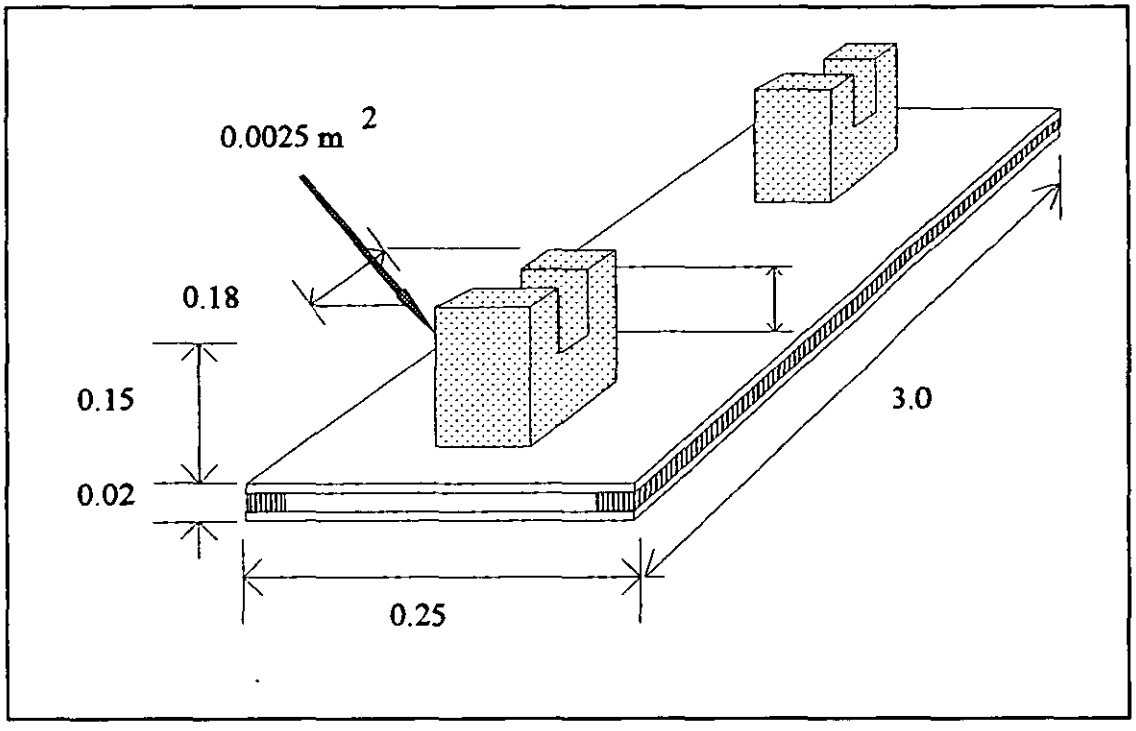
0.0025 m 2
0.18
0.15
0.02
3.0
0.25

Temperature Considerations

Applying an energy balance to the magnet such that;

Change in Internal Energy = Energy Generated - Heat Flow from Surface

$$m\ C_p\ \delta T = \dot{q}\ V\ \delta t - h\ A\ T\ \delta t \qquad \textbf{A6.1}$$

Where t = time (s)

T = excess temperature

m = mass (kg)	= 15 kg
C_p= Specific Heat Capacity (Fe)	= 500J kg^{-1} K^{-1}
C_p= Specific Heat Capacity (Al)	= 920J kg^{-1} K^{-1}
qV= heat generated (W)	= I_o^2R = 255.7W
h = film coefficient $Wm^{-1}K^{-1}$	= 16 W m^{-1} K^{-1}
A = surface area of device (m^2)	= 0.102 m^2

The film coefficient is dependent on the nature of the surrounding fluid not the nature of the material from which the heat is radiated and this is clearly air.

$$\frac{dT}{q\ V - h\ A} = \frac{dt}{m\ C_p} \qquad \textbf{A6.2}$$

Integrating

$$\int \frac{1}{h\ A}\ \frac{dT}{(\frac{q\ V}{h\ A} - T)} = \int \frac{dt}{m\ C_p} \qquad \textbf{A6.3}$$

$$\frac{1}{h\ A}\ \ln[\frac{q\ V}{h\ A} - T] + Constant = -\frac{t}{m\ C_p} \qquad \textbf{A6.4}$$

At t=0 then T=0 so the constant may be defined;

$$C = -\frac{1}{h\ A}\ln[\frac{q\ V}{h\ A}] \qquad \textbf{A6.5}$$

$$-\frac{t}{m\ C_p} = \frac{1}{h\ A}\left[\frac{\ln[\frac{q\ V}{h\ A} - T]}{\frac{q\ V}{h\ A}}\right] \qquad \textbf{A6.6}$$

At final temperature;

$$\frac{dT}{dt} = 0 \qquad \textbf{A6.7}$$

Hence the following applies;

$$\frac{[q\ V - h\ A\ T_{max}]}{m\ C_p} = 0 \qquad \textbf{A6.8}$$

This leads to the most significant results that;

$$T_{max} = \frac{q\ V}{h\ A} \qquad \textbf{A6.9}$$

$$T = T_{max}\ [1 - e^{(\frac{h\ A\ t}{m\ C_p})}] \qquad \textbf{A6.10}$$

Substituting the parameters given the following steady state values can be calculated;

$$T_{max} = \frac{255.7}{16 \cdot 0.102} = 156.6\ ^{\circ}C \qquad \textbf{A6.11}$$

This maximum temperature is that of the two aluminium coils mounted on one core. No account is taken of the heat conduction through the core and flexible beam. Hence this

value should be the very worst case.

$$\textit{Time Constant}\ ,\ \tau = \frac{11 \cdot 920}{16 \cdot 0.102} = 6555\ s = 1\ hr\ 56\ \text{min} \qquad \textbf{A6.12.}$$

Appendix 7: Control Software

A number of programs are include in this thesis as examples of the control law implementation

The program "d19.c" is the basic levitation program for the whole rig. The phase advance function is included after "d19.c" in a series of programs "pa.h", "pa.c", as well as the programs to calculate the filter coefficients "fltdpa.h" and "fltdpa.c".

These listing are only intended to give an overview of the implementation. The listing is not complete in that a number of the functions and the interrupt routine IO_init.s are not included.

Program "d19.c" Classical Maglev Modal Controller

```
/*************************************************************************
        Use of notch filters on the basic modal suspension

        Remember that the accelerometer data is now band limited to 110Hz


        Introduces the real airgap small variation and still uses the electonic
        self zeroing integrator. The digital self-zeroing integrator is present
        but cancelled out.


        Single Degree of freedom levitation program for the JEP Maglev
        Rig.

        This program can drive either Magnet

        The compensator filters are implemented using the delta filter

        16 Channels are read at 1kHz sampling rate using a new interrupt
        routine, IO_init().

        Language:       DSP32C Assembler
        Compiler:       AT & T `d3as'
        Compiler switches:  -Q (DSP32C mode only)
        Compiler Version:   1.6.1
        Function description:  Driver software for LSI DAC and ADC cards.
                               Initialises buffers and interrupts. Contains
                               interrupt service routines.
        Status:         Experimental


        Program compiled using the following;

        xcc -Q -lad -lda -lm -o %1.x a.o i5.o %1.c

        Where i5.o is the compiled version of ioinit5.s which is compiled
        for the DSP32C using the following;
```

```
                d3as -Q ioinit5.s

                Similarly a.o is the definition program for the DSPLINK addresses
                supplied by ONYX as addinit.s

                J.E.Paddison        Program name originally :  MO_DEM2.C
                                    Version;
                              :     4.0       15/12/94
                              :     3.0       dated 03/10/94
                              :     2.0       dated 10/08/94
*************************************************************************/

#include "libad32c.h"                   /* library for the a to d LSI32 In- Card */
#include "libda32c.h"                   /* library for the d to a LSI16 Out- Card */
#include "math.h"                       /* maths library */
#include "malloc.h"
#include <xstdio.h>                     /* I/O library */
#include "fdintc.c"
#include "dint1.c"
#include "pa.c"                         /* Delta Phase Advance Filter */
#include "fltdpac.c"                    /* Delta Discrete Filter Coefficients for the PA */
#include "pi.c"                         /* Delta Proportional + Integral */
#include "fltdpic.c"                    /* Delta Discrete Filter Coefficeints for the PI */
#include "limit.c"                      /* Limit on the voltage command in response to a current measurement */
#include "filtntc.c"                    /* Calculate the notch filter discrete coefficients */
#include "notch.c"                      /* Function for notch filter */
#include "filthpc.c"                    /* High Pass Filter Coefficients */
#include "hp.c"                                 /* High Pass Filter Function */
#include "filtlpc.c"                            /* Low Pass Filter Coefficients */
#include "lp.c"                                 /* Low Pass Filter Function */

#define MASK   1 + 2 + 4 + 8 + 16               /* ie selects channels 0 and 1, from 2^0, 2^1 */
#define pifact 3.142

#define N_SAMPLES           4000                /* set the number of samples (1000Hz sampling represents 10s)*/
#define KI          5.8333e-2                   /* Current/Flux Density relation ship Bo/Io */
#define ADC_FACTOR          32767               /* ADC/DAC  Maximum values */
#define MAX_AIRGAP          0.033               /* Maximum Airgap [m] */
#define MAX_FLUX  1.5                           /* Maximum Flux [T] */
#define MAX_Z               0.00858             /* Maximum Displacement [m] */
#define MAX_ACCEL           3.17                /* Maximum Acceleration [m/s^2] */
#define MAX_VELOCITY        0.00905             /* Maximum Velocity [m/s]*/
#define CLK_TRG             125e-9              /* Clock Trigger Period [s] */

extern ADC_ptbuff;
extern ADC_flag;
extern ANALin_base;

short data1[N_SAMPLES][25];                     /* readings */

short outdat[16];                               /* array for output of command output and signals */

main()
        {
        FILE *fp;
        float gap_scale = MAX_AIRGAP/ADC_FACTOR;        /* airgap scaling factor */
        float z_scale = MAX_Z/ADC_FACTOR;               /* dispalcement scaling factor */
        float flux_scale = MAX_FLUX/ADC_FACTOR;         /* flux scaling factor */
        float accel_scale = MAX_ACCEL/ADC_FACTOR;       /* acceleration scaling factor */
        float velocity_scale = MAX_VELOCITY/ADC_FACTOR;
        float cg=0;                                     /* airgap coupling factor */
        float nomg0=0.010,nomg1=0.010;                  /* nominal airgap */
        float kpi0=600, tpi0=0.002;                     /* PI Continuous filter coefficients */
        float kpa0=15, tpa0=0.06, apa0=0.13;            /* Continuous Filter Coefficients for PA */
        float kpa1=5, tpa1=0.06, apa1=0.13;             /* Continuous Filter Coefficients for PA */
        float wn1=19.1*2*3.142, dmp1=0.1;               /* Notch filter frequency for 1st resonant mode */
        float wn2=36.08*2*3.142, dmp2=0.05;             /* Notch filter frequency for 2nd resonant mode */
        float whp=1.5*2*3.142;                          /* High Pass Filter Frequency */
        float wlp=1.5*2*3.142;                          /* Low Pass Filter Frequency */
        float tint1=0.47;
```

```
float tint2=0.946;
float tint3=2.2;
float tint4=2.2;

short sample_freq1=1000;
float sp1 = 1 / (float)sample_freq1;                    /* 'False' Sample Interval Seconds */
short sample_int1 = (short)(sp1 / CLK_TRG);             /* sample rate in terms of clock triggers */
float end_sim = 60;                                     /* end of the loop in seconds */
short jmax=1;                                           /* number of intermediate cycles in each loop */
float ipa0,ipi0,ipa1,ipi1,time=0,uint=0;                /* input and output variable of pi and pa */
float z0,z1,bourmp=0.010,pitrmp=0.00;
short channel=0;
float g0,g1,cengap,cenang,zdd0,zdd1;
short flag=0,m=0;                                       /* general short variables */
register short i,j;
dintc ic1;
dint iout0;
dint iout1;
pidc picoef0;
pidc picoef1;
pic varpi0;
pic varpi1;
padc pacoef0;
pac bounce;
padc pacoef1;
pac pitch;
lpdc lpfcoef0;                                          /* Low Pass Filter Coefficients */
lpc lpout0;                                     /* Low Pass Carry Structure */
lpc lpout1;                                     /* Low Pass Carry Structure */
hpdc hpfcoef0;                                  /* High Pass Filter Coefficients */
hpc hpout0;                                     /* High Pass Carry Structure */
hpc hpout1;                                     /* High Pass Carry Structure */
ntdc notcoef1;                                  /* notch filter coefficients */
ntdc notcoef2;
ntc vntf1;
ntc vntf2;                                      /* Notch carry structure */
short *outptr;                                  /* data output mask */
short *ptr0;                                    /* define pointers */
ptr0=(short *)malloc(16*2);


outptr = &outdat[0];

intcoef(&ic1,tint1,tint2,tint3,tint4,sp1);

pacoef(&pacoef0,kpa0,tpa0,apa0,sp1);
pacoef(&pacoef1,kpa1,tpa1,apa1,sp1);

picoef(&picoef0,kpi0,tpi0,sp1);

hpcoef(&hpfcoef0,whp,sp1);                      /* calculate all of the high pass filter coefficients */

lpcoef(&lpfcoef0,wlp,sp1);                      /* calculate all of the low pass filter coefficients */

ntcoef(&notcoef1,wn1,dmp1,sp1);                 /* calculate all of the notch filter coefficients */
ntcoef(&notcoef2,wn2,dmp2,sp1);

LSIADC_cal();                                   /* Calibrate the ADC Card */

LSIADC_set_int( sample_int1 );                  /* Set sample interrupt to the equivalent of 1000Hz */

while( !LSIDAC_single_out( 0,channel++ ));      /* sends zero to all channels */
                                                /* initialise the filter coefficients */
bounce.wpac=0,pitch.wpac=0,varpi0.wpic=0,varpi1.wpic=0,vntf1.xntc=0,vntf1.wntc=0,vntf2.xntc=0,vntf2.wntc=0;
lpout0.whpc=0,lpout0.xhpc=0,lpout0.ohp=0,lpout0.wlpc=0,lpout0.xlpc=0,lpout0.olp=0,lpout1.whpc=0,lpout1.xhpc=0;
lpout1.ohp=0,lpout1.wlpc=0,lpout1.xlpc=0,lpout1.olp=0;
iout0.wint1=0,iout0.wint2=0,iout0.wint3=0,iout0.oint1=0,iout0.oint2=0,iout0.oint3=0;
iout1.wint1=0,iout1.wint2=0,iout1.wint3=0,iout1.oint1=0,iout1.oint2=0,iout1.oint3=0;
```

```
        j=0;
        m=0;

        ptr0 = (short *)&ADC_ptbuff;                    /* initialise pointer */
        for(i=0; i<32; i++)
        *ptr0++ =0;

        ptr0 = (short *)&ADC_ptbuff;
        ADC_flag=0;
        IO_init(INT_1,0);

/* ************************************************************************************ */
        while( time<end_sim ){                          /* outer loop */
                for(j=1;j++<=jmax;){

                while(ADC_flag==0);                     /* wait for interrupt to finish */

                ADC_flag=0;                             /* reset flag */

                LSIDAC_multi_out( outdat,MASK );        /* output for all signals in control loop - note this statement*/
                                                        /* outputs the values from the last control cycle */
                                                        /* but operates as soon as the interrupt is finished - this means it */
                                                        /* does not vary with calculation length */
                if (time < (end_sim - 20)){
                        bourmp = bourmp-0.0000005;      /* Ramp to raise the magnet in 2 seconds */
                        if (bourmp< -0.002 ) bourmp= -0.002;
                }
                else {
                        bourmp=bourmp + 0.0000004;
                        if (cengap <= -0.014){
                                varpi0.opi = 0;
                                }
                }
                g0= nomg0 + bourmp - (float)( *( ptr0 + 1 ) - 4965) * gap_scale;        /* airgap */
                g1= nomg1 + bourmp - (float)( *( ptr0 + 5 ) - 4965) * gap_scale;

                z0 = (float) *(ptr0+3) * z_scale;                                       /* absolute coordinate */
                z1 = (float) *(ptr0+7) * z_scale;

                zdd0 = (float) *(ptr0+8) * accel_scale;                                 /* acceleration */
                zdd1 = (float) *(ptr0+9) * accel_scale;

                /* Self Zeroing Double Integrators */
                dintf(&iout0,ic1.dintp,ic1.dintq,ic1.dintd1,ic1.cint01,ic1.cint11,ic1.cint02,ic1.cint12,zdd0,iout0.wint1,iout0.
                wint2,iout0.wint3,iout0.oint3);
                dintf(&iout1,ic1.dintp,ic1.dintq,ic1.dintd1,ic1.cint01,ic1.cint11,ic1.cint02,ic1.cint12,zdd1,iout1.wint1,iout1.
                wint2,iout1.wint3,iout1.oint3);
                /* High Pass Filters */
                hpf(&hpout0, hpfcoef0.php, hpfcoef0.qhp, hpfcoef0.rhp, hpfcoef0.dhp1, hpfcoef0.dhp2 ,(iout0.oint2/2.4),
                hpout0.xhpc, hpout0.whpc);
                hpf(&hpout1 ,hpfcoef0.php, hpfcoef0.qhp, hpfcoef0.rhp, hpfcoef0.dhp1, hpfcoef0.dhp2, (iout1.oint2/2.4),
                hpout1.xhpc,hpout1.whpc);
                /* Low Pass Filters */
                lpf(&lpout0,lpfcoef0.plp, lpfcoef0.qlp, lpfcoef0.rlp, lpfcoef0.dlp1, lpfcoef0.dlp2,g0,lpout0.xlpc,lpout0.wlpc);
                lpf(&lpout1,lpfcoef0.plp, lpfcoef0.qlp, lpfcoef0.rlp, lpfcoef0.dlp1, lpfcoef0.dlp2,g1,lpout1.xlpc,lpout1.wlpc);

                ipa0 = (g0 + g1)/2;                                                     /* Position Demand */
                ipa1 = (-g0 + g1)/(2*0.75);                                             /* Pitch Demand */


                nt(&vntf1,notcoef1.pnt,notcoef1.qnt,notcoef1.rnt,notcoef1.dnt1,notcoef1.dnt2,ipa0,vntf1.xntc,vntf1.wntc);

                nt(&vntf2,notcoef2.pnt,notcoef2.qnt,notcoef2.rnt,notcoef2.dnt1,notcoef2.dnt2,ipa1,vntf2.xntc,vntf2.wntc);

                paf(&bounce,pacoef0.ppa,pacoef0.qpa,pacoef0.dpa1,ipa0,bounce.wpac);     /* Phase advance */
                paf(&pitch,pacoef1.ppa,pacoef1.qpa,pacoef1.dpa1,ipa1,pitch.wpac);       /* Phase advance */

                ipi0= bounce.opa - pitch.opa*0.75 + ((float)*ptr0 - 200) * flux_scale;  /* Flux Density Demand */
                ipi1= bounce.opa + pitch.opa*0.75 + ((float)*(ptr0+4) - 200) * flux_scale;  /* Flux Density Demand */
```

```
                pif(&varpi0,picoef0.cpi0,picoef0.cpi1,ipi0,varpi0.wpic);        /* Proportional + Integral */

                pif(&varpi1,picoef0.cpi0,picoef0.cpi1,ipi1,varpi1.wpic);        /* Proportional + Integral */


                *outptr = 740 * limit((short)varpi0.opi,40,-40) - 2200;         /* Control output demand magnet 1 */
                *(outptr+1) = 740 * limit((short)varpi1.opi,30,-30) - 2200;     /*Control output demand magnet 2 */
                *(outptr+2) = (short)( ipa0 / gap_scale );                      /* Analysis Outputs */
                *(outptr+3) = (short)( g1 / gap_scale );
                *(outptr+4) = flag*4000;

                data1[m][16]= (short)(hpout0.ohp / z_scale);                    /* store additional data in array */
                data1[m][17]= (short)((lpout0.olp + hpout0.ohp)/gap_scale);
                data1[m][18]= (short)(iout0.oint2 * 32767);
                data1[m][19]= (short)(lpout0.olp / gap_scale);
                data1[m][20]= (short)(ipa0 / gap_scale);

                if (flag++ == 1 ) flag=0;
                time = time + sp1;
                }
                if(time>25 && m<N_SAMPLES){                                     /* store latest set of interrupt driven data */
                        for( i=0;i<16;i++){
                                data1[m][i] = *ptr0++;
                                }
                        m++;
                        ptr0 = (short *)&ADC_ptbuff;
                        }
                }
/* ********** disable output ************************************************************************** */
                outptr= &outdat[0];
                for(j=0; j++<=16;){                             /* reset the outputs of the DAC for channels */
                        *outptr++ = 0;
                }
                LSIDAC_multi_out( outdat,MASK );                        /* send 0 signal to output */
                *(short *)ANALin_base = 0;                              /* disable interrupt */

/* ********** save the array ************************************************************************** */

        if (!(fp=fopen("d2.dat","w+"))){                                /* w+ create a file for read/write */
                printf("Cannot Open the file\n");
                exit(1);}

        for(i=0; i<N_SAMPLES; i++){                                     /* write data to file in scaled format */
                        fprintf(fp," %f",i*sp1*jmax);
                        fprintf(fp," %f",(float)data1[i][0] * flux_scale);
                        fprintf(fp," %f",(float)data1[i][1] * gap_scale);
                        fprintf(fp," %f",(float)data1[i][2] * 1e-3 - 0.75);
                        fprintf(fp," %f",(float)data1[i][3] * z_scale);
                        fprintf(fp," %f",(float)data1[i][4] * flux_scale);
                        fprintf(fp," %f",((float)data1[i][5] - 4965) * gap_scale);
                        fprintf(fp," %f",(float)data1[i][6] * 1e-3 - 0.75);
                        fprintf(fp," %f",(float)data1[i][7] * z_scale);
                        fprintf(fp," %f",(float)data1[i][8] * accel_scale);
                        fprintf(fp," %f",(float)data1[i][9] * accel_scale);
                        fprintf(fp," %f",(float)data1[i][10] * accel_scale);
                        fprintf(fp," %f",(float)data1[i][11]);
                        fprintf(fp," %f",(float)data1[i][12] * velocity_scale);
                        fprintf(fp," %f",(float)data1[i][13] * velocity_scale);
                        fprintf(fp," %f",(float)data1[i][14] * velocity_scale);
                        fprintf(fp," %f",(float)data1[i][15] * z_scale);
                        fprintf(fp," %f",(float)data1[i][16] * z_scale);
                        fprintf(fp," %f",(float)data1[i][17] / 32767);
                        fprintf(fp," %f",(float)data1[i][18] / 32767);
                        fprintf(fp," %f",(float)data1[i][19] * gap_scale);
                        fprintf(fp," %f",(float)data1[i][20] * gap_scale);
```

Files for the phase advance filter

File "fltdpac.h" header file to file calculating the phase advance filter coefficients

```
#ifndef _fltdpac_h_
#define _fltdpac_h_
typedef struct {
        float ppa;                      /* Modified Canonic Coefficients for the Delta Filter */
        float qpa;
        float dpa1;
        } padc;
void pacoef();                          /* Phase Advance Filter Coefficients */
#endif
```

File "fltdpac.c" file calculating the phase advance filter coefficients

```
#include "fltdpac.h"
#include "math.h"

/* delta filter phase advance */

void pacoef(anypac,kpa,tpa,apa,sp)
        padc *anypac;
        float kpa;
        float tpa;
        float apa;
        float sp;
        {
        anypac->ppa = ( kpa*sp + 2*kpa*tpa ) / ( sp + 2*apa*tpa );
        anypac->qpa= kpa;
        anypac->dpa1= ( 2* sp )/( sp + 2* apa * tpa);
        }
```

File "pa.h" header file for actual phase advance operation

```
#ifndef _pa_h_
#define _pa_h_

typedef struct {                        /* Structure to pass data from Phase Advance */
        float opa;
        float wpac;
        } pac;
void paf();                             /* Phase Advacne Function */
#endif
```

File "pa.h" actual phase advance operation

```
#include "pa.h"
void paf(anypa,ppa,qpa,dpa1,upa,wpa)    /* Phase Advance */
        pac *anypa;
        float ppa;
        float qpa;
        float dpa1;
        float upa;
        float wpa;
                {
                float v=0;
                v = upa - wpa;
                anypa->opa = ppa * v + qpa * wpa;       /* perform delta operations */
                anypa->wpac = wpa + dpa1 * v;           /* Update value for outer loop */
                }
```